CRANFIELD UNIVERSITY

W RAWES

THE APPLICATION OF SIGNAL ANALYSIS TECHNIQUES BASED ON CHAOS THEORY TO FLOW REGIME IDENTIFICATION

SCHOOL OF MECHANICAL ENGINEERING

PhD THESIS

CRANFIELD UNIVERSITY

SCHOOL OF MECHANICAL ENGINEERING

PhD THESIS

Academic Year 1996-7

W RAWES

The application of signal analysis techniques based on chaos theory to flow regime identification

Supervisor: H Yeung

December 1996

Crutchfield J.P.,Farmer J.D.,Packard North N.H.,Shaw R.S.
('Chaos' Sci. American V255 p35-50 1986)
Even the process of intellectual progress relies on the injection of new ideas & on new ways of connecting ideas. Innate creativity may have an underlying chaotic process that selectively amplifies small fluctuations & moulds them into macroscopic coherent states that are experienced as thoughts. In some cases the thoughts may be decisions, or what are perceived to be the exercise of the will. In this light, chaos provides a mechanism that allows for free will within a world governed by deterministic laws.

Davies, P.C.W.
('The Matter Myth', with Gribbon, J. (Simon & Schuster/Viking 1991))
We are necessarily ignorant of ultrafine detail.. & so is the universe itself ...
The universe is its own fastest simulator.

Wigner, E.
('The unreasonable effectiveness of mathematics in the natural sciences', comm.pure&appl.maths.V13 p1-14 1960)
The enormous usefulness of mathematics in the natural sciences is something bordering on the mysterious & ... there is no rational explanation for it. ...
Newton's law .. a monumental example of a law, ...simple to the mathematician, which has proved accurate beyond all reasonable expectation. ...
The miracle occurred only when matrix mechanics was applied to problems for which Heisenberg's calculating rules were meaningless. Heisenberg's rules presupposed that [they] could not be applied to cases [such as Helium (He)]. Nevertheless, the calculation of the lowest energy level of He [1960] agree with the experimental data within the accuracy of .. 1 part in 10 million.
Surely in this case we 'got something out' of the equations that we did not put in. ...
we do not know why our theories work so well.

Einstein, A. ('Out of my later years' (Thames & Hudson 1950))
We should take care not to make the intellect our god; it has, of course, powerful muscles, but no personality.

Kepler, J. ('Cosmic History')
Thanks be to Thee, O Lord our Creator, who hast granted me visions of beauty in Thy creation

Born, M. (Letter to Einstein 15/7/44)
I had a kind of breakdown last winter. It was the result of many causes: the most depressing idea was always feeling that our science, which is such a beautiful thing in itself & could be such a benefactor for human society, has been degraded to nothing but a means for destruction & death. We've really put our foot in it this time, poor fools that we are & I am truly sad for our beautiful physics!

Ecclesiastes 1:18
For with much wisdom comes much sorrow; the more the knowledge, the more the grief.

Ecclesiastes 3:11
[God] has made everything beautiful in its time.
He has also set eternity in the hearts of men; yet they cannot fathom what God has done from beginning to end.

ACKNOWLEDGEMENTS

I wish to express my thanks to my supervisor, Hoi Yeung, for his useful suggestions to improve the research and production of this thesis. Thanks to Gary Oddie for his encouragement and useful suggestions for improvement to the research. Thanks is also due to those who have helped me to carry out the experimental work notably Gary, Duncan Mcleod and Chris Evans. Thanks also to Gerry McNulty and Najim Beg of CALtec Ltd. for supplying me with gamma-ray densitometer signals from air-water flows. Thanks to Ruth and Sam and friends at DFEI for moral support.

ABSTRACT

The aim of the research presented in this thesis has been to develop an objective measurement technique to improve the detection of flow patterns in closed ducts. This activity is important for the safe and efficient running of many processes, particularly within the oil production, nuclear power, chemical and process industries. Signal analysis techniques based on nonlinear dynamic (chaos) theory have been applied to simulated and experimental transducer signals measuring properties of gas-liquid (air-water) flows in horizontal and vertical pipes. The techniques provide a method of measuring properties of the signals that are related to patterns within the signals. Signals from various non-invasive transducers (including differential pressure transducers, an electrical conductance transducer, a light attenuation transducer, an ultrasonic transducer and a gamma-ray densitometer) have been analysed. Signal analysis techniques include the use of singular value decomposition, the correlation integral and power spectra analysis.

The results of signal analysis on the simulated signals illustrate their potential for flow regime identification. When applied to experimental signals it is shown that changes in some of the signal characteristics correlate well with changes in the flow regimes. Discernment between horizontal stratified-wavy, plug and slug and vertical slug and bubbly flow regimes has been achieved. The most successful analysis technique (using singular value decomposition) is more robust than previously used techniques and can be computed much more efficiently.

CONTENTS

FIGURES

TABLES

NOTATION

Roman

A	pipe cross section area
A, V, E, L	simple statistical measures used in signal analysis
$\underline{a}$	vector average
$C_m(r)$	correlation integral
$c'(m',r)$	intermediate parameter for $C_m(r)$ computation
c	constant
D	pipe internal diameter
D_2	correlation dimension
D'_2	gradient of $\log(C_m(r))$-$\log(r)$ curve
$D(r)$	integer estimate of number of degrees of freedom
D_p	fractal dimension related to power spectra
D_s	number of significant singular values
D_δ	an average of $D(r)$'s
G_g, G_l	gas and liquid (respectively) mass flow rates
g	acceleration due to gravity
H	scaling component
$\underline{I}_k$	Eigenvector of covariance matrix
i, j, k, n	various indices used
idf, *sign*, *mf*,	intermediate parameters for $C_m(r)$ computation
i_{min}	parameter for D_δ calculation
jd	parameter for binary search for list construction for $C_m(r)$ computation
L_p	length of simulated plug or slug
m_e	embedding dimension (suitable)
m, m'	embedding dimension (not necessarily suitable)
N	number of measurements
$P(\omega)$	spectral power
p	index identifying a particular intermittent flow structure
p_i	simulated signal during passage of a plug
p(i), pp(i)	pointers used in $C_m(r)$ computation
Q_G, Q_L	Volumetric flow rates
r	size of hypercube
rmin, *mx'*	$C_m(r)$ computation time saving parameters
S_k	sum of first k singular values

s_i	simulated signal during passage of a slug
T_p	simulated delay between successive plugs or slugs
T_0	average simulated delay between successive plugs or slugs
U	matrix constructed from vectors $\underline{u}_i$
U_g, U_l, U_T	average superficial gas, liquid and total velocities (respectively)
$\underline{u}_i$	vectors with zero average
$\underline{v}_i$	vector constructed from time series
X, Y, Z	dynamic variables of the Lorenz system
x_i, $x(t)$	measurements taken at regular time intervals (a time series)
$\underline{x}_i$	vector constructed from time series

Greek

α	scaling factor
$\beta(\tau)$	measure for determining suitability of τ
$\delta_m(r)$	Savit and Green (1991) delta measures
$\delta\underline{x}_i$	separation vector
ϕ_k	random phase used in simulation of noise signal
φ, λ	dimensionless parameters in terms of ratios between densities, surface tensions and viscosities
Θ	Heaviside function
θ_i	angle between neighboring vectors
μ_{pi}	random variable used in simulation of intermittent structures
ν_i	noise signal used in simulations
σ_k	singular values of Ξ
σ, r, b	constant parameters of the Lorenz system
τ	delay time
ω	angular frequency
ω_0	highest frequency component of simulated noise signal
Ξ	covariance matrix
ξ	$\delta_m(r)$ noise threshold

CHAPTER 1

INTRODUCTION

Many industries use mixed flows of gas, liquid and/or solid in ducts, known as multiphase flows. Those in which multiphase flow is particularly important include the oil production, nuclear power generation, chemical and process industries. The behaviour of the components of the flow can play a crucial role on the efficient and safe working of a plant. In the nuclear power generation industry it is particularly important that heat transfer, which often involves multiphase flows, occurs safely. Accurate metering of multiphase flows is becoming increasingly important in the oil production industry as oil fields need to be exploited more efficiently. The interactions of the phases with each other and with the duct walls are very complex and difficult to predict from a given set of flow parameters such as phase flow rates and duct geometry.

Clearly it is advantageous to know the fluid flow behaviour occuring within a duct and research is still being carried out to investigate ways of detecting and predicting flow conditions and their interactions with the duct walls. The need for objective experimental data is still an important requirement which is the primary issue addressed by the research presented in this thesis.

Typical flow conditions can be catergorised into various flow 'patterns' or 'regimes'. The detection and prediction of these regimes is very important in many industrial processes. A particular regime may be either desirable (e.g. by improving the efficiency of a process) or undesirable (by having a hazardous effect on a plant). The author describes the development and testing of a method to improve the objectivity of identifying certain characteristic behaviours of multi-phase flow.

Since the late sixties there has been an increase in the understanding of the principles of chaotic, non-linear systems. These systems are governed by very simple processes but display surprisingly complex behaviour. They have measurable properties which has resulted in the development of novel measuring techniques that can be applied to signals that are related to the system.

These techniques have been applied to signals collected from non-invasive transducers sensing various properties of multiphase flows. The measured signal properties have then

been compared with the flow regime in order to determine if there is a correlation between the two.

A previously unused measuring technique investigated in this thesis has been successful in detecting changes in the signal properties which correspond with changes in the multiphase flow patterns. It is based on a standard technique known as singular value decomposition. The detection of such changes could accordingly be used for discriminating between different flow patterns. Additionally such measurements will provide objective data to assist in the development of more comprehensive models of multiphase flows, based on approximating appropriate flow parameters to dynamic variables governed by a finite number of non-linear equations, to enhance flow regime prediction.

§1.1 Justifications for multiphase flow research

Although multiphase flows are highly complex and their complete numerical modelling not yet practical there are components of their behaviour which are not beyond analysis and possible prediction. For example, Sæther, et al. (1990) have made measurements of a particular multiphase flow (known as slug flow and described in Chapter 2) which indicate that predictable properties do exist. These results would be useful for the development of a model of the flow properties.

Hewitt and Hall-Taylor (1970) rather tentatively commented that it could be considered fortunate that the distribution of fluid-fluid interfaces is such that it falls into a number of characteristic patterns which could hopefully be predicted from the independent variables of the system such as the flowrates of each phase and their physical properties. Twenty five years later Hewitt (1995) highlights the development of computer codes which are currently used in industrial applications where validation data is difficult to obtain. These codes appear to give realistic results and these tools have now become of enormous significance to industry. However it is emphasised that the models used for prediction are of limited generality. There is still need for more objective data related to many multiphase phenomena.

The characteristic phenomena of multiphase flows are called flow patterns or flow regimes. It was first suggested by Kosterin (1949) that flow regime maps might prove useful for estimating the flow regime in a conduit given certain flow parameters. Parameters that have been used include superficial phase velocities, mass flow rates and

various dimensionless numbers. Many maps have been compiled since the first one developed by Baker (1954) and it has become apparent that the boundaries between different flow regimes are very sensitive to many factors including conduit geometry and inclination. Figure 1.1 shows the original Baker map with the boundaries determined empirically by relatively simple relationships between the dimensionless parameters. Figure 1.2 shows a later map constructed by Taitel and Dukler (1976) using superficial phase velocities and determined by mechanistic arguments accounting for pipe geometry, inclination and fluid properties. The maps are related to gas-liquid flows in a horizontal pipe. Another flow map developed is shown in Figure 1.3. It was constructed by Spedding and Nguyen (1980) for vertical upward gas-liquid flows and uses different parameters related to flow conditions, as do many of the other maps. To illustrate the continuing development in the understanding of multiphase flows Spedding and Spence (1993) conducted a detailed survey comparing many of the commonly used maps and found serious discrepancies between them.

Some of these discrepancies have been known to exist for some time (Weisman, et al. (1979) and Vince and Lahey (1982) describe some examples). Partly in response to this situation there have been investigations of time varying flow parameters in an attempt to estimate flow patterns by more direct methods. Problems have also arisen in this area and are discussed in Chapter 2. A great many flow patterns have been defined in the relevant literature owing to the present subjective nature of flow regime identification. Different names have often been given to (essentially) the same pattern (a more detailed description of the main flow regimes is given later). A useful history of the developments in the understanding of multiphase flows can be found in Brill and Arirachakaran (1992). There is a need for an objective, generally applicable flow regime identification technique. The research presented by the author is an investigation of signal analysis techniques which measure properties that have not been identified using the more traditional statistical measurements or measurements associated with the power spectra.

As well as practical applications in industry there is much purely academic interest in the nature of multiphase flows. Pure scientific and mathematical research often tends to be carried out from aesthetic motives, the results of which later lead to the research of practical applications. The signal analysis techniques described in Chapter 4 and used by the author for analysis of multiphase flows provide a very apt example. The techniques are the results of investigations of naturally occuring patterns carried out in the 1960's and 1970's concerning clouds and coastlines (Mandelbrot (1968)). This led to investigations of mathematical systems with similar properties and which turned out to be

unexpectedly beautiful and complex. Figure 1.4 shows one of the most spectacular of these patterns, known as the Mandelbrot set, which is generated by an incredibly simple rule (the rule involves repeated squaring of a complex number and adding the result to the initial complex number).

Measurement and signal analysis techniques were developed (Mandelbrot (1968), Grassberger and Procaccia (1983)) which could be used to extract information from complex patterns which related directly to the complexity (or simplicity) of the rules generating the pattern. These techniques have been shown to be potentially useful in multiphase flow research. Complex flows, including turbulence, still pose many challenging problems.

The numerical modelling/simulation of multiphase flows is being improved and will have many useful applications as progress continues (Hewitt (1995)).

§1.2 Flow regime identification

There are many applications for flow regime identification. Some of the most important of which are in the chemical, process, oil production and nuclear power industries, particularly with regard to the safety and efficiency of various industrial plant. The importance of flow regime identification is apparent in many industrial fields including the following examples.

Hewitt (1982) pointed out that the vast majority of technical calculations on two-phase flow were made without any reference whatsoever to flow-pattern maps. Research subsequently demonstrated that more accurate results could be obtained by giving specific attention to specific flow patterns. Hewitt (1982) suggested that it would be likely that calculation methods based on flow-pattern delineation would ultimately supercede those that take no account of the nature of the flow and that the understanding of flow patterns would become increasingly important in the future. This indeed seems to be the case.

In the design and operation of two-phase flow systems, it is essential to know the two-phase flow pattern because hydro- and thermo-dynamic data such as pressure drop, void fraction and quality depend on flow pattern. It is therefore important to develop techniques to evaluate a flow pattern in an opaque pipe or duct (Matsui (1984)).

Continuous knowledge of flow patterns is essential in multiphase production not least in order to prevent hazardous events such as slug arrivals at processing plant for example. Flow patterns play a crucial role in the estimation of gas-oil contents in order to have a better knowledge of overall mass flow rates (Leducq and Hervieu (1991)).

Certain flow patterns can be damaging to equipment over long periods such as the apparent increase in corrosion rates of large oil lines during slug flows (Wood (1993)).

Within the nuclear power generation industry the successful analysis and design of light water reactors demands basic information on the boiling processes of two-phase flow. One of the most important aspects of this research field is the identification of two-phase flow patterns (King, et al. (1989)).

Pressure drop and stability characteristics of the three-phase oil/gas/water flows in sub-sea oil well lines are important factors in the proper operation of off-shore oil well platforms, and they depend intimately on the flow regimes that occur (Acikgoz, et al. (1992)).

A more specific example in which the knowledge of flow regimes is important is in an oil-well riser. An oil well riser separates gas and liquid components most efficiently during the bubble type flow regime. If churn or plug type flows develop an undesirable overload of the separation process may occur. This change in flow behaviour needs to be detected and responded to. The analysis techniques presented here could be applicable to the development of such a diagnostic system.

Another very important area in which knowledge of flow patterns is needed is the metering of flows. It is known that flow meters are sensitive to the changes in fluid dynamics caused by the addition of another phase. Delaye (1974), Baker (1970), Oddie (1992) and Kraft (1994), amongst others, give examples of the serious effects that multiphase flows have on the behaviour of various types of meters.

The increasing importance of accurate multiphase flow measurement for the oil production industry is emphasised by Ashkuri and Hill (1985). Multiphase flow meters will be increasingly needed for optimizing oil production over the life of an oil field and in saving costs in developing and building phase separation systems which are used at present for the measurement of the individual oil, gas and water flow rates.

The awareness of the need for multiphase flow metering is increasing as noted by Baker (1989). Baker indicates that an increasing number of industrial processes result in a flow which is not single phase and in which the second phase can no longer be disregarded. Also that the efficiency of processes could be improved if multiphase metering were possible without the need of a separation process. There has been a rather extreme attitude towards multiphase metering summed up by Hayward (1977) suggesting that engineers proposing to meter two-phase flow should not even start because of the complexity. With the increased availability of computing power for signal analysis and modelling which has occurred within the last decade there is less justification for this pessimism. Baker (1989) acknowledges that there is still a lack of experience and data with regard to metering multiphase flows and distinguishing between flow patterns.

The research presented in this thesis directly addresses this issue. It presents the improvement of signal analysis techniques for obtaining objective data related to multiphase flows which is needed for the improvement of industrial diagnostic systems and the development of non-linear models of variables associated with multiphase flows.

Some of the justifications and applications for the research of multiphase flow patterns presented in the thesis have been outlined.

§1.3 Scope of the thesis

Chapter 2 provides an overview of the research that has been carried out in the development of flow pattern analysis. Reviews by other authors describing the present state of affairs and the problems associated with present detection methods are highlighted. Research that has stimulated the line of approach and the use of the particular methods employed by the author is highlighted. Finally justification for this approach is given.

Chapter 3 describes the experimental apparatus including the methods of signal production and collection. The transducers that are used to detect properties related to multiphase flows and their interaction with the flow is described. The system has been set up to generate a variety of typical air-water flow patterns.

Chapter 4 outlines the approach adopted for flow pattern detection. The methods of signal analysis that have been used are described. The signal analysis techniques include those that are based on recent developments in the theory of nonlinear dynamic systems.

These developments are found to be useful in a great number of applications and have recently demonstrated potential usefulness in the field of multiphase flows. The authors original improvements to the methods for application to flow regime identification are described. The methods are applied to signals simulating transducer responses to various multiphase flows to illustrate how they can be used on experimental signals. Thus the potential of the methods for flow regime identification is demonstrated from a theoretical point of view.

Chapter 5 describes the experiments that have been carried out by the author. Transducer signals have been collected using the transducers described in Chapter 3 and the signal analysis techniques described in Chapter 4 have been applied. Results of the signal analysis are presented. The results of measurements from signals provided by CALtec (of the British Hydromechanics Research Group) are also presented. It has been found that some of the signal analysis techniques are successful in detecting changes in the transducer signal properties which correlate with changes in the flow patterns.

Chapter 6 draws conclusions from the results. Potential advantages of the techniques applied are described. Areas where further work is required are highlighted. This includes testing the signal analysis techniques on a greater variety of flow configurations.

CHAPTER 2

LITERATURE REVIEW

§2.1 Definitions of flow regimes

Before reviewing the work presented in the literature it is appropriate at this point to present a brief description of the typical flow regimes that are encountered in horizontal and vertical two-phase gas-liquid flows. It should be noted, however, that the precise definitions of certain flow regimes is problematical and this will be discussed further in Section 2.2. The descriptions that follow apply to flow patterns within pipes of circular cross section, though similar patterns often occur in ducts of other shapes. They are based on those suggested by Hewitt and Hall-Taylor (1970) and cover the most widely recognised patterns. There has been much debate on the nature and existence of many flow patterns which is made apparent by the large number of flow maps that have been produced since the Baker flow regime map (see Oddie (1992)).

In horizontal flow six typical flow regimes shown in Figure 2.1 are commonly classified as follows (very approximate mass flux in Kg hr^{-1} m^{-2} are given in brackets):-

i) **Stratified flow**. At low liquid and gas flow rates the liquid flows along the bottom of the pipe and the gas along the top. The liquid surface is flat. ($G_g<10^3$,$G_l<10^5$)

ii) **Stratified-wavy flow**. Waves are formed on the gas-liquid interface at higher gas flow rates due to the friction forces between the fast moving gas and slower moving liquid. ($G_g<10^4$,$G_l<10^5$)

iii) **Annular-dispersed flow**. This flow pattern occurs at high gas flow rates. The gas flows through the center of the pipe while the liquid flows as a film on the pipe wall. Often liquid droplets are entrained in the gas core and gas bubbles entrained in the liquid film. In horizontal annular flows the film along the bottom of the pipe is thicker than that at the top, due to the effect of gravity. ($G_g>10^4$,$G_l<10^6$)

iv) **Intermittent flows (plug/slug flows)**. These flows are characterised by the flow of large bubbles between slugs or plugs of liquid. Plug flow is characterised by bullet shaped bubbles flowing along the top of the pipe. Slug flow involves slugs of liquid with high entrainment of gas bubbles (a frothy mixture of gas and liquid) flowing between

long bullet shaped bubbles. The intermittent structures in semi-slug flow take the form of frothy waves which do not touch the top of the pipe. Franca and Lahey (1992) distinguish slug and plug flows by considering the phase which drives the flow. In slug flow the large bubbles become more unstable with wavy interfaces typical of gas driven flows. Jones and Zuber (1975) observe that slug flow can be considered as a combination of bubbly and annular flows. ($G_g<10^4$,$G_l<10^7$)

v) **Dispersed-bubble flow**. At higher liquid flow rates and low gas flow rates bubbles of gas are dispersed within a liquid continuum. At high flow rates the dispersion is reasonably uniform where as at lower flow rates the bubbles congregate near the top of the pipe. ($G_g<10^2$,$G_l\sim10^6$)

(vi) **Mist flow**. At very high gas flow rates and lower liquid flow rates the liquid becomes dispersed throughout the gas as small droplets. If there is no heat transfer from the pipe wall to droplets adhering to it then this regime tends to change to annular flow. ($G_g>10^6$,$G_l<10^2$)

In vertical flow there are six commonly described flow regimes. Typical phase configurations are shown in Figure 2.2. The Spedding and Nguyen (1980) vertical upward flow regime map can be referred to (Figure 1.2). Commonly used regimes are:-

i) **Bubbly flow**. There is a continuous liquid phase containing a dispersion of bubbles. Spedding and Nguyen (1980) found this regime very difficult to obtain. They have defined bubble type flow as an intermittent flow of gas bubbles and liquid that is more like the following description of Hewitt's plug flow.

ii) **Slug or plug flow**. At higher gas (or secondary fluid) flow rates bubbles congregate eventually forming large bullet shaped bubbles of similar size to the pipe diameter. In slug flow the liquid between the long bubbles contains a dispersion of bubbles (frothy in nature and similar to those of horizontal slug flow). It is not uncommon for the liquid film around the slugs to fall in the opposite direction to the total average fluid-fluid flow. Spedding and Nguyen (1980) describe the plug type flow as bubble type flow. As the gas flow rate is increased the length of the bubbles increases and the gas-liquid interface becomes more disturbed, eventually leading to slug type flow. As the gas region moves upwards liquid drains down the side of the pipe and disturbs the liquid below it causing a froth to develop.

iii) **Churn flow**. At higher flow rates the slug flow bubbles break down leading to a complicated movement of irregularly shaped bubbles. Oscillatory motion of the liquid occurs in tubes of sufficiently large internal diameters. This flow regime has been debated as being similar to slug flow and its existence has been questioned (see Hewitt and Jayanti (1993) and Mao and Dukler (1993) and references therein).

iv) **Annular flow**. This flow occurs at high gas flow rates. The gas flows through the center of the pipe while the liquid flows as a film on the pipe wall. The interfacial friction between the gas and the liquid provides upward force on the liquid. Often liquid droplets are entrained in the gas core and gas bubbles entrained in the liquid film.

v) **Wispy annular flow**. When the liquid flow rate is high enough the droplets entrained in the gas core of annular flow congregate forming large streaks (wisps) of liquid. Flows of this type have a high mass flux.

vi) **Mist flow**. This flow has the same flow structure as mist flow in horizontal ducts.

§2.2 Review of previous work

In the early days of multiphase flow research various classifications of the types of phase distributions were recognised (Kosterin (1949)). This resulted in the first of many flow regime maps (Baker (1954)). The map was an attempt to estimate the conditions necessary to produce some of the possible flow patterns in terms of phase flow rates and various fluid properties. Since then many more maps have been produced in attempts to improve the generality and accuracy of flow pattern prediction. By 1980 it was clear that a general flow map which could take into account phase flow rates, pipe geometry and inclination was not possible (Spedding and Nguyen (1980)). Problems concerning the actual definition and behaviour of various flow regimes also existed (and still does). Research has tended towards more detailed analysis of flow patterns using measurable properties of the flow such as pressure fluctuations at the pipe wall. Analysis of collected signals of these fluctuations using traditional statistical and frequency measurements had some success in identifying changes in flow behaviour. Improvements to analysing techniques are still taking place. These include the use of linear regression models (King, et al. (1989)), wavelet analysis (Leducq and Hervieu (1991)), neural networks (Beg and Toral (1993)) and fractal techniques (Sæther, et al. (1990)). These techniques are briefly described in the following sections including some of the advantages and disadvantages that have been found in their use. Improvements are still necessary to most of the

techniques currently used. This thesis describes improvements that can be made to the measurements of fractal properties of signals related to multiphase flows in an attempt to gain more objective information about the complexity of the signals and hence the processes that govern the behaviour of the flow patterns.

This section provides an overview of prominent researchers' work to high light common methods that have been employed in multiphase flow regime identification research.

Table 2.1 (on the following page) summarises a cross section of the research that has been done. Information includes the flow regimes covered, the ranges of superficial flow velocities (or flow/mixture rates), the measuring techniques used and the methods of analysing flow parameters and determining the flow regimes of air-water mixtures (except set d investigated by Leducq, et al. (1991) which was for a gas-oil mixture).

§2.2.1 Some explanatory notes for Table 2.1

The flow regime denoted by Sb consists of axially symmetric shaped bubbles occuring between plugs in vertical flow.

The probability distribution function (PDF) of a variable gives the probability of the variable having a particular value. It is estimated by calculating a histogram from the signal.

Characteristic functions (CHAFs) include functions such as the PDF, cross-correlation functions and power spectral densities.

The auto-regressive moving average (ARMA) model is a statistical model usually based on the assumption that each point of a time series is linearly dependent on a finite number of the previous points of the time series. Parameters used in the model can be used for characterisation. Beg and Toral (1993) also describe the use of such parameters by neural networks applied to flow regime identification (refer to Section 2.2.5).

Wavelet analysis is a recently developed method for efficiently detecting intermittent components of a given frequency (Grossman and Morlet (1984)). It has similarities to applying a windowed fourier transform to a signal. The signal is decomposed into a set of short lived pulses which are given a particular position and frequency (refer to Section 2.2.5).

Table 2.1 Experimental data from various authors

	Flow regimes covered	Method of identifying flow regime	Frequency range analysed / Hz	Superficial gas velocity / ms^{-1}	Superficial liquid velocity / ms^{-1}	Pipe I.D. / $10^{-2}m$	Pipe Orientation	Measurement technique
Nishikawa, et al. (1969)	B,S,C, A	CHAFs	0-15	0.03-8	0.01-3	2.6	Vertical	DPS
Jones, Zuber (1975)	B,S,A	PDFs	0-100	[a]0-37	[a]0-37	.5×6.4 rectangle	Vertical	X-ray attenuation
Wiesman, et al. (1979)	B,P,St, W,S,A	Signal amplitude ratios	-	[c]103-105	[c]105-107	1.2-5	Horizontal	DPS
Barnea, et al. (1980)	B,P,S, C,A,St, W	Signal trace analysis	-	0.1-30	0-3	2.5	Various	Electrical conductance probe
Vince, et al. (1982)	B,S,C, A	CHAFs	0-100	0.05-5	0.1-0.5	2.54	Vertical	X-ray attenuation
Lubbesmeyer, et al. (1983)	B,M, C,A	CHAFs	0.2-66	0.1-8	0.1-1.4	2.5	Vertical	Light attenuation
Matsui (1984)	B,Sb,S, C,A,M	PDFs	-	0.009-13	0-0.49	2.2	Vertical	DPS
King, et al. (1989)	Sb,B,S, C	ARMA model	0-100	0.05-3.3	0.07-0.31	2.5	Vertical	Neutron noise
Franca, et al. (1991)	P,S,W, A	Fractal techniques	0-70	0.2-17	0.3-6.8	1.9	Various	DPS
Leducq, et al. (1991)	B,S,C	Wavelet Analysis	0-48 0-48[d]	~0-7 [b]1-12.5	~0-5 [b]0.5-4	0.1-4 7.62	Vertical Vertical	vibration & DPS
Das and Pattanayak (1993)	B,S,C, A	PDFs	205	<12	2	1.1	Vertical	Electrical conductance probe
Beg,Toral (1993)	St,S,P	Neural Networks	-	0.2-8	0.05-2	406	Horizontal	γ-ray densitometer & DPS

Key

a - mixture flow rate
b - flow rates in litres s^{-1}
c - flow rates in Kg $hr^{-1}m^{-2}$
d - gas-oil mixture
I.D. - internal diameter
CHAF - characteristic function
PDF - probability distribution function
DPS - differential pressure signals
ARMA - auto-regressive moving average
P - Plug flow
A - Annular flow
M - Mist flow
W- Wavy flow
B - Bubble flow
St - Stratified flow
C - Churn flow
Sb - Spherical bubble flow
S - Slug flow

Signal trace analysis involves visual observation of signal traces.

Fractal techniques are those employed by the present author and are described in Chapter 4. They provide an objective measurement of the apparent complexity of a signal.

The various flow regimes that have been identified do not always agree between different authors (such as the difference between vertical upward bubbly and bubble flow described in Section 2.1). Examples of other discrepancies are detailed in Spedding and Spence (1993).

§2.2.2 Experimental techniques used

As can be seen from the table the analysis of differential pressure signals is a widely used technique. Pressure signals potentially contain useful information required about flow-regimes since pressure fluctuations from disturbances caused by multiphase structures are transmitted along and across the duct at the speed of sound in the fluids. It is relatively cheap to extract signals using this method and installation is also relatively simple. Flush mountings with the pipe wall are important to keep interference with the flow to a minimum.

The electrical conductance probe used by Barnea, et al. (1980) consisted of three needle like probes and a large flat electrode, and would be likely to be insufficiently robust in some industrial applications. The probe used by Das and Pattanayak (1993) was similarly fragile. The authors also mention that the presence of such probes in high liquid velocities can interfere with the flow and hence interfere with the behaviour of the other neighbouring probes. However, a variation of the apparatus using flush electrodes may be suitable for many applications where a significant difference in electrical conducting properties between the phases exists.

Capacitance sensors for water-oil flows have been used by Xie, et al. (1989), using an arrangement of eight electrodes that enable tomographic imaging of the phase distributions across the pipe section. The setup proves to be adequate in retrieving suitable information for the purposes of flow regime identification. A simpler version (without the use of tomographic imaging) using just one capacitor has been used by Midttveit, et al. (1992) for the purposes of void fraction measurements. It is important to note that the capacitance across a duct is substantially reduced when the water fraction exceeds 30-40% (typically). The variation in the subsequent signals produced is small.

This is due to the high conductance of the water. These authors illustrate the strengths of the capacitance sensor for use in the appropriate environment (particularly where low conductance fluids are used).

Photon attenuation proves to be suitably sensitive, however, the light attenuation sensor used by Lubbesmeyer and Leoni (1983) will only work for transparent or translucent fluids. The X-ray void measurement system of Jones and Zuber (1975) has certain drawbacks concerning extra safety precautions required and installation costs (partly because of these factors Lubbesmeyer and Leoni (1983) developed their light attenuation method).

Oddie (1992) has measured the intensity of an ultrasonic beam which is attenuated and diffracted at the phase boundaries in oil-water flows. It has proved to be suitably sensitive for detecting flow parameter changes in oil-water flows, however, at a liquid-gas boundary the transmitted ultrasonic waves experience very large attenuation (most of the energy of the wave is scattered away from the transducer) which makes detection and signal interpretation across a pipe diameter very difficult. The reflected waves can be detected from receivers placed on the same side of the pipe as the transmitter.

Some authors were aware of the need for future application of experimental techniques. Leducq and Hervieu (1991) took industrial environments into consideration and remarked that to be available on a production installation the measuring technique should be non-intrusive, using flush mounted or external sensors and the signal processing hardware to be reduced as much as possible (on microcomputer for example). Lubbesmeyer and Leoni (1983) noted the following criteria for suitable transducers:
-sensitivity for one of the fluid-inherent natural noise sources like temperature, conductivity, density or transparency.
-suitable response times to changes in the flow.
also recommended were:
-minimal flow restriction.
-mechanical and chemical stability at high pressures and temperatures.
-low cost.

§2.2.3 Analysing techniques used

A common method of determining flow regimes has been by visual analysis of the flows, often with the aid of high speed photography (Jones and Zuber (1974) and Vince and

Lahey (1982) include the pictures taken) . Though flow regime identification is important there is, as yet, no generally accepted method to carry this out with satisfactory objectivity. Indeed it has, in the past, been acknowledged that, because of the lack of absolute methods for the determination of flow pattern, data on the patterns should be treated with some reserve (Hewitt (1982)). A decade later Franca, et al. (1991) amongst others acknowledged that this still needs to be borne in mind.

Most methods that have been used to attempt flow regime identification have involved analysis of statistical properties of the signals from the flow. Typically characteristic functions (CHAFs) have been measured and their various patterns correlated with recognised flow regimes. Common CHAFs include the probability density function (PDF), auto-correlation function and power spectral density function (PSD). The PDF is usually estimated by producing a histogram of a signal (a count of the frequency of occurrences of a particular signal value). The auto-correlation function involves the comparison of the signal with a translation in time of itself. It is a function over a range of translations. The PSD is commonly estimated by squaring the components of a fast fourier transform of the signal.

Once a CHAF has been constructed it requires subsequent analysis. This has been done by comparisons between the visual shape of the CHAF and the visually determined flow pattern and also by objective methods which involved making measurements related to their shape such as moments around the mean value of a PDF or ratios of particular peak heights (Jones & Zuber (1974) and and Vince and Lahey (1982)).

§2.2.4 Theoretical techniques used

When flow patterns have been defined and observed under various flow conditions attempts have been made to give theoretical explanations for the behaviour. Many expressions have been formed which attempt to describe quantitatively the boundaries between different flow regimes in terms of parameters related to flow rates and fluid properties. The Baker map (1954) was the first empirically obtained result of this technique and many others have followed. Taitel and Dukler (1976) later used mechanistic arguments to derive various transition boundaries. Reviews have been carried out by Weisman, et al. (1979) and Spedding and Spence (1993) amongst others. A great variety of expressions have been produced and little consistency has so far been attained. Weisman, et al. (1979) and Spedding and Spence (1993) high light the difficulties.

§2.2.5 Problems encountered with analysing techniques

Using characteristic functions for flow regime identification has not been entirely successful. A typical problem that is encountered is described by Vince and Lahey (1982). They show that all moments associated with the PSD of X-ray attenuation signals exhibit a strong dependence on superficial liquid velocity. This characteristic is very undesirable for a flow regime indicator because any correlation would require prior knowledge of this variable. Since void fraction measurements are sufficiently difficult the additional requirement of a simultaneous liquid velocity measurement renders the use of PSD moments impractical. Moreover, they found that only the variance of the PSD has potential as a flow regime indicator. They conclude that the moments of the PSD are not considered to be as valuable as the moments of the PDF for flow regime identification.

King, et al. (1989) found that in certain cases different flow patterns have similar CHAFs making discrimination between CHAFs very difficult. They acknowledged that there was no well established method for two-phase flow pattern identification suitable for certain processes relevant to the nuclear power industry. In a detailed analysis of the relationship between CHAFs and flow regimes carried out by Lubbesmeyer and Leoni (1983) the similar conclusions were reached. For example, they found that the high-void bubbly and churn-turbulent flow-patterns had very similar CHAFs while in other cases, some CHAFs were very sensitive to different bubble sizes in bubbly-flows.

The comprehensive review of flow regime maps and analysis by Spedding and Spence (1993) concluded that existing regime maps and the theories for the prediction of phase boundary transitions did not satisfactorily predict observed flow pattern regimes, particularly when the geometrical parameters and physical properties of the phases were varied.

Other investigations include Hubbard and Dukler (1966), Jones and Zuber (1975), Weisman, et al. (1979), Barnea, et al. (1980), Nishikawa, et al. (1969), Akagawa, et al. (1971) and Tutu (1982). All have had difficulty in precisely determining flow regime boundaries. Spedding and Nguyen (1980) point out the need for care when using maps that are drawn with sharp line boundaries since the uncertainty of flow regime is greatest near such lines. Maps drawn by Weisman, et al. (1979) used bands to indicate smooth transitions. Franca, et al. (1991), summarize the state of affairs:-

'Despite the variety of methods adopted up to now, there is no accepted method to objectively distinguish between the flow regimes. Methods suitable for vertical flows cannot be used for horizontal flow since the phases show a different distribution. Moreover, the roll waves which are present in wavy and annular horizontal flows, give an output similar to those from intermittent flows. Clearly better objective flow regime indicators are needed.'

§2.2.6 Potential improvements investigated

Some of these authors have started to investigate a few methods that show promise in attaining a higher degree of objectivity. It is the aim of this thesis to improve the situation further by carrying out research required of methods that depend less on subjective determination of flow pattern.

The use of CHAFs coupled with developments in pattern recognition systems such as neural networks (implemented by Beg (1993)) and large data bases (implemented by Annunziato (1991)) have more recently been tested with reasonable success. CHAFs used by Annunziato (1991) include:-

(i) The ratio of the low density peak area to total area of the two peaked PDF arising from intermittent type flows.

(ii) The 'characteristic frequency' (the frequency corresponding to the maximum value of the PSD).

(iii) The perturbation velocity (the velocity of dominant structures in the flow e.g. bubble velocity in bubbly flow, slug velocity in slug flow, etc.). This parameter is calculated using cross correlation functions.

(iv) The 'characteristic length' between the dominant structures such as those described above.

Annunziato (1991) reports success rates of greater than 90% using a pattern recognition system and database.

The use of neural networks has recently been applied to multiphase flow analysis by Beg and Toral (1993). Various simple statistical measures and parameters associated with a linear prediction model (similar to those used by King, et al. (1989)) were estimated from pressure and gamma ray densitometer signals. Flow patterns covered were of the stratified and intermittent types. The neural network was then trained using the parameters to directly estimate flow rates. Flow rates of gas and liquid phases were sometimes estimated to accuracies of less than $\pm$10%. The use of trained neural networks

is very computationally efficient, however performance is critically dependent on the availability of a good quantity of well distributed training data (Beg, et al. (1993)). The actual training process for the neural networks can be very computationally expensive. There are difficulties in demonstrating that a trained network will continue to generate reliable outputs from input data which differs significantly from the data used to train the network.

Another promising technique is that provided by the wavelet transform (Grossman and Morlet (1984), Strang (1989), Mallat (1989)). The wavelet transform is a more powerful and efficient advancement of the windowed Fourier transform. Information about the frequency and location of structures within a signal can be extracted (more quickly than using a Fourier transform). A particular wavelet component provides information about the location of disturbances of a particular characteristic frequency. Initial studies applied to multiphase flows have been carried out by Leducq and Hervieu (1991). They conclude that two wavelet components seem sufficient to characterize the flow configuration, which could lead to simplified signal processing. However because the wavelet components only transform signal information (very efficiently) the results still require a further level of recognition and correlation with flow regimes using some appropriate method.

Franca, et al. (1991), used what they called fractal techniques. These are measuring techniques that have arisen out of the analysis of mathematically generated objects which have proved to be applicable to a vast field of physical phenomena. Differential pressure signals from a horizontal 19mm internal diameter pipe were obtained. PSDs and PDFs of the signals were calculated and two types of fractal measure were obtained (one of these is fully described in Chapter 4). The fractal measures they obtained showed potential for better discrimination between flow patterns than the PSDs or PDFs and they concluded that fractal techniques offer a promising way to objectively classify flow patterns. However, with reporting only four measurements, they acknowledge that more work is needed before truly objective techniques are available. This thesis is written largely in response to the recommendations and initial results presented by Franca, et al. (1991). Other fractal measures have been used which the present author has found to be more robust and more efficient to compute. These are described in detail in Chapter 4, together with background information to fractal measuring techniques.

§2.2.7 Fractal measuring techniques applied to multiphase flows

Fractal measuring techniques applied to data analysis have developed in the last two decades mostly because of the increased availability of computing power. They have been applied to a vast range of applications and are used throughout many of the sciences. They have been applied to single phase turbulence and found to be useful (Huang and Huang (1989)). Only in the last few years have they been applied to multiphase flows. The relevance of fractal measurement techniques to this field arises from the property of fractal measures being related to pattern (Mandelbrot (1977)). This property enables a pattern to be measured or classified in an objective manner. For example a line that has a very complicated and jagged appearance will have a higher fractal measure than a smoother and less complicated line. Measurements such as these have a great potential to be well suited to the discernment between different multiphase flow patterns using transducer signals from the flows.

The main motivation for this thesis has been stimulated by the application of the fractal techniques carried out by Franca, et al (1991), Oddie (1992), Sæther, et al. (1990), Fabre and Liné (1992) and Lusseyran (1990). These authors have indicated the potential of fractal measurements to distinguish between flow patterns. The research presented describes particular methods that are more robust than those used by the above investigators.

Oddie (1992) has measured a fractal property known as the correlation dimension (described in Chapter 4) for a vertical upward dispersed oil-water flow, showing a possible chaotic type behaviour which might be detectable by the use of fractal measuring techniques.

Sæther, et al. (1990) have carried out investigations on horizontal gas-liquid slug type flows. They measured a fractal property known as the Hurst dimension (Mandelbrot and Van Ness (1968)) of slug lengths. The results indicated that the slug lengths were governed by a non-random influence. Also the Hurst dimension showed some dependence on superficial gas velocity which could prove useful for multiphase metering. These results are further discussed by Bernicot, et al. (1993).

Lusseyran (1990) made one fractal measurement of a signal related to vertical upward slug flow. Fabre and Liné (1992) discuss the result and conclude that this indicates that such slug flow could be described by a model with a small number of degrees of freedom

(meaning that a few differential equations may describe the behaviour sufficiently. See Chapter 4).

They conclude that the behaviour of slug flow has properties that are measurable by fractal techniques and that such measurements could be useful in developing more accurate models of slug type flows.

Franca, et al (1991) have carried out measurements using the Hurst and correlation dimensions which suggest that measurements of fractal properties of signals show promise in objectively determining flow patterns.

The fractal techniques described in Chapter 4 and used by the previously mentioned authors provide measures that are related in an objective and quantitative way to pattern and complexity (Mandelbrot (1977)). It is therefore well worth applying the use of such measures to flow regime identification. Because of the sensitivity of these techniques to various signal properties and variables used in the signal analysis some arbitrarily chosen factors are introduced. These factors are maintained as constants throughout the analysis carried out by the author to minimise their influence on the discernment between flow regimes.

Measurements of fractal properties, though less computationally efficient and more difficult to apply do not require the training of neural networks. Suitably objective measurements of signal properties related to the flow patterns may provide information fundamentally useful for the development of models of some aspects of multiphase flow behaviour as well as providing a tool for distinguishing and classifying different types of flow.

§2.3 Summary

This chapter has highlighted the current difficulties in classifying and identifying flow patterns. Research by investigators using more recently developed techniques such as fractal analysis and neural networks has been discussed. The potential of the fractal analysing techniques have been shown to have a potential for improving the determination and classification of flow patterns, particularly because an objective measurement of signal properties can be made. However only a few results were published by the initial investigators of the technique for flow regime identification (Franca, et al. (1991)), namely measurements from four time series from different flow

situations. This may have been because of the large amount of computing time that is required by the particular techniques used. The sensitivity and robustness of the methods was not discussed. It can be concluded that improvements to the methods are required.

The present author has carried out further testing and development of some of the techniques that have indicated potential in improving flow regime identification. Improvements to the analysing techniques has been done with regard to improving the robustness of the techniques to the effects signal noise and simplifying computational complexity. A well established signal analysis technique known as singular value decomposition that has not (to the author's knowledge) been applied to flow regime identification has been investigated and provided results that indicate this method to be more effective and robust than those employed by the previous authors.

§2.4 Justifications and objectives

Research has been discussed which suggests that fractal measuring techniques have the potential of providing objective data related to multiphase flows. This is because the measuring techniques provide a method of analysing and classifying patterns. It has been acknowledged that there is a growing need for more such information for the classification, understanding and modelling of multiphase flows and that the use of fractal techniques has not yet been fully investigated.

The objectives of the research presented in this thesis have been the following.

- To develop a method of measuring fractal properties of transducer signals related to multiphase flows that is :

(i) suitably sensitive to changes in flow pattern,
(ii) less sensitive to different signals from the same flow patterns and
(iii) more efficient to compute than those previously used.

- To extend the testing of such a method on relevant signals (including simulated signals).

The methodology and results of the research are presented in the following chapters.

CHAPTER 3

EXPERIMENTAL SETUP AND PROCEDURES

§3.1 Introduction

Multiphase flows were produced in an air-water flow loop. Flow patterns (regimes) included horizontal slug, plug and dispersed bubble flows and vertical bubble and slug flows. A variety of non-invasive transducers were used to provide signals which were collected by digital computer and subsequently analysed. Details of the flow loop, flow production and the transducers are presented.

§3.2 Flow rig

Figure 3.1 shows the layout of the main components of the rig. The experimental rig for producing water-air flows consisted of a loop of 50mm ID plastic and perspex pipe sections. Two straight 2.4m sections of perspex pipe held the various transducers. One section of 50mm ID was orientated vertically and horizontally. The other section of 25mm ID was orientated vertically.

The water was circulated via a tank of approximately $3m^3$ capacity using a pump that produced a maximum head of $3.5\times10^5 Nm^{-2}$. Flow rates between $1\times10^{-4}m^3s^{-1}$ and $15\times10^{-3}m^3s^{-1}$ were used to obtain the various flow patterns. Air was supplied from a $7\times10^5 Nm^{-2}$ air line at flow rates between $5\times10^{-6}m^3s^{-1}$ and $2\times10^{-3}m^3s^{-1}$ (when at S.T.P. using the pressure regulators). The details of the arrangements for entraining the air into the water are shown in Figure 3.1.

Various flow patterns were produced using the full range of measurable air and water flow rates. Slug, plug and bubble flows were directly visually determined from the structures observed through the perspex pipe sections. The temperature of the water varied between 18°C and 24°C. This variation did not affect the result of visual estimation of a particular flow regime.

§3.2.1 Flow meters

Two turbine meters provided measurements of the various water flow rates that were used. The meters were manufactured by Fisher Controls Ltd. (U.K.). Model numbers were 7185-4015-A (this smaller range meter was connected via a 25mm by-pass line) and 7102-0008-A. Refer to Figure 3.3 for the calibration curves.

Pelton wheel meters were used to measure small air flows which were necessary to produce vertical bubble flows. The meters were manufactured by Quadrina Ltd. (U.K.). Model numbers were PWG7 (7 l/min max. flow) and PWG2/EP1 (2 l/min max. flow). Refer to Figure 3.2 for the calibration curves.

A turbine meter for the larger air flows was used (A Quadrina meter, model number QEG13B. Refer to Figure 3.3 for the calibration curve).

The necessary air meters (in parallel with each other) were used in series with pressure regulators to enable a greater range of flow rates at different pressures to be obtained (refer to Figure 3.1).

§3.3 Data collection

Various types of transducers were selected to collect information related to the flow phenomena in the pipe. During experiments the data collection was started when flow meter readings had stabilised. Visual estimation of a flow pattern was made by identifying the characteristic structures of a particular flow pattern as described in Section 2.1.

An IBM PC (with a processor clock speed 25MHz) was used with an analogue to digital converter (ADC) to record the signals. The ADC was manufactured by Pico Technology Ltd. (U.K.). Maximum sampling frequencies of the order of 5KHz for 1 channel were obtainable. Up to four channels were recorded simultaneously. About 300,000 data points could be collected without interruption.

§3.4 Transducers

A wide variety of sensors have been used in the literature for flow pattern analysis. These included pressure transducers, photon attenuation meters (using γ-rays, X-rays and

visible light) and electrical properties (eg. conductance and capacitance). They all are sensitive to parameter changes that are affected by the instantaneous distribution and/or momentum of the fluids in the pipe and have therefore been used for flow regime research.

Transducers are required which respond suitably quickly to the passage of the various bubbles and droplets that are encountered in the multiphase flow across a pipe cross section. The movement of such structures past some transducers may be faster than the response time of the transducers or not close enough to them to be detected. A device such as a thermocouple is unlikely to detect much of the useful information that is provided by small bubble or droplet movement that occurs away from its immediate vicinity. Its fragility, particularly, makes it an impractical sensor for multiphase flows.

Transducers that are able to respond quickly enough include those that measure electrical properties of the fluids and densitometers which relate to the local 'instantaneous' void fraction.

Pressure transducers are also suitable due to the relatively high speed of sound compared to flow velocities and their sensitivity to effects that occur across the whole pipe section in the vicinity of the transducer. They have been used extensively in this field. They are cost effective and usually pose relatively few implementation problems which are also important criteria to consider.

Non-invasive transducers are recommended, since flow patterns are directly influenced by the geometry of the flow duct. Turbine meters and vortex meters will interact with bubble formations and are very likely to cause disturbances that change the fluid-fluid interfaces. Such devices are therefore unsuitable for flow regime indicators.

The requirement of high durability sensors in multi-phase environments makes the use of turbine meters and hot wire anemometry impractical.

Due to their suitable sensitivity, robustness and cost effectiveness the sensors that were used were pressure transducers, a light attenuation sensor, an electrical conductance sensor and an ultrasonic transmitter and receiver system. Their arrangement on the perspex pipe sections is shown in Figure 3.4. Details of the pressure tappings are included.

§3.5 Transducers and their interaction with air-water flows

i) Pressure transducers.

Pressure transducer tappings were arranged diametrically opposite and axially along the perspex test sections. The differential pressure ranges measured were up to $3.5\times10^{4}Nm^{-2}$ (the larger range) and $1.25\times10^{3}Nm^{-2}$ (the smaller range). The larger range differential pressure transducer was also used as an absolute pressure transducer (having one side at atmospheric pressure). The transducers were acquired from RS Components Ltd. (U.K.). Response times for both were less than $10^{-3}s$. The signals produced were amplified to a range of 0-2.5V. The connecting tubes between the differential pressure transducers and pipe wall introduced problems that affected the signals due to bubbles entering the tubes. Absolute pressure measurements were subsequently taken having the transducer mounted flush with the inner pipe wall. Typical differential and absolute pressure transducer signals are shown in Figures 3.5 and 3.6. The vertical flows described as bubble flows in the subsequent Figures use the Spedding and Nguyen (1980) description given in Section 2.1.

The pressure transducers produced large signal fluctuations when slugs passed the tappings. These intermittent fluctuations were dominant features of the signals. In the horizontal plug flows and vertical bubble flows the signals were dominated by more continuous higher frequency components. This occurred due to the transmission of vibrations from the pump via the liquid phase which was in contact with the transducer. A small set of signals from dispersed bubble flows were collected using the absolute pressure transducer. These signals were characterised by noisy high frequency components in a similar fashion to those of the plug and bubble flows.

Vibration produced by the pump was transmitted through the pipe walls and the water which affected the pressure transducer signals. It would be reasonable to expect large amounts of such vibration in many industrial applications.

Difficulties were found in discerning flow regimes using the differential pressure signals. This was caused by the increased noise sensitivity of the devices due to the flexibility of the pipes between the transducers and the tappings. The absolute pressure transducer was not susceptible to such problems. Its signals were also sampled at a higher sampling frequency than the differential pressure signals. Initially it was hoped that the signal analysis techniques would enable discernment using the noisey differential pressure

transducer signals, but there were insufficient differences in signal quality from the different flows regimes.

ii) Light attenuation sensor.

The light sensor consisted of a laser and a photodiode similar to that used by Lubbesmeyer and Leoni (1983). A low power laser beam (15mW HeNe with wavelength 632.8nm) was directed through the perspex test section via an opaque 15mm tube and onto a semiconductor photodiode (also via an opaque tube). The beam passed along a diameter of the perspex test section. Figure 3.7 shows the arrangement of the sensor and the typical behaviour of a light beam during the passage of a bubble through the pipe. The beam went through many reflections and refractions which often resulted in very little light reaching the diode for short periods of time. The signal produced by the photodiode was in the range 0-0.5 V.

Typical signals produced by the photodiode are shown in Figure 3.8. Bubbles as small as the diameter of the laser beam (1mm approx.) dramatically affected the amount of light reaching the diode as the beam was reflected and refracted from the air-water boundary. When many bubbles in complex arrangement passed through the pipe it was common for the amount of light reaching the diode to be substantially reduced. This often occurred when a frothy slug passed through the pipe (shown particularly clearly in the slug signal from the 25mm pipe). In the example of the slug flow signal from the 50mm pipe most of the light was impeded and scattered by froth in the annular flow as well as in the slugs.

Occasionally light was focused towards the photodiode by a suitable configuration of air/water boundaries. This is shown clearly by the increased signal detected during vertical bubble flow in the 25mm diameter pipe (labelled B in Figure 3.8).

During the passage of clear water in the horizontal plug and vertical bubble flows a steady, high signal level was produced.

iii) Electrical conductance sensor.

The electrical conductance sensor consisted of eight brass electrodes situated around the inside of the pipe and connected as shown in Figure 3.9. The arrangement was such that variations occuring in the water distribution across the whole cross section of the pipe were detected. The resistors R1, R2 and R3 were set to give a potential difference in the

range 0-2.5 V (resistances are of the order of 10 kΩ). Figure 3.10 shows typical signals collected by the electrical conductance transducer.

Wet structures such as plugs and slugs (P and S) that passed the sensor increased the conductivity around the pipe wall, thus producing an increase in signal strength. When large bubbles passed through the sensor the signal voltage decreased at rates dependent on the rate at which water drained from the sides of the pipe and on the depth and length of the bubble(s).

Difficulties were found in discriminating between some of the signals produced by plug and slug type flows where the difference was dependent on the intermittent structure being either a homogeneous liquid (plug) or a frothy mixture of air and water (slug). The froth containing many small bubbles tended to have similar conductance properties to that of clear water especially near the pipe surface where the electrodes were placed. Surface tension tended to keep the electrodes and pipe wall between them wet whether a slug or plug had passed them.

iv) Ultrasonic reflection sensor.

The ultrasonic sensor consisted of a piezoelectric transmitter and receiver placed on one side of the pipe (see Figure 3.11). The transducers were silver coated piezo-electric ceramic discs (diameter 10mm) that resonate at 2MHz. They were arranged inclined towards each other to maximise the sensitivity of the system. The transmitter was driven by a constant frequency (at 2MHz) with an amplitude of 10V. The receiving transducer detected reflections of the transmitted ultrasonic wave that occurred at phase boundaries. A 2MHz signal with an amplitude dependent on the intensity of reflected waves was produced. Reflections occurred at perspex-water, water-air and perspex-air boundaries. The amplitude of the reflected wave received by the transducer changed as the configuration of air and water changed near the transducers. It was very sensitive to the angle, area and position of the boundaries present in the region where the transmitter and receiver interacted. The signal generated by the receiver was amplitude modulated (producing signals up to 2KHz) and amplified to a range of about 0-2V. Figure 3.12 shows typical ultrasonic transducer signals collected. Only signals from vertical flows were collected.

Bubbles that passed through the pipe near the transducers tended to increase the amount of energy reflected producing a larger amplitude wave at the receiver. This was

particularly clear from the signals produced by a bubble type flow. As the edge of a bubble (B in the Figure) passed the transducer a strong reflection was detected. Smaller peaks in the signal are produced by the occasional small trailing bubbles. During slug flow many reflections were almost continuously detected due to the air-water boundary being close to the pipe wall. In a typical slug, S, and in the annular type film following it there were many small bubbles of air that passed the transducer which produced reflections of the incident wave (due to their close proximity to the pipe wall). These reflections were apparent by the many small peaks that were present throughout the signal.

§3.6 Gamma-ray densitometer signals

A set of signals from a gamma-ray densitometer was kindly provided by CALtec Ltd., part of the British Hydrodynamics Research Group Ltd. Signals were from horizontal stratified wavy and intermittent air-water flows in a 406mm diameter, 400m long pipe. The signals are shown in Figure 3.13. During the passage of an intermittent plug or slug structure the signal increases quickly and then tails off as the water level decreases and water drains from the pipe wall. During the wavy flows the occasional small peaks appear in the signals as the result of single large waves passing, but generally a very complicated, noisy signal is produced.

§3.7 Conditions investigated

Table 3.1 shows the flow conditions investigated using the experimental flow rig and those investigated by CALtec Ltd. The author's experiments were carried out over a period of about 2 years. The absolute pressure transducer signals were taken after considering the need to improve on the poor results obtained from the differential pressure transducers. These are all documented in Chapter 5.

Figure 3.14 shows the superficial velocities of the air and water plotted on a Taitel and Dukler (1976) flow map for horizontal flow. The visually estimated slug and plug flow patterns agreed with the Mandhane, et al. (1974) transition band. The points labelled with a * indicate dispersed bubble flows that did not agree with the corresponding Taitel and Dukler (1976) boundary.

Figure 3.15 shows the superficial velocities of the air and water obtained in the vertical 25mm and 50mm pipes. Figure 3.16 shows the transformed points on the Spedding and

Nguyen (1980) flow map, where U_T is the total average superficial velocity of both phases, D the pipe diameter, g the acceleration due to gravity and Q_G and Q_L the volumetric flow rates of air and water, respectively. The point labelled with a * indicates a bubble type flow that did not agree with the map boundary.

Table 3.1 Conditions investigated

No. flow conditions covered	Pipe arrangement	Flow patterns covered	Transducers used	Sampling frequency (KHz)
53	Horizontal (50mm)	slug, plug	P_L, P_s, El, Lt	0.8
52	Vertical (50mm)	slug, bubble	P_L, El, Lt	0.97
29	Vertical (25mm)	slug, bubble	P_L, Us, Lt	1.6
8	Horizontal (50mm)	slug, plug dispersed bubble	P_a	4
8	Vertical (50mm)	slug, bubble	P_a	4
6	Vertical (25mm)	slug, bubble	P_a	4
11	Horizontal (406mm)	slug, stratified-wavy	γ	0.02

P_L-Large range differential pressure transducer
P_s-Smaller range D.P.
P_A-Absolute pressure transducer
El-Electrical conductance transducer
Lt-Light attenuation transducer
Us-Ultrasonic transducer
γ - gamma-ray densitometer

CHAPTER 4

SIGNAL ANALYSIS TECHNIQUES

The signal analysis techniques which have been used are based on the theory of non-linear dynamics or chaos theory. This is the study of systems which display complex behaviour but which are governed by comparatively simple rules. These systems and the measuring techniques developed are described. Their application to typical signals related to multiphase flows is then illustrated.

§4.1 A brief summary of chaotic systems

Before discussing the application of chaos theory to signal analysis a brief summary of definitions and properties displayed by chaotic systems is given. The discovery of these systems has enabled the measurement of properties which are potentially very well suited for detecting changes in flow patterns.

A deterministic system is such that its behaviour can be fully described by a finite number of state variables which are governed by the same number of differential equations or mappings. In principle the state of a deterministic system can be calculated at any instant (given the initial conditions) using the governing equations. Since the sixties it has become known that many of these deterministic systems display dynamics that are non-repeating in behaviour, having an apparently random quality. Such aperiodic behaviour is called chaotic behaviour (the variables never repeat exactly any previous pattern of behaviour). At first sight it seems surprising that such systems (with no external random influences) could behave in such a way, but it has become apparent that most deterministic systems when forced at certain rates do (even very simple ones such as the forced pendulum).

Chaotic behaviour is different from purely random or stochastic behaviour in that it is, in principle, predictable since the governing system is deterministic. In practice finite accuracy (incomplete knowledge) of a systems present state severely limits the success of prediction to finite times. This is due to the system being extremely sensitive to initial conditions. With the discovery of chaotic behaviour there has been the definition of measures which quantify how predictable these types of systems are (measures of chaos). These measures have been very useful in classifying different types of chaotic behaviour. Two classic examples of such systems are the logistic map (Holden (1986)) and the Lorenz equations (Lorenz (1963)).

The logistic map produces a series of numbers, x_i, each of which is calculated from the preceding number, x_{i-1}, according to :-

$$x_i = 4\, x_{i-1}(1-x_{i-1}) \qquad 0<x_0<0.5\ ;\ 0.5<x_0<1 \qquad (4.1)$$

It has been used to model fluctuations in predator-prey populations. Figure 4.1 shows the erratic behaviour of the numbers that can arise. Typical measures of chaos associated with the logistic map have values between 0 and 1 because each number is only dependent on the one immediately preceding number (described as having 1 degree of freedom). These measures are known as fractal dimensions.

The Lorenz equations describe the behaviour of 3 variables that are dependent on each other in the following way:

$$\frac{dX}{dt} = \sigma(Y - X), \qquad (4.2a)$$

$$\frac{dY}{dt} = rX - Y - XZ, \qquad (4.2b)$$

$$\frac{dZ}{dt} = -bZ + XY. \qquad (4.2c)$$

The system models the convection of a steadily heated fluid. Figures 4.2-4.4 show typical chaotic behaviour of the variables (the following parameter values were used: σ=10, b=8/3, r=28 with initial conditions: X=20.4, Y=24, Z=20). It is important to appreciate the complexity of the behaviour of the system variables given the simplicity of the governing system. From the Figures it can be noted that there is an apparent qualitative difference between the behaviour of Z and X or Y. These differences are not detected by analysis based on chaos theory since the underlying system which generates each signal is the same. Fractal dimensions (measures of chaos) associated with this system have values between 2 and 3 since the system behaviour is dependent on three variables (described as having 3 degrees of freedom). The higher fractal dimensions associated with the Lorenz equations indicate that it is a more complex system than that governed by the logistic map. This distinction between the level of complexity of the systems gives these measures their potential for distinguishing between signals associated with different multiphase flows.

A powerful aspect of chaos theory is that information regarding the whole system can be obtained from sufficiently large amounts of measurements of a single dynamic system variable (e.g. measurements of any one of the variables, X, Y or Z, of the Lorenz system). It is this aspect that provides the practical application of analysis methods based on chaos theory to the analysis of signals measuring multiphase flow phenomena.

§4.2 The application of chaos theory to flow regime identification

It is suspected that the dynamic variables describing multiphase flow of fluids in a pipe may exhibit chaotic behaviour or at least may be modelled by a chaotic system which has a minor random influence incorporated within it. Certainly there are apparently random fluctuations in the behaviour of many of the parameters associated with multiphase flow and the complexity of such behaviour is observed to have different qualities for different flow regimes (Sæther, et al. (1990) have investigated the apparent chaotic behaviour of slug lengths and frequencies). It is this property of the flows which may enable the measures of chaos associated with different flow regimes to be used to distinguish between them. The use of these measures depends on :-

i) whether the behaviour of relevant, measurable parameters is chaotic (or at least if the behaviour can be adequately modelled by a chaotic system)

ii) whether the measures of chaos for each flow regime are measurable and distinguishable.

Initial tests of this method have been carried out already, most notably by Franca, et al. (1991), and they show some promising results (see Section 4.6). The present author has not reproduced them and has adopted signal analysis techniques that are more practical to implement and robust than those used by Franca, et al. (1991) and others.

It is worth noting that the measures of chaos obtained from complex, noisy experimental signals will not necessarily give accurate estimates of the properties of a fundamental model of the system. With regard to a multiphase flow system (a fluidised bed) this has been indicated by Tam and Devine (1992). However, when using the methods for comparing properties of different signals the measures can perform a very useful role since the measures, though possibly inaccurate for predicting a model, still detect changes in the complexity of signal behaviour.

An outline of the theory of obtaining measures of chaos from dynamic systems is presented below.

§4.3 Measures of chaos from dynamic systems

The behaviour of a deterministic dynamic system is fully described by all the independent state variables or parameters of the system. The number of these variables is called the embedding dimension, m_e, and it is equal to the number of degrees of freedom that the system has. A set of vectors which have components made up of these variables can be plotted in an m_e dimensional space (called a phase space) and their evolution through time can be observed. Chaotic systems behave in such a way that the object drawn in the m_e dimensional phase space has an infinitely detailed structure and is known as a strange attractor. Figure 4.5 shows examples of two strange attractors (the double looped attractor is from the Lorenz system. The other attractor is known as the Rössler attractor (Rössler (1976))). These are unlike periodic systems in which the variables tend to an attractor which is a closed loop or a point (once initial fluctuations known as transients have dissipated). Transients in the Lorenz system can be seen in the behaviour of the variables X, Y and Z where $0<t<3$ in Figures 4.2-4.3. Once the transients have dissipated the variables describe the double looped Lorenz attractor shown in Figure 4.5. Also shown in Figure 4.5 are examples of non-chaotic attractors generated by periodic systems such as simple unforced pendulums.

The infinitely fine structure of a strange attractor is due to the aperiodic behaviour of the state variables, i.e. the attractor is made up of an infinite number of orbits, which, though they may be close to each other, *never* actually touch each other (i.e. the system never returns exactly to a previously obtained state). A consequence of this is that the attractor has a non-integer dimension that lies between m_e and m_e-1. This dimension, known as a fractal dimension, and the embedding dimension give measures of the complexity of the system. If the dimension has a non-integer (fractal) value then the system exhibits chaotic behaviour.

Another property of the strange attractor is that orbits within it that initially are close together will tend to diverge away from each other at an exponential rate as the system evolves in time. This is an inherent property of chaotic systems which makes itself apparent by the extreme sensitivity of the system to initial conditions. Measuring the exponential rate at which such orbits diverge gives a measure of the amount of chaotic

behaviour the system displays. These measures are known as Lyapunov exponents (Wolf, et al. (1985)).

§4.4 Fractal dimensions

The fractal dimension of an object describes how much the object fills space. A square requires a two dimensional space in which to draw it, and its surface area and perimeter are finite in value. However a fractal dimension object, such as the Lorenz attractor, is drawn using a one dimensional line that tends to erratically fill the three dimensional space in which it is drawn (because no part of the line ever overlaps exactly another part of itself). The line has an infinite length and yet is contained in a finite volume. These are the distinguishing properties of strange attractors. The term fractal refers to the non-integer dimension values that most strange attractors have. There are various methods for calculating the fractal dimensions of strange attractors. Some of these dimensions are easier to estimate than others (particularly with regards to factors such as computation time). Most of the methods involve the reconstruction of the attractor which is assumed to exist for the system. To extract the information about the attractor of a dynamic system a time series of measurements of one of the relevant parameters needs to be collected. The attractor can be reconstructed from this time series using the method of delays developed by Takens (1982).

Given a series of measurements of a suitable variable taken at regular time intervals, $x_i = x(t+i\tau)$ (where $i = 1, \ldots, N$), a series of vectors $\underline{x}_i$ can be constructed as follows :-

$$\underline{x}_j = (x_j, x_{j+1}, \ldots, x_{j+m-1}) \qquad (4.3)$$

where $j = 1, \ldots, N-m+1$,
m is known as an embedding dimension (though not necessarily suitable)
and τ is known as the sampling or delay time.

When these vectors are plotted in the m dimensional phase space they follow a trajectory (a line in the phase space) which forms an attractor that has the same topological properties (such as dimension) as the original attractor constructed from all the independent variables describing the system dynamics (see Figure 4.6). This produces a mapping (denoted by Φ in the Figure) of the original attractor onto a reconstructed attractor which can be analysed and has proved to be an elegant and very useful method in the analysis of non-linear systems. The process of constructing an attractor in the phase space is known as embedding the attractor.

The two parameters τ and m play a crucial role in the reliable and accurate estimation of measures associated with the attractor. Estimates are sensitive to the values of τ and m. This applies particularly in the case of experimental signals which tend to be noisy, are of finite resolution and are limited in length. Such problems are highlighted by Broomhead and King (1986), Fraedrich and Wang (1993), Buzug and Pfister (1992[a & b]), Ding, et al. (1993), Lawkins, et al. (1993) and Abarbanel and Kennel (1993). They describe methods of estimating suitable values of τ and m by observing the behaviour of attractors embedded in the spaces using a range of values of τ and m. Tam and Devine (1992), who have applied chaos measures to fluidised-bed pressure fluctuations, emphasise the need for careful utilisation of these measuring techniques to avoid drawing spurious conclusions about the governing models (i.e. the measures may not be accurate estimates of the governing system's dimension).

The value of m is restricted for practical reasons to a maximum of about 10. This is because as m gets larger the number of points required to describe the attractor sufficiently increases exponentially. All dimension estimates require a suitable density of points throughout the phase space to give reasonable estimations of averages of various parameters that are needed. Reliable measurement of high dimensional chaos (eg. dimensions of the order 10 and above) cannot practically be made at the moment by methods such as these which estimate various statistical properties associated with a reconstructed attractor (data sets with more than the order of 10^5-10^6 points often result in impractical computer analysis time, if not sampling time and space). Tam and Devine (1992) suggest that fluidised bed behaviour is likely to be of a high dimensional nature (rendering inaccurate model prediction) but are still able to use these measurement techniques to obtain limited but useful information about changes in behaviour. A similar philosophy has been adopted by the author applying these methods to multiphase flow pattern identification since unreliable dimension estimates were obtained for the purpose of accurate model construction.

§4.5 Effects of the delay time, τ

The delay time, τ, is especially important for accurate model construction and there are numerous methods of estimating a suitable value (Broomhead and King (1986), Buzug and Pfister (1992[a & b]), Stelter and Pfingsten (1991)). However most of these methods are at least as computationally intensive as the estimation of the chaos measures themselves. This is because they involve a detailed analysis of the structure of the

reconstructed attractor or they require the analysis of the behaviour of the dimension estimate itself as τ is varied. Some of the methods do not clearly determine a suitable value for τ particularly from noisy experimental data sets.

For flow regime identification which requires detecting an appropriate change in signal properties the sampling time was used as the delay time. When the sampling time proved to be inadequate (i.e. no change in signal properties were detected with flow regime change) an attempt to provide a suitable delay time using a robust and fast method of delay time estimation method developed by the author was used. The method adds little extra computation time to the signals analysis by measuring the angle, θ_i, between successive tangent vector approximations on the attractor for a given delay time. The method described has not been used before, to the author's knowledge. Its implementation is described in Section 4.9.1.

For an attractor that has been reconstructed using a delay time, τ, that is too small most angles between successive tangent vectors will tend to have a value of $\theta_i \approx 0$. This is because the attractor lies very closely along the direction vector (1, 1, ... ,1) as the components of the vector describing the attractor point are all too similar. A few values of θ_i will tend to be $|\theta_i| \approx \pi$, when the trajectory changes to the opposite direction of the unit vector. Figure 4.7 shows the appearance of such a reconstructed Lorenz attractor.

If too large a value of τ has been chosen then typically $\pi/2<|\theta_i|<\pi$ as most successive points on the attractor jump from one side to another without clearly following a smooth trajectory around the attractor (see the reconstructed Lorenz attractor in Figure 4.8).

For a suitable value of τ then typically $0<|\theta_i|<\pi/2$ as successive attractor points flow along a smooth trajectory which bends around the attractor (see the reconstructed Lorenz attractor in Figure 4.9).

§4.6 The correlation dimension

A commonly measured dimension from experimental data is that known as the correlation dimension, D_2, due to the large amount of useful information that can be extracted about the attractor from its computation. There are problems with the application of this method to experimental signals, however, which will be discussed later.

Once the attractor has been reconstructed an estimate of the correlation dimension is obtained using the following definition (Grassberger and Procacia (1983)):-

Given the correlation integral

$$C_m(r) = \frac{2}{N(N-1)} \sum_{i=1}^{N} \sum_{j=i+1}^{N} \Theta(r - | \underline{x}_i - \underline{x}_j |), \qquad (4.4)$$

where the Heaviside function $\Theta(y) = 0$ for $y \leq 0$ and $\Theta(y) = 1$ for $y > 0$
and $| \underline{x} |$ is usually taken as the maximal norm, the correlation dimension, D_2, is given by:-

$$D_2 = \lim_{m\to\infty} \lim_{r\to 0} \lim_{N\to\infty} \frac{\mathrm{d} \log(C_m(r))}{\mathrm{d} \log(r)} . \qquad (4.5)$$

$C_m(r)$ is the probability that a pair of randomly chosen points on the attractor both lie within the same hypercube of side r (refer to Figure 4.10 showing an example of a three dimensional reconstructed attractor). D_2 then gives a measure of how rapidly this probability changes over different scales of the attractor (this is a typical sort of analysis related to dimension measurements). It is known (Takens (1982)) that for sufficiently large and clean data sets and for a suitable range of r that the gradient

$$\frac{\mathrm{d} \log(C_m(r))}{\mathrm{d} \log(r)} = D'_2 \to D_2 \qquad \text{as } m \to 2m_e+1 \text{ (m_e the original attractor's embedding dimension)} \qquad (4.6)$$

There is also evidence that it is possible for the convergence to occur for lower values of m (Ding, et al. (1993)). However there are many problems that arise from attempting to estimate D_2 from experimental measurements. Some of these include :-

(i) Only approximations to the limits of equation (4.5) can be calculated. i.e. N can only be large rather than infinite (and needs to be at least of the order of n^{D_2}, where $n > 5$. See Fraedrich and Wang (1993) and Grassberger, et al. (1991)), r has a lower bound restricted by measurement resolution and noise and the maximum size of m is restricted by failings in the method of delays for experimental data (these failings are similarly due to finite amounts and resolutions of the data set). The data set also needs to be large enough for the measured variable to be stationary (that is the statistical properties of the data being independent of time). Another consequence of the data set not being large enough is that unreliable estimates of the probabilities $C_m(r)$ are obtained. This is because as m increases the density of points on the attractor decreases rapidly.

(ii) $C_m(r)$ is sensitive to the sampling time, τ (as discussed in the previous section).

(iii) The estimation of D_2 involves the estimation of the gradient d $\log(C_m(r))$/d $\log(r)$. Practically this is done using a least squares method with a suitably large set of values of $C_m(r)$ calculated at different r values which introduces errors particularly from experimental data. It was found that these errors combined with the difficulty of determining whether D'_2 had converged sufficiently often made an estimation of D_2 very difficult. These procedures are very computationally intensive.

Unfortunately the tests carried out by Franca, et al. (1991), did not indicate how much these problems interfered with the dimension estimates that they obtained for signals from various flow regimes. The tests were carried out on pressure transducer signals produced by wavy, plug, slug and annular flows (in a 19mm internal diameter (ID) horizontal pipe) with dimension estimates of 6.2, 7.2, 5.1 and 5.9 respectively. One set of flow rates for each flow regime was tested. Some measurements carried out by Vitsikounaki (1995) showed some correlation with fluid component flow rates and possible correlation with flow regimes, though the flow regime information was not available to be able to draw conclusions about responses to flow regimes. Added to computation times for the correlation integrals for many values of r was the additional processing to provide useful measures that were then correlated with flow conditions. Vitsikounaki (1995) made no comment about the computation times.

Because of these problems in estimating D_2 the author has not found it to be very practical for the application of flow pattern identification. Figure 4.11 shows the typical behaviour of $C_m(r)$ that occured for many of the experimental signals obtained by the author. The behaviour of the gradients, D'_2, is also shown. Typically there is insufficient convergence of D'_2 to a fixed value as m increases to obtain reliable estimates of D_2. m cannot be increased indefinitely because the reliability of the probability estimates decreases due to the rapidly decreasing density of points. A more robust method has been adopted. The results of this method applied to the noisy and relatively small experimental signals do seem to provide a measure that plays a role in the discernment between signals from different flow patterns. It must be emphasised, however, that the dimension estimates obtained do not necessarily reflect the true nature of the underlying dynamics governing the behaviour of the measured variable due to the restrictions on the size of m particularly.

The method is based upon properties of the correlation integral as previously defined and was developed by Savit and Green (1991). It seems to be more robust at detecting signal properties from noisy data. They introduced a delta measure, $\delta_m(r)$, defined as:-

$$\delta_m(r) = 1 - \frac{C_m^2(r)}{C_{m-1}(r)\, C_{m+1}(r)} \qquad (4.7)$$

These $\delta_m(r)$'s give a measure of the dependency of x_i on x_{i-m} aside from the dependencies of x_i on x_k for $i-m < k < i$.

For a chaotic signal produced by a system with m_e degrees of freedom the following behaviour tends to result :-

$$\delta_m(r) > \xi \text{ for } m = 1, \ldots, m_e \text{ and } \delta_m(r) < \xi \text{ for } m > m_e \qquad (4.8)$$

The parameter ξ represents a threshold below which a given $\delta_m(r)$ is influenced more by noise factors rather than deterministic mechanisms. Typical behaviour of $\delta_m(r)$ from experimental signals is shown in Figure 4.12. There is a general trend for $\delta_m(8)$ to decrease as m increases. Where $\delta_m(8)$ is above the noise threshold then there are at least m degrees of freedom. Savit and Green (1991) recommended r to be one half of the standard deviation, ε, of the time series, x_i. However the signals that have been analysed by the author show that $\delta_m(r)$ has a dependence on the flow conditions for values other than at $r=\varepsilon/2$ (and hence provided potentially useful information). The authors particular method of using the delta measures is further described in Section 4.9.2.

§4.7 Singular value decomposition

This method has been widely used in signal analysis and is an application of the Karhunen-Loève expansion of a random process (Bundick (1973) gives a good introduction). Ciliberto and Nikolaenko (1991) applied the method to investigate single phase fluid dynamic behaviour between sliding moving surfaces. To the author's knowledge singular value decomposition (SVD) has not been successfully applied to flow regime identification. An unsuccessful attempt by Vitsikounaki (1995) was probably due to lack of sufficiently large data sets. Also, unfortunately, the flow regimes were not known. Tam and Devine (1992) used SVD for the noise reduction in the analysis of signals obtained from fluidised beds (upward fluid/solid flows), but they did not

implement SVD to extract more directly a dimension estimate as has been carried out by the author.

Karhunen-Loève expansion involves the construction of a matrix from a set of vectors describing a reconstructed attractor from a time series. This is the same reconstruction process as for the correlation integral calculations, except that different parameter values are used. The square roots of the eigenvalues of this matrix are called singular values. They give information about the relative strengths of deterministic properties within the original signal. Information about the amount of stochastic noise in the signal can also be extracted. The Karhunen-Loève expansion is efficient at projecting the reconstructed attractor onto a special space such that the information about the deterministic and stochastic influences in the signal can be extracted via the singular values. Figure 4.13 shows a reconstructed attractor in the space and the singular values related to the spread of the attractor along individual axes in the space.

The method was implemented by constructing an $m \times m$ covariance matrix, Ξ, from a time series of N measurements, x_i, i=1, ... , $N = n \times m$, using a set of vectors describing an attractor, $\underline{v}_j$, $j = 1, \ldots, m$. $\underline{v}_j$ are given by :-

$$\underline{v}_j = (x_j, x_{j+n}, \ldots, x_{j+(m-1)n}) \tag{4.9}$$

and an average vector, $\underline{a}$, given by:

$$\underline{a} = \frac{1}{n} \sum_{j=1}^{n} \underline{v}_j = (a_1, a_2, \ldots a_m)$$

$$= \frac{1}{n} (\Sigma x_j, \Sigma x_{j+n}, \ldots, \Sigma x_{j+(m-1)n}). \tag{4.10}$$

m is an embedding dimension playing the same role as that of the correlation integral. However it is practical to use larger values with SVD than can be used with the correlation integral because the computation process is much faster.

Ξ is then given by:

$$\Xi = \frac{1}{n} U^T U \tag{4.11}$$

where U is the $n \times m$ matrix of n row vectors $\underline{u}_j = \underline{v}_j - \underline{a}$, $j = 1, \ldots, n$.

The eigenvalues, σ_k^2, k=1, ... , m of Ξ (a real symmetric matrix) have the following important property:

$$\sigma_1^2 \geq \sigma_2^2 \geq \ldots \geq \sigma_m^2 \geq 0. \qquad (4.12)$$

The eigenvalues can be easily computed using one of the routines produced by the Numerical Algorithms Group (NAG) which produces numerical analysis software for many computer systems.

The orthonormal eigenvectors of Ξ form the basis vectors onto which the vectors $\underline{y}_i$ can be projected. These projections are called principle components. The largest eigenvalue, σ_1^2, gives a measure of the energy contributed by the most significant (and most likely deterministic) principle component (Broomhead and King (1986)). The smaller σ_k^2, k=D_s+1, ... , m, correspond to the energy contributions from principle components that represent noise in the original attractor where D_s can be considered as an upper bound of the dimension of the attractor if suitable values of N, m and sampling time have been chosen. These parameters are difficult to determine for accurate estimates. Values were selected which provided discernable differences in D_s which were dependent on the flow pattern (though accurate dimension estimates are unlikely). This was done since changes in D_s were of most interest for this particular research. The embedding dimension, m, was typically of the order of 20, which provided a large enough variation in D_s to be observed for signals from different flow patterns. The large value in m meant that N needed to be as large as possible (of the order of 10^5 data points).

Estimations of D_s have been obtained by counting the number of singular values that make up at least 90% of the total energy of the system, i.e.

$$100\% \times S_{D_s} / S_n \geq 90\%, \qquad (4.13)$$

where $S_k = \sum_{i=1}^{k} \sigma_i$

D_s is the number of significant singular values that may be considered to be related to deterministic influences in the original signal (Broomhead and King (1986)). The value of 90% was somewhat arbitrarily chosen, leaving what was considered a reasonable value (10%) for random influences in the signal.

Figure 4.14 shows the typical behaviour of the ratio, S_k / S_n, as k increases for signals from bubble and slug type flows. The labels, p and s, indicate the the values of $k=D_s$ where the singular values above the threshold are considered as insignificant and related only to signal noise. The position of the vertical lines indicate the estimated value of $k=D_s$. As can be seen from the figure the rate of increase of S_k / S_n occurs at different rates for the different flow patterns. E.g. the light signal from slug flow has many more significant singular values than the light signal from plug flow and hence has a larger number of degrees of freedom.

§4.8 Power spectra analysis

Another method of estimating a measure of the complexity or roughness of a signal, $x(t)$, is to measure the exponential rate of decay of the power spectra, $P(\omega)$, with respect to $\log(\omega)$. This method was applied to anemometer signals from two-phase bubbly flow and single phase turbulent flow by Wang, et al. (1990) to analyse the turbulent nature of the flows.

A signal, $x(t)$, has fractal properties if for a range of a scaling factor, α,

$$x(\alpha t) \propto \alpha^H x(t) \quad (\alpha>0), \tag{4.14}$$

where H is known as the scaling exponent (Barnsley, et al. (1988)).

The decay of the broad band power spectra, $P(\omega)$, of the signal is a consequence of this scaling property and tends to have the following behaviour

$$P(\omega) = c\,|\omega|^{2D_p-5}, \qquad 1 < D_p < 2 \tag{4.15}$$

where D_p is a fractal dimension related to the roughness of the signal, $x(t)$ (in this case the smallest integer greater than D_p is not the same as the number of degrees of freedom of the system producing $x(t)$) and c is a constant (Fowler (1993) and Prechner (1993)). These authors describe practical implementations of this method.

The gradient $(2D_p\text{-}5)$ of the $\log(P(\omega))$-$\log(\omega)$ graph was estimated by a least-squares best-fit line and so provided a non-iterative method for estimating fractal dimension. A Bartlett window was applied to each signal prior to Fourier transforming to reduce undesirable effects of using discrete data (this simply involved the following operation :

$x_i \rightarrow 2ix_i/N$ when $i \leq N/2$ and $x_i \rightarrow 2(N-i)x_i/N$ when $i > N/2$). Typical logarithmic behaviour of the smoothed power spectra from some of the experimental signals is shown in Figure 4.15. Smoothing was done using a moving average of 90 neighbouring points. Different average slopes can be seen in the curves from light signals from bubble and slug flows. Errors in D_p estimates occured due to large and isolated frequency components (examples are indicated by a and b in Figure 4.15) which deviated from the law described by equation (4.15). The effects of peaks in the spectra representing these components (which reflected regular structures in the signal) were reduced by applying the moving average. The variation in D_p of signals obtained from the same flow patterns was also reduced by the smoothing process.

§4.9 Improvements to the signal analysis techniques

Improvements to some of the analysing techniques were made to improve, where possible, the detection of signal properties that changed with the flow regime and to improve the speed and efficiency of the computations. These included (i) the introduction of a fast and robust method for estimating a delay time when the sampling time proved to be ineffective and (ii) improvements to the speed of the analysis techniques that used the correlation integral.

§4.9.1 Estimation of the delay time, τ

The most commonly used delay time in the analysis of the experimental signals was the sampling time (i.e. the smallest delay time available) in the initial attempt to detect changes in signal properties which correlated with flow regime. When the sampling time proved to be inadequate (i.e. no change in signal properties were detected with flow regime change) an attempt to provide a suitable delay time using a robust and fast method of delay time estimation method developed by the author was used. The method added little extra computation time to the signals analysis by measuring the angle between successive tangent vectors on the attractor for a given delay time. The method described has not been used before, to the author's knowledge. It involved finding the cosine of the angle between successive tangent vectors on the reconstructed attractor trajectory:-

$$\beta(\tau) = \cos(\theta(\tau)) \qquad (4.16)$$

where $\cos(\theta(\tau))$ is the most frequently calculated cosine of the angle between successive tangent vectors. This was estimated by calculating a histogram of the cosines.

The cosines were computed efficiently using the cosine rule :-

$$\cos(\theta_i) = \delta\underline{x}_i \cdot \delta\underline{x}_{i+1} / (|\delta\underline{x}_i||\delta\underline{x}_{i+1}|) , \qquad (4.17)$$

where $|\underline{x}_i|$ represents the Euclidean norm of the m dimensional vector $\underline{x}_i$ and $\delta\underline{x}_i = \underline{x}_i - \underline{x}_{i-1}$ (Figure 4.16 shows the angles θ_i on a trajectory)

The most likely $\cos(\theta(\tau))$ was estimated by finding the most frequently occuring $\cos(\theta_i)$ within a given small range using a histogram.

$\beta(\tau)$ gives a measure of the average cosine of the angle found between successive tangent vectors lying on the reconstructed attractor. It was generally found that the contributions to $\beta(\tau)$ from each m correlated with each other. Because of this all the attractors from a range of embedding dimensions (m=2, ..., 7) were used to produce the histogram of cosines measurements.

The behaviour of $\beta(\tau)$ is shown for various time series. Figure 4.17 shows $\beta(\tau)$ for numerically generated data from the X variable of the Lorenz system. The effects of noise on $\beta(\tau)$ are shown (Gaussian noise was added to the numerically produced time series in various amounts indicated). Generally as the noise levels increase the angles between successive tangent vectors become more obtuse (due to the deviation of points from the 'clean' trajectory) and the value of $\beta(\tau)$ decreases. For the Lorenz system a suitable delay time is known to be $\tau \approx 0.1$ corresponding to $\beta(\tau)$ satisfying $0 \leq \beta(\tau) \leq 0.8$.

Figures 4.18 and 4.19 show $\beta(\tau)$ for experimental data collected from the rig described in Chapter 3. It was found that often the most suitable delay time provided by the given data was the smallest possible (i.e. the sampling time). This was decided by the fact that often $\beta(\tau)<0$, corresponding to reconstructed attractors with delay times that were too large. Although this is a serious problem with regards extracting information about the true nature of the underlying dynamics governing the data it has not prevented discernment between signals from different flow regimes. This is because the dimension estimates (though not necessarily accurate for system model prediction) still responded to fundamental changes in signal properties resulting from changes in the flow properties.

The structures of the reconstructed attractors from experimental signals are shown in Figures 4.20-4.22. Figure 4.20 shows two attractors, (a) and (b), reconstructed from light transducer signals from horizontal plug flow. Attractor (a) was reconstructed using τ=sampling time and attractor (b) reconstructed using τ=20×sampling time. It can be seen that many angles, θ_i, between successive tangent vectors on each attractor satisfy $\pi/2<|\theta_i|<\pi$, hence $\beta(\tau)$ (shown in Figure 4.18) is less than 0. This is due to the nature of the light transducer signals, which tend to have magnitudes which congregate around the maximum or minimum values possible (refer to Figure 3.8). Figure 4.21 shows attractors (c) and (d) reconstructed from light transducer signals from horizontal slug flow (τ=sampling time for attractor (c) and τ=20×sampling time for attractor (d)). The structure of the attractors from the light signals all look very similar due to the signals tending to have either maximum or minimum values. The attractors are embedded into a 3-dimensional phase space which is not large enough to reveal differences in structure which are detected by the signal processing methods.

Figure 4.22 shows attractors from absolute pressure transducer signals from horizontal plug and slug flows. A delay time of τ=3×sampling time was used for each attractor (since $\beta(\tau)\approx 0$ suggested that this value of τ was suitable). The differences in the structure of the attractors are more clear than those from the light signals. During slug flow there are more orbits in the attractor (denoted by O in Figure 4.22) that extend from the main body of the attractor (denoted by M) due to the larger fluctuations that occur during the passage of a slug. These differences in attractor structure are reflected in suitable fractal measures of the attractors. These are shown in the results presented in Chapter 5 (refer to Tables 5.1 and 5.2).

In an attempt to reduce the computation times for signal analysis the most common recommended sampling time was maintained as a constant for all signals from a whole set of flow rates. In the analysis of the experimental signals it was found that with many of the successful cases discernment between flow patterns could be obtained using τ equal to the sampling time and that often the use of an optimised value of τ did not always improve the discernment.

§4.9.2 Efficient use of the correlation integrals

In Section 4.6 the use of delta measures was introduced, since they improve the efficiency of extracting information from signals using the correlation integral. The

information contained in the behaviour of delta measures was analysed by defining a measure, D_δ, which included information over a range of hypercube sizes (described in Section 4.6 and shown in Figure 4.10).

$$D_\delta = \sum_{i=0}^{i_{max}} D(2^i) / i_{max} \qquad (4.18)$$

where the embedding dimension estimate, $D(r)$ is such that $\delta_{D(r)+1}(r) < \xi$ and $\delta_k(r) > \xi$, k=1, ... ,$D(r)$ and ξ is the threshold parameter given in equation (4.8).

The parameter i_{max} was chosen such that the $\delta_k(r)$ values were observed to vary with a change in flow pattern as much as possible. i_{max} governs the maximum size of hypercube used and is restricted by the maximum possible size of r, (i.e. r=1024=2^{10} (i_{max}=10) in the case of the 10 bit signals collected by the author). Useful values of i_{max} were typically less than this (i_{max}~5), since too many of the attractor points were contained in hypercubes with large r (r>2^5) and information with regards the more detailed attractor structure was excluded. Computation times were greatly reduced by using small values of i_{max} since less pairs of points were enclosed (and therefore less points counted) in smaller hypercubes. The value ξ was set to 0.08 representing a noise floor of 8%.

Note that D_δ is not a fractal dimension but an average of integer embedding dimensions. It does not therefore have the same meaning as the correlation dimension, D_2.

§4.9.3 Improvements in computation speed of the correlation integral

A very important factor in the use of fractal measuring techniques applied to practical situations is the computation time. Optimisation of algorithms is often essential if a method is to be used in an industrial situation. Also for extensive and practical research to be carried out excessive computation time can be prohibitive. The computation of the correlation integral is a very intensive process and the author has developed a fast algorithm which is given in detail in Appendix A and Figures A.1 and A.2. Computation of the correlation integral is intensive because ideally the distance between all pairs of points on the reconstructed attractor needs to be calculated. The algorithm minimises the number of times that this calculation is made.

§4.10 Signal analysis techniques applied to simulated signals related to multiphase flows

The particular method using the correlation integral and delta measures and the SVD method of signal analysis have not been successfully applied to modelled or experimental signals associated with multiphase flows (to the author's knowledge). The results of these measuring techniques are illustrated by applying them to signals produced by a hypothetical transducer which is presumed to detect typical multiphase flow structures such as slugs, plugs, bubbles or waves. The results show the sensitivity of these measurements to the complexity of the signals which is directly related to the 'visible' complexity of the signal generating algorithms.

Signals that contain characteristics reflecting the response of the hypothetical transducer to multiphase flows have been simulated by considering the appearance of typical transducer signals acquired by the author. Dispersed bubble, stratified wavy, plug and slug type flows have been considered (see Chapter 2).

It has been assumed that a suitable transducer is sensitive to the shape of the gas-liquid boundaries in the location of the transducer across the pipe (such as the light signals shown in Figure 3.8) or to the void fraction of the mixture. The measures D_δ, D_s and D_p have then been estimated from the signals to provide information on how they could be expected to respond to different experimental signals.

§4.10.1 Simulated signals related to dispersed bubble, stratified, plug and slug flows

In the case of a dispersed bubble or stratified wavy horizontal flow it is assumed that a noisy signal will be produced which has a homogeneous structure. The characteristics of the noise would be dependent on the many frequent and complex interactions that the transducer has with either the small bubbles or moving gas-liquid boundary passing it.

In the case of a horizontal plug or vertical bubbly flow the same noisy signal is assumed to exist during the passage of a bubble where a complex, moving gas-liquid boundary passes the transducer. However when a section of clear liquid passes it is assumed that the transducer produces a constant signal.

In the case of a horizontal or vertical slug flow during the passage of a slug it is assumed that a complex interaction between the transducer and the frothy slug occurs, producing a visible change in signal structure. The signal modelling the stratified flow is assumed to be produced during the absence of a slug.

The basic noise signal, v_j, (j=1, ... , N) is produced using the following function:-

$$v_j = \sum_{k=1}^{1000} \frac{1000}{k+100} \sin(kj\omega_0+\phi_k) \qquad (4.19)$$

where ϕ_k is a random phase satisfying $-\pi \leq \phi_k < \pi$ (see the probability function shown in Figure 4.23) and $\omega_0=1.25\times10^{-4}$.

The transducer response to plug type structures is crudely modelled by a constant:-

$$p_j = 812 \text{ for } T_p < j < T_p + L_p. \qquad (4.20)$$

Where the length of the plug, L_p, (or slug, L_s, for the next case) (indexed by p=1, 2, ...) is described by:-

$$L_p = 50\mu_{p1} + 350, \qquad (4.21)$$

where μ_{pi} (i=1,2) is a random variable with a Gaussian probability distribution (see Figure 4.23). The time delay, T_p, (or T_s for slugs,) between plugs p-1 and p is given by:-

$$T_p = (90\mu_{p2} + 500)T_0. \qquad (4.22)$$

T_0 governs the average delay in slug or plug arrival.

The transducer response during the passage of a slug type structure is modelled by amplifying and displacing the noise signal, v_j. The signal is given by:-

$$s_j = 1.2(v_j + 300). \qquad (4.23)$$

The simulated time series for the various flow regimes are given by:-

$x_j=v_j$ for the dispersed or stratified flow regimes,
$x_j=p_j$ when $T_p<j<T_p+L_p$, $x_j=v_j$ otherwise for plug flow and
$x_j=s_j$ when $T_p<j<T_p+L_p$, $x_j=v_j$ otherwise for slug flow

Figure 4.24 shows the simulated signals, using values of T_0=1 and T_0=5 for the intermittent flow regimes.

§4.10.2 Measurements of the simulated signals

Measurements of D_δ, D_s and D_p have been carried out on each signal. The most appropriate delay of τ=(3 sample intervals) (i.e. time series given by x_1, x_4, ...) was used having measured $\beta(\tau)$ for each signal.

For the D_δ measurement the following parameter values were used : N=15,000 and i_{max}=5. Five sections of each time series were analysed.

For the D_s measurement the following parameter values were used : N=120,000 and m=40. Ten sections of each time series were analysed.

For the D_p measurement the following parameter values were used : N=4,096. Ten sections of each time series were analysed.

The results of the measurements (averaged over the sections) are shown in Table 4.1.

Table 4.1 Measurements made on simulated signals

Signal	D_δ	D_s	D_p
Dispersed bubble or Stratified	3.3	12	1.94
Slug (T_0=1)	4.1±0.2	6	1.85
Slug (T_0=5)	4.0±0.3	7	1.86
Plug (T_0=1)	1.5±0.5	2	1.71
Plug (T_0=5)	2.6±0.3	2	1.74

The measures D_s and D_p seem to indicate that the most complicated signal is the basic noise signal used to model the dispersed bubble or stratified flow whilst D_δ indicates that

the slug flow signals are more complicated. In terms of computational effort to generate the signals the slug flow signal requires greater effort and hence a more complex generating algorithm is required (as is apparent from the fact that equation (4.19) is sufficient for the basic noise whilst the additional equations (4.21)-(4.23) are required for the slug flows). D_δ may then be considered to provide more fundamental information in terms of the governing system. However in terms of the appearance of the signal the slug flow signal might be considered simpler in that the response to slugs break up the irregularity of the basic noise, which is reflected in the lower values of D_s and D_p. This becomes more apparent when considering the signal representing the higher frequency of slug arrival time. The signal structure seems to become simpler with the higher frequency, according to D_s and D_p. In terms of computational effort per data point the higher frequency slug flow signal requires greater computational effort, as is reflected by the increase in D_δ. In terms of usefulness for flow regime identification the measures D_s and D_p vary less for different sections of the same signal analysed and perform adequate discernment.

All three measures behave consistently with regard the plug flow signal. Although the plugs are of random length and arrive at unpredictable times the transducer response is very simple during each plug interaction. The constant nature of the signal reduces the computational effort per data point required to generate it. For the higher frequency plug flow signal this simplicity in generation reduces the computational per data point and hence D_δ is smaller. The signal simplicity of the modelled plug interaction has a significant reducing influence on each of the measures.

From this analysis of simulated signals the use of measures of chaos demonstrate a potential use for multiphase flow regime identification.

§4.11 Summary

The use of fractal measuring techniques based on chaos theory has been described. The calculation of three measures, D_δ (using correlation integrals), D_s (using singular value decomposition) and D_p (using power spectra) have been described. Computation times are an important factor and the author has introduced original improvements to the effectiveness and computation efficiency of the calculations. Measurements have been made on simulated signals that contain structures typical of various multiphase flows. The results show that fractal measuring techniques have potential for discriminating between flow regimes.

CHAPTER 5

PRESENTATION OF RESULTS

5.1 Introduction

The results of measurements of chaotic properties of experimental time series related to various multiphase flows is presented. A variety of horizontal and upward vertical flow patterns were obtained and the measures described in Chapter 4 were calculated. Some simpler statistical measures were also calculated for comparisons to be made.

§5.1.1 Conditions investigated

The signal analysis techniques described in Chapter 4 have been applied to signals collected from the transducers described in Chapter 3 and to signals collected from a gamma-ray densitometer on a 406mm internal diameter horizontal pipe (kindly provided by CALtec Ltd. of the BHR Group Ltd.). Using the test sections described in Chapter 3 data from the situations shown in Table 3.1 was collected.

§5.1.2 Signal analysis

Each of the 477 transducer signals (time series) from the author's experiments contained 120,000 data points to a maximum resolution of 10 bits (0-1023). Each time series was analysed several times by taking up to 50 measurements from various sections of each time series. This provided an indication of how much variation in the measures could be expected. For measures using large numbers of data points (more than half those in the complete time series) the variation is under estimated due to overlapping sections of time series being analysed more than once.

The following measures were calculated from each time series:-

i) D_δ (using N=15,000 data points) from 5 time series sections. Fewer sections were tested due to the rather long computation time required for each D_δ estimation (between 2 and 5 minutes on a 175MHz clock speed workstation). The parameter i_{max} (in equation (4.11)) which produced some suitable changes in D_δ with the flow pattern had a value of 5. Variations in D_δ were of the order of $D_\delta \pm 1$.

ii) D_s (using N=100,000 data points) from 20 overlapping time series sections. The size of the embedding dimension (given by m in equation (4.13)) was set at 20. This gave a reasonable sized sample of 5000 points to be used in the calculation of the average vector, $\underline{a}$ in equation (4.14). Standard deviations in D_s for each set of flow rates were of the order of 0.05 (though the over lapping of time-series is considerable, so this is an underestimate).

iii) D_p (using N=8192 data points) from 20 overlapping time series sections. A moving average of 90 neighbouring points was used to smooth each power spectra to reduce excessive variation of D_p estimates (see Figure 4.15). Standard deviations in D_p for each set of flow rates were of the order of 0.05.

iv) the average,

$$A = \sum_{i=1}^{N} x_i / N \qquad (5.1)$$

v) a variance measure (the mean absolute deviation),

$$V = \sum_{i=1}^{N} | x_i - A | / N \qquad (5.2)$$

vi) the mean absolute difference between successive data points (high when high frequency signal components are present),

$$E = \sum_{i=2}^{N} |x_i - x_{i-1}| / N \qquad (5.3)$$

vii) a measure of how often a certain threshold is exceeded (high when points approximately larger than the median are visited frequently),

$$L = \sum_{i=1}^{N} \Theta(x_i - 600) / N \qquad (5.4)$$

where Θ is the Heaviside function as described in equation (4.4).

The simple measures A, V, E and L were calculated using N=100,000 from 50 overlapping time series sections. They were included as comparisons with the measures based on the fractal techniques. Standard deviations in A, V, E and L for each set of flow rates were of the order of 0.05 (though the over lapping of time-series is considerable, so this is an underestimate).

§5.2 Presentation format

Results are presented for measures that could be used to successfully detect changes in the flow pattern. Measurements are as a function of the air and water flow rates. The visually estimated flow patterns are also indicated. Successful flow pattern identification is possible when a change in a measure correlates with a change in the the visually estimated flow pattern. In the surface plots this is apparent by a step or dip in the surface where measures associated with one of the flow patterns are above or below a threshold separating the measure values associated with the other flow pattern.

Many measurements were made which showed negative results, i.e. there was no consistent change in the value of a measure with a change in the flow pattern. Most figures included in Appendix B show these results. Figures which show a jagged and messy surface or line with flow pattern labels appearing mixed clearly indicate an unsuccessful measurement for flow pattern discrimination. Different axes orientations are used in the surface plots in order to provide as clear a view of the surface as possible. Though such results are negative they reflect the difficulties of detecting multiphase flows which were described in Chapter 2.

The signal source is given in the title. For most of the measurements the minimum delay time, τ, was used (restricted by the sampling time of the time series). Where correlation with flow pattern changes could be improved (or if it was not obtained with the use of the sampling time) a different delay time was used having used the delay estimation parameter, $\beta(\tau)$, described in Section 4.9.1. Where a delay time was used that was different from the sampling times given above it is indicated in the Figure title. For all the measurements on the absolute pressure signals a delay time of 7.5×10^{-4}s was used having measured $\beta(\tau)$ from each time series (except for D_s measures from horizontal flows where τ is shown in Figure 5.4).

Included on the bases of the surface plots are labels indicating the visually estimated flow patterns to indicate the approximate air and water flow rates at which the flow patterns occured. 'p' indicates horizontal plug flow, 'b' vertical upward bubble flow (as described by Spedding and Nguyen (1980)), 's' horizontal or vertical slug flow and 'd' horizontal dispersed bubble flow. The behaviour of the successfully discriminating measures for the different flow conditions is displayed in Figures 5.1 to 5.20.

§5.3 Results from horizontal plug and slug flows in the 50mm pipe

Table 5.1 shows the measures that discriminate between the plug and slug flow patterns. Successful measures are shown in Figures 5.1 to 5.5. It is worth noting that the measure, D_S, (Figure 5.4) applied to light signals which seems to be correlated with the visually estimated flow pattern indicates a gradual change in signal complexity with respect to the flow rate. This suggests that the transition boundary between the horizontal slug and plug flow patterns may not be clearly definable justifying the use of bands defining flow pattern boundaries that have been used in some of the later flow regime maps (e.g. Weisman, et al. (1979)). The theoretically simulated signals in Section 4.10 also produced similar behaviour.

The successful results from the absolute pressure transducer signals from the horizontal plug and slug flows are included in Figures 5.2, 5.3 and 5.9 to 5.12. However none of the measures could be used to successfully discriminate absolute pressure transducer signals from the dispersed bubble flow pattern from the slug or plug flow patterns (see Figures B.78 to B.85). Absolute pressure transducer signals in Figure 3.6 show some similarity in the higher frequency noise content in signals from a typical dispersed bubble flow and a plug flow. This is possibly due to the large amount of system vibration that is transmitted through the dominating liquid fraction of both flows and detected by the transducer. It seems that the effect of the bubbles tended to be over-shadowed by the system noise. The behaviour of D_S reflects the similarity of the signals as shown in Figure B.83.

Table 5.1 Measures discriminating between plug and slug flow (50mm horizontal pipe)

Signal source	Measure	Limits recorded for :- Plug flow	Slug flow	Figure
Light	L	$0.457>L>0.202$	$0.186>L>0.023$	5.1
Absolute pressure	E	$45>E>15$	$10>E>5$	5.2
Absolute pressure	D_s	$D_s\geq 2$	$D_s=1$	5.3

The measures which showed no overlapping across the flow pattern boundary were L on the light transducer signals and E and D_s on the absolute pressure transducer signals (neglecting the dispersed bubble flow). The next best discriminating measure was the D_s measure on the light transducer signals using a delay time of 0.00375s (three times the original sampling time). The trend was $D_s\geq 9$ for slug flows and $D_s\leq 8$ for plug flows. The use of a delay time of 0.00375s was prompted by $\beta(\tau)$ indicating a possible improvement in attractor structure on the other transducer signals. Although for the light transducer signals the minimum delay time available was recommended by $\beta(\tau)$. With regard to this matter it can be noted that there is little qualitative difference between the behaviour of D_s shown in Figures B.24 and 5.4. The ambiguity of D_s in discriminating between slug and plug flows occurs for one flow condition (air flow: 94 l/min, water flow: 100 l/min). $D_s \leq 8$ for all plug flows except for this one flow condition where $D_s=9$. Also of the 20 sections of time series used 2 produced measurements of $D_s=8$ for the slug flow at an air flow of 117 l/min and a water flow of 200 l/min. Of 1060 measurements of D_s 22 gave incorrect discernment (2% failure rate). Taking into consideration the over lapping of sections of time series the error could be more safely estimated as 2 failures out 53 (4% failure rate).

Table 5.2 gives a summary of the behaviour of D_s and also V which had a similar failure rate.

Table 5.2 Measures discriminating between plug and slug flows with failure rates < 5% (50mm horizontal pipe)

Signal source	Measure	Limits recorded for :- Plug flow	Slug flow	No. failures out of 53	Figure
Light	D_s	$5\leq D_s\leq 8$	$9\leq D_s\leq 12$	2	5.4
Light	V*	$400>V\geq 259$	$255\geq V>100$	2	5.5

* margin for discernment < 1% of total range of V (not particularly safe)

Poor results from the differential pressure transducer signals are due to the noise inherent in them, partly due to electrical interference and mechanical vibration of the rig. Further signal analysis and filtering might have isolated the flow regime dependent properties, however this would have increased computation time. The author was interested to see whether the fractal measuring techniques would be less sensitive to the noise, since the signal properties may change to some extent with the more obvious changes in flow pattern. The electrical conductance transducer signals tended to show little difference in properties from bubble and slug type flows due to its lack of sensitivity to small air bubbles in the frothy slugs (the conductance still increased dramatically whether a slug or plug passed the transducer). Because of this insensitivity there was no discrimination between the flow patterns from the electrical conductance transducer signals and the differential pressure transducer signals analysed by the author.

§5.4 Results from upward vertical bubble and slug flows in the 50mm pipe

Table 5.3 shows the measures that successfully discriminate between the vertical bubble and slug flow patterns in the 50mm internal diameter pipe. Figures 5.2 and 5.6 to 5.12 show the behaviour of the various successful measures from the transducer signals (unsuccessful measures are included in Appendix B). The differential pressure and electrical conductance transducers failed to provide any discriminating measures for the same reasons as given in the previous section. The measures related to light signal complexity (D_s in Figure 5.8 and D_p in Figure 5.13) that seem reasonably well correlated with flow pattern show an increase with air flow rate during the bubble flows, possibly related to the increase in frequency of the bubbles. During the slug flows these measures then become reasonably stable, probably due to the majority of the signal complexity resulting from the transducer interaction with the highly complex frothy structures between slugs rather than from the pattern of slug arrivals. All the statistical measures (A, V, E and L) from the absolute pressure transducer signals were reasonable discriminators. A, V and L from light transducer signals displayed similar qualitative behaviour as D_s and D_p (Figures 5.6, 5.7 and 5.14). A, V and L changed by only small amounts near the transition boundaries and hence disadvantageous for flow pattern discrimination..

The measure which changed most significantly with a change in flow pattern was D_s. The success of the statistical measures did not continue when applied to flows from the

smaller 25mm vertical pipe shown in the next section (with the exception of V from the absolute pressure transducer and A from the light transducer signals).

Table 5.3 Measures discriminating between bubble and slug flow (50mm vertical pipe)

Signal source	Measure	Limits recorded for :- Bubble flow	Slug flow	Figure
Light	A*	$461>A>36$	$35>A>14$	5.6
Light	V**	$331>V>57$	$54>V>21$	5.7
Light	D_s	$3\leq D_s\leq 8$	$11\leq D_s\leq 13$	5.8
Absolute pressure	A***	$470<A<541$	$544<A<570$	5.9
Absolute pressure	V	$60<V<85$	$105<V<170$	5.10
Absolute pressure	E	$42>E>17$	$10>E>5$	5.2
Absolute pressure	L	$0.05<L<0.23$	$0.33<L<0.47$	5.11
Absolute pressure	D_s	$D_s\geq 2$	$D_s=1$	5.12

* margin for discernment < 0.25% of total range (not particularly safe)

** margin for discernment < 1% of total range (not particularly safe)

*** margin for discernment < 1.5% of total range (not particularly safe)

Small failure rates resulted in the following measures (Table 5.4). The D_p failures occurred for less than 10% of the sections from about 12 of the time series (1040 sections were measured). Average D_p measurements are shown in Figure 5.13 with variation of approximately ± 0.1.

Table 5.4 Measures discriminating between bubble and slug flows with failure rates < 5% (50mm vertical pipe)

Signal source	Measure	Limits recorded for :- Bubble flow	Slug flow	No. failures	Figure
Light	D_p	$1.5<D_p<2$	$2.1<D_p<2.3$	25 out of 1040	5.13
Light	L	$0.6>L>0.032$	$0.017>L>10^{-3}$	1 out of 52	5.14

§5.5 Results from upward vertical bubble and slug flows in the 25mm pipe

Table 5.5 shows the measures that successfully discriminate between the bubble and slug flow patterns in the smaller 25mm internal diameter pipe. Figures 5.10, 5.12 and 5.15 to 5.19 show the behaviour of the various successful measures from the transducer signals (unsuccessful results are shown in Appendix B).

In contrast to the results from the vertical 50mm pipe the behaviour of the successful statistical measures A, V, E and L during slug flows was not stable (Figures 5.10, 5.15, 5.16 and 5.17). The visible difference between the light transducer signals in Figure 3.8 from the vertical slug flows in the different sized pipes is that those from the smaller pipe indicate that more light reaches the photodiode. This may have caused the statistical measures to be more sensitive to the frequency of slug arrivals which depends on the air flow rate.

Both measures D_p and D_s maintain their stability during the slug flows (Figures 5.12, 5.18 and 5.19), remaining consistent with the results from the larger pipe. This suggests that these types of measures related to signal complexity are less dependent on factors such as pipe diameter. The complexity of light signals increased with the transition from the bubble to slug flows as measured by D_p and D_s. The complexity of absolute pressure signals decreased with the transition from the bubble to slug flows as measured by D_s. This difference in behaviour can be explained by considering the transducer signals shown in Figures 3.6 and 3.8. The light transducer is highly sensitive to small bubbles (e.g. in slug froth) and not clear liquid (during bubble flow) whereas the pressure transducer is very sensitive to system vibrations when clear liquid is present during the bubble flow.

Table 5.5 Measures discriminating between bubble and slug flow (25mm vertical pipe)

Signal source	Measure	Limits recorded for :- Bubble flow	Slug flow	Figure
Light	A*	$700>A>370$	$365>A>100$	5.15
Light	E	$18<E<75$	$80<E<130$	5.16
Light	L	$0.9>L>0.35$	$0.3>L>0.03$	5.17
Light	D_s	$2\geq D_s\geq 5$	$6\geq D_s\geq 7$	5.18
Light	D_p	$1.3<D_p<1.75$	$1.88<D_p<2.17$	5.19
Absolute pressure	V	$80<V<105$	$160<V<200$	5.10
Absolute pressure	D_s	$D_s\geq 2$	$D_s=1$	5.12

* margin for discernment < 1% of total range of A (not particularly safe)

With 29 flow conditions tested no other measures had less than 5% failure rates.

§5.6 Results from horizontal air-water intermittent and stratified flows in a 406mm pipe

The 11 gamma-ray densitometer signals provided by CALtec, BHR, covering horizontal air-water intermittent (slug) and stratified-wavy flows were analysed. The signals were sampled at 20Hz and up to 16,000 data points were collected. The 7 measures were estimated using the same number of sections described in Section 5.1.2, however because fewer data points were available the value of N used for the measures D_s, D_δ, A, V, E and L was reduced to 9000 (for the D_p measure N was maintained at 8192). For the D_s measure it was necessary to use a value of 10 for the parameter m in equation (4.11) (this gave 900 points for the each estimation of the average vector, $\underline{a}$, in equation (4.12)). The smallest possible delay time of 0.05s was used for all estimates.

Table 5.6 shows the results of the measures applied to the normalised time series (such that $0\leq x_i\leq 1023$). Table 5.7 show the measures (D_s and E) that successfully discriminated between the slug and stratified-wavy flow patterns.

Table 5.6 Results from gamma-ray densitometer signals from slug and stratified wavy flows (406mm horizontal pipe)

Flow	U_g /ms^{-1}	U_l /ms^{-1}	Successful discriminating measures		Unsuccessful measures (* Estimates which do not correlate with flow pattern boundaries)				
			D_s	E	D_δ	D_p	A	L	V
slug	7.57	0.486	1	20	1	1.63	196	.04*	107*
slug	7.25	0.724	1	30	1.8±0.8*	1.9*	184	.09*	189
slug	2.71	0.73	1	33	1.5±0.5*	1.67	212	.1*	213
slug	1.16	0.985	1	20	1.2±0.2	1.68	80	.14*	79*
slug	1.18	0.486	1	25	1	1.68	130	.05*	137
slug	1.12	1.195	2	48	2.3*	1.56	548*	.39	292
slug	2.29	1.461	2	33	1	1.56	381*	.16*	195
wavy	1.08	0.0976	3	175	2±0.3*	1.94	467	.16	104
wavy	3.62	0.0976	3	65	2*	1.85	391	.07	101
wavy	6.41	0.245	4	73	1.5±0.5*	1.9	348	.05	101
wavy	6.64	0.0976	5	116	3	2.06	407	.14	124

Table 5.7 Measures discriminating between slug and stratified wavy flow

Measure	Limits recorded for :- Stratified wavy flow	Slug flow
D_s	$D_s \geq 3$	$D_s \leq 2$
E	$E>60$	$E<50$

Figure 5.20 shows the results of D_s on the superficial velocity flow map, which includes the slug/stratified-wavy flow pattern boundary predicted by the Taitel and Dukler horizontal flow pattern map (Taitel and Dukler (1976)).

The only measures which successfully discriminated between slug and stratified wavy flows were D_s (slug: $D_s \leq 2$; wavy: $D_s \geq 3$) and E (slug: $E<50$; wavy: $E>60$). As can be seen from the normalised signals in Figure 3.13 those from stratified-wavy flow appear more complex than those from slug type flow (due to the lack of the occasional large structure which reduces the apparent randomness of the signal). D_s is therefore larger for

the stratified-wavy signals. The response of D_s to the qualitatively similar simulated signals was comparable (shown in Table 4.1).

The measure, E, is successful because there is a large difference in relative amplitude of the high frequency noise components of the normalised signals from the different flow patterns.

§5.7 Interpretation of the results

The signals that have been analysed have come from very complex situations involving the interactions between two turbulently moving fluids. Various properties have been measured using non-invasive transducers which each reflect some of the aspects of the systems complex behaviour. The apparent structure in different signals can be very different even though the same situation is measured. For example, the light transducer signals shown in Figure 3.8 show very different behaviour to the corresponding electrical signals shown in Figure 3.10. Because such differences in the transducer signals exist differences in behaviour of the various measures that have been obtained also exists. The qualitative behaviour of the measures has been illustrated by use of the simulated signals in Chapter 4. These help to explain the behaviour displayed in the results of Chapter 5, but with not much quantitative accuracy, due to the nature of measures based on non-linear dynamics and their sensitivity to certain important parameters such as sampling frequencies (and hence delay times) and number of sample points.

Even for signals produced by numerical methods the behaviour of various measures classifying signal properties can be complex and difficult to predict. The signals shown in Figures 4.2 to 4.4 show the variety in signal behaviour that can arise from a system as simple as the Lorenz system described in Chapter 4. The example of such measures known as Lyapunov exponents (Wolf, et al. (1985)) applied to 'clean' numerically produced signals illustrates this. These measures are ideal indicators of how chaotic a system is by describing how quickly two very close states of a system diverge from each other as the system evolves in time. They are difficult to measure from experimental data and tend to require more computation time than even the correlation dimension estimates described in Section 4.6. Hence the author has not carried out such measurements for the present application. Wolf, et al. (1985) tabulate a series of Lyapunov exponents from different chaotic mathematical systems which clearly shows that their behaviour is in no way simply related to the apparent complexity of the systems. Since this is the case for clean numerical systems one should not necessarily expect to be able to infer what

underlying mechanisms may be causing the particular behaviour of the measures from systems as complex and noisy as the multiphase flow systems analysed here.

§5.8 Summary

The most consistent measure which changed coherently with visually estimated flow patterns from horizontal and vertical pipes was D_S using the light transducer, absolute pressure transducer and γ-ray densitometer signals (with the exception of the 4% of failures for horizontal plug/slug flow discernment from the light signals described in Section 5.3). Table 5.8 shows the values of D_S associated with particular signal sources and flow patterns.

The table shows the consistency with which D_S is a measure of signal complexity, particularly when applied to the absolute pressure transducer signals (i.e. D_S=1 during slug flows and $D_S \geq 2$ during the intermittent bubble and plug flows). For the light signals D_S is greater during the slug flows. This provides evidence that D_S does provide an objective and robust measurement of signal complexity that is dependent on flow pattern.

Table 5.8 Summary of successful D_S measurements

Pipe arrangement	Flow patterns (a;b)	Signal Source	Range of D_S (a;b respectively)	Relevant Figure no.
Horizontal 50mm pipe	Slug;Plug	Lt*	≥9 ; ≤8	5.4
		Ap	=1 ; ≥2	5.3
Horizontal 406mm pipe	Slug;Wavy	γ	≤2 ; ≥3	5.20
Vertical 50mm pipe	Slug;Bubble	Lt	≥11 ; ≤8	5.8
		Ap	=1 ; ≥2	5.12
Vertical 25mm pipe	Slug;Bubble	Lt	≥6 ; ≤5	5.18
		Ap	=1 ; ≥2	5.12

Ap - Absolute pressure transducer Lt - Light transducer γ - Gamma ray densitometer * 4% failure rate

Other measures which successfully showed a significant change in behaviour with a change in flow pattern for the various pipe orientations are summarised in Table 5.9.

Table 5.9 Summary of successful measures other than D_s

Pipe arrangement	Successful Measures(Signal Source)	Relevant Figure no. (respectively)
Horizontal 50mm pipe	*E* (Ap), *L* (Lt)	5.2, 5.1
Horizontal 406mm pipe	*E* (γ)	5.20
Vertical 50mm pipe	*E* (Ap), *L* (Ap), *V* (Ap)	5.2. 5.11, 5.10
Vertical 25mm pipe	*E* (Lt), *L* (Lt), D_p (Lt), *V* (Ap)	5.16, 5.17, 5.19, 5.10

Ap - Absolute pressure transducer Lt - Light transducer γ - Gamma ray densitometer

These other measures are less robust than D_s (comparing Table 5.8 with Table 5.9). As can be seen the measure E is the next most consistent measure, but it is not consistent for one type of transducer (unlike D_s).

§5.8.1 Trends in the behaviour of successful discriminating measures

The figures presented in this chapter show the behaviour of the successfully discriminating measures with significant changes in behaviour that correlate with flow pattern change.

D_s indicates that light signals are more complex for vertical or horizontal slug flows than the bubble or plug flows. This suggests that the slug structures introduce a more complex contribution to the these signals than was estimated in the simulations of Section 4.10. The behaviour is consistent with the trends shown in D_p and D_δ applied to the light and ultrasonic transducers. This is a clear indication of a more complex signal content for these transducers for slug flows. For the absolute pressure signals from horizontal slug/plug flows and vertical slug/bubble flows the opposite trend is observed (Figures 5.3 and 5.12). This suggests that the interaction of a slug on the absolute pressure transducer introduces a simplification to the signal. From considering the example signals in Figure 3.6 this is consistent, since the slug arrivals introduce a simplification to the signal structure by reducing the proportion of system noise in the signal. This follows the behaviour demonstrated by the theoretical simulations given in Section 4.10 for the D_s and D_p measures.

The magnitude of D_s for the light signals from the bubble or plug flows in the different pipes varies and is not particularly consistent. This is likely to be because different delay times were used. Very approximate estimates of the embedding dimension of the

processes governing the light transducer signals could be suggested as of the order of 5 for plug/bubble flows and of the order of 10 for slug flows.

Trends in the statistical measures are somewhat easier to explain since the contribution of each individual signal point measurement can be visualised. Non-linear measures are more reliant on contributions from a whole series of neighboring points which become near impossible to visualise when dealing with complex signals. This limits the possibility of interpreting generalised explanations from the results of the chaos measures.

The larger values of L for light signals from plug flows (Figure 5.1) are a result of the signal spending more time above a normalised value of 600 (see equation (5.4)) during a clear plug than during a frothy slug. Similar behaviour exists in the vertical flow cases (Figures 5.14 and 17). For the absolute pressure signals from the 50mm vertical pipe it can be seen from Figure 3.6 that more signal points are above the normalised value of 600 during the slug flow, which is consistent with the results shown in Figure 5.11.

The larger values of E for absolute pressure signals from plug/bubble flows (Figure 5.2) in the 50mm horizontal and vertical pipe are a result of the plug/bubble structures producing larger disturbances to the transducer behaviour than slugs structures (Figure 3.6). The light signals in the 25mm pipe (Figure 3.8) clearly show many more fluctuations during slug flow than for bubble flow which is reflected in the values shown in Figure 5.16. From the γ-ray signals shown in Figure 5.20 it is clear that the normalised stratified wavy flows contain many more fluctuations than in the slug flow signals which is consistent with the behaviour of E (which is higher for the stratified flows) shown in Table 5.7.

The measure V from absolute pressure signals from vertical flows has larger values during the slug flows.

§5.8.2 Measures and signals appropriate for flow regime identification

The measure that changes most consistently with a change in flow pattern and could therefore be used to discriminate between flow patterns is the measure D_S, computed using singular value decomposition and described in Section 4.7. Because of this consistent behaviour it is possible that D_S could be used to help classify flow patterns and possibly to aid the development of nonlinear models of important multiphase flow variables.

The successfully used transducer signals were the light attenuation signals, the absolute pressure signals and the gamma-ray densitometer signals. The electrical conductance transducer was insufficiently sensitive to the small bubbles present in the frothy slugs. The small and large range differential pressure transducers were seriously affected by tapping arrangements and pipe vibration. Improvements may be made by introducing signal filtering and by the use of more rigid and narrower tubes between the test section and pipe walls.

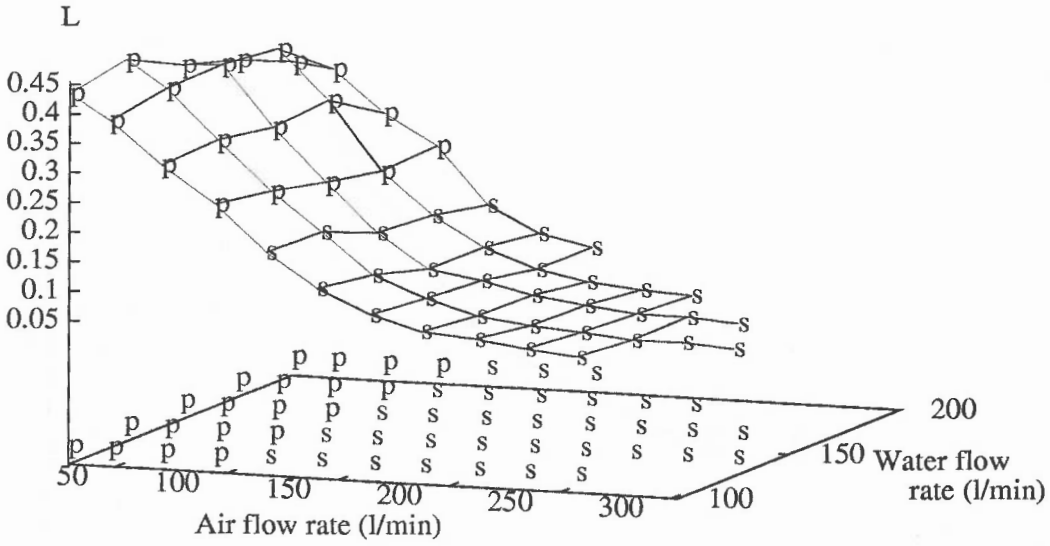

Figure 5.1 L From Light tranducer signals
(Horizontal 50mm pipe)

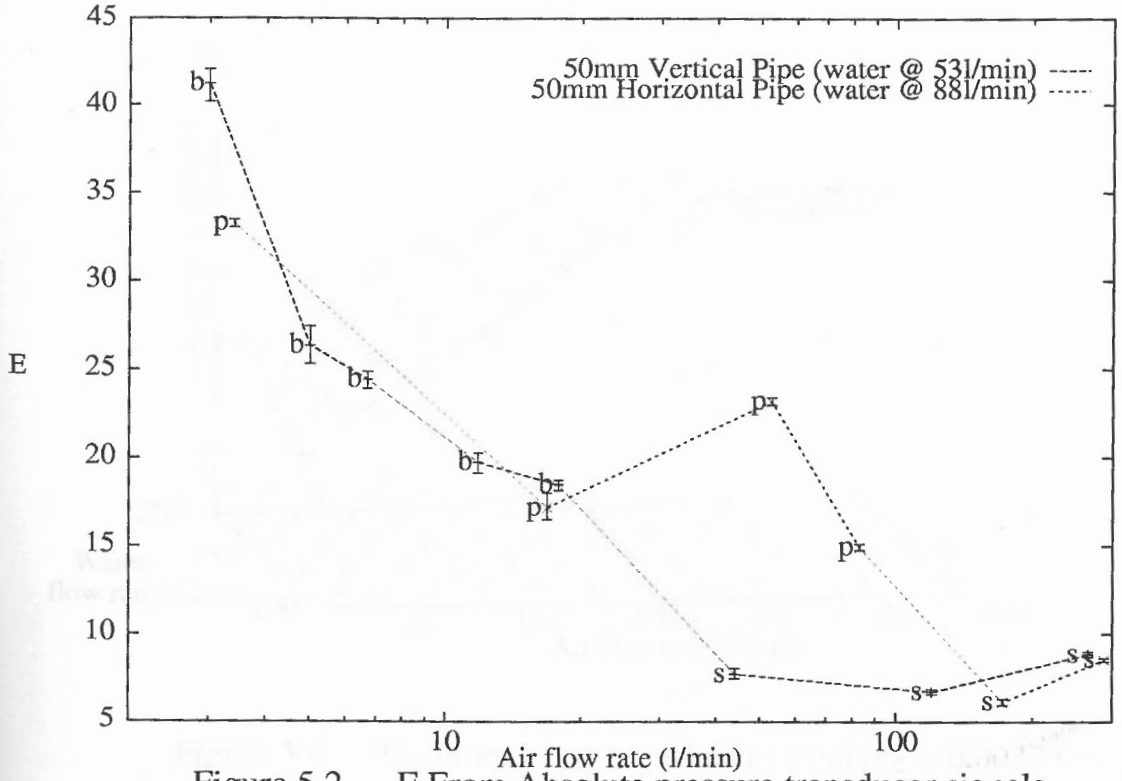

Figure 5.2 E From Absolute pressure transducer signals

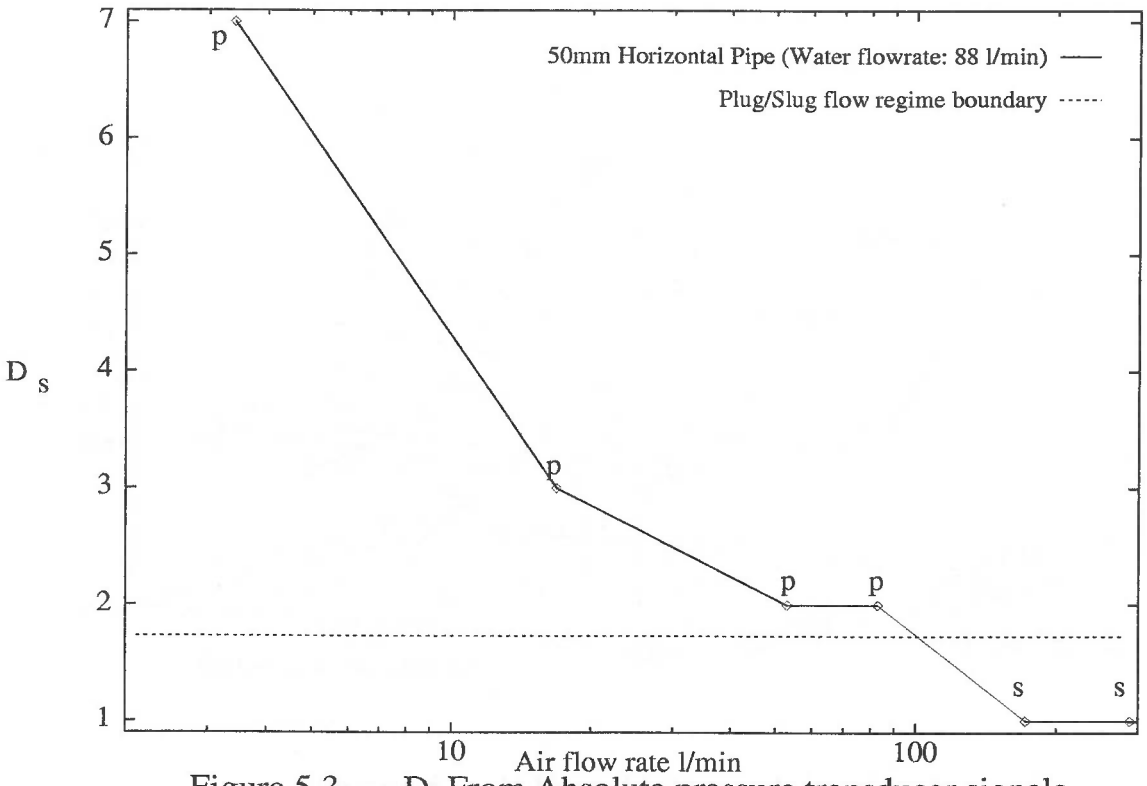

Figure 5.3 D_S From Absolute pressure transducer signals (τ =0.00275s)

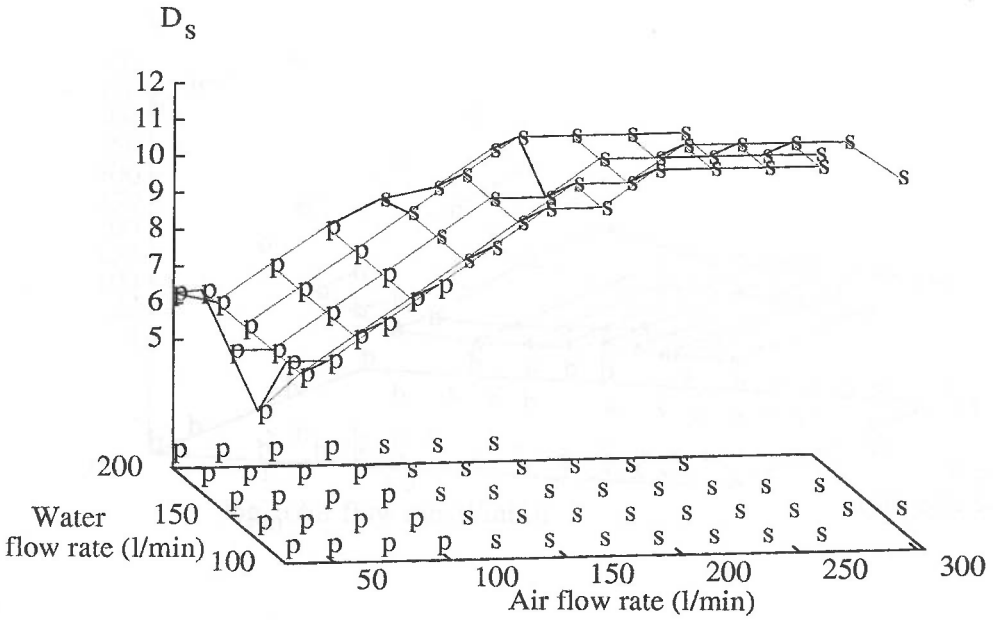

Figure 5.4 D_S From Light transducer signals (τ = 0.00375 s) (Horizontal 50mm pipe)

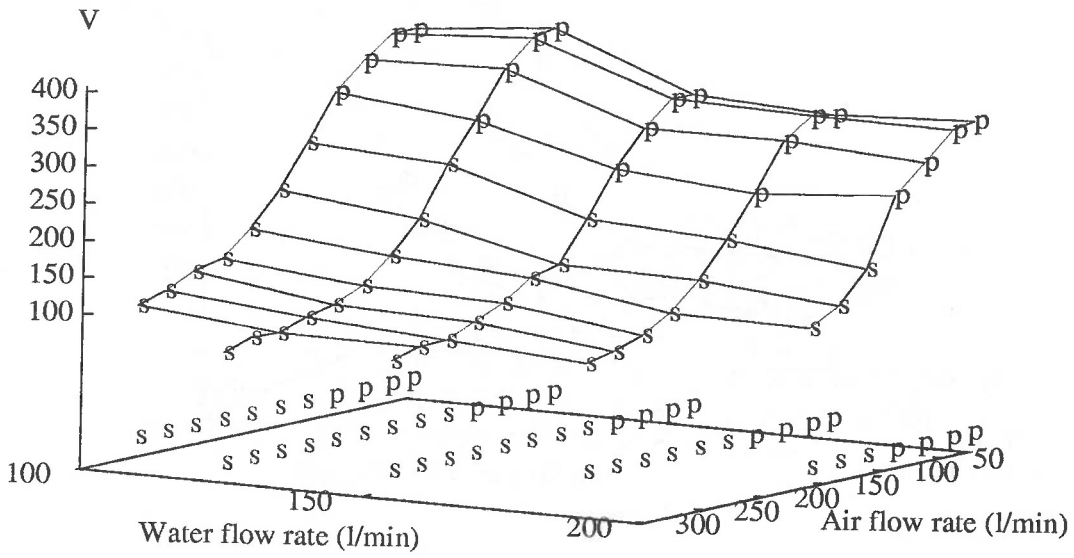

Figure 5.5 V From Light tranducer signals
(Horizontal 50mm pipe)

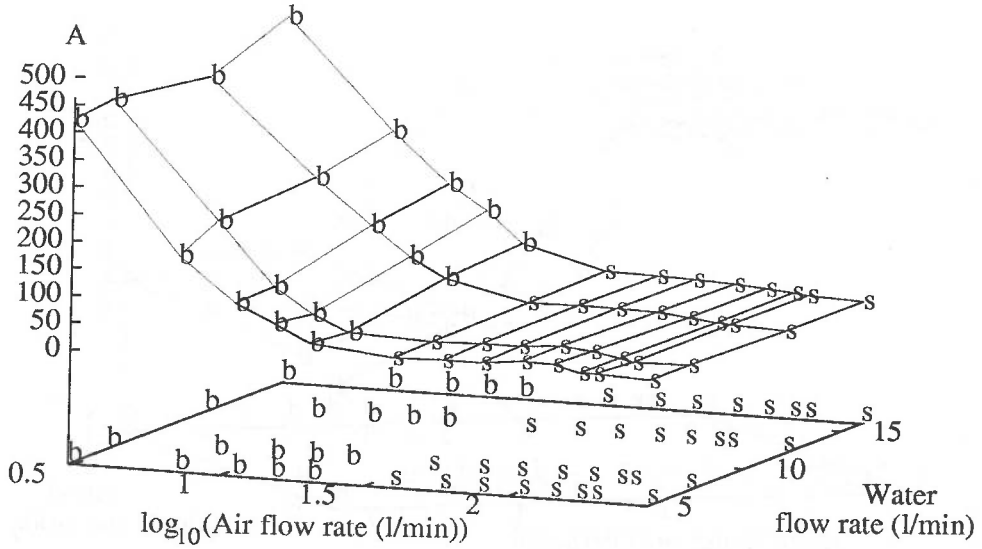

Figure 5.6 A From Light transducer signals
(Vertical 50mm pipe)

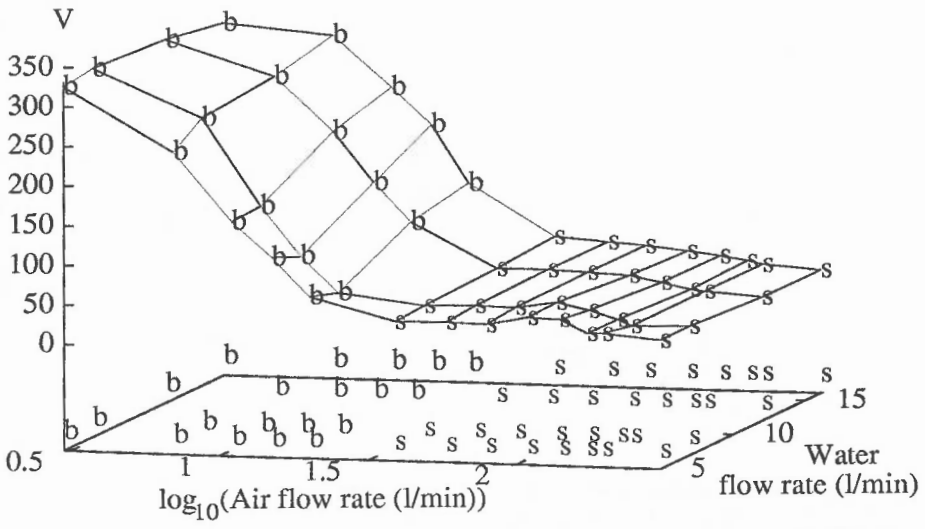

Figure 5.7 V From Light transducer signals
(Vertical 50mm pipe)

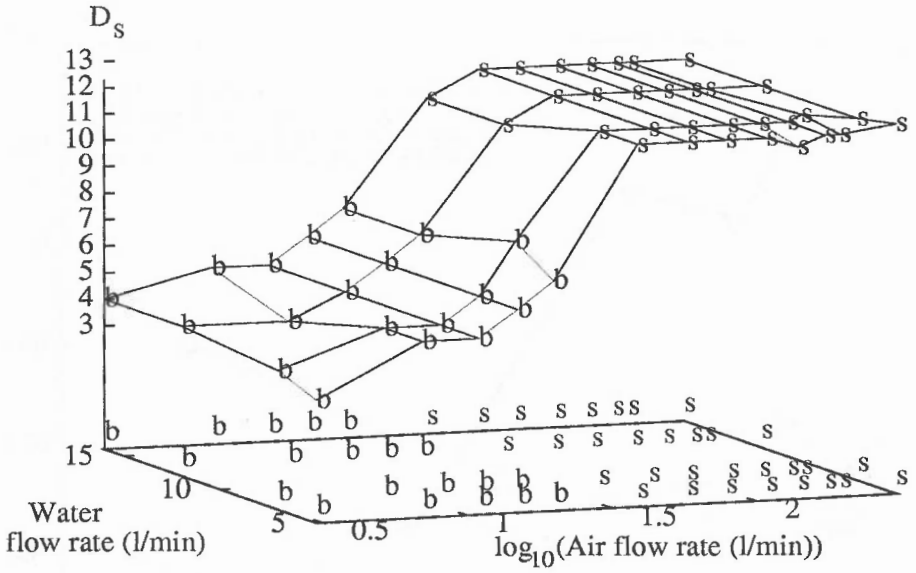

Figure 5.8 D_S From Light transducer signals
(Vertical 50mm pipe)

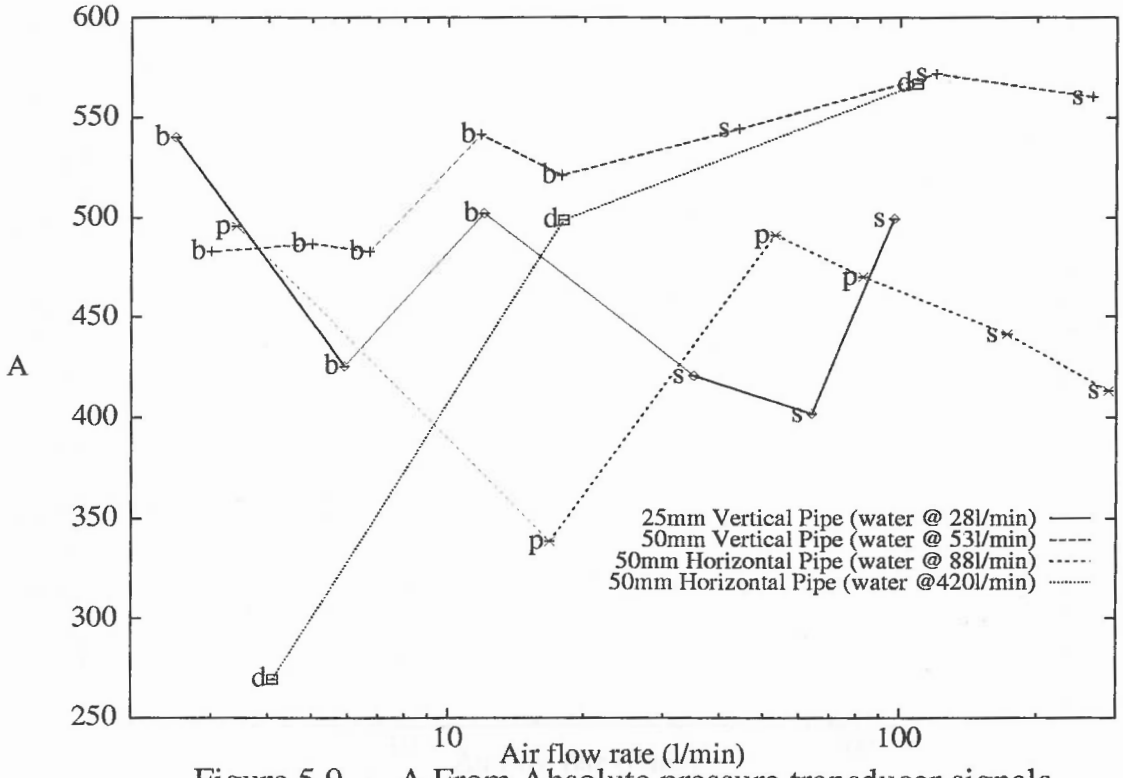

Figure 5.9 A From Absolute pressure transducer signals

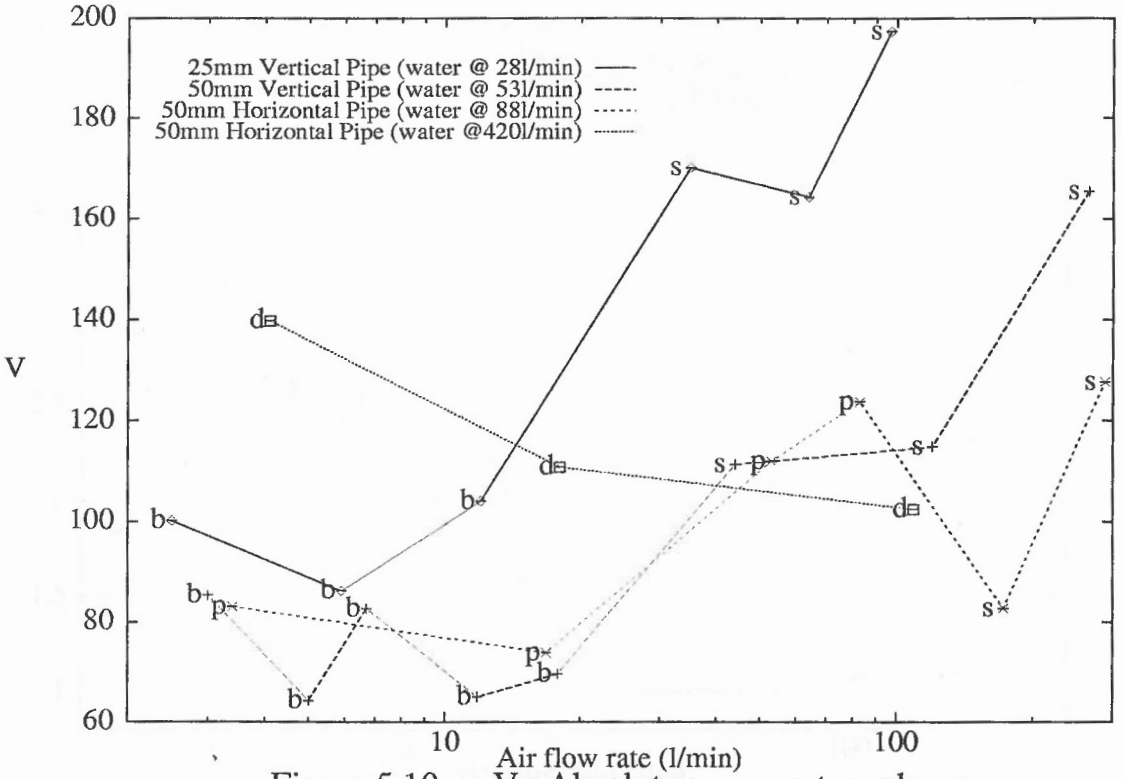

Figure 5.10 V : Absolute pressure transducer

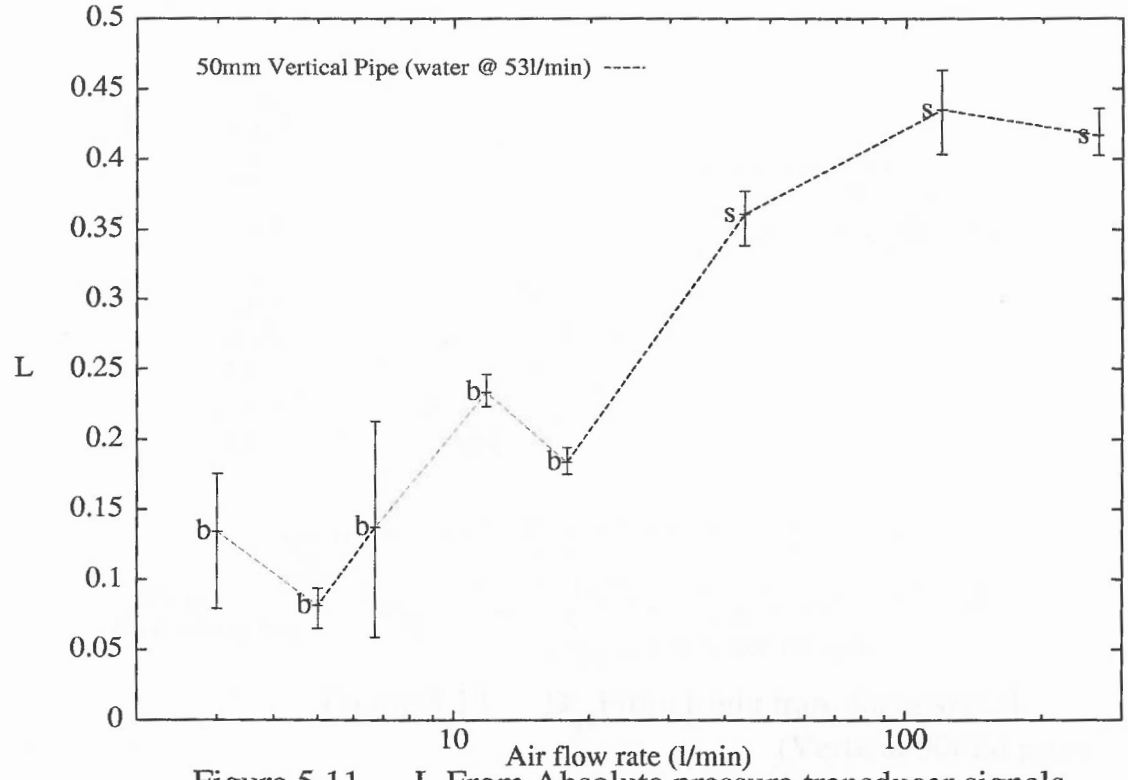

Figure 5.11 L From Absolute pressure transducer signals

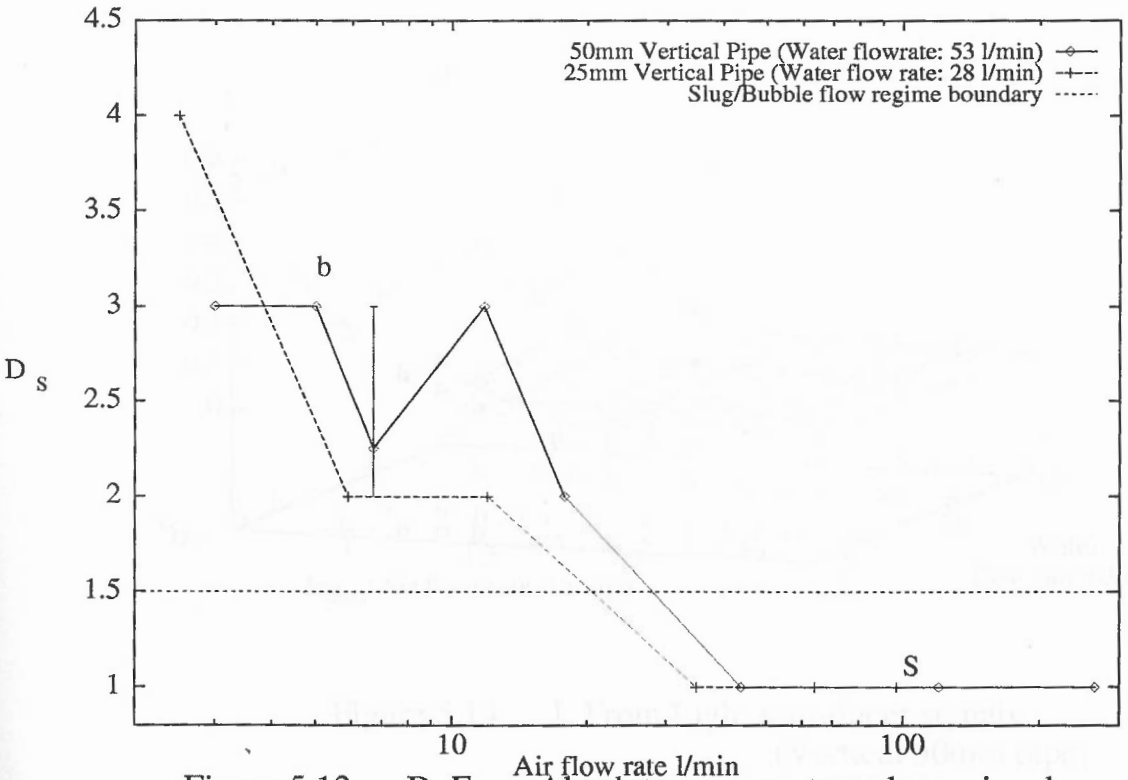

Figure 5.12 D_S From Absolute pressure transducer signals

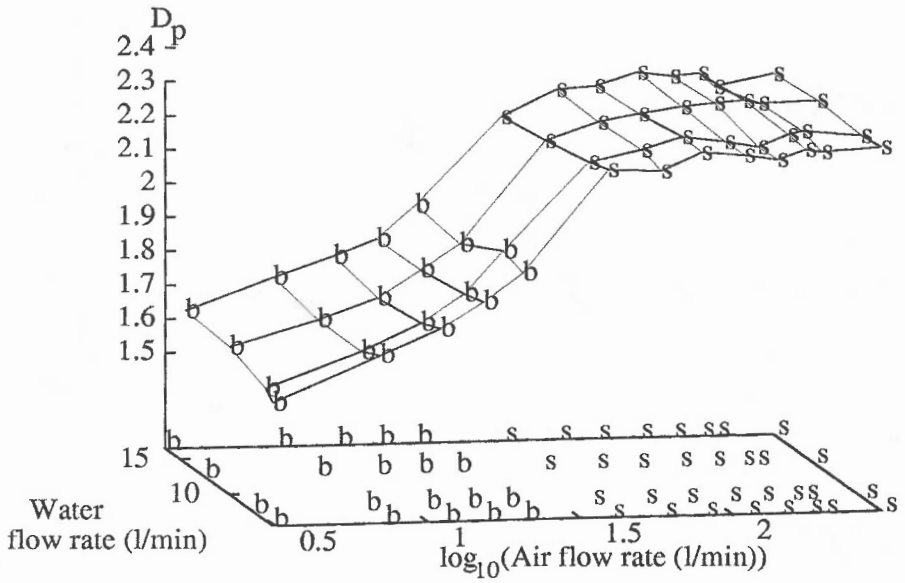

Figure 5.13 D_p From Light transducer signals
(Vertical 50mm pipe)

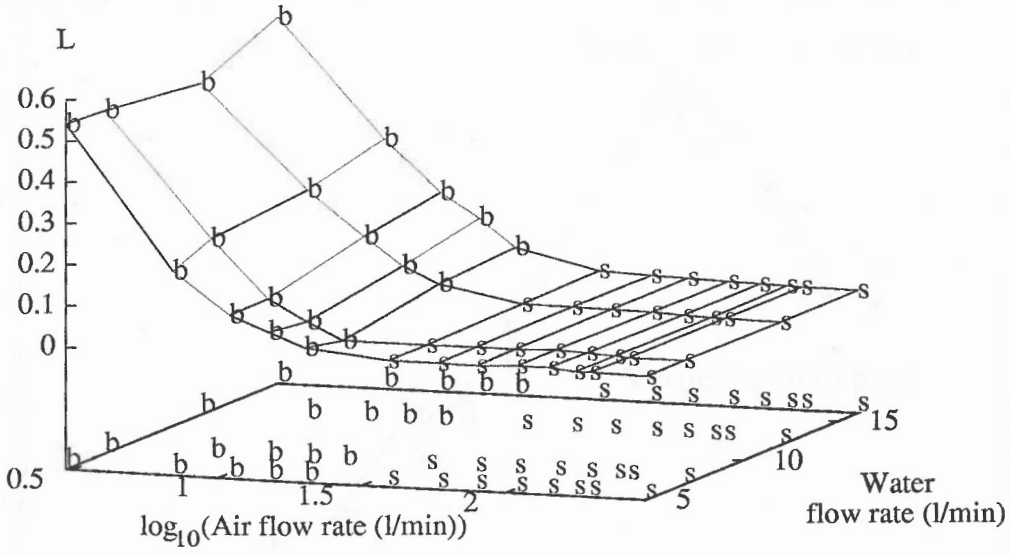

Figure 5.14 L From Light transducer signals
(Vertical 50mm pipe)

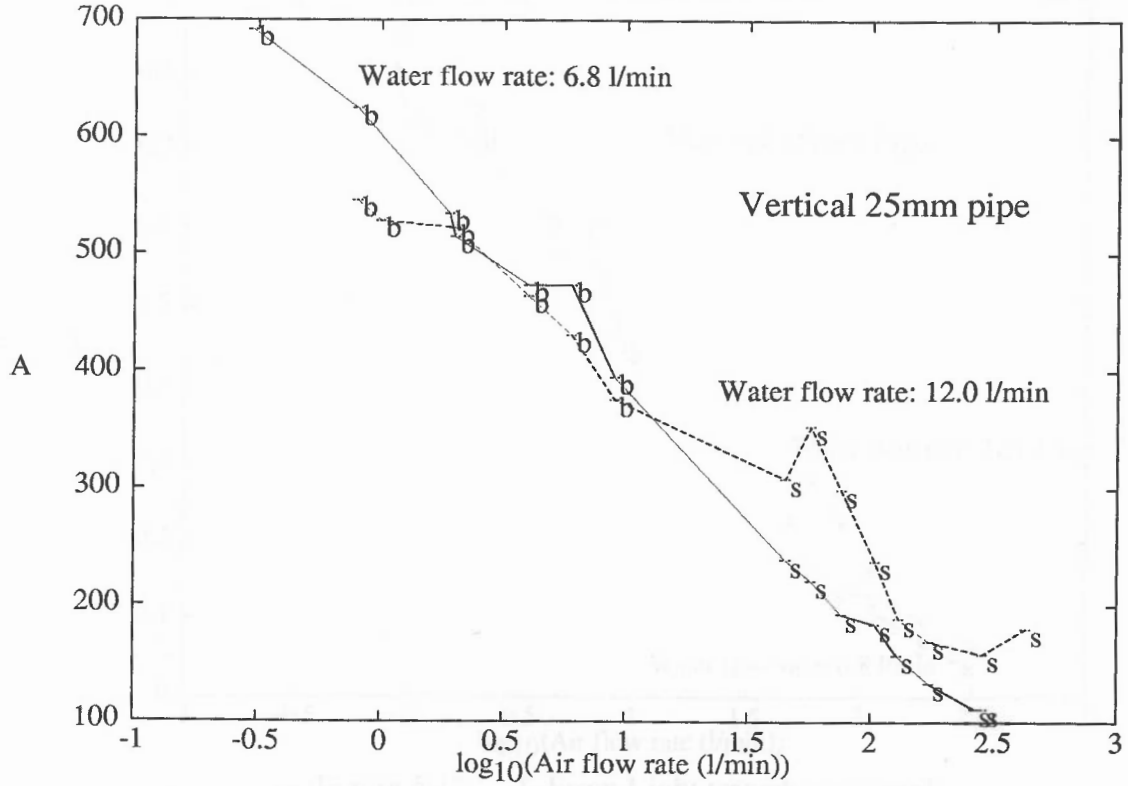

Figure 5.15 A From Light transducer signals

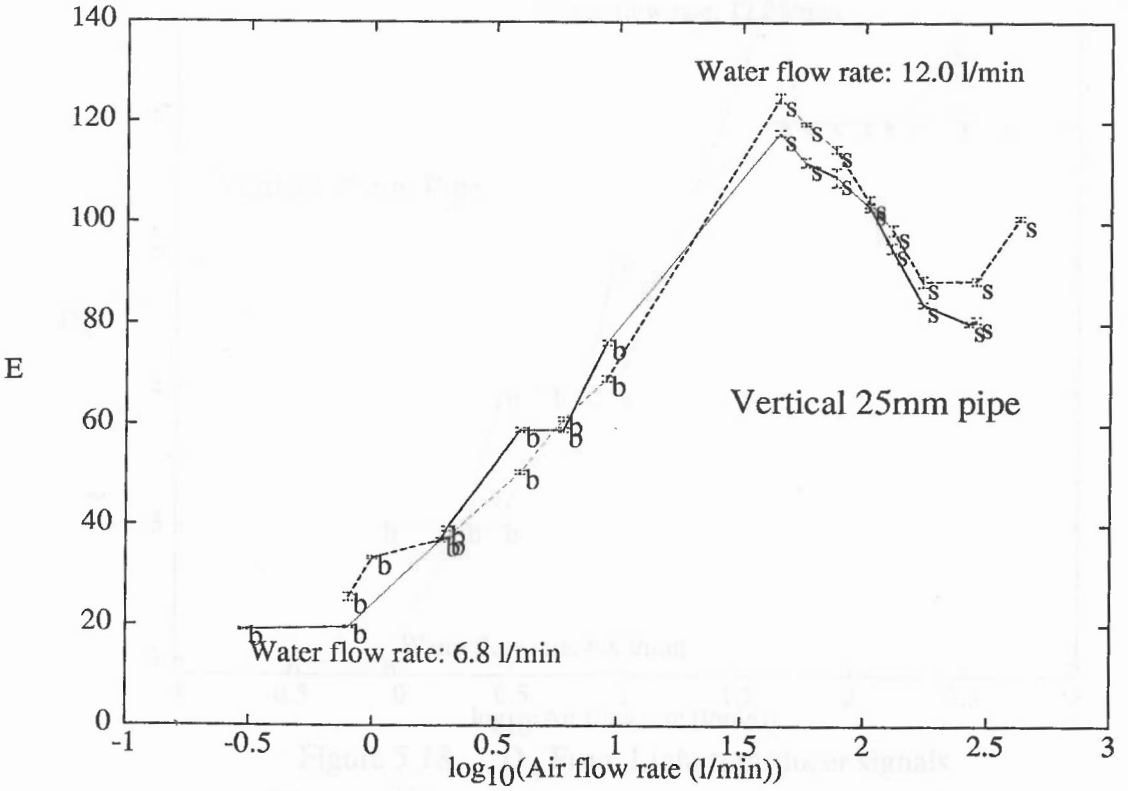

Figure 5.16 E From Light transducer signals

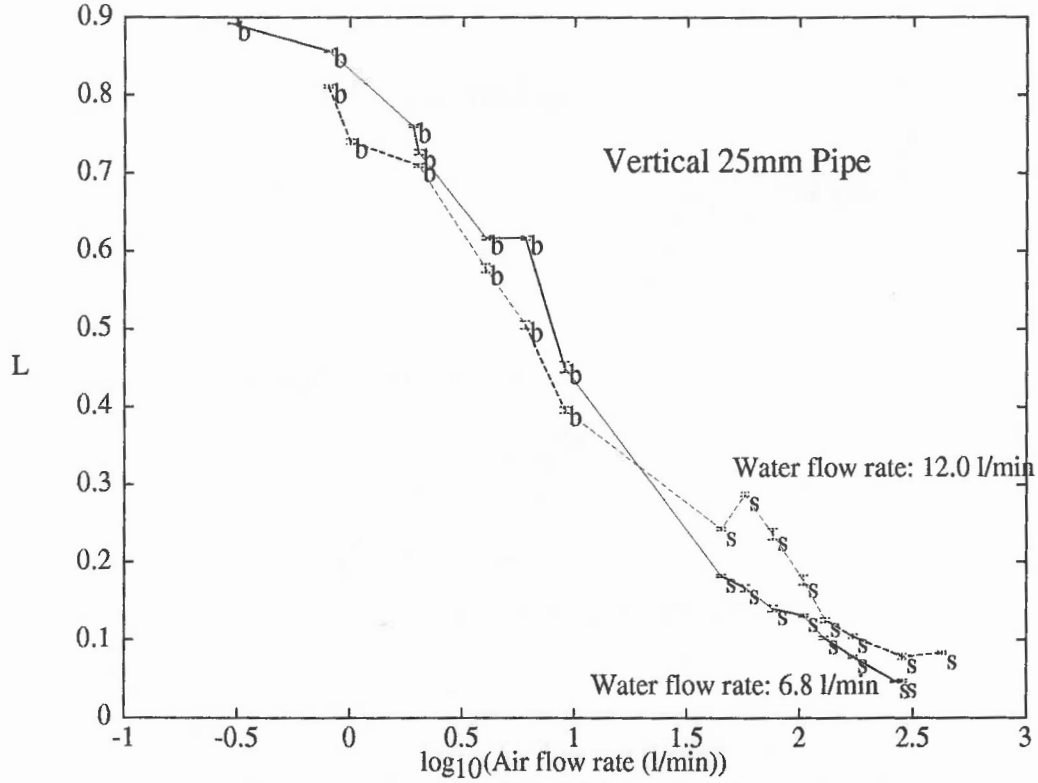

Figure 5.17 L From Light transducer signals

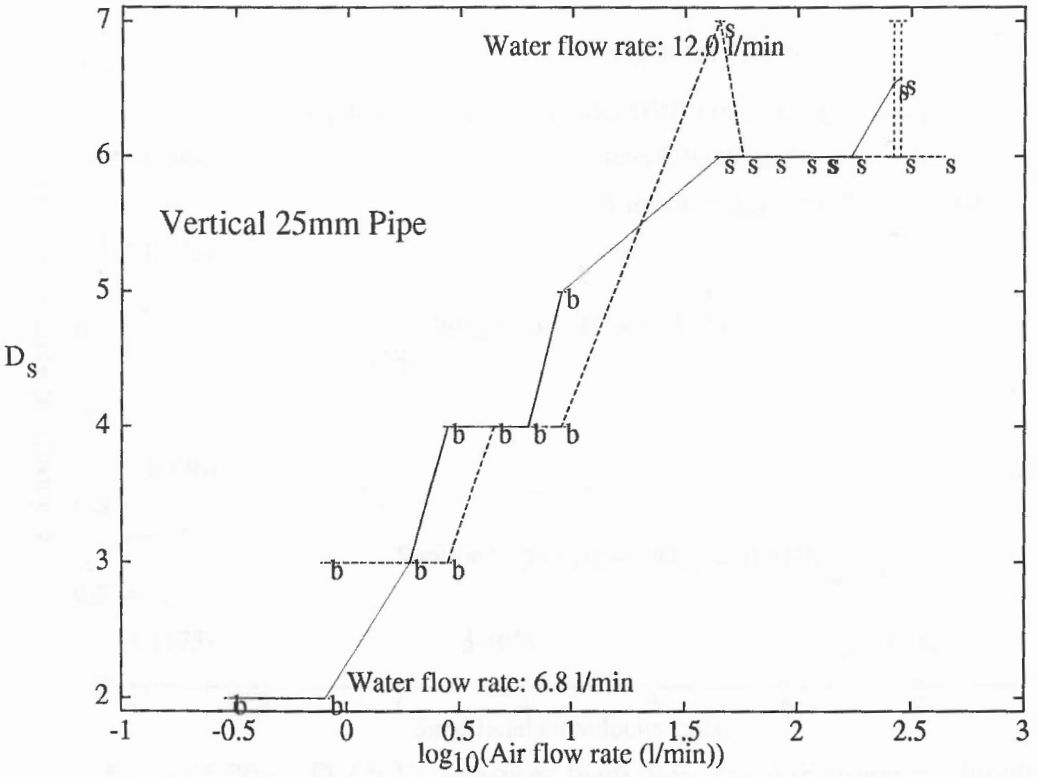

Figure 5.18 D_S From Light transducer signals

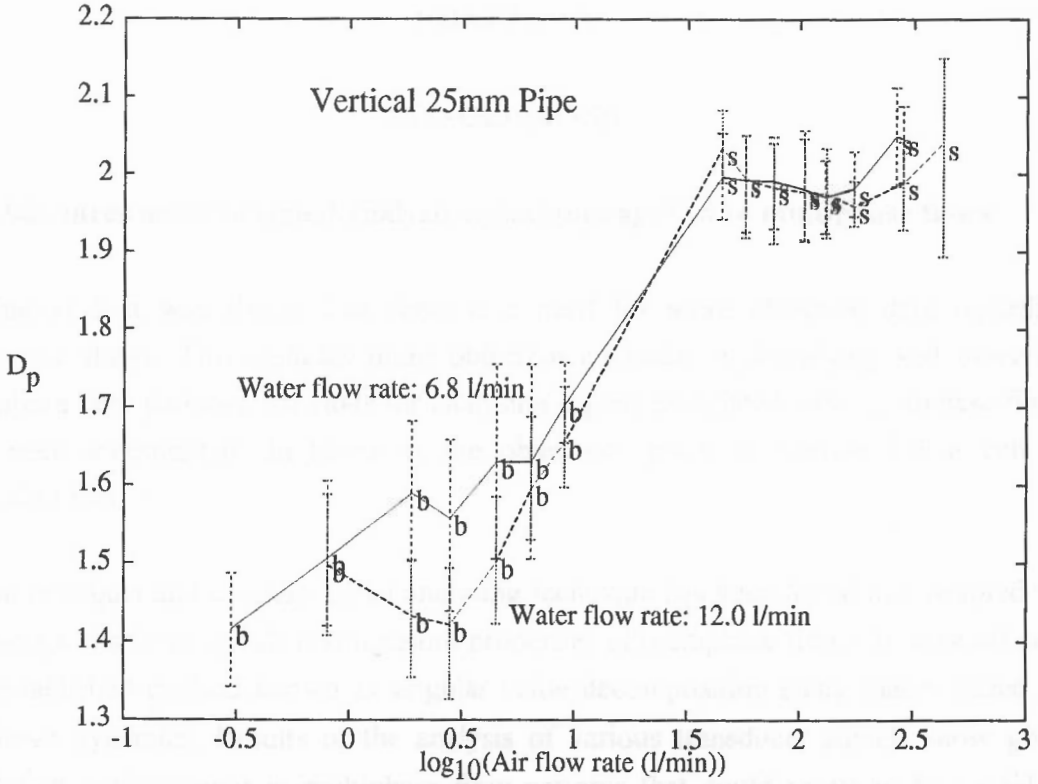

Figure 5.19 D_p From Light transducer signals

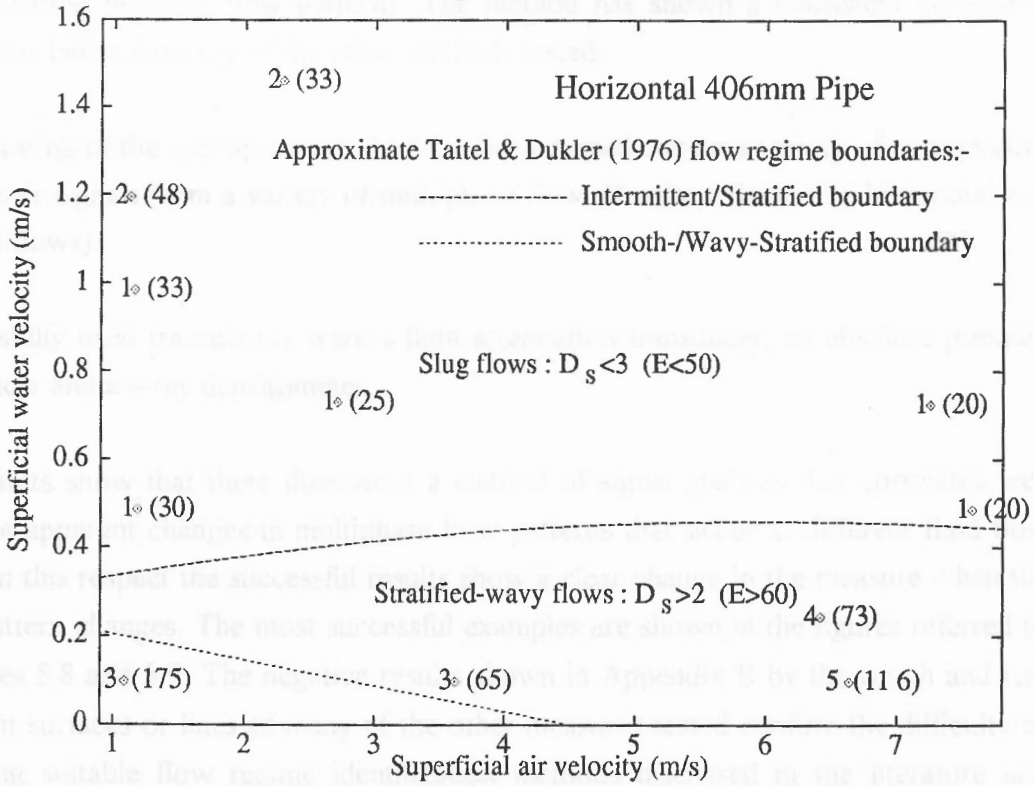

Figure 5.20 D_s(& E) measures from the γ-ray densitometer signals

CHAPTER 6

CONCLUSIONS

§6.1 Advances made in signal analysis techniques applied to multiphase flows

In Chapter 2 it was shown that there is a need for more objective data regarding multiphase flows. This includes more objective methods of classifying and detecting multiphase flow patterns. Methods for analysing signals associated with multiphase flows have been investigated. In terms of the objectives given in Section 2.3 it can be concluded that :-

- A more robust and efficient signal analysing technique has been found and adapted for analysing transducer signals that measure properties of multiphase flows. It is based on a well established method known as singular value decomposition using theory based on non-linear dynamics. Results of the analysis of various transducer signals show good correlation with changes in multiphase flow patterns that could prove to be useful in discriminating between flow patterns. The method has shown a consistent behaviour, noticeably better than any of the other methods tested.

- The testing of the appropriate method has been carried out on a variety of non-invasive transducer signals from a variety of multiphase flow situations (including horizontal and vertical flows).

Successfully used transducers were a light attenuation transducer, an absolute pressure transducer and a γ-ray densitometer.

The results show that there does exist a method of signal analysis that correlates well with the apparent changes in multiphase flow patterns that occur at different fluid flow rates. In this respect the successful results show a clear change in the measure when the flow pattern changes. The most successful examples are shown in the figures referred to in Tables 5.8 and 5.9. The negative results shown in Appendix B by the rough and less coherent surfaces or lines of many of the other measures tested confirm the difficulty of obtaining suitable flow regime identification methods discussed in the literature and referred to in Chapter 2.

The analysis method which provides the measure D_S that displays most clearly a behaviour which is related to the flow pattern is singular value decomposition (described in Section 4.7). From the measurements that have been carried out by the author this method seems robust, though further testing on more signals is obviously required. The relevant measure, D_S, has a high value associated with light attenuation transducer signals from slug flow (where many small bubbles in the frothy structures produce many peaks) and a lower value with plug or bubble type flow signals (where highly complex frothy structures are not present). With gamma-ray signals D_S is high for wavy flows and is lower for slug type flows where the intermittent slugs introduce a simplification of the signals. With the absolute pressure transducer signals D_S=1 for all the slug flows and $D_S \geq 2$ for all the bubble or plug flows.

With regards to providing information that may be useful for the development of nonlinear models of two-phase flow behaviour the results presented by the author are limited, probably to the development of signal simulations rather than fluid dynamic modelling (which ultimately will only be achieved by sufficiently comprehensive computational fluid dynamics). This has been made apparent by the sensitivity of the signal processing methods to various parameters that have so far been chosen in a some what arbitrary manner. For singular value decomposition the parameters concerned are the delay time, τ, and the embedding dimension m. The author has used values that optimise the response of the measure, D_S, to flow pattern changes. Where unsuitable delay times caused poor discrimination a better value of τ was estimated using a simple, fast and robust method developed by the author (Section 4.9).

The measure, D_S, provides an improved method of objectively measuring the complexity of a signal from a multiphase phenomena for flow regime identification. It must also be pointed out that the estimation of D_S is very much faster than the more common methods that require the calculation of the correlation integral or a similar type of measure. The computational intensity of these methods is probably the reason that only a small amount of data has been produced in the literature. The faster estimation of D_S will enable more extensive and practical research to be carried out.

§6.2 Future work

Having concluded that singular value decomposition provides a measure of a suitable transducer signal that seems to be related to flow pattern a useful development would be to use it in conjunction with a system such as the neural networks developed by Toral

and Beg (1993), to improve the success rates obtained by such methods. The method employed by Toral and Beg (1993) requires the training of the neural networks using any measure that is likely to be dependent on the flow patterns and/or flow rates, thus that provided by SVD would be highly appropriate. Neural networks are trained by inputting large amounts of series of relevant parameters that can be distinguished between by possible subtle differences in the parameter values. A training algorithm is run to adjust the state of the network so that it produces an output that is related to patterns within the input data. This training takes many hours and requires large amounts of data from a great variety of input possibilities. Using the measure D_s as a network input parameter may improve the speed and efficiency of the neural network training process.

An improvement to the D_s measurement itself can be made. Currently it has been calculated as an integer since it represents the significant number of singular values of a matrix (see Section 4.7). However a non-integer value can be produced by calculating the intersection of the curve that passes through the points S_k/S_n and the threshold line which represents the cut off for significant singular values (refer to Figure 4.14). The non-integer value of the ordinate of this intersection point will provide a higher resolution measure, that is directly related to D_s. In fact it would be much more like a fractal dimension with the great advantage of being much more efficient to compute than most (this is due to the fundamental efficiency of the SVD process). The process of finding the intercept of the S_k/S_n curve with the threshold line will add negligible computation times. The improved resolution will enable better investigation of signal structure.

Improvements to the other signal processing methods described in Chapter 4 may make some of the other measures (such as D_δ and D_p) more effective at discriminating between flow pattern changes. The correlation integral method (giving D_δ) may well benefit from the use of signal filtering prior to analysis. This however would increase the already intensive amount of computational effort involved in the signal processing.

The estimation of the fractal measures known as Lyapunov exponents could be applied to signals. However the measurement process is more complicated and more computationally expensive than even the correlation integral calculations. It was for this reason that this method was not investigated by the author. An implementation of the method could have the following steps:

i) estimation of a suitable delay time using the method described in Section 4.9.1

ii) application of singular value decomposition to reconstruct the attractor a second time in the space described in Section 4.7.

iii) application of the correlation integral computation to find points in the second reconstructed attractor that are close together.

iv) estimation of the rate at which the trajectories from the points diverge away from each other along each axis of the space in which the second attractor is reconstructed.

The application of the analysis methods to more signals from a greater variety of flow conditions is also essential to the testing of these measurement techniques to evaluate further their reliability. Detailed analysis of the behaviour of fractal measures at flow regime transition boundaries will help classify regimes and may reveal characteristics that were previously unobserved, leading to better definitions of flow regimes.

REFERENCES

Abarbanel, H.D. & Kennel, M.B., 'Local false nearest neighbors and dynamical dimensions from observed chaotic data', Physics Review E **47** 3057-3068 (1993)

Acikgoz, M, Franca, F. & Lahey Jr., R.T., 'An experimental study of three-phase flow regimes', International Journal of Multiphase Flow **18** 327-336 (1992)

Akagawa, K., et al., Bulletin JSME **14** 447-469 (1971)

Annunziato, M., 'A measurement system for two-phase flow pattern recognition using statistical analysis', Proceedings Multiphase Flow and Heat Transfer 2nd International Symposium, Xi'an P.R.C., Xue-Jun Chen, Veziroglu, T.N. & Tien, C.L. (eds.) (Hemisphere, New York) 1990

Ashkuri, S. & Hill, T.J., 'Measurement of multiphase flows in crude oil production systems', Petroleum Review **Nov.** 14-16 (1985)

Baker, O., 'Simultaneous flow of oil and gas', Oil Gas Journal **26** 185-195 (1954)

Baker, R.C., 'Effects of non-uniform conductivity in electromagnetic flowmeters', Journal Physics D Applied Physics **3** 637-639 (1970)

Baker, R.C., 'Multi-phase flow moves on', Control & Instrumentation **21** 35-37 (1989)

Barnea, D., Shoham, O. & Taitel, Y., 'Flow pattern characterisation in two-phase flow by electrical conductance probe', International Journal of Multiphase Flow **6** 387-397 (1980)

Barnsley, M. F., Fractals Everywhere, (Academic Press, San Diego) 1988

Beg, N.A. & Toral, H., 'Off-site calibration of a two-phase pattern recognition flowmeter', International Journal of Multiphase Flow **19** 999-1012 (1993)

Beg, N.A., McNulty, J.G., Sheppard, C. & Frith, A., 'Non-intrusive multiphase metering using artificial neural networks', Proceedings 6th International Conference Multiphase Production, Wilson, A. (ed.) (Elsevier) 1993

Bernicot, M., Dhulesia, H. & Deheuvels, P., 'On fractal dimension and modelling of slug and bubble flow processes', Proceedings 6th International Conference Multiphase Production, Wilson, A. (ed.) (Elsevier) 1993

Brill, J.P. & Arirachakan, S.J., 'State of the art in multiphase flow', Journal Petroleum Technology **May** 538-541 (1992)

Broomhead, D.S. & King, G.P., 'Extracting qualitative dynamics from experimental data', Physica D **20** 217-236 (1986)

Bundick, W.T., 'A unified development of several techniques for the representation of random vectors and data sets', Report no. NASA TR R-398, NASA, Hampton, Va., USA, 1973.

Buzug, T. & Pfister, G., 'Optimal delay time and embedding dimension for delay-time coordinates by analysis of the global static and local dynamical behaviour of strange attractors', Physics Review A **45** 7073-7084 (1992[a])

Buzug, T. & Pfister, G., 'Comparison of algorithms calculating optimal embedding parameters for delay time coordinates', Physica D **58** 127-137 (1992[b])

Ciliberto, S. & Nikolaenko, B. 'Estimating the number of degrees of freedom in spatially extended systems', Europhysics Letters **14** 303 (1991)

Daubechies, I., 'Orthonormal bases of compactly supported wavelets', Communications Pure & Applied Maths. **41** 909-996 (1988)

Das, R.K. and Pattanayak, S., 'Electrical impedence method for flow regime identification in vertical upward gas-liquid two-phase flow', Measurement Science Technology **4** 1457-1463 (1993)

Delaye, J.M., 'Two phase flow measurement', Bulletin d'informations Scientifiques et Techniques - Commisariat a l'Energie Atomique **197** 5-20 (November 1974)

Ding, M., Grebogi, C., Ott, E., Sauer, T. & Yorke, J.., 'Plateau onset for the correlation dimension: When does it occur?', Physics Review Letters **70** 3872-3875 (1993)

Eckmann, J.-P. & Ruelle, D., 'Ergodic theory of chaos and strange attractors', Review Modern Physics **57**, 617-656 (1985)

Fabre, J. & Line, A., 'Modelling of two-phase slug flow', Annual Review Fluid Mechanics **24** 21-46 (1992)

Fowler, E., 'Interpretation of synthetic aperture radar images using fractal geometry', PhD Thesis, Cranfield University (1993)

Franca, F., Acikgoz, M., Lahey, Jr, R.T. & Clausse, A., 'An application of fractal techniques to flow regime identification', Proceedings 5th. International Conference on Multiphase Production, Burns, A. (ed.) (Elsevier) June 1991.

Franca, F. & Lahey Jr., R.T., 'The use of drift-flux techniques for the analysis of horizontal two-phase flows', International Journal of Multiphase Flow **18** 787-801 (1992)

Fraedrich, K. & Wang, R., 'Estimating the correlation dimension of an attractor from noisy and small datasets based on re-embedding', Physica D **65** 373-398 (1993)

Grassberger, P. and Procacia, I., 'Measuring the strangeness of strange attractors', Physica D **9** 189- (1983)

Grossman, A. & Morlet, J., 'Decomposition of Hardy functions into square integrable wavelets of constant shape', SIAM Journal Mathematical Analysis, **15** 723-736 (1984)

Hewitt, G.F., Flow regimes, Handbook of multiphase systems, Hetsroni, G. (ed.) (McGraw-Hill) 1982.

Hewitt, G.F., 'Transient multiphase flows - programme definition document', Marine Technology Directorate (MTD) Ltd. Managed Programme (11th May 1995)

Hewitt, G. F. & Hall-Taylor, N. S., Annular Two-Phase Flow (Pergamon Press) 1970.

Hewitt, G.F. & Jayanti, S., 'To churn or not to churn', International Journal of Multiphase Flow **19** 527-529 (1993)

Holden, A.V. (ed.), Chaos (Princeton University Press) 1986

Hubbard, M. & Dukler, A., Proceedings Heat transfer & Fluid Mechanics Institute (Stanford University Press, California) 1966.

Huang, Y. & Huang, Y., 'On the transition to turbulence in pipe flow', Physica D **37** 153-159 (1989)

Jones, O. & Zuber, N., 'The interrelation between void fraction fluctuations and flow patterns in two-phase flow', International Journal of Multiphase Flow **2** 273-306 (1975)

King, C.H., Ouyang, M.S., Pei, B.S., 'Identification of 2-phase flow regimes by neutron noise-analysis', Nuclear Technology **86** 70-75 (1989)

Kosterin, S.I., Izv. Akad. Nauk SSSR, Otdel Tekh. Nauk **12** 1824-1830 (1949)

Kraft, R., 'Multiphase flow in electromagnetic flowmeters', PhD Thesis, Cranfield University (1994)

Lawkins, W.F., Daw, C., Downing, D. & Clapp Jr., N., 'Role of low-pass filtering in the process of attractor reconstruction from experimental chaotic time series', Physics Review E, **47** 2520-2535, (1993)

Leducq, D. & Hervieu, E., Proceedings 5th. International Conference on Multiphase Production, Burns, A. (ed.) (Elsevier) June 1991.

Lorenz, E.N., 'Deterministic nonperiodic flow', Journal of Atmospheric Science **20** 130-141 (1963)

Lubbesmeyer, D. & Leoni, B., 'Fluid-velocity measurements and flow-pattern identification by noise-analysis of light beam signals', International Journal of Multiphase Flow **9** 665-679 (1983)

Lusseyran, F., 'Caractéristiques cellulaires du régime à poches en écoulement gaz-liquide co-courant vertical. Transition vers le régime déstructuré', Thèse Inst. Natl. Polytech. Lorraine, Nancy, France (1990)

Mallat, S., 'A theory for multiresolution signal decomposition: The wavelet representation', IEEE Transactions Pattern Analysis & Machine Intelligence, **11** 674-693 (1989)

Mandelbrot, B.B., Fractals: Form, chance and dimension (W.H. Freeman & Co., San Francisco) 1977.

Mandelbrot, B.B. & Van Ness, J.W., 'Fractional Brownian motion, fractional noises and applications', S.I.A.M. Review **10** 422-437 (1968)

Mandhane, J.M., Gregory, G.A. & Aziz, K., 'Flow pattern map for gas-liquid flow in horizontal pipes', International Journal of Multiphase Flow **1** 537-553 (1974)

Mao, Z.S. & Dukler, A.E., 'The myth of churn flow', International Journal of Multiphase Flow **19** 377-383 (1993)

Matsui, G., 'Identification of flow regimes in vertical gas-liquid two-phase flow using differential pressure fluctuations', International Journal of Multiphase Flow **10** 711-720 (1984)

Midttveit, Ø., Berge, V., Dykesteen, E., 'Multiphase flow metering using capacitance transducer and multivariate calibration', Modeling, Identification & Control **13** 65-76 (1992)

Nishikawa, K., Sekoguchi, K. & Fukano, T., 'On the pulsation in gas-liquid two-phase flow', Bulletin JSME **12** 1410-1416 (1969)

Oddie, G.M., 'The characterisation of multicomponent (liquid) flows using scattered ultrasound', PhD Thesis, Cranfield Institute of Technology (1992)

Parlitz, U., 'Identification of true and spurious Lyapunov exponents from time series', International Journal of Bifurcation & Chaos **2** 155 (1992)

Prechner, P.B., 'Texture models in coherent imaging', PhD Thesis, Cranfield University (1993)

Rössler, O.E., 'An equation for continuous chaos', Physics Letters A **57** 397 (1976)

Sæther, G., Bendiksen, K., Müller, J. and Frøland, E., 'The fractal statistics of slug lengths', International Journal of Multiphase Flow **16** 1117-1126 (1990)

Savit, R. & Green, M., 'Time series and independent variables', Physica D **50** 95-116 (1991)

Spedding, P.L. & Nguyen, V.T., 'Regime maps forair-water two phase flow', Chemical Engineering Science **35** 779-793 (1980)

Spedding, P.L. & Spence, D.R., 'Flow regimes in two-phase gas-liquid flow', International Journal of Multiphase Flow **19** 245-280 (1993)

Stelter, P. & Pfingsten, T., 'Calculation of the fractal dimension via the correlation integral', Chaos, Solitons & Fractals **1** 273-280 (1991)

Strang, G., 'Wavelets and dilation equations: a brief introduction', SIAM Review **31** 614-627 (1989)

Takens, F., 'Detecting strange attractors in turbulence', Lecture notes in Mathematics **898** (Springer) 1981.

Taitel, Y. & Dukler, A.E., 'A model for predicting flow regime transitions in horizontal and near-horizontal flow' American Institute of Chemical Engineering Journal **22** 47-55 (1976)

Tam, S.W. & Devine, M.K. 'A study of fluidized-bed dynamical behaviour: a chaos perspective', Applied Chaos, Jong, H. K. & Stringer, J. (eds.) (Wiley & Sons, Inc.) 1992.

Tutu, N., 'Pressure fluctuations and flow pattern recognition in vertical 2 phase gas-liquid flows', International Journal of Multiphase Flow **8** 443-447 (1982)

Vitsikounaki, D., 'Fractal techniques for the interpretation of multiphase flow', MSc Thesis, Imperial College of Science, University of London (1995)

Vince, M.A. & Lahey Jr., R.T., 'On the development of an objective flow regime indicator', International Journal of Multiphase Flow **8** 93-124 (1982)

Wang, S.K., Lee, S.J., Jones Jr, O.C., Lahey Jr, R.T., 'Statistical analysis of turbulent two-phase pipe flow', Journal Fluids Engineering **112** 89-95 (1990)

Weisman, J., Duncan, D., Gibson, J. & Crawford, T., 'Effects of fluid properties and pipe diameter on two-phase flow patterns in horizontal lines', International Journal of Multiphase Flow **5** 437-462 (1979)

Wolf, A., Swift, J.B., Swinney, H.L., & Vastano, J., 'Determining Lyapunov exponents from a time series', Physica D**16** 285-316 (1985)

Wood, D.G., 'Slug Flow - occurrence, consequences and prediction', Proceedings 6th International Conference Multiphase Production, Wilson, A. (ed.) (Elsevier) 1993

Xie, C.G., Plaskowsi, A. & Beck, M.S. '8-electrode capacitance system for 2-component flow identification. 2. flow regime identification', IEE Proceedings **136** 184-190 (1989)

APPENDIX A

Computation of the correlation integral, $C_m(r)$

A simplistic implementation of the definition of $C_m(r)$ given by equation (4.6) is very computationally intensive and therefore not very practical, particularly when large data sets are analysed. This is because every x_i is compared with all others in the data set to obtain the separation between points on the attractor. Particularly for experimental data it is often important to maximise the size of the data set thus increasing the need for efficient computation.

A fast algorithm has been developed by the author which minimises the number of calculations of $|x_i-x_j|_{j\neq i}$. A list of the x_i's in order of their magnitudes is constructed. A pointer is then used that enables the neighbours, x_j, of a given x_i to be immediately accessed from the list. The pointer is constructed such that the x_j's giving the smallest $|x_i-x_j|$ are accessed first. Once a given $|x_i-x_j|$ has exceeded r all the other subsequent x_j's accessed by the pointer from the list are outside the r limit and therefore do not need to be used.

The flow charts which give the details of the list construction and calculation of $C_m(r)$ are shown in figures A.1 and A.2. The flow charts are drawn to make it easy to translate the chart into a computer program. The statements in the diamonds can be easily translated into 'if' statements. Statements of the form $x \rightarrow f(x)$ are to assign a new value, $f(x)$, to the variable x. Statements of the form $x=f(i)$, $i=a,..,b$ are to assign new values to x, looping through i starting from $i=a$ and ending at $i=b$.

Figure A.1 shows the construction of the following necessary pointers:

- p(k) (such that $x_{p(1)}$ is the smallest of the x_i's through to $x_{p(N)}$ being the largest of the x_i's),
- pp(k) (such that $x_{p(pp(i+j))}$ is the $|j|^{th}$ nearest x greater or less than x_i (depending on the sign of j)). It is this pointer that provides the main time saving mechanism.

Figure A.2 shows the use of the pointers for calculating the correlation integral. Before the computation the x_i's are normalised between 0 and 1023, hence r values (giving hypercube sizes) increase exponentially in powers of 2 starting from 1.

i is the index of the current x value. *sign* determines whether to check x's greater (*sign*=1) or lesser (*sign*=-1) in magnitude than x_i. pt1 points to the next largest or smallest x to x_i, where pt2 is the index of that x. Once this x_{pt2} (=x(pt2)) has been determined the separation of the (m'+1) dimensional attractor points (x_i,x_{i+1},..,$x_{i+m'}$) and (x_{pt2},x_{pt2+1},..,$x_{pt2+m'}$) can be calculated and compared with the hypercube sizes r=2^0,..,2^7. If the separation is less than r for m'<mx' then the intermediate integrals, $c'(m',r)$ are incremented. Incrementing the $c'(m',r)$ values is terminated as soon as possible. When a pair of points do not fit inside an m' dimensional hypercube then higher dimensional cubes and smaller cubes can be ignored. The largest dimension is set using the statement *mx'=m'* and the smallest hypercube is set using the statement *rmin=r*.

idf is a parameter that prevents counting points of an attractor that are close together simply because they are on parts of the trajectory that are close in time to each other (such counting would produce errors in the estimate of $C_m(r)$ from finite sized data sets). *mf* is the maximum embedding dimension used (*mx'* is an intermediate maximum that can be reduced to save computation time). *rmin* is an intermediate minimum of r that can be increased for time saving.

The final computation which sums the intermediate $c'(m',r)$ values (m'=*mf*,..,1) uses the fact that m' dimensional points within an m' dimensional hypercube of side r also contain the correspondingly positioned m'-1 dimensional points within the m'-1 dimensional hypercube of side r.

This method improves the speed of computation of $C_m(r)$ by orders of magnitude.

APPENDIX B

Presentation of results

Many results have been computed showing the behaviour of the measures defined in Chapters 4 and 5. They are plotted as surfaces or lines showing the relationship between the measure related to some property of a transducer signal and the air and water flow rates producing a particular multiphase flow (which has been visually determined).

Most of the measurements resulted in lines or surfaces that often cross over the flow regime boundaries, apparent by jagged and messy lines with different flow pattern labels spreading over similar ranges of vertical axis coordinates. Such negative results show that the measure does not detect flow pattern dependent properties. Generally the measure D_δ showed very poor correlation (particularly when compared with the success of D_s). One reason may be because not enough data points were used in the D_δ computation, however this would only lengthen the already long computation process.

The large number of negative results show that flow patterns are an elusive quality to measure, classify and detect. This is also shown by the variety of classifications that have been made of multiphase flow phenomena in the literature (refer to Chapter 2). The successful measurements that the author has carried out are described in Chapter 5 and stand in stark contrast to the unsuccessful measurements as is easily seen by the difference in the shapes of the lines or surfaces. Successful measures show a marked change in the line or surface which correlates well with the flow pattern.

Figures B.1-B.30 show the measures A, V, E, L, D_δ, D_s and D_p estimated from large and small range pressure, light and electrical transducer signals (respectively) from the 50mm horizontal pipe.

Figures B.31-B.54 show the measures A, V, E, L, D_δ, D_s and D_p estimated from large range pressure, electrical and light transducer signals (respectively) from the 50mm vertical pipe.

Figures B.55-B.77 show the measures A, V, E, L, D_δ, D_s and D_p estimated from ultrasonic, light and large range pressure transducer signals (respectively) from the 25mm vertical pipe.

Because no correlation was found between the differential pressure transducer signal properties and flow patterns a set of measurements were made using an absolute pressure transducer which did not require pipes between the transducer and pipe wall. Figures B.78-B.85 show the measures A, V, E, L, D_δ, D_s and D_p estimated from the absolute pressure transducer signals from the 50mm horizontal pipe and the 25mm and 50mm vertical pipes. It was originally hoped that the signal processing techniques might detect structure in the rather messy and inadequate differential pressure transducers but this proved to be over optimistic. Much better flow regime detection was found with the absolute pressure transducer signals.

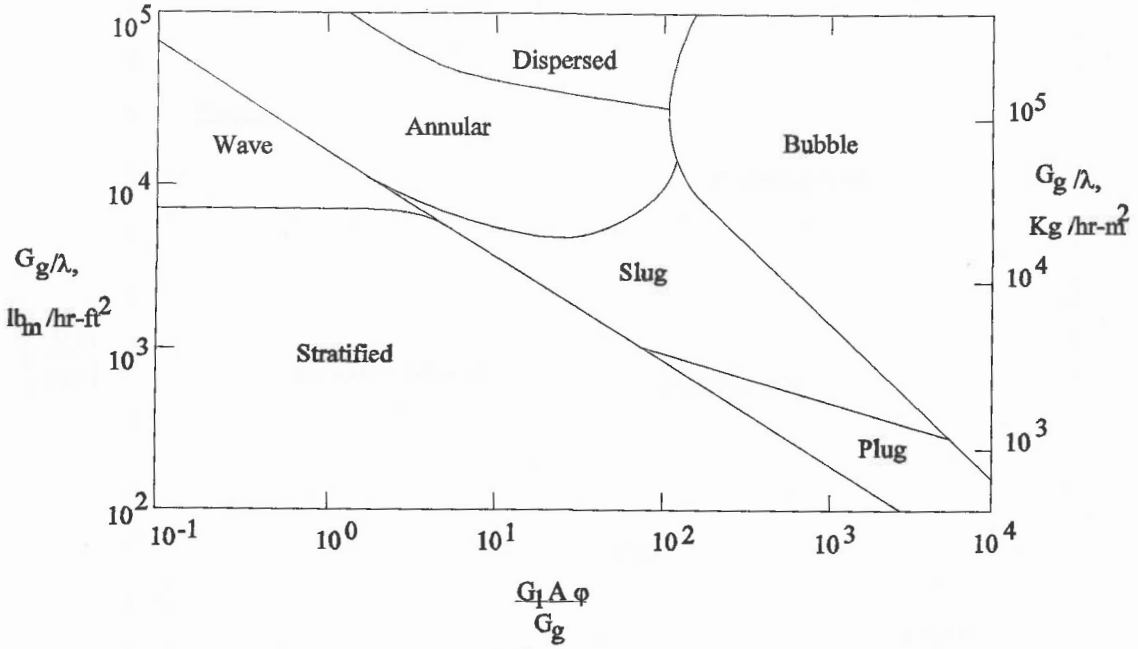

Figure 1.1 Baker (1954) horizontal gas-liquid flow regime map

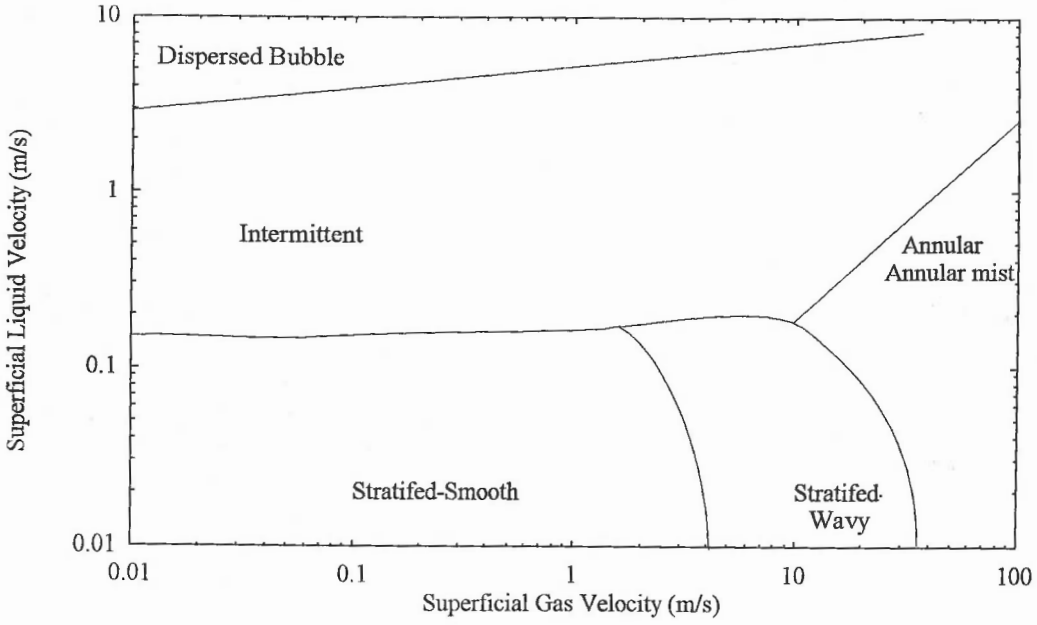

Figure 1.2 Taitel & Dukler (1976) gas-liquid flow regime map
(50mm horizontal pipe, air-water flows)

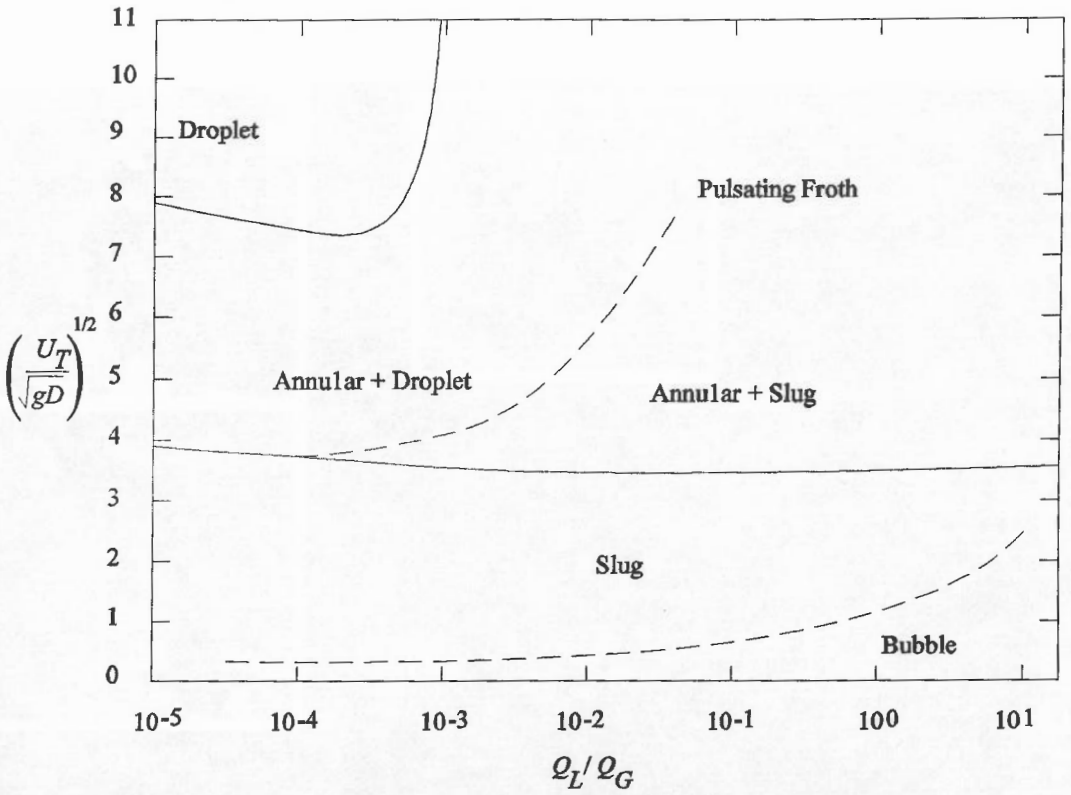

Figure 1.3 Spedding & Nguyen (1980) vertical upward air-water flow regime map

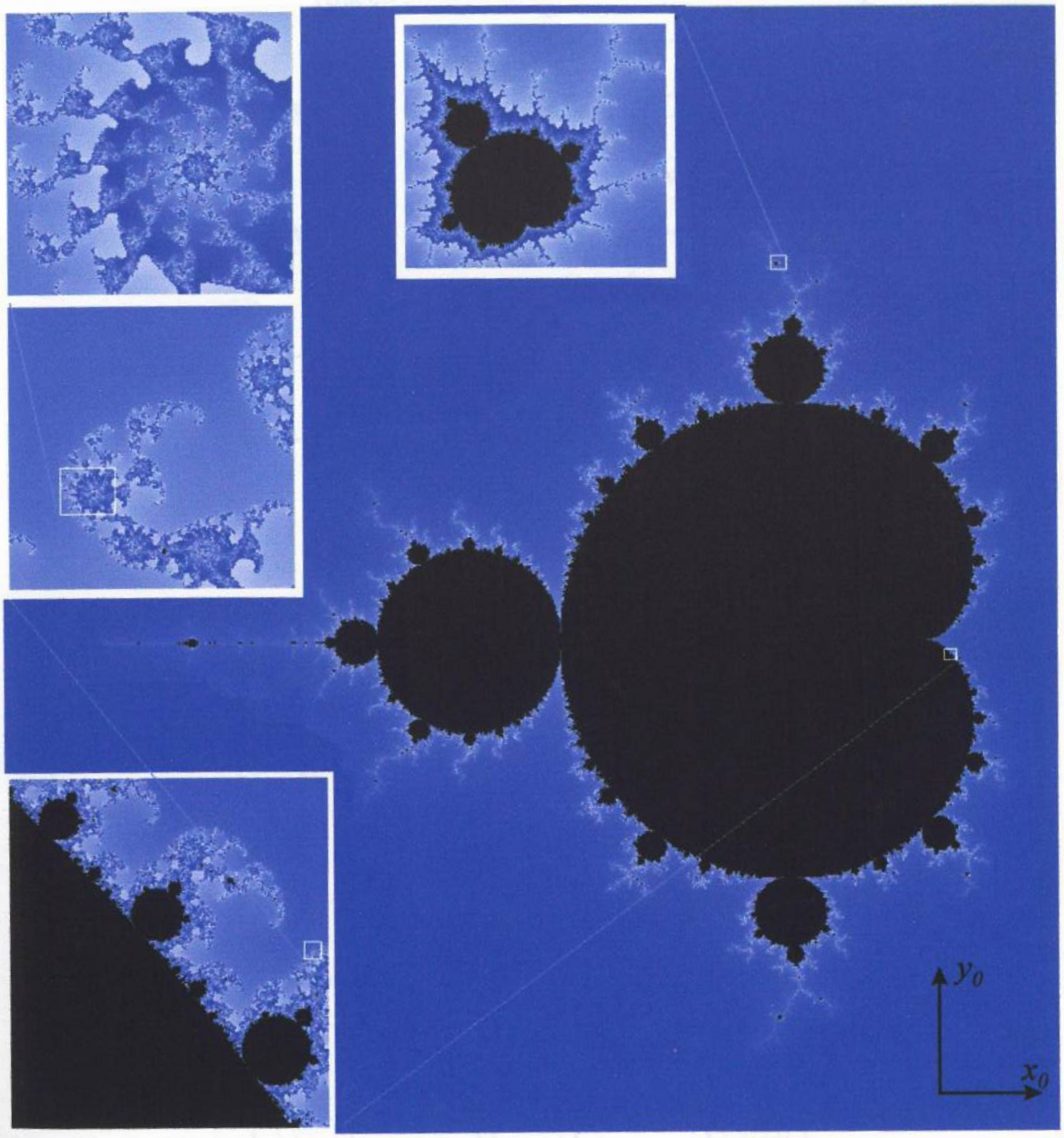

Figure 1.4 The Mandelbrot Set

The set is generated by taking the complex number $Z_0=x_0+iy_0$ and performing the iteration $Z_{n+1}=Z_n^2+Z_0$.
As n tends to infinity $|Z_n|$ remains finite or tends to infinity itself. If the latter occurs then a the point Z_0 is plotted with a colour dependent on the rate at which $|Z_n|$ increases.

The complexity and beauty of the set is all the more stunning when the simplicity of this generating equation is considered. Fractal measurements of the object are directly related to the generating equation.

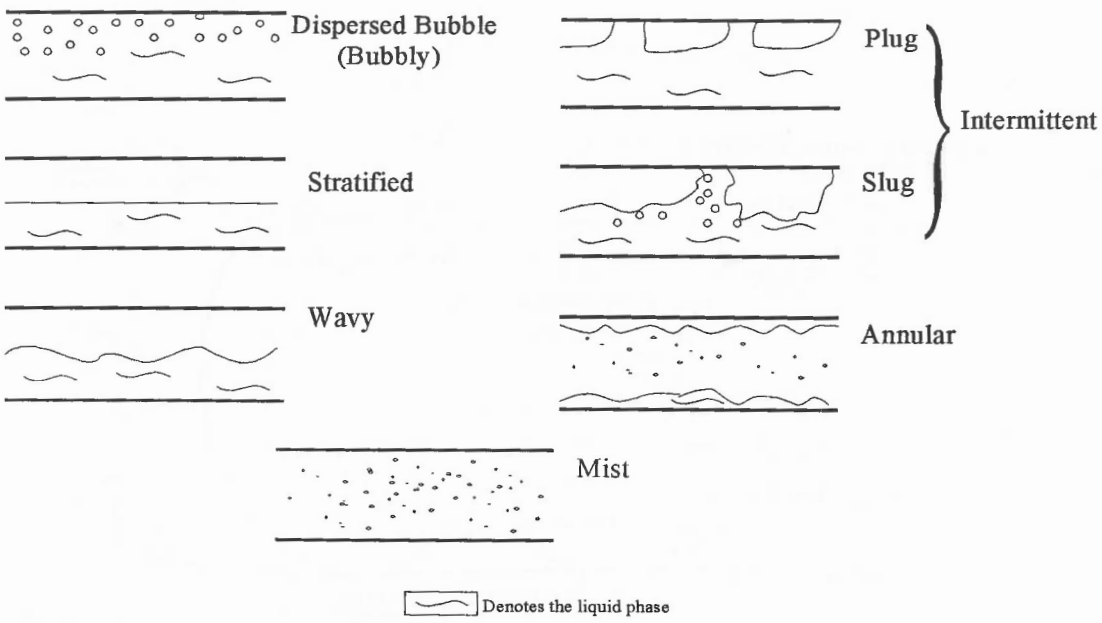

Figure 2.1 Horizontal Gas-Liquid Flow Regimes

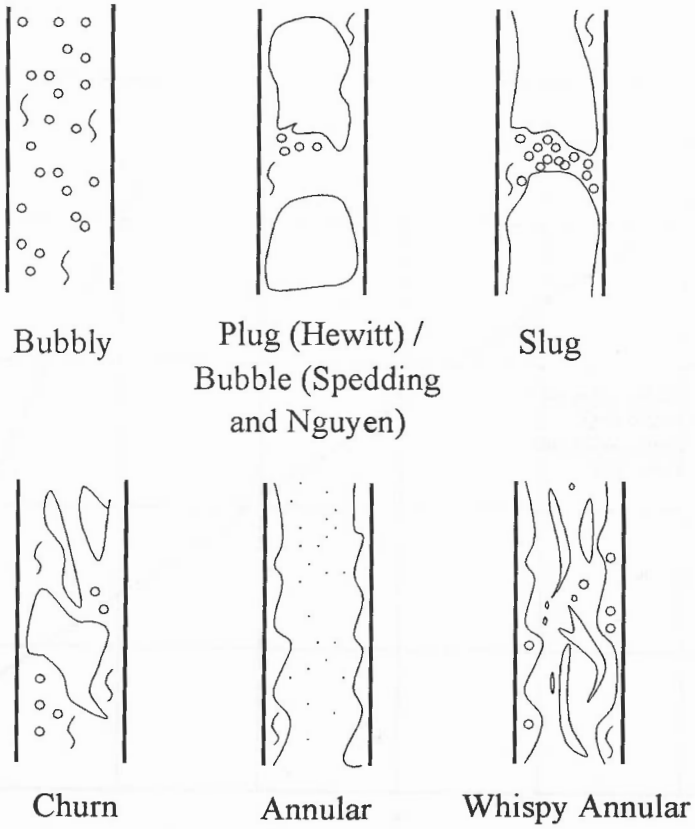

Figure 2.2 Vertical Gas-Liquid Flow Regimes

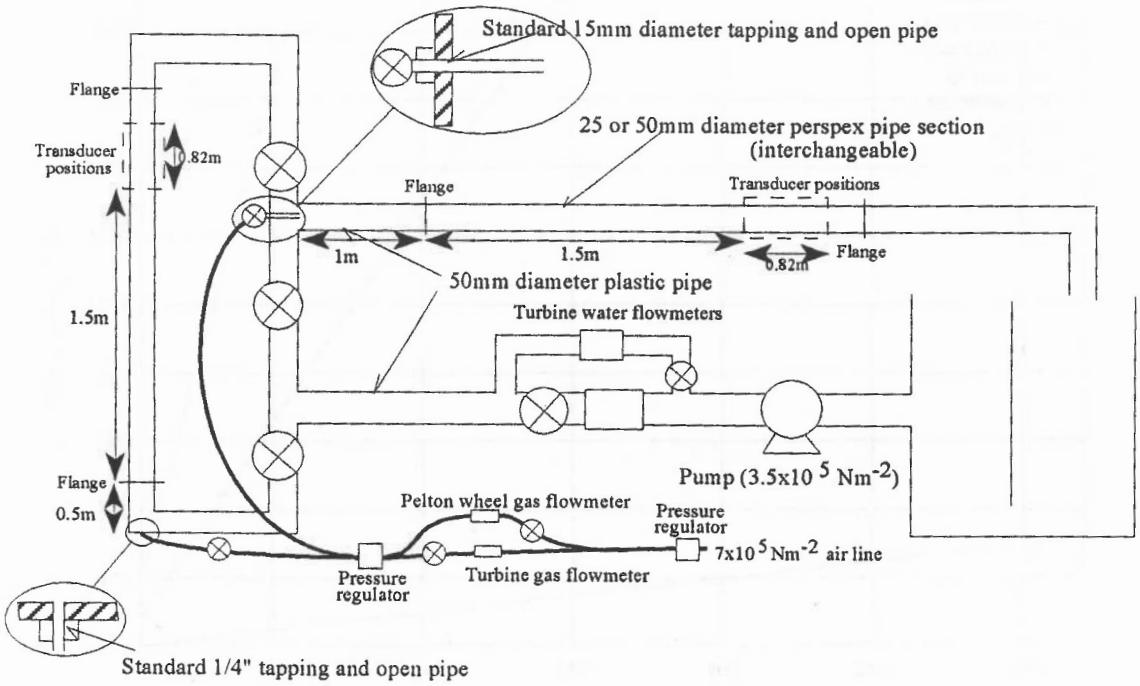

Figure 3.1 Main components of flow rig

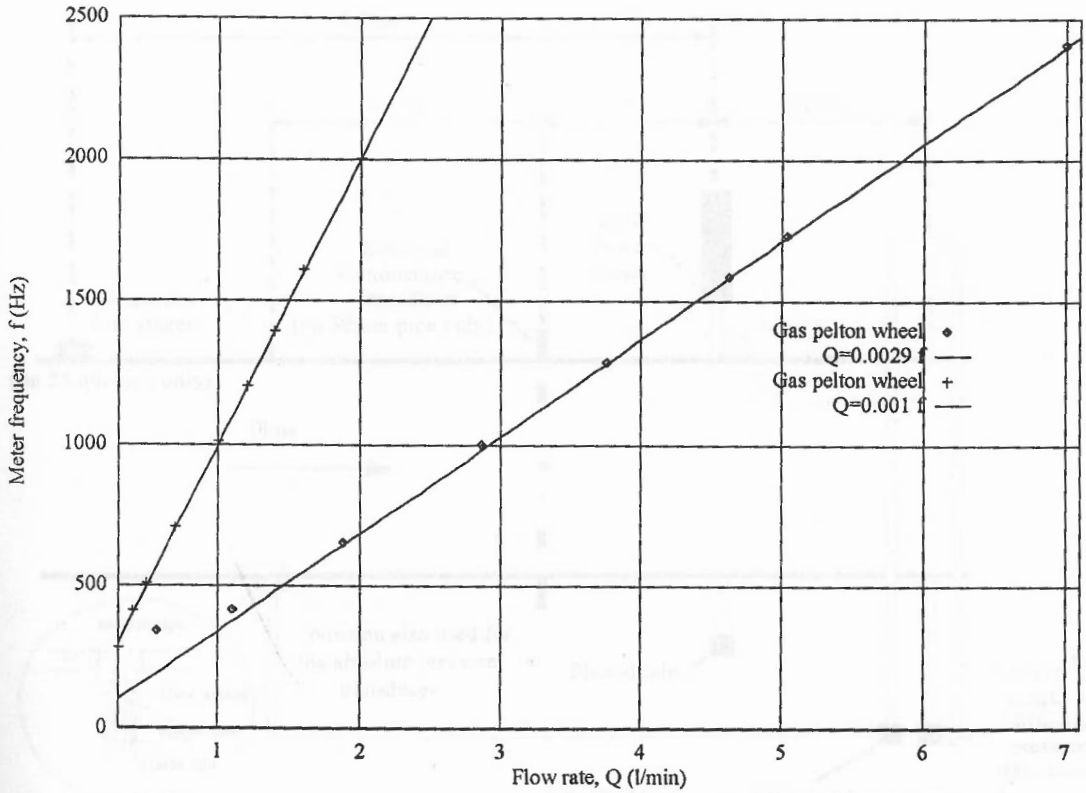

Figure 3.2 Calibration curves for pelton wheel flow meters

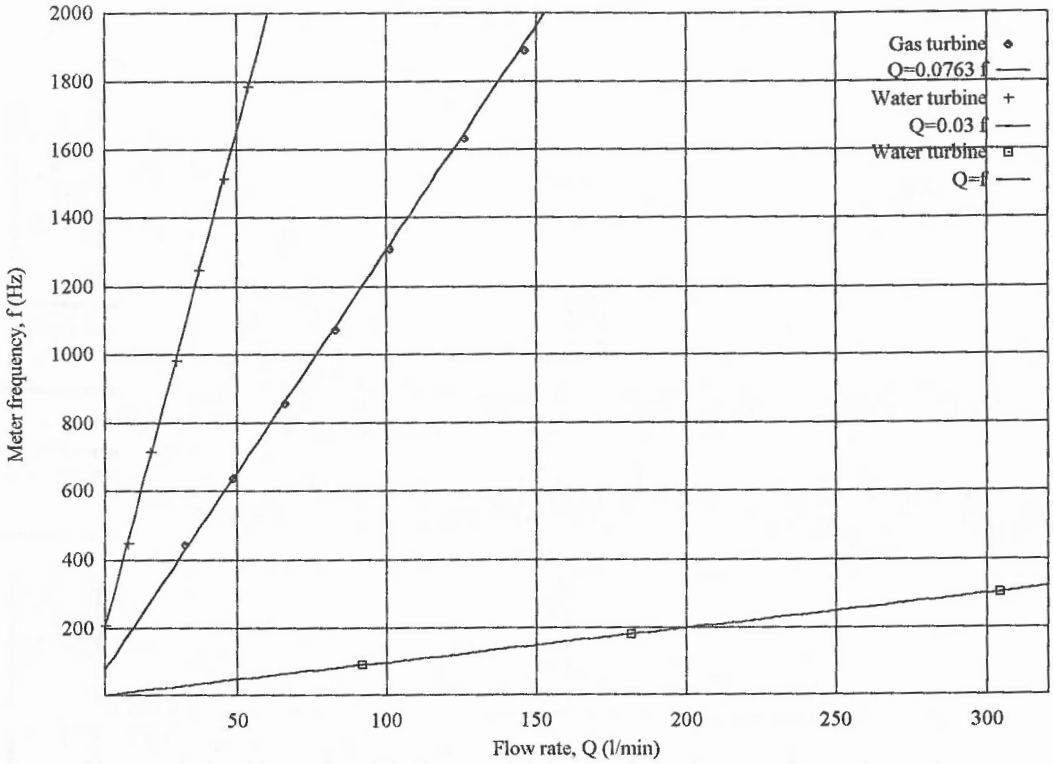

Figure 3.3 Calibration curves for turbine flow meters

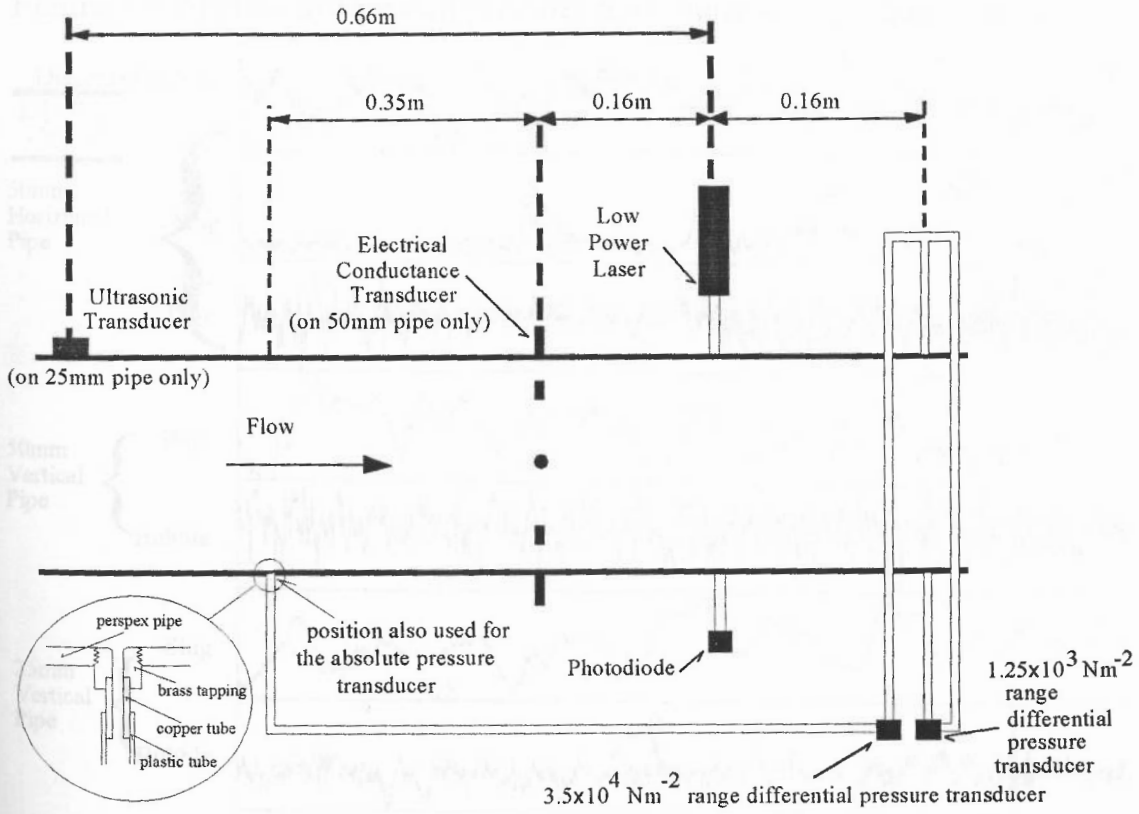

Figure 3.4 Arrangement of transducers

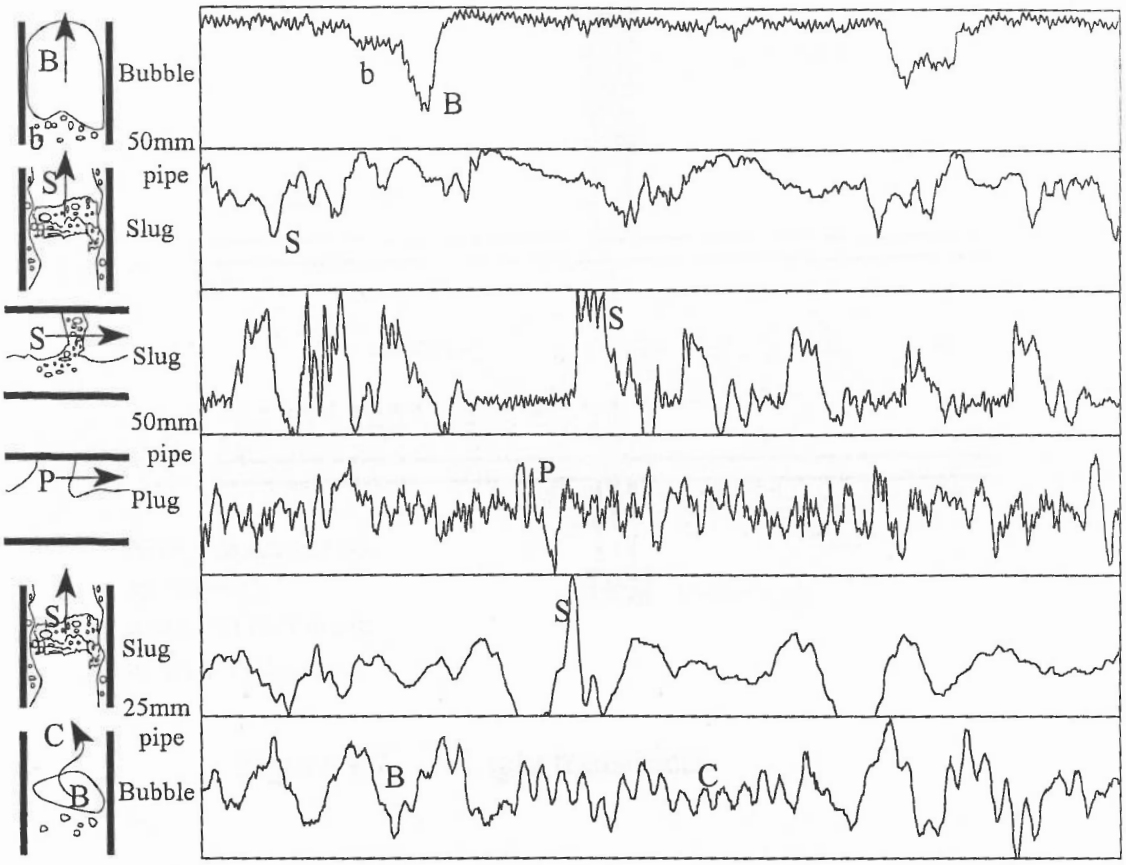

Figure 3.5 Typical differential pressure transducer signals (large range)

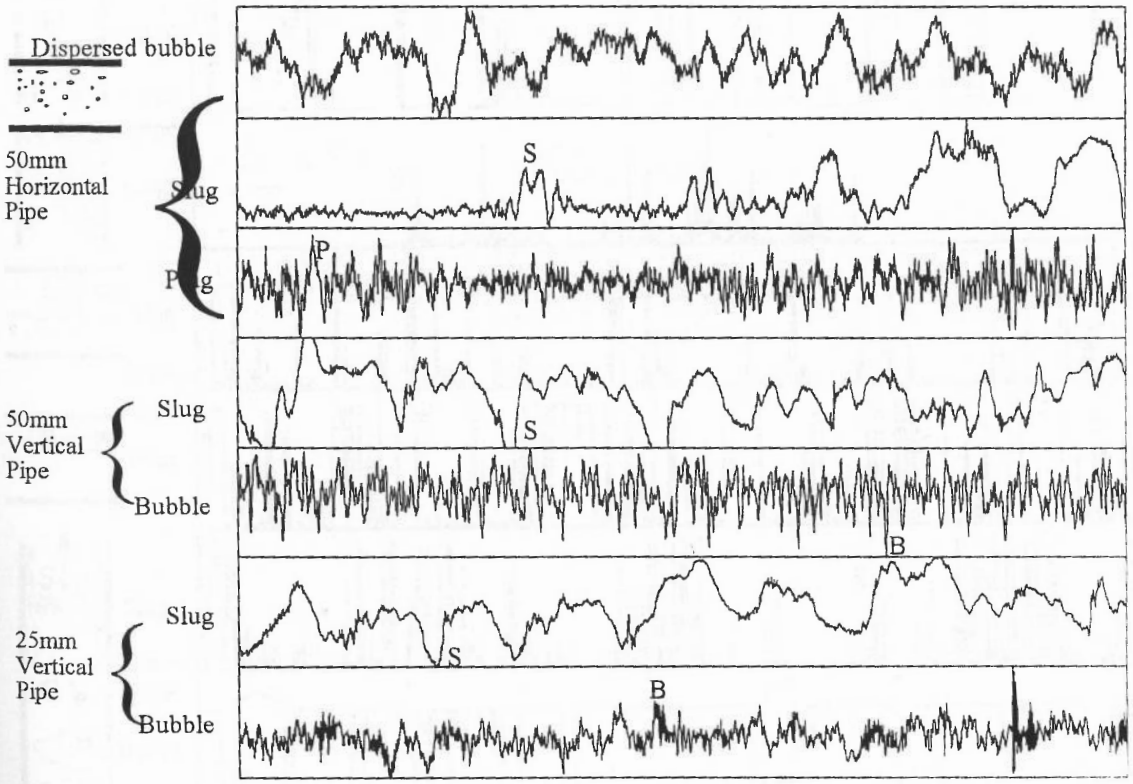

Figure 3.6 Typical absolute pressure transducer signals

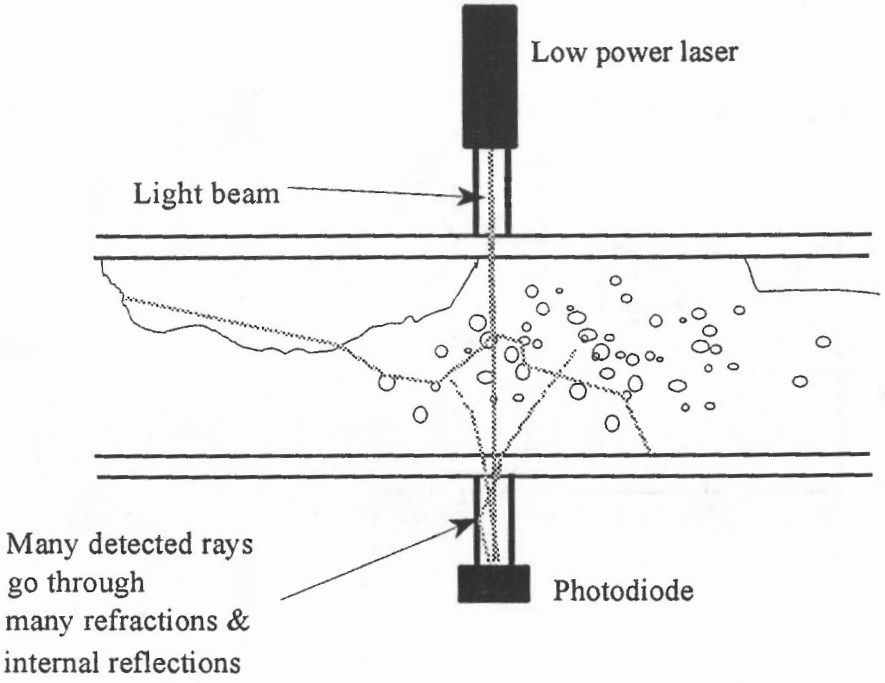

Figure 3.7 Light transducer

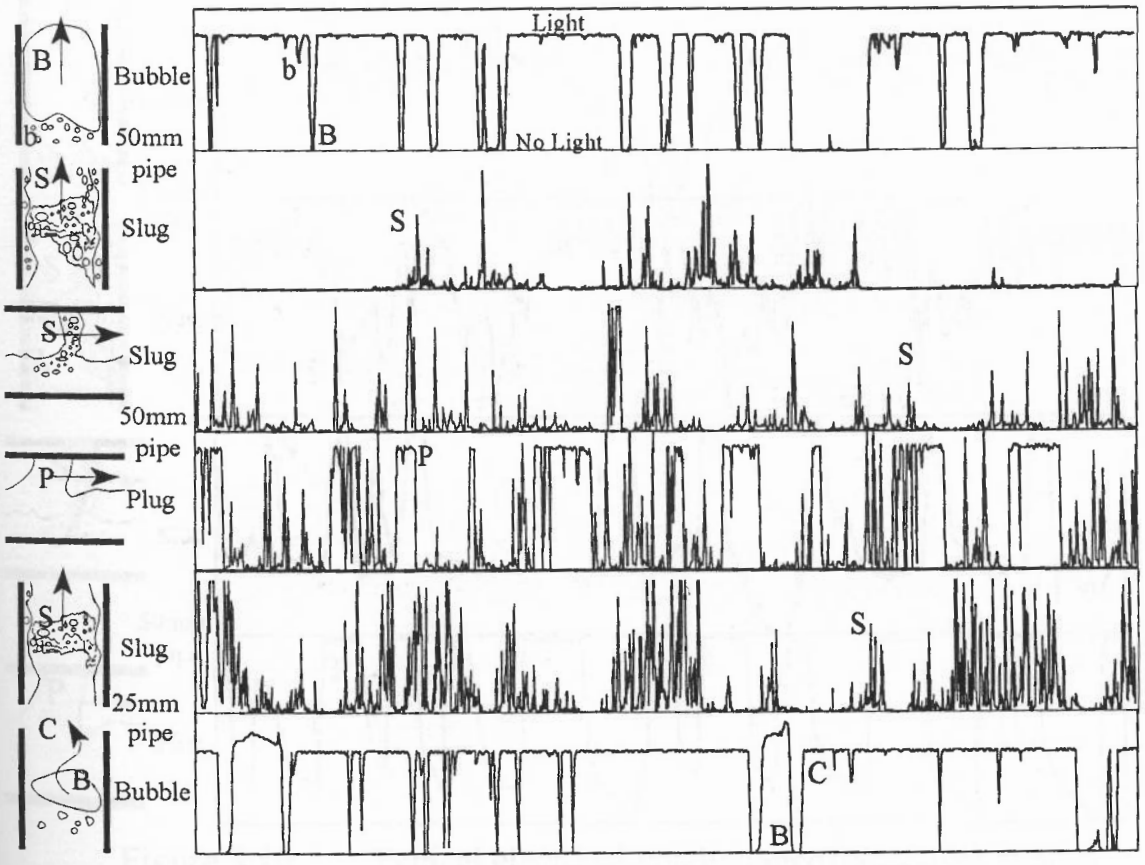

Figure 3.8 Typical light transducer signals

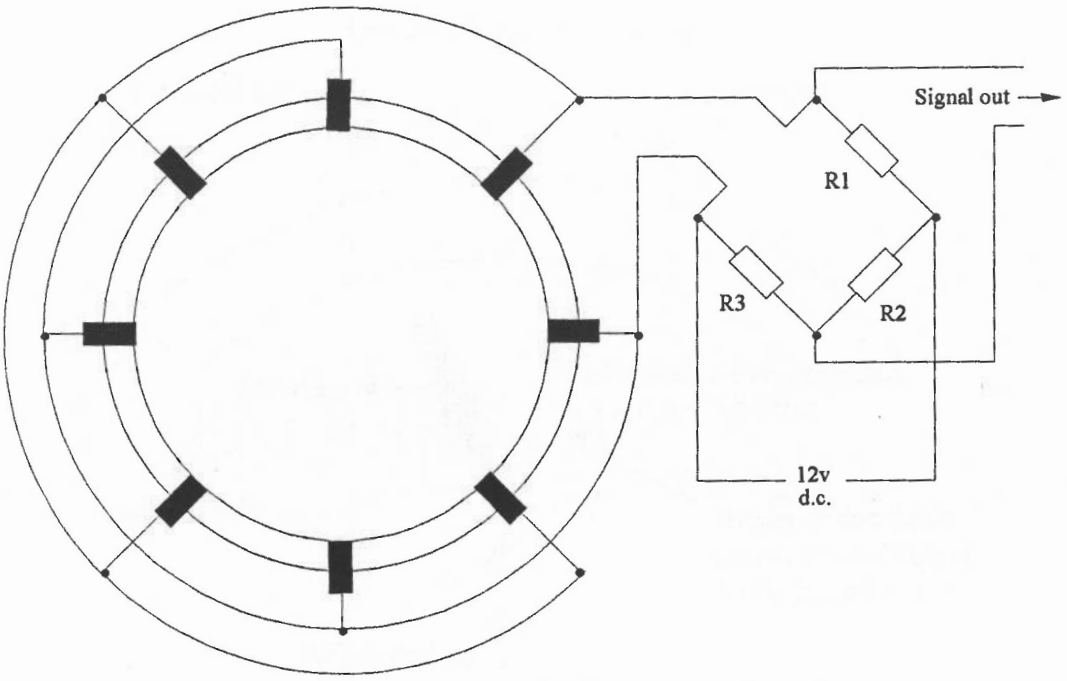

Figure 3.9 Electrical conductance transducer

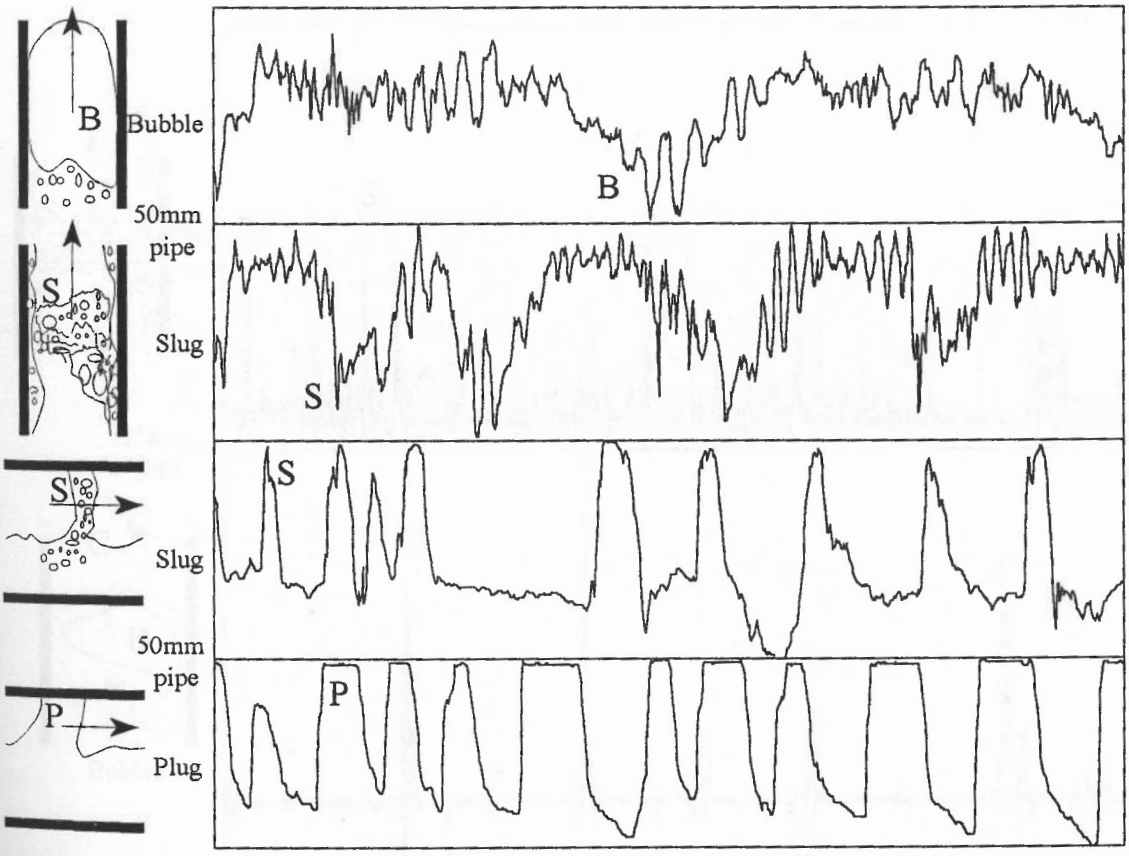

Figure 3.10 Typical electrical conductance transducer signals

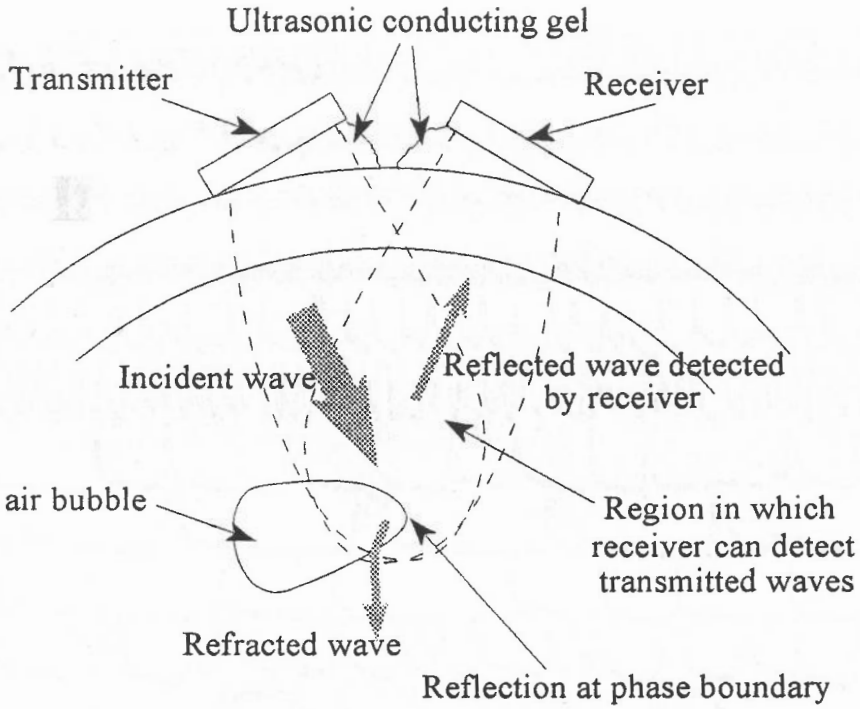

Figure 3.11 Ultrasonic transducer

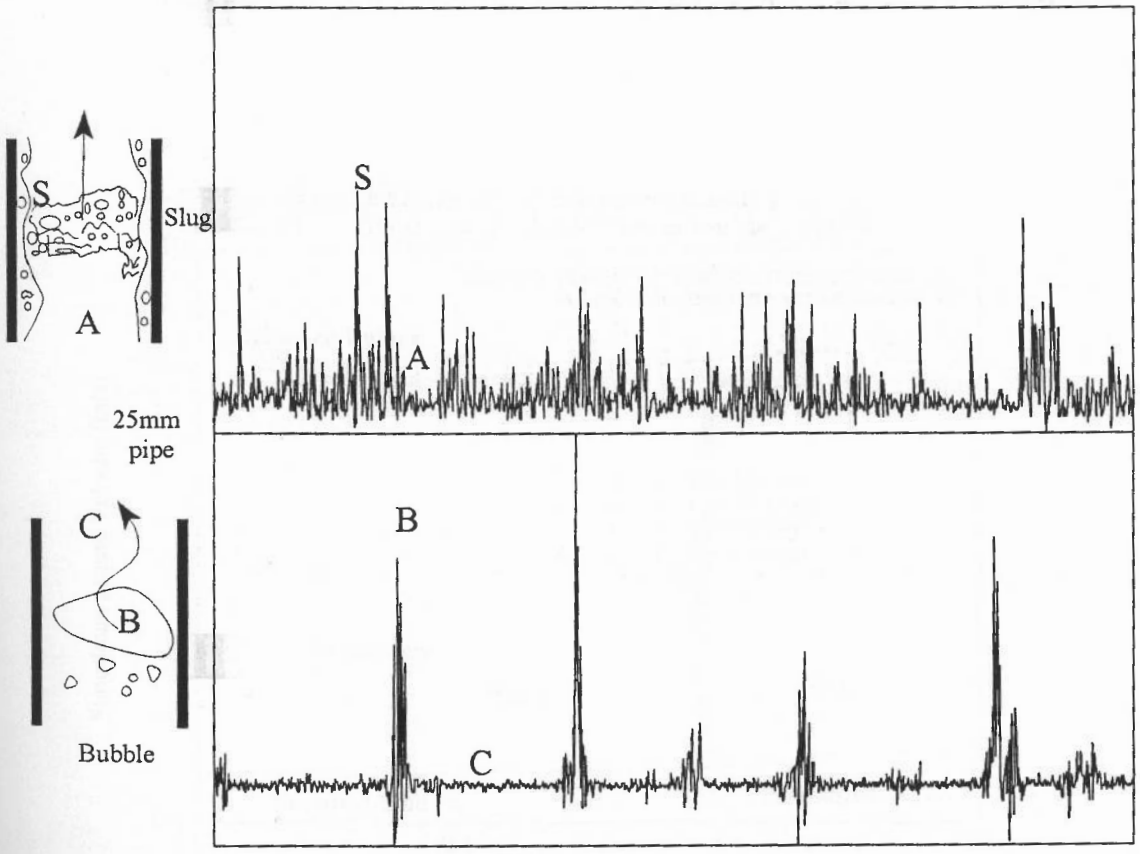

Figure 3.12 Typical ultrasonic transducer signals

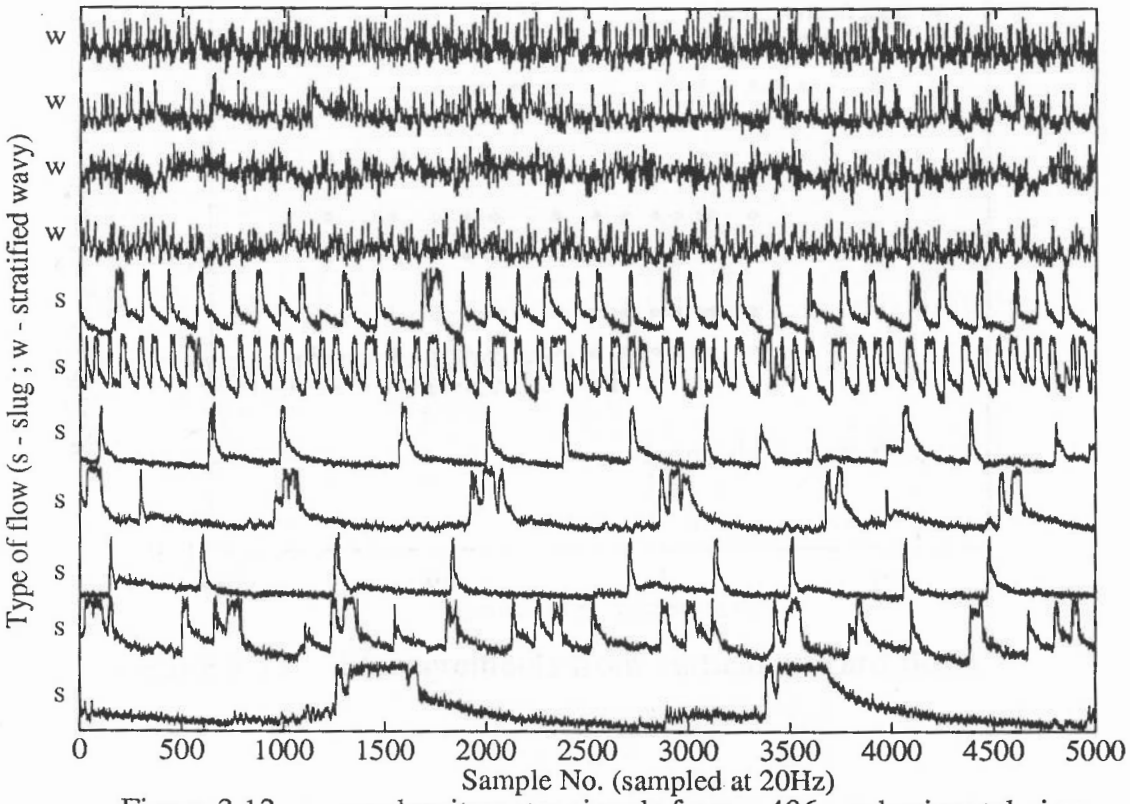

Figure 3.13 γ -ray densitometer signals from a 406mm horizontal pipe

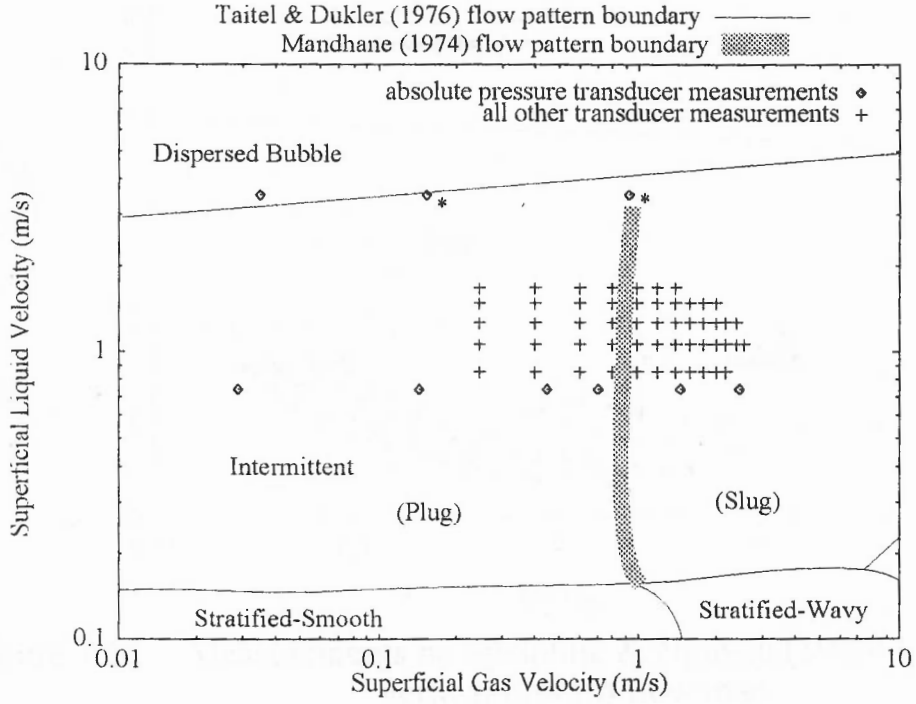

Figure 3.14 Measurements from 50mm horizontal pipe

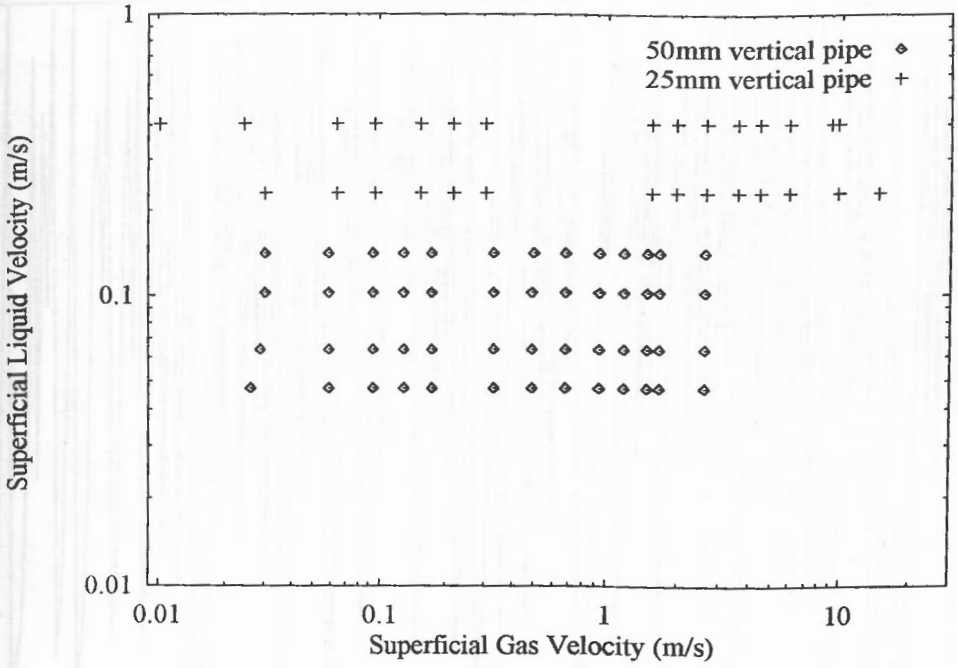

Figure 3.15 Measurements from vertical upward flows

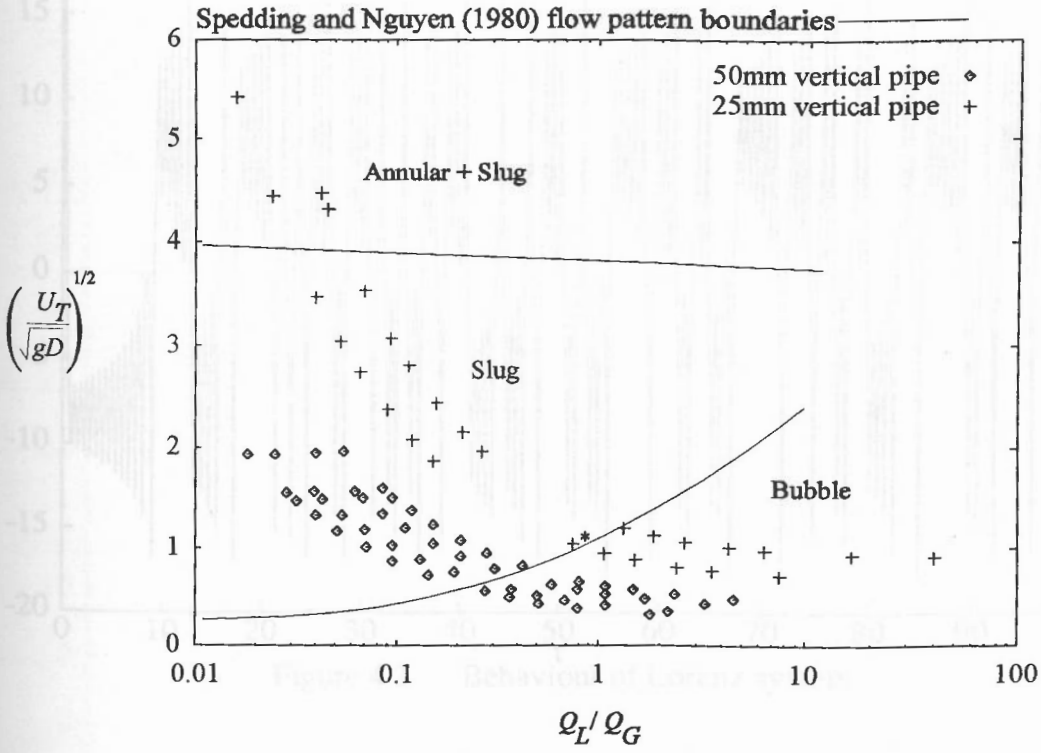

Figure 3.16 Measurements on Spedding & Nguyen (1980) vertical upward flow map

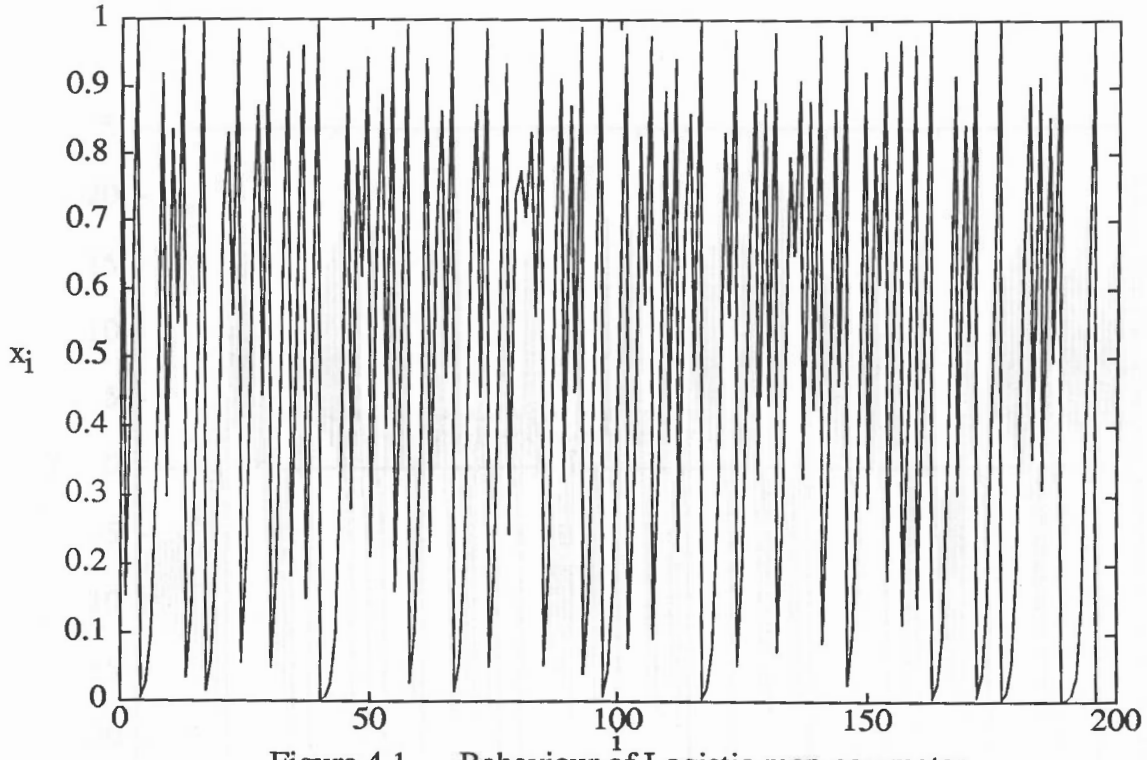

Figure 4.1 Behaviour of Logistic map parameter

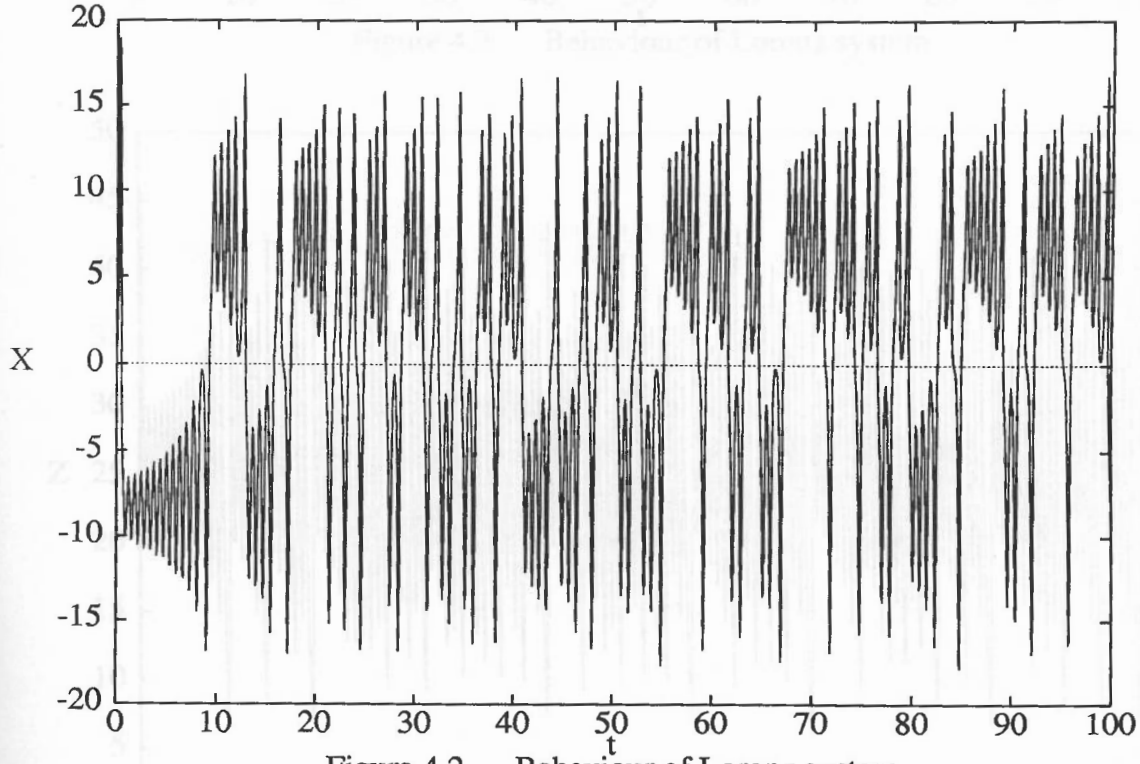

Figure 4.2 Behaviour of Lorenz system

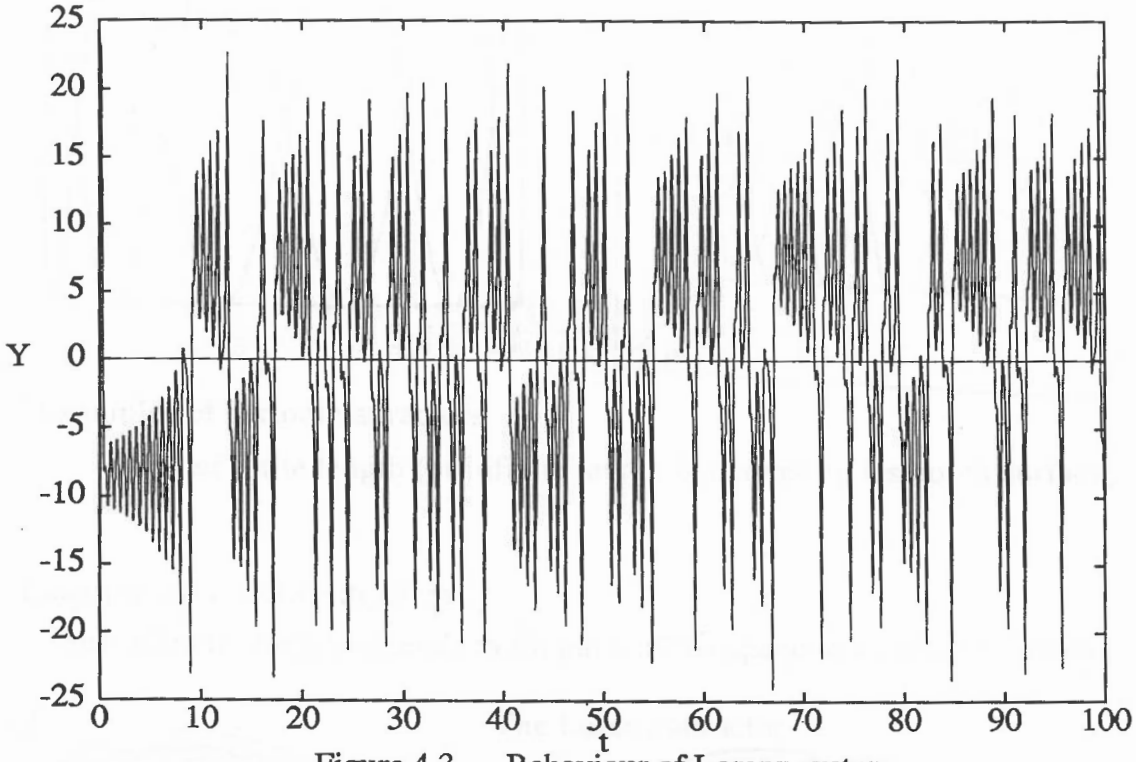

Figure 4.3 Behaviour of Lorenz system

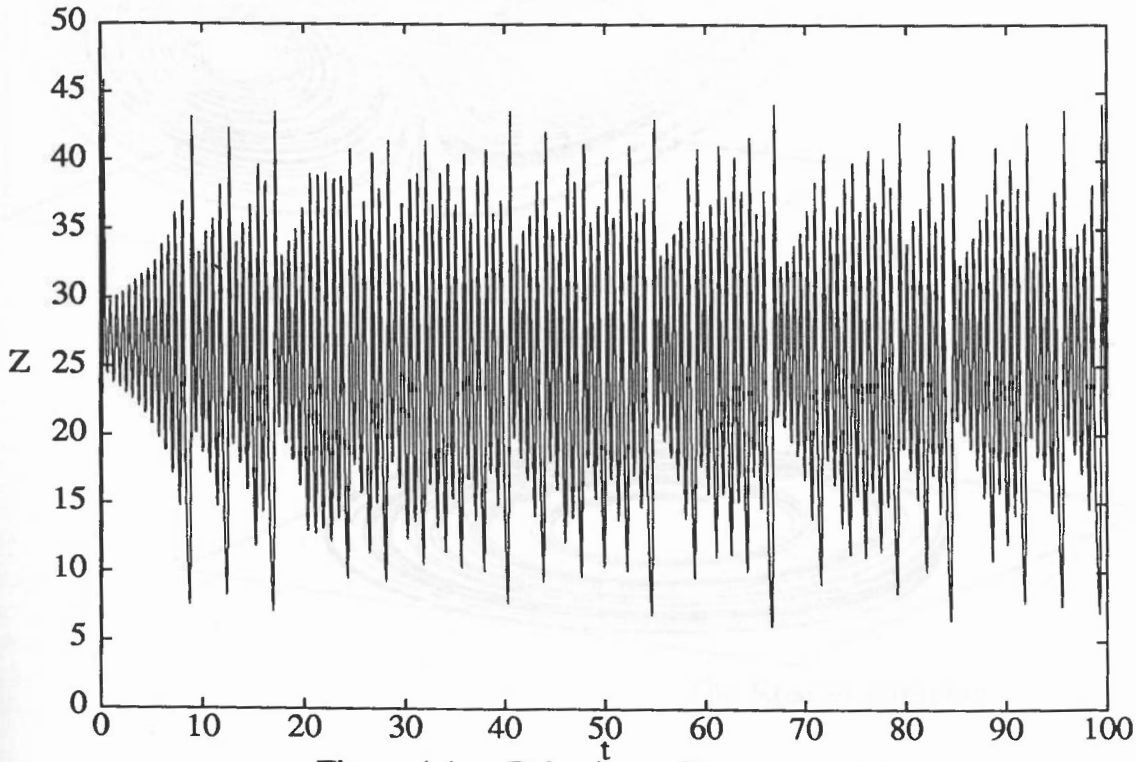

Figure 4.4 Behaviour of Lorenz system

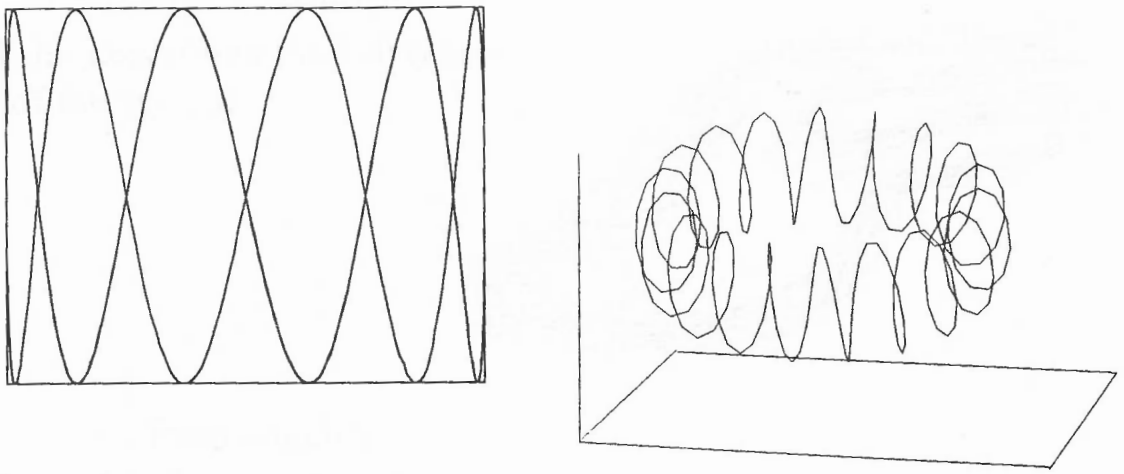

Examples of periodic attractors

-a line of finite length (or infinite length but covering a smooth surface)

Examples of chaotic attractors

-the infinetly long line tends to fill parts of the space in a complex manner

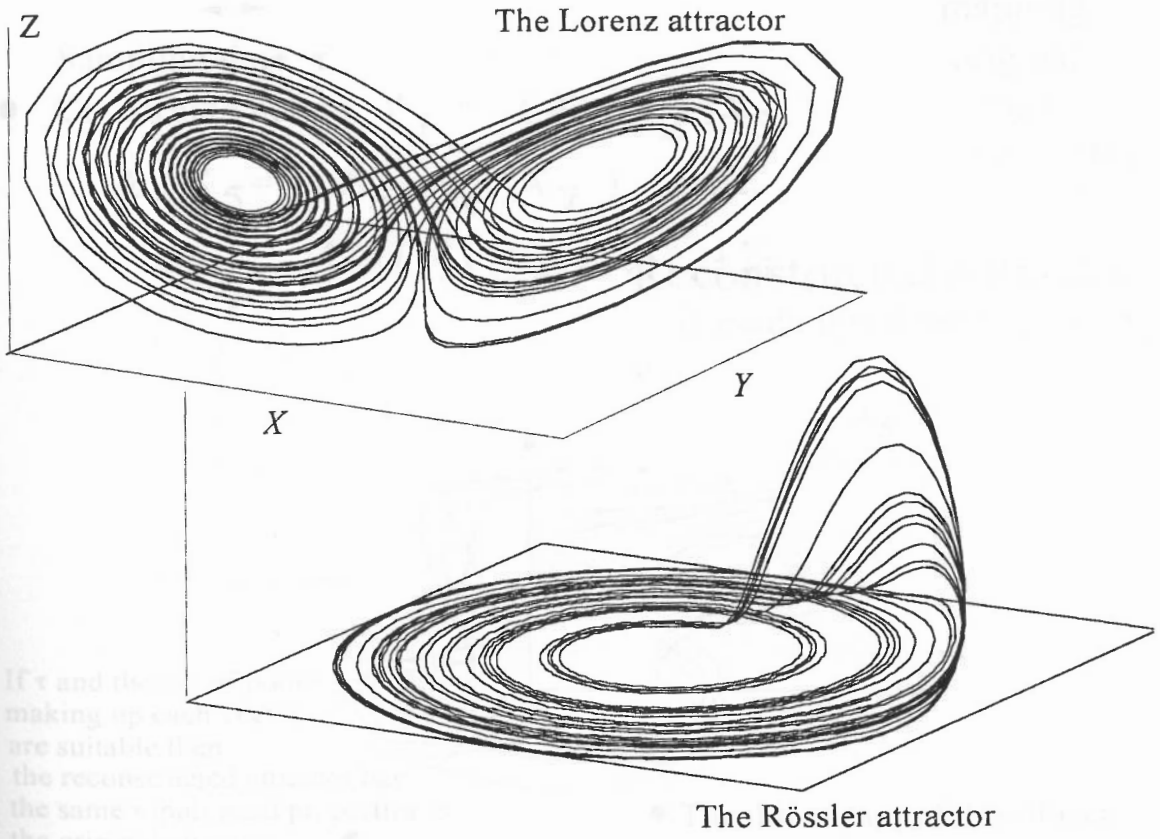

Figure 4.5 Examples of various attractors

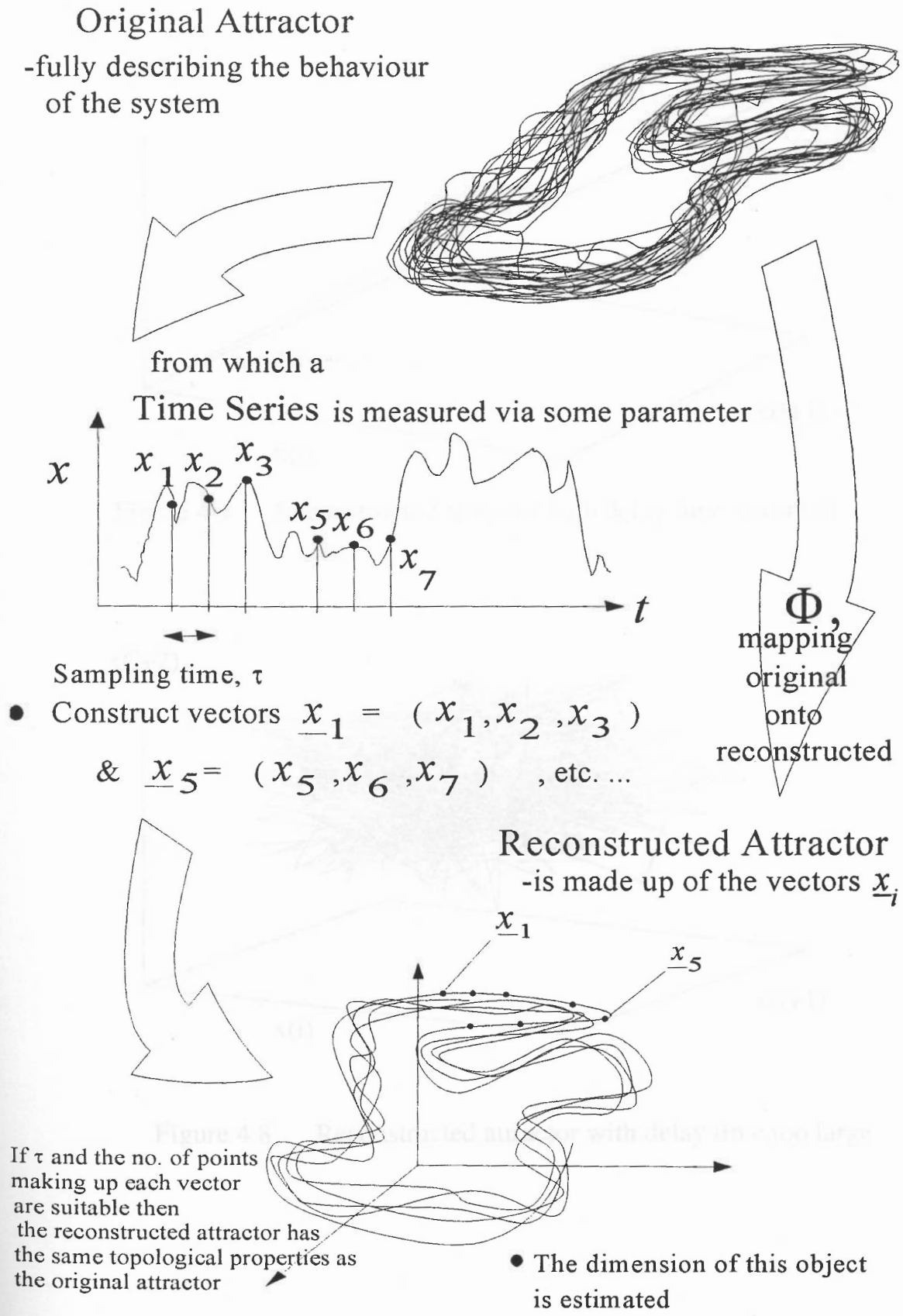

Figure 4.6 Reconstruction of an Attractor

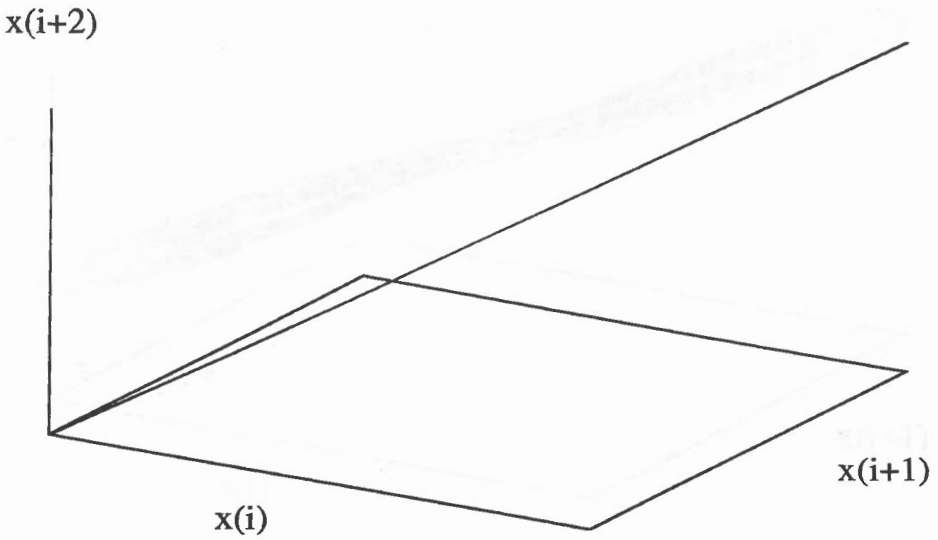

Figure 4.7 Reconstructed attractor with delay time too small

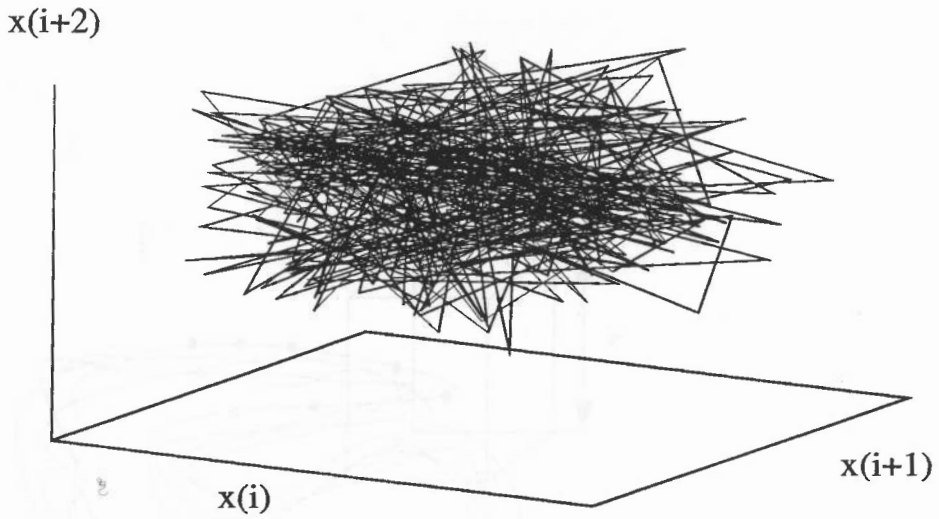

Figure 4.8 Reconstructed attractor with delay time too large

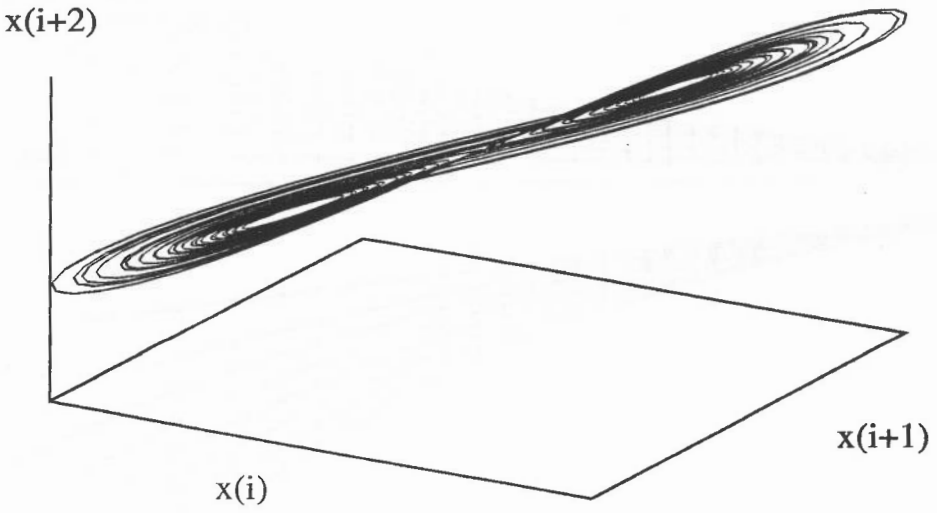

Figure 4.9 Reconstructed attractor with a suitable delay time

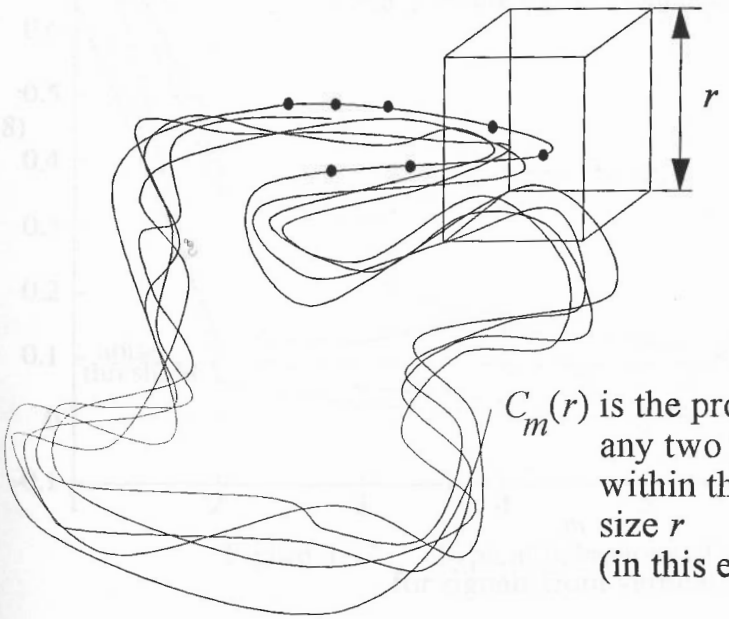

$C_m(r)$ is the probability of finding any two points on the attractor within the same hypercube of size r (in this example m=3)

Figure 4.10 Definition of the correlation integral

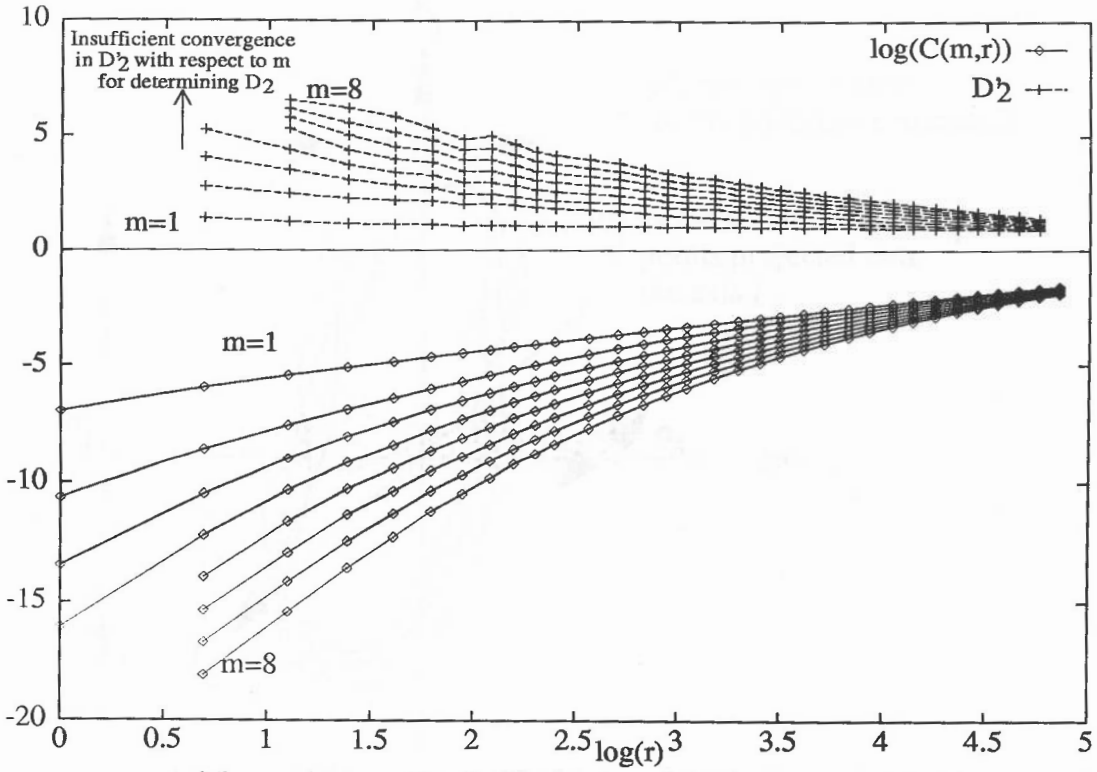

Figure 4.11 Typical behaviour of C(m,r) and D'$_2$(m,r)

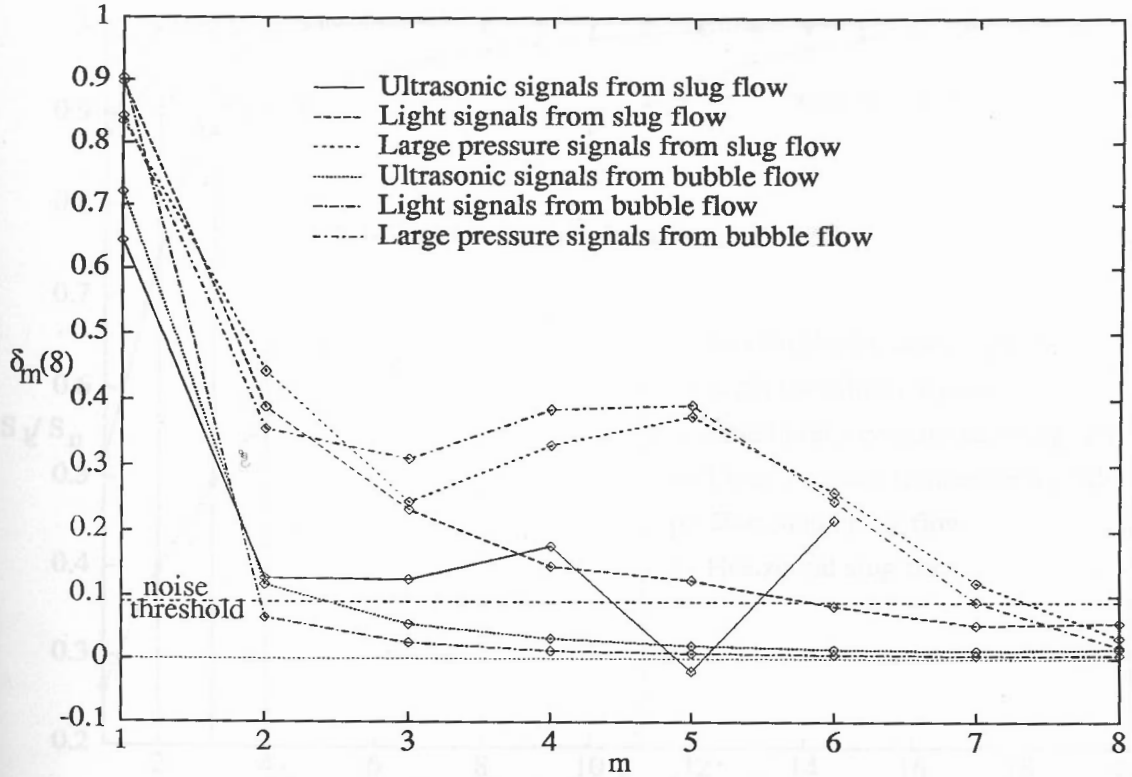

Figure 4.12 Typical behaviour of delta measures
for signals from vertical upward flows

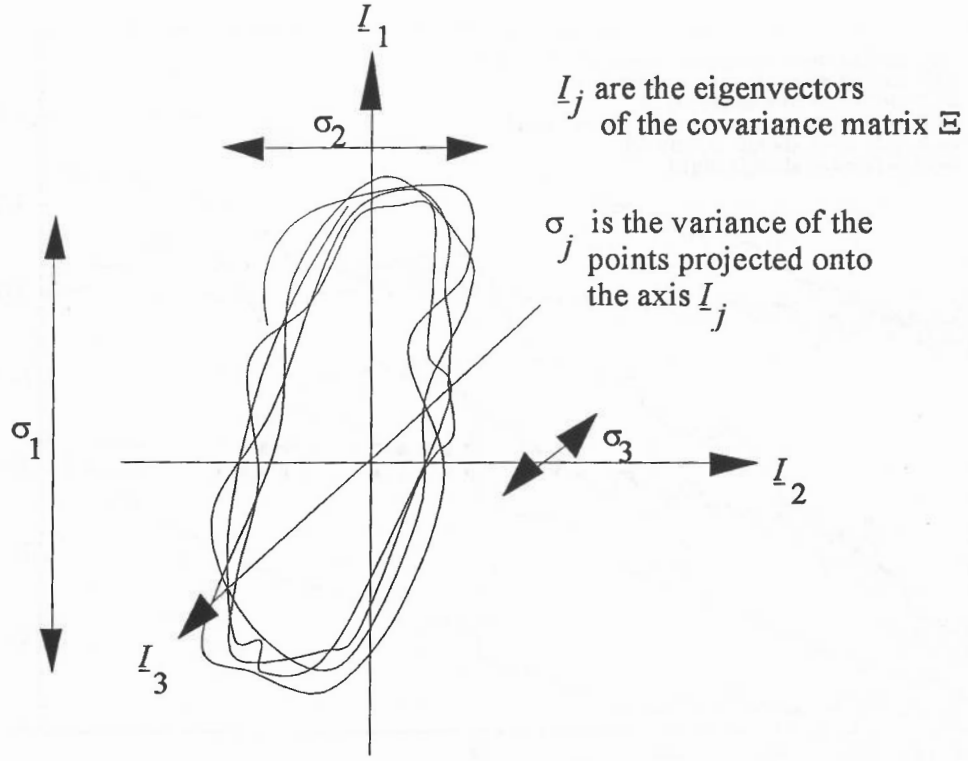

Figure 4.13 Definition of singular values σ_j

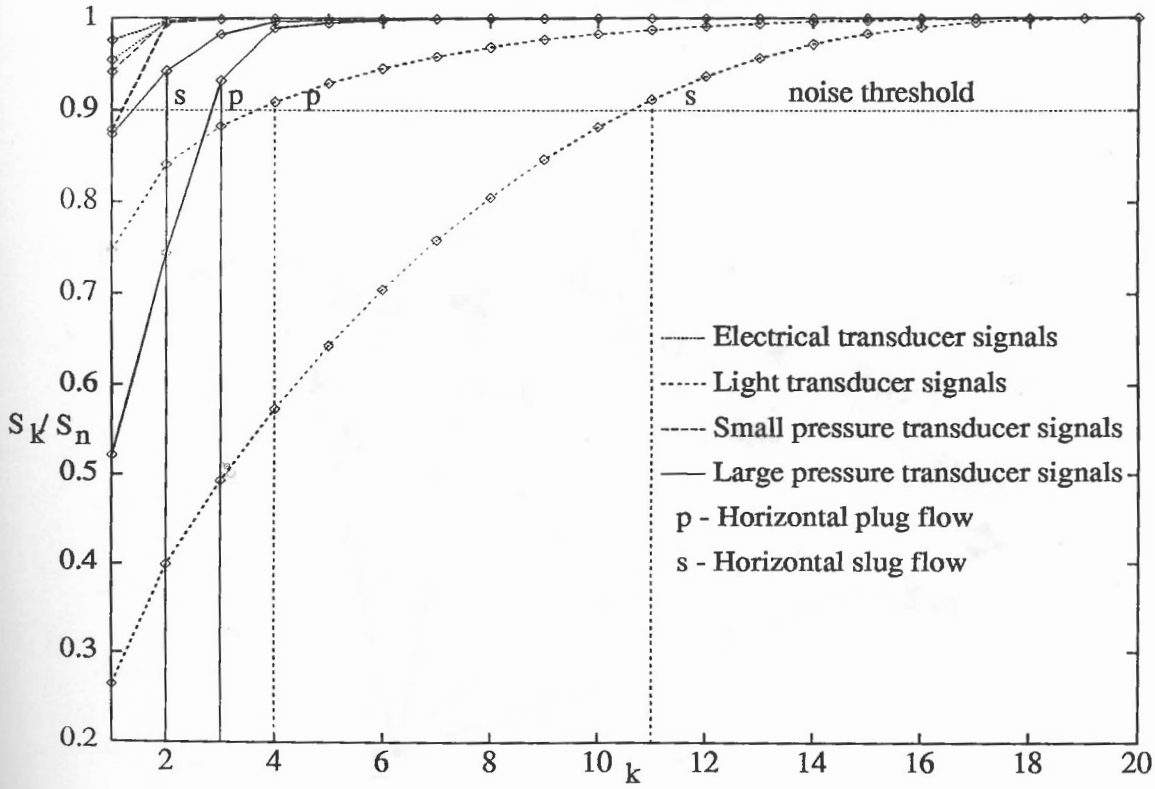

Figure 4.14 Typical behaviour of S_k/S_n from various transducer signals

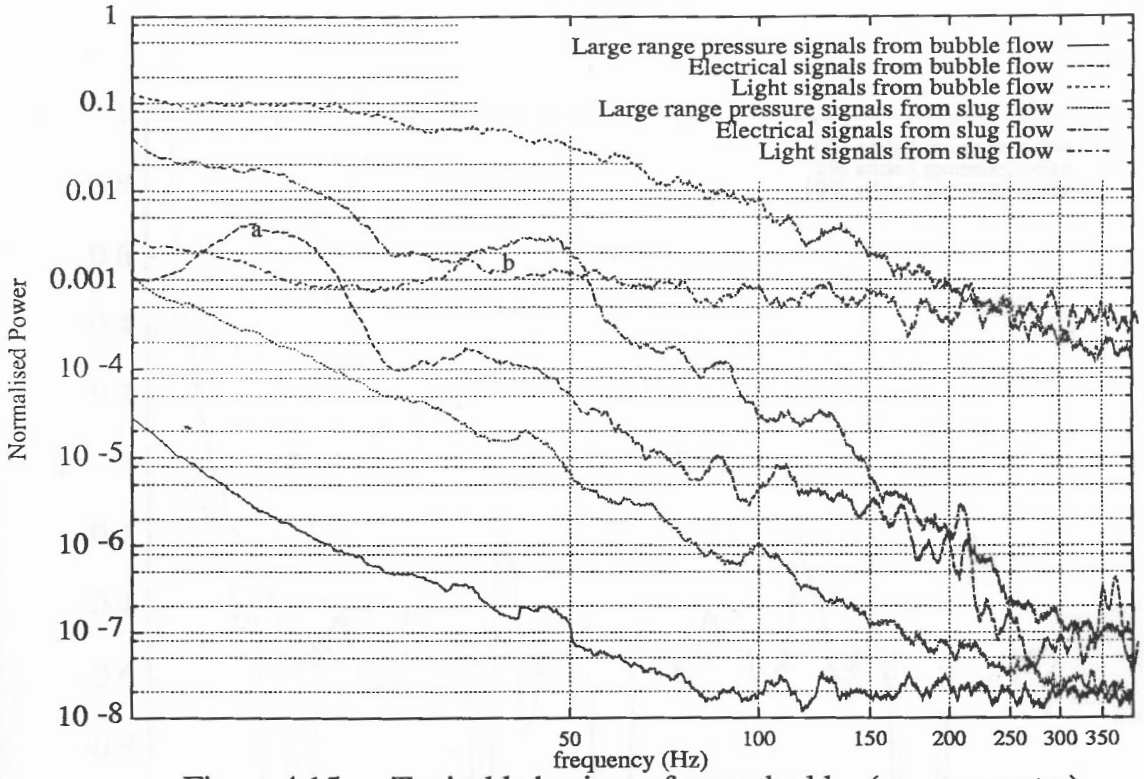

Figure 4.15 Typical behaviour of smoothed log(power spectra) for signals from vertical flows

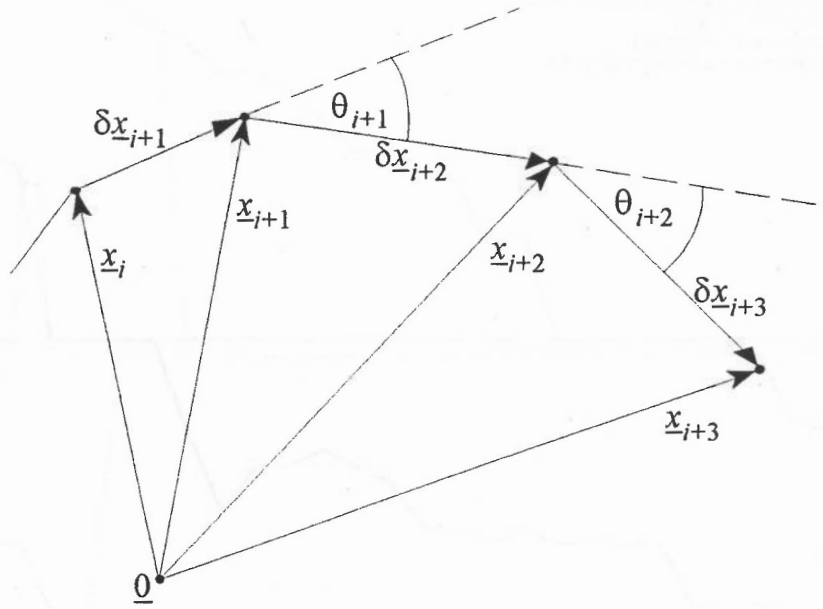

Figure 4.16 Tangent vector approximations of reconstructed attractor

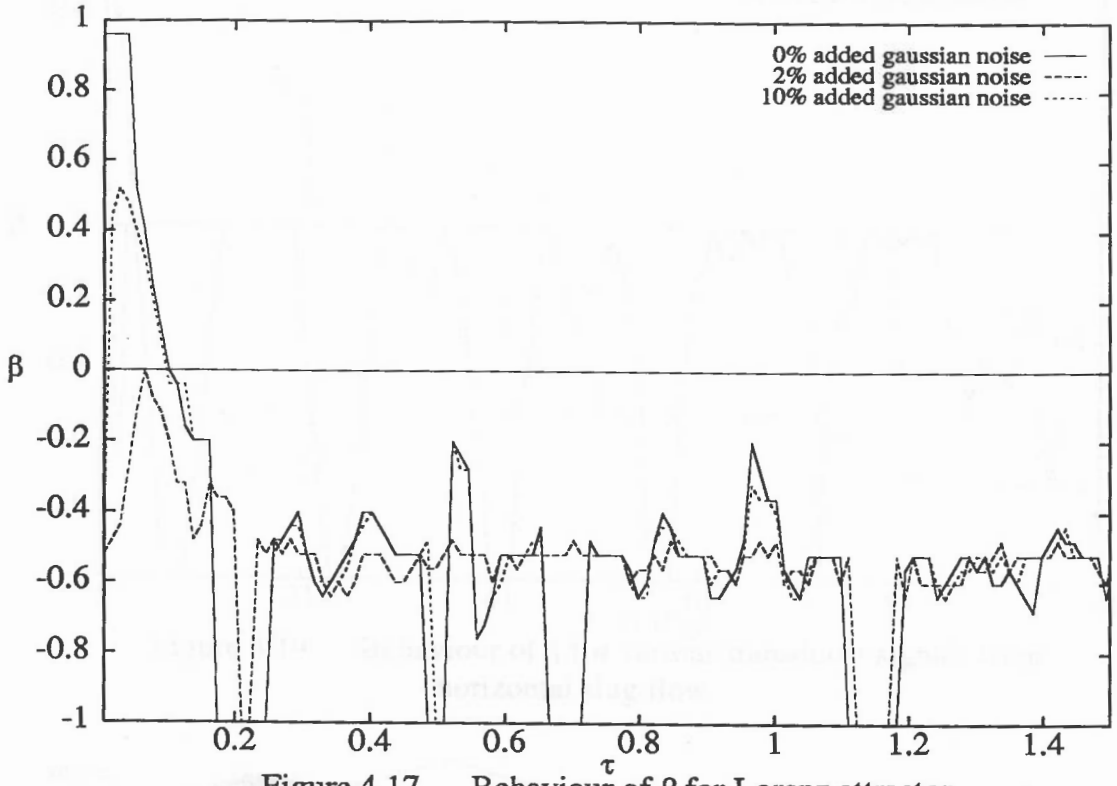

Figure 4.17 Behaviour of β for Lorenz attractor

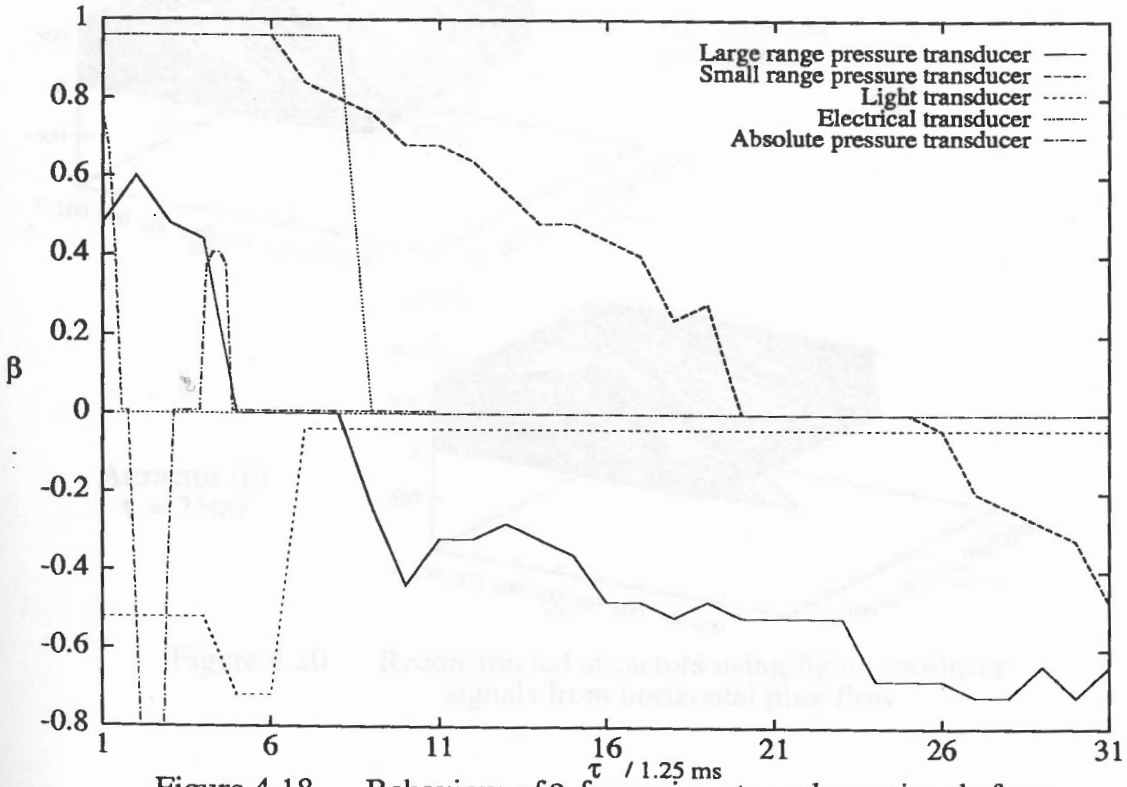

Figure 4.18 Behaviour of β for various transducer signals from horizontal plug flow

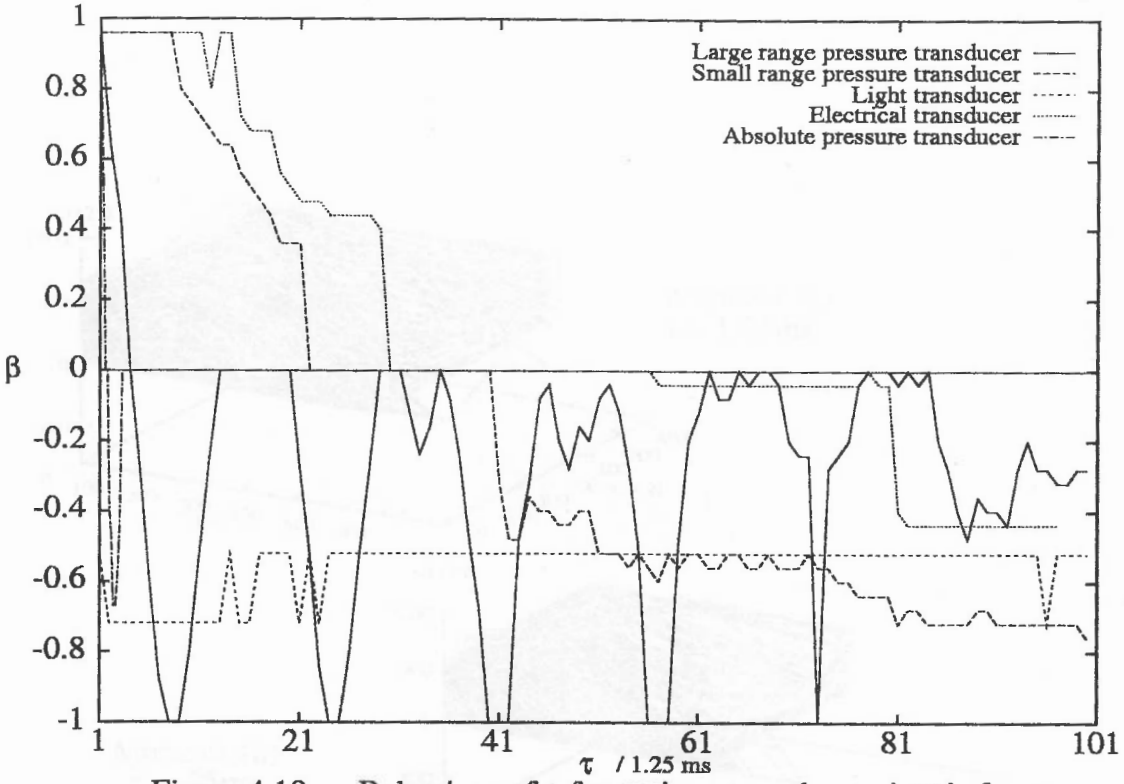

Figure 4.19 Behaviour of β for various transducer signals from horizontal slug flow

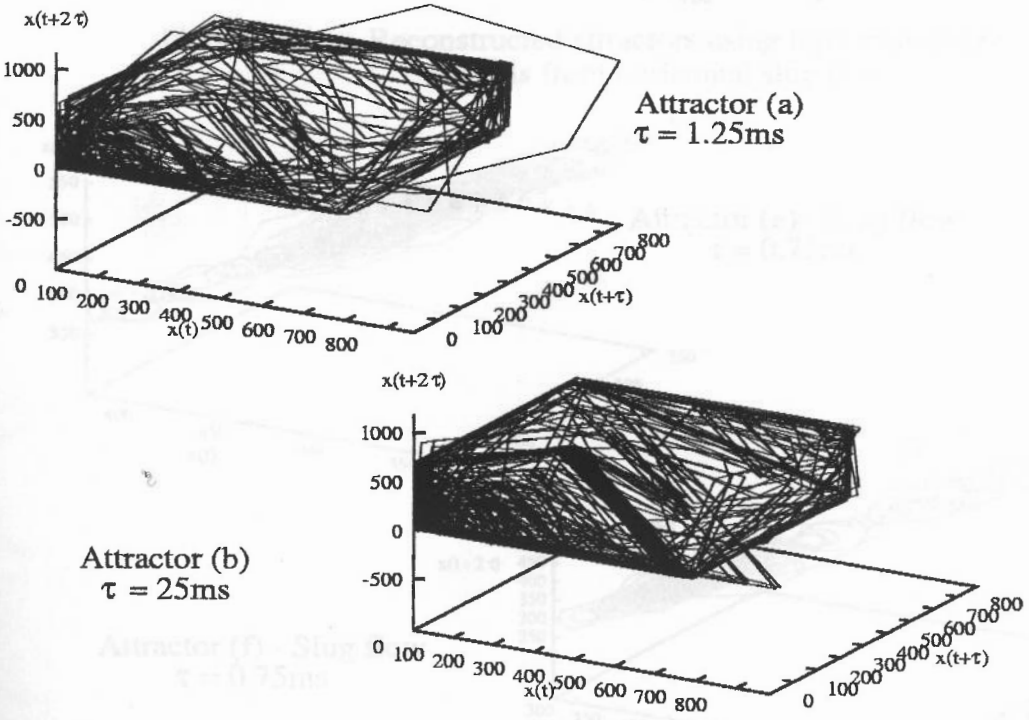

Figure 4.20 Reconstructed attractors using light transducer signals from horizontal plug flow

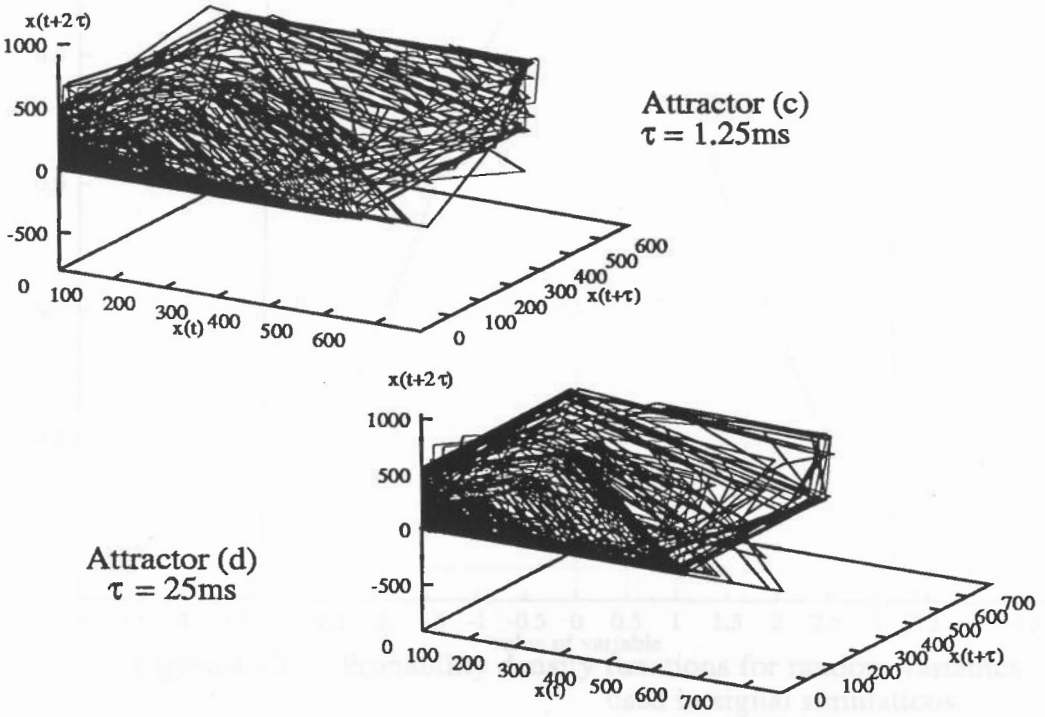

Figure 4.21 Reconstructed attractors using light transducer signals from horizontal slug flow

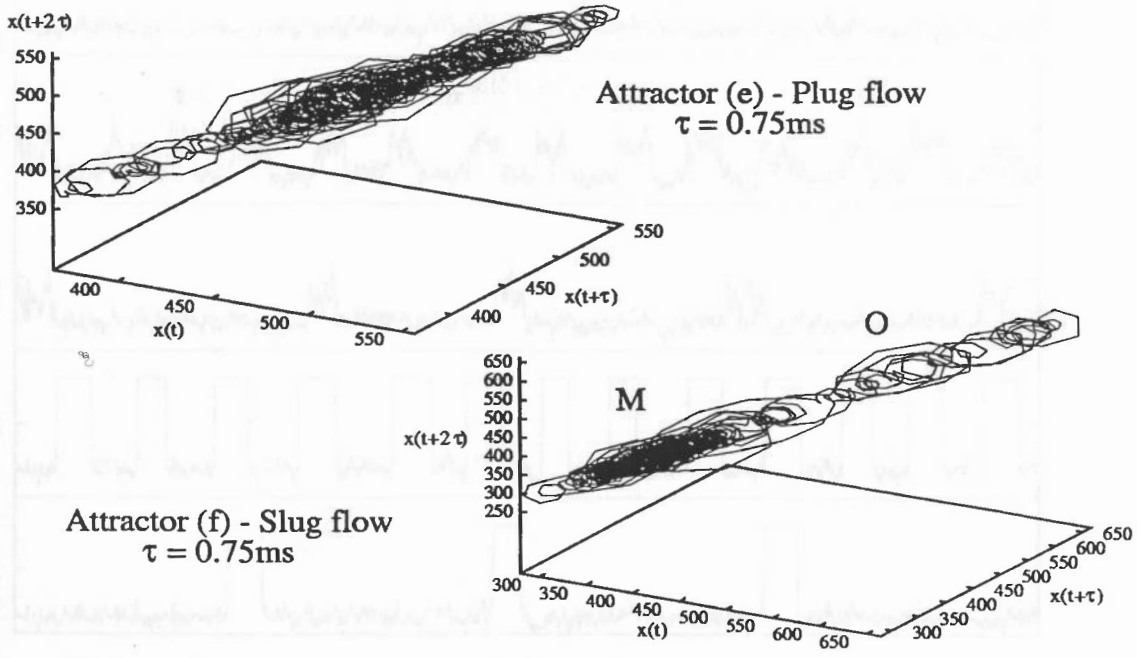

Figure 4.22 Reconstructed attractors using absolute pressure transducer signals from horizontal plug and slug flows

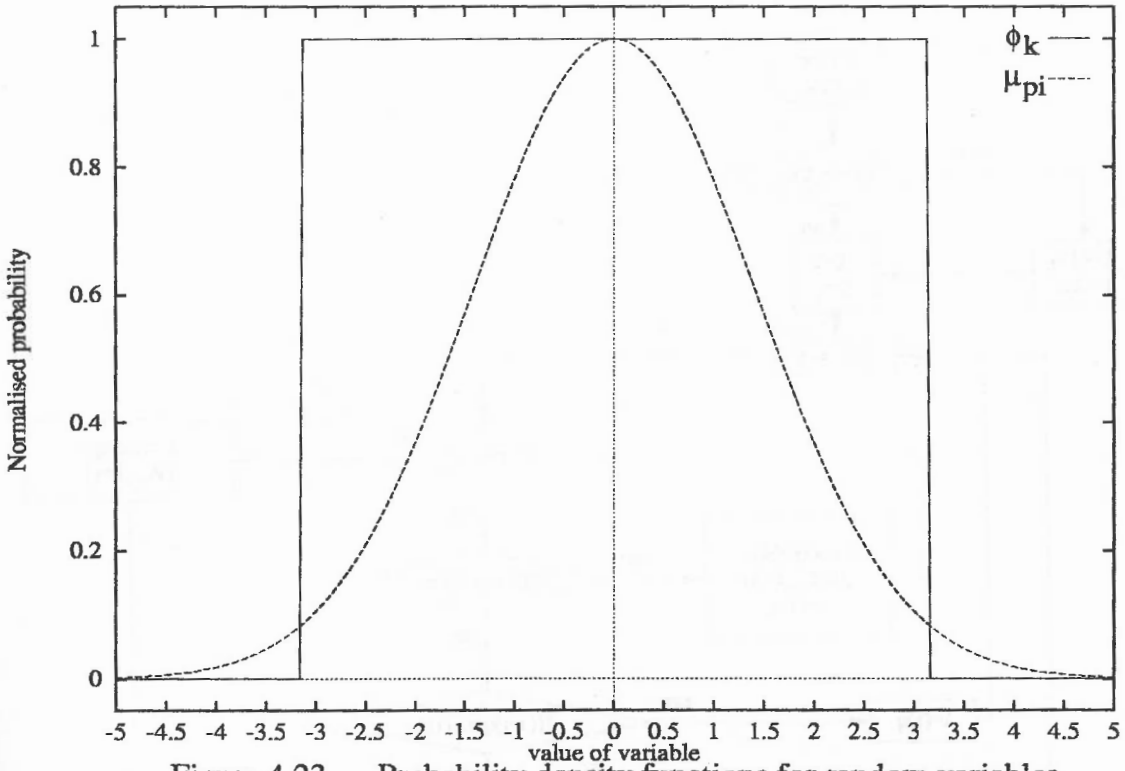

Figure 4.23 Probability density functions for random variables used in signal simulations

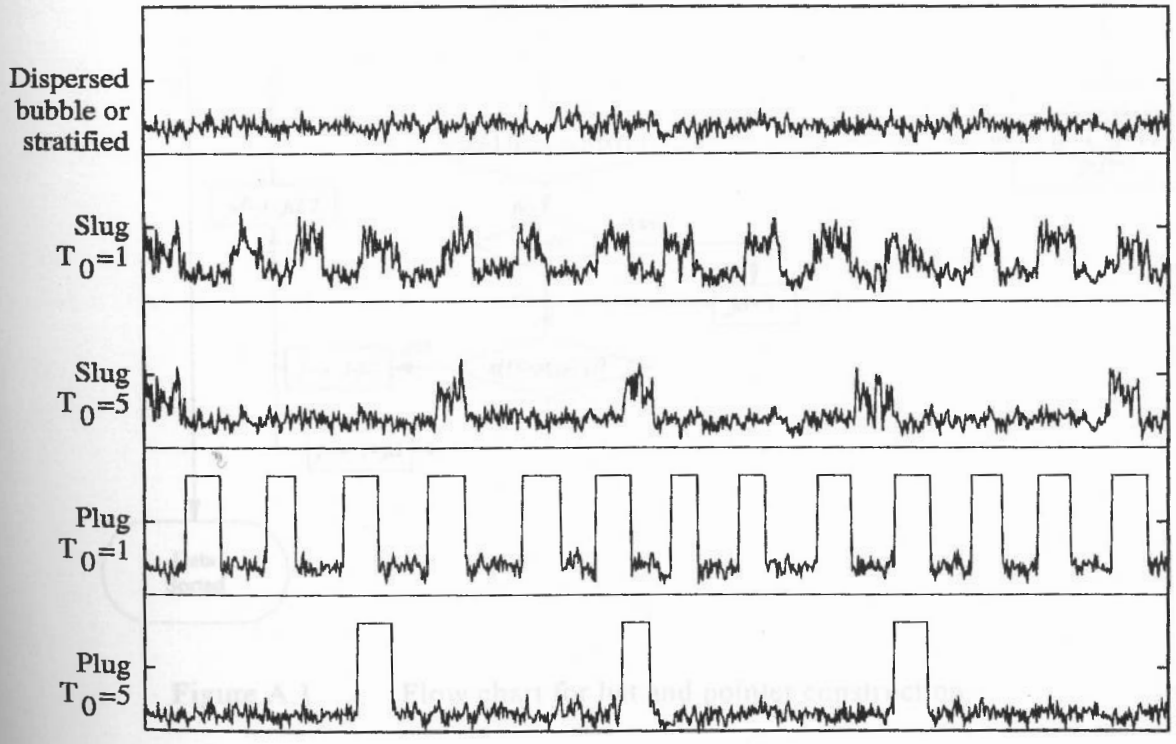

Figure 4.24 Simulated signals for various multiphase flow regimes

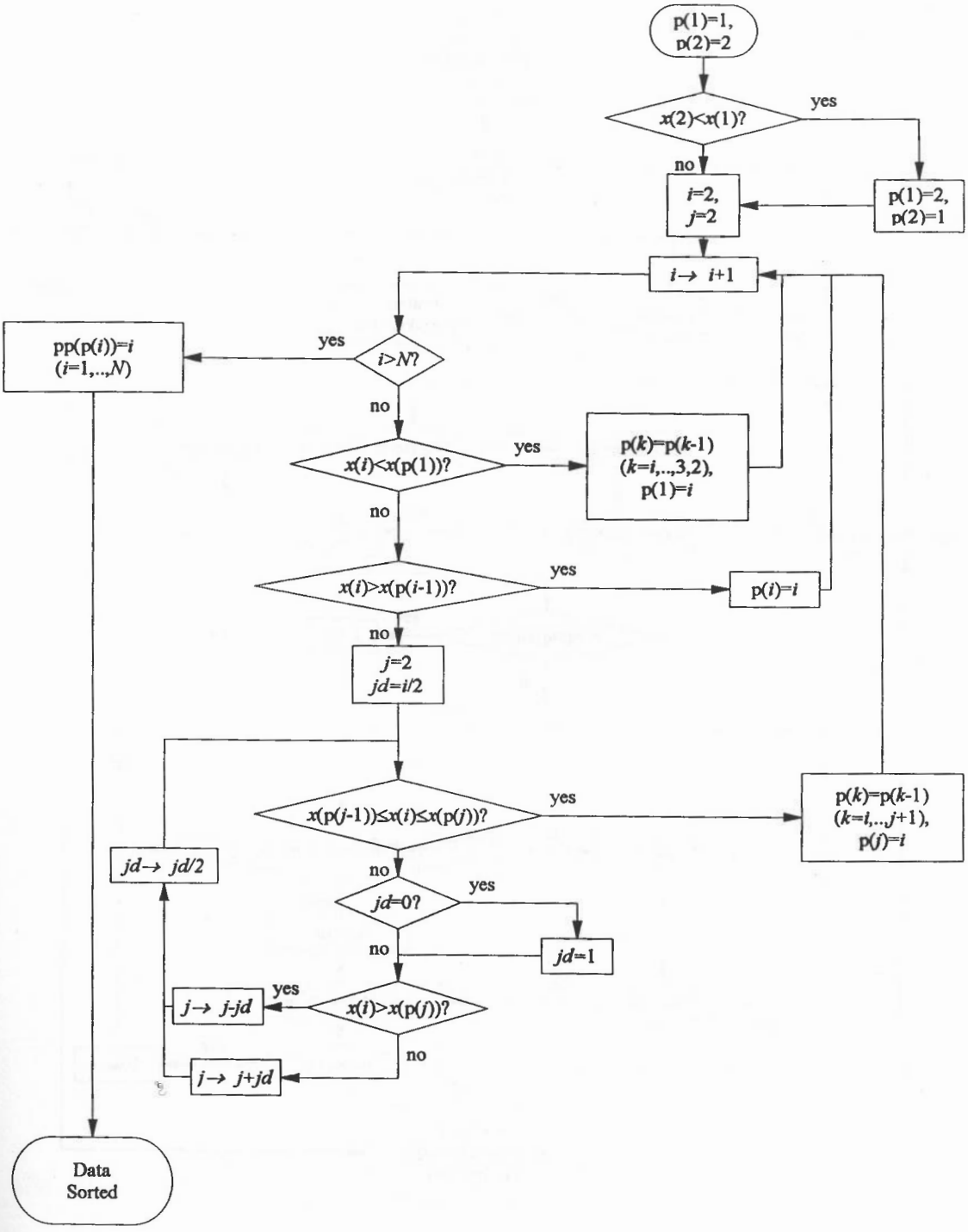

Figure A.1 Flow chart for list and pointer construction

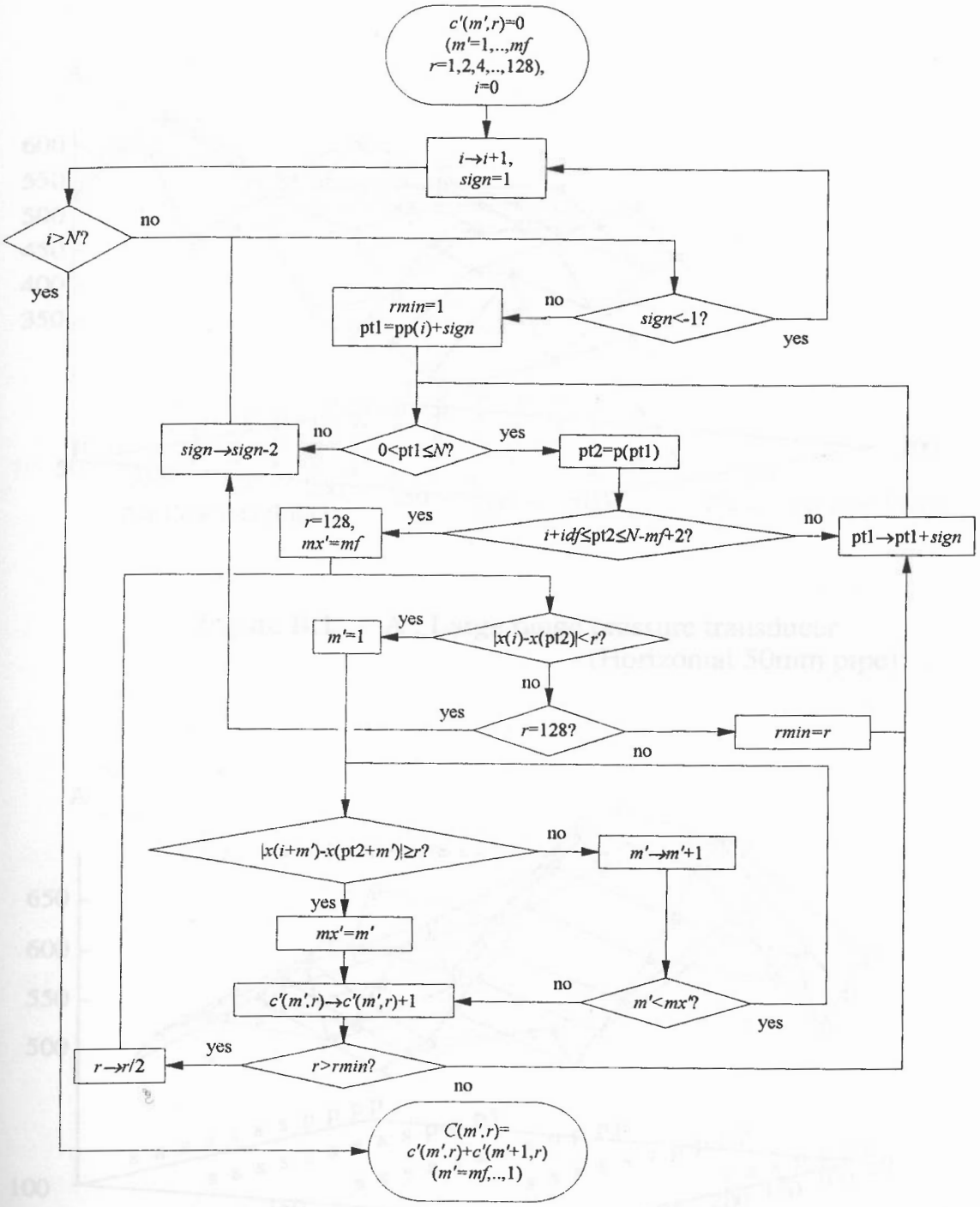

Figure A.2 Flow chart for correlation integral computation

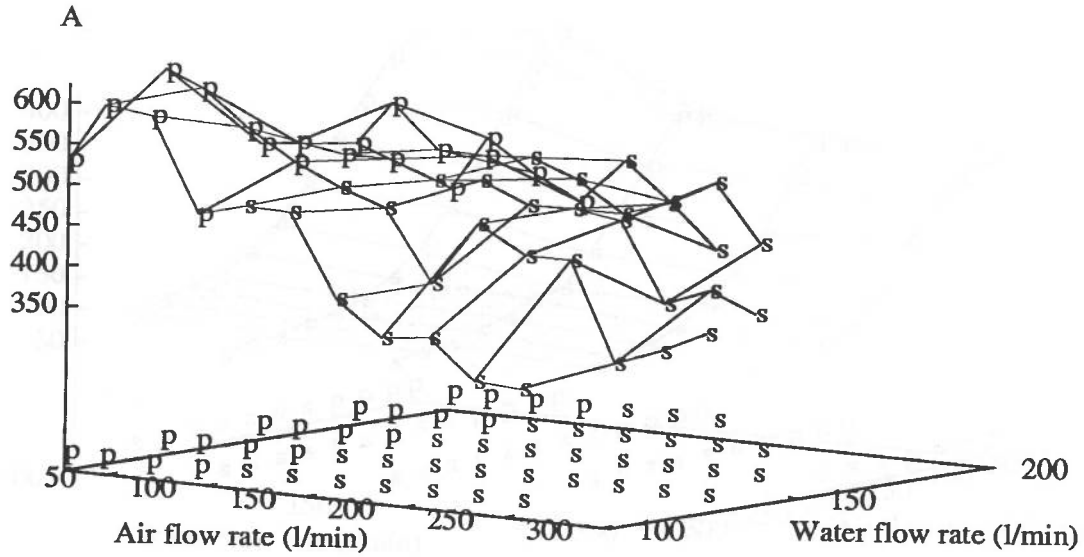

Figure B.1 A : Large range pressure transducer
(Horizontal 50mm pipe)

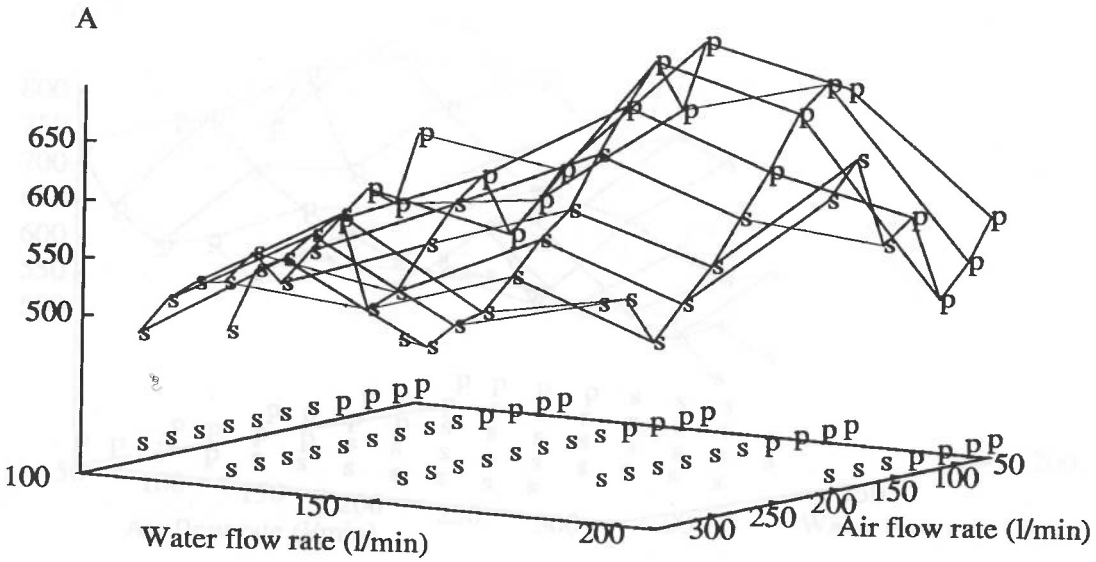

Figure B.2 A : Small range pressure transducer
(Horizontal 50mm pipe)

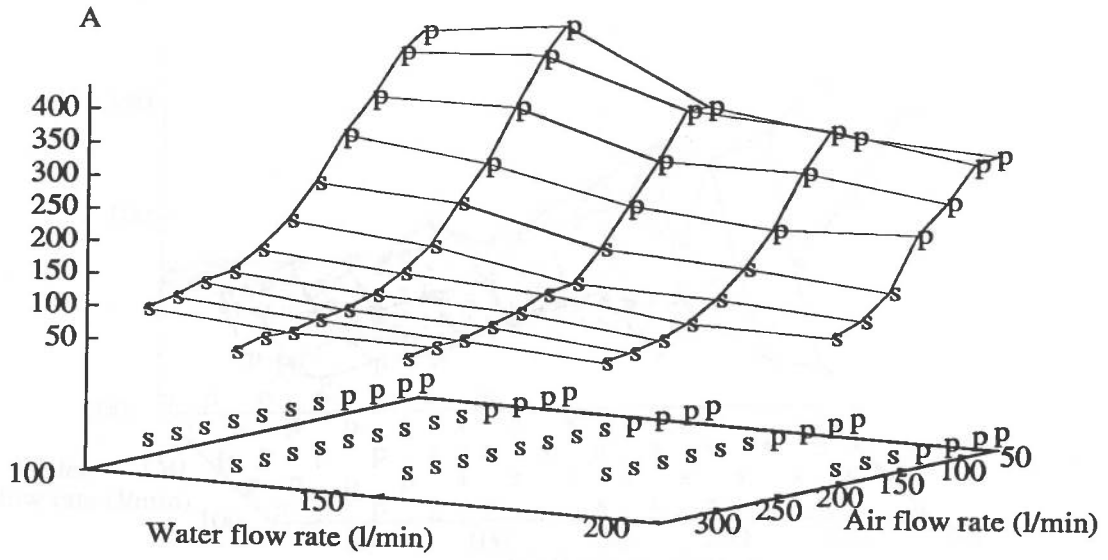

Figure B.3 A : Light transsducer
(Horizontal 50mm pipe)

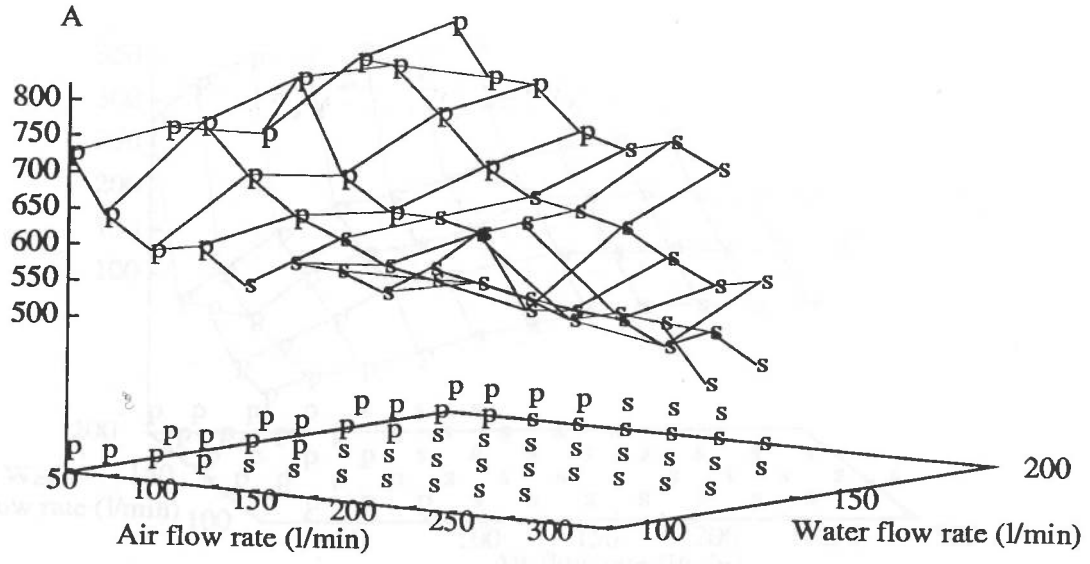

Figure B.4 A : Electrical transsducer
(Horizontal 50mm pipe)

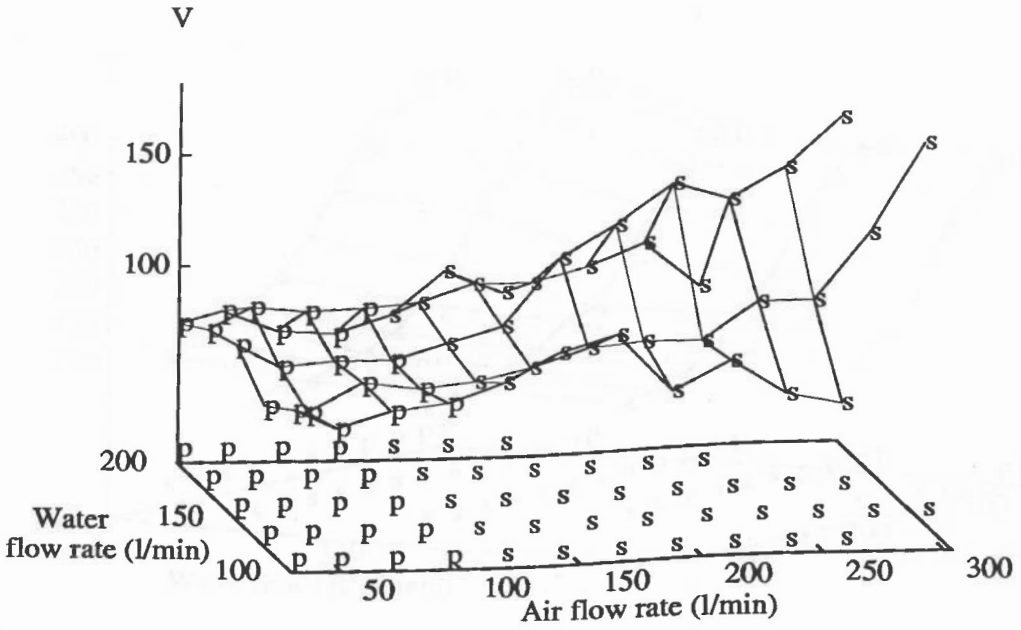

Figure B.5 V : Large range pressure tranducer
(Horizontal 50mm pipe)

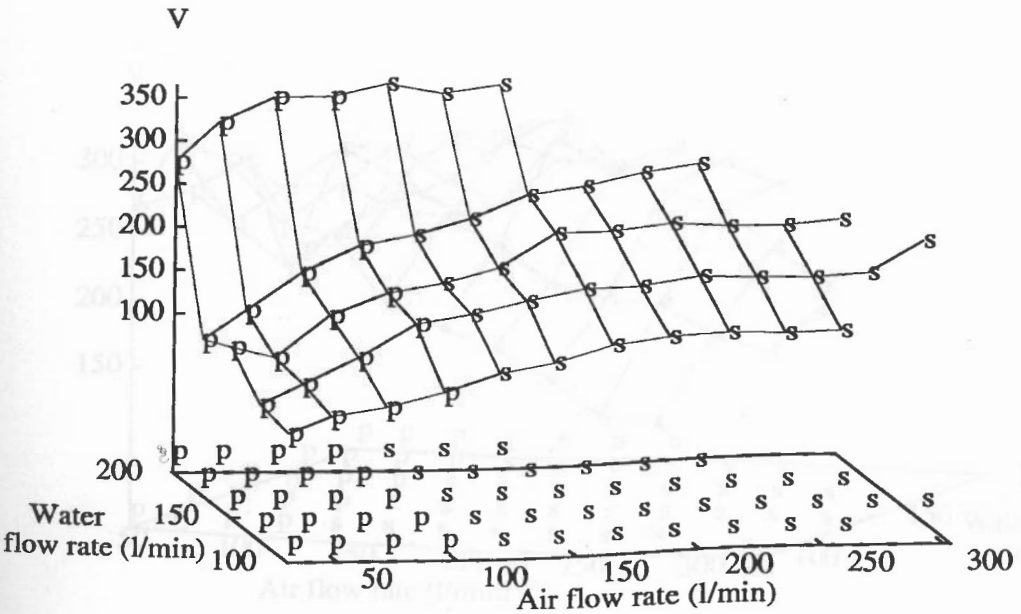

Figure B.6 V : Small range pressure transducer
(Horizontal 50mm pipe)

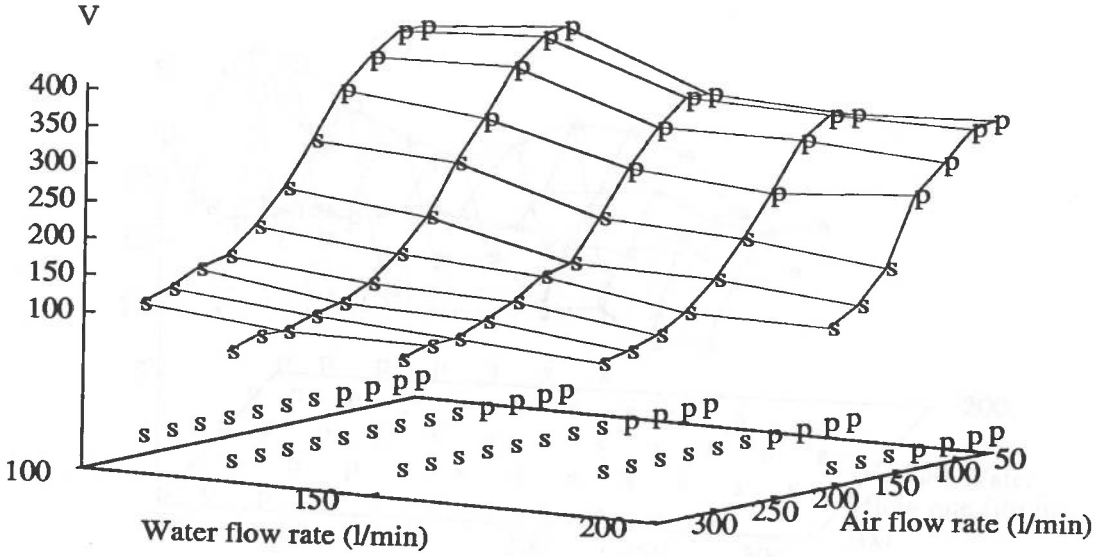

Figure B.7 V : Light tranducer
(Horizontal 50mm pipe)

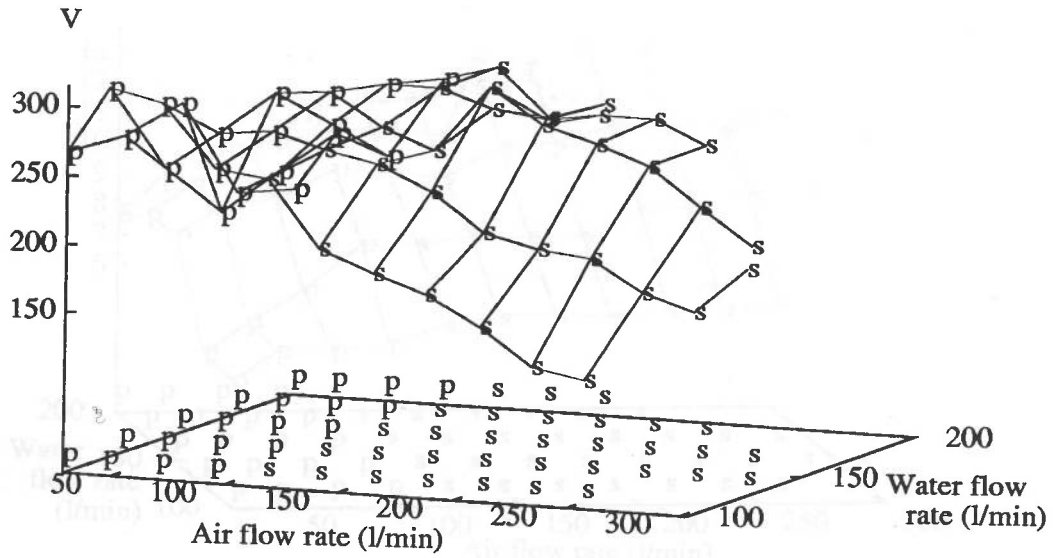

Figure B.8 V : Electrical transducer
(Horizontal 50mm pipe)

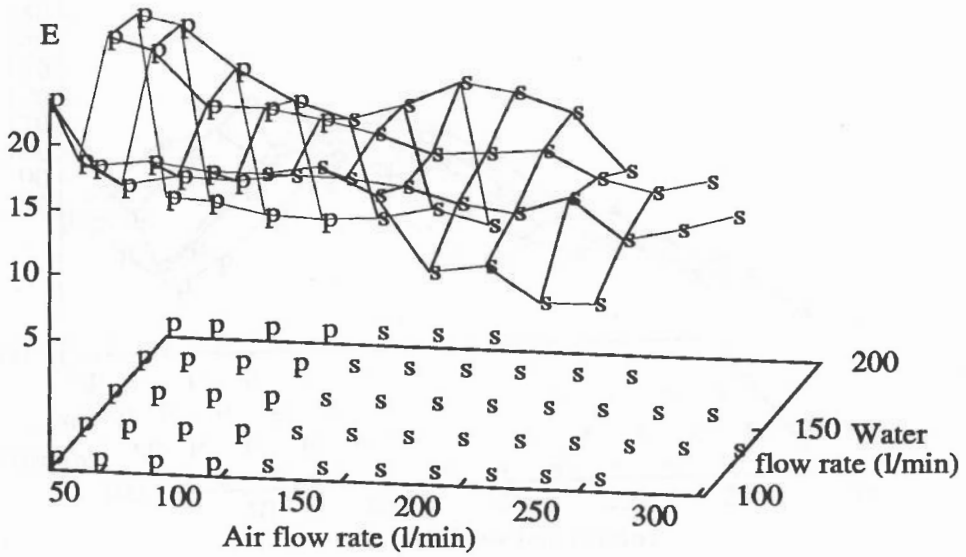

Figure B.9 E : Large range pressure tranducer
(Horizontal 50mm pipe)

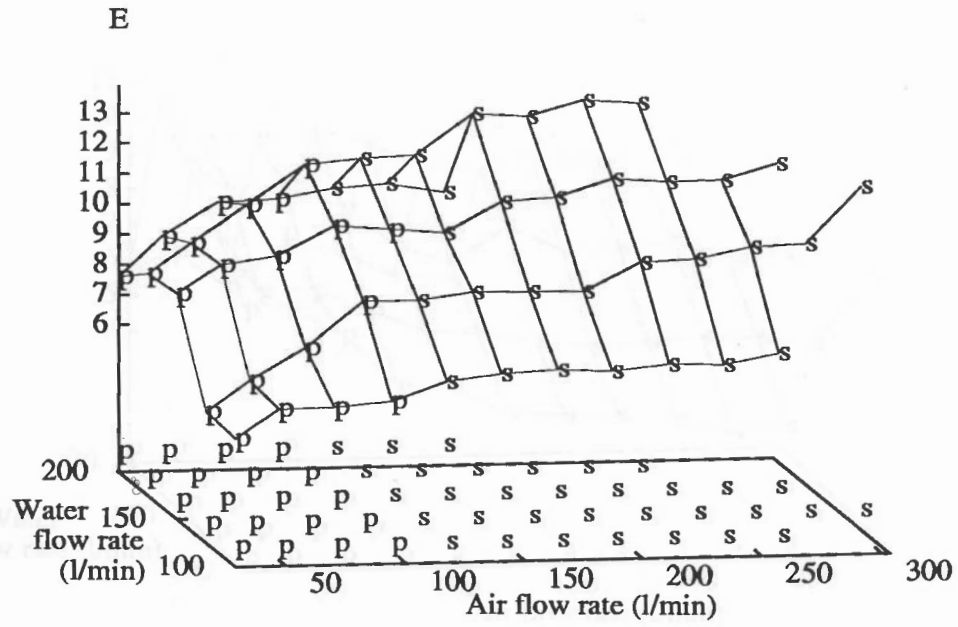

Figure B.10 E : Small range pressure transducer
(Horizontal 50mm pipe)

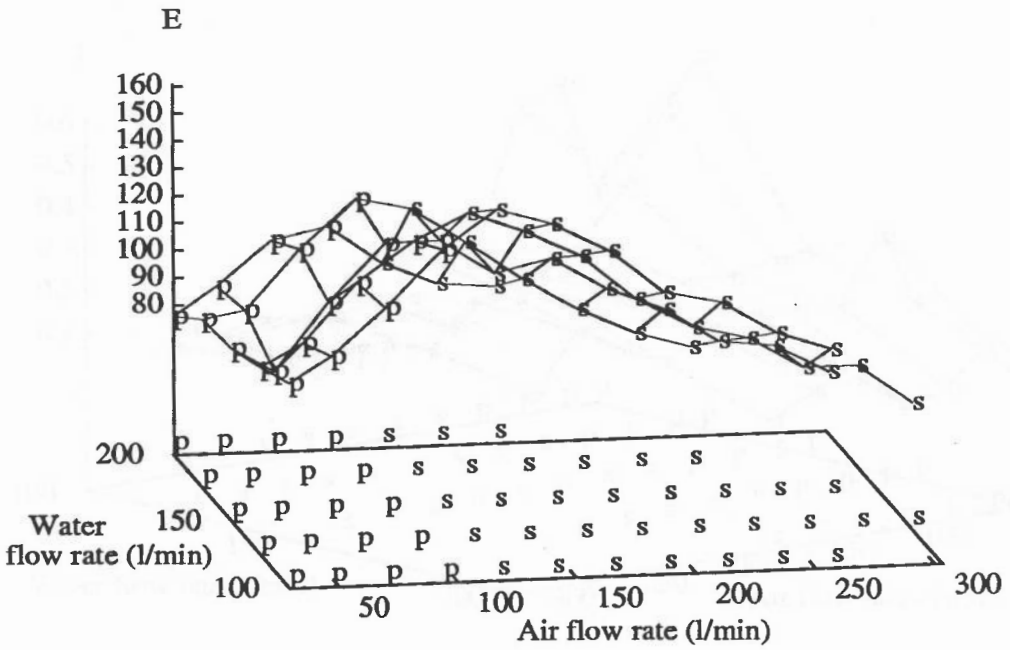

Figure B.11 E : Light tranducer
(Horizontal 50mm pipe)

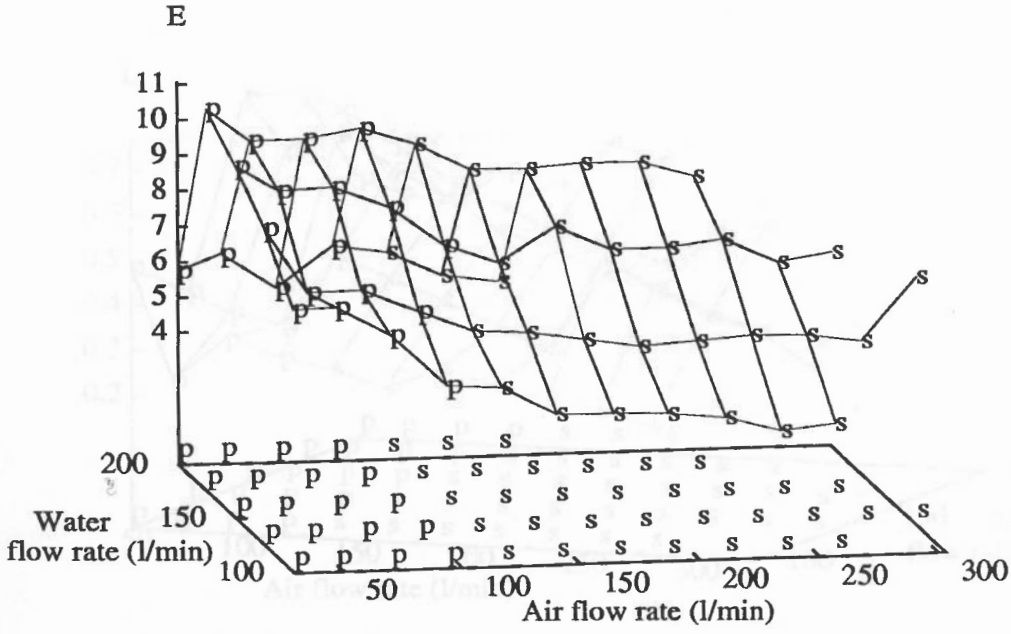

Figure B.12 E : Electrical transducer
(Horizontal 50mm pipe)

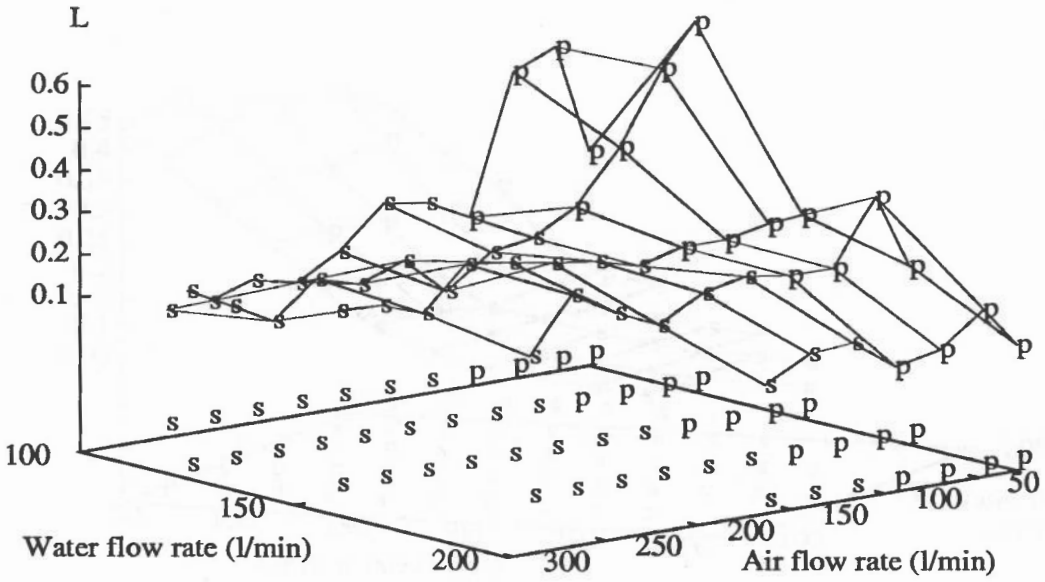

Figure B.13 L : Large range pressure tranducer
(Horizontal 50mm pipe)

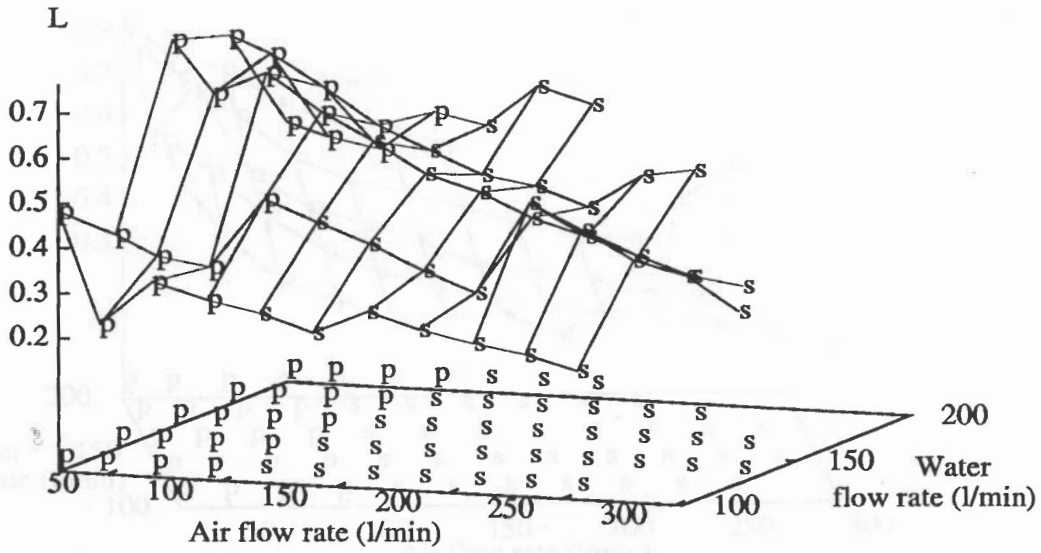

Figure B.14 L : Small range pressure transducer
(Horizontal 50mm pipe)

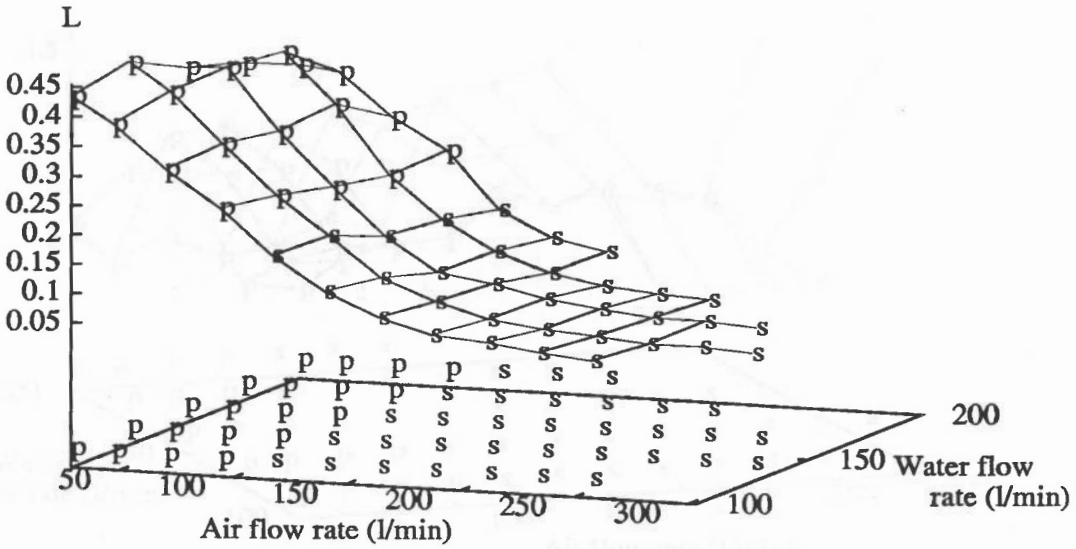

Figure B.15 L : Light tranducer
(Horizontal 50mm pipe)

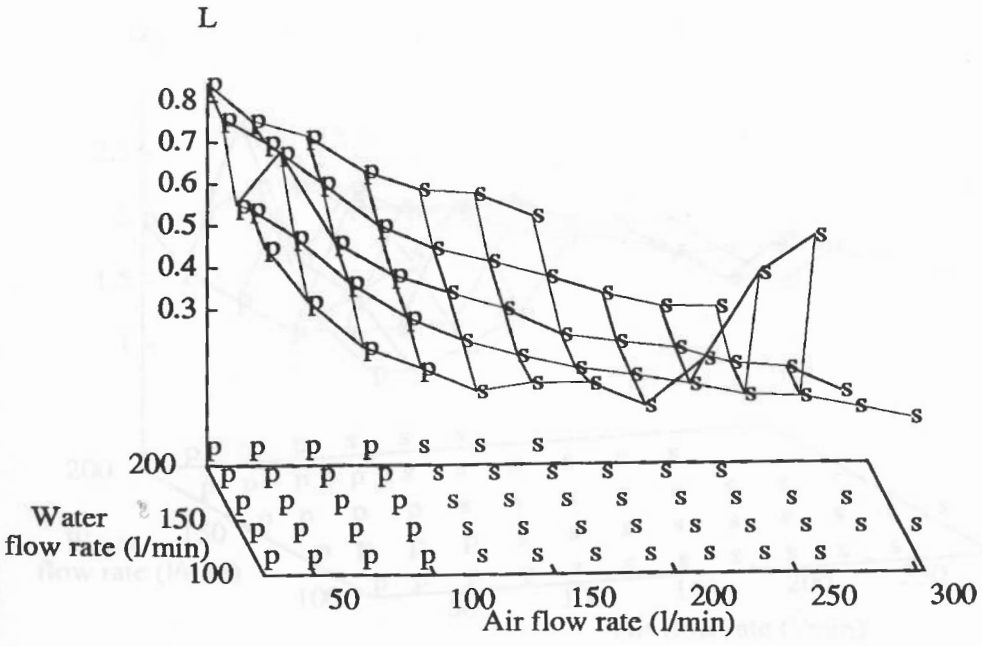

Figure B.16 L : Electrical transducer
(Horizontal 50mm pipe)

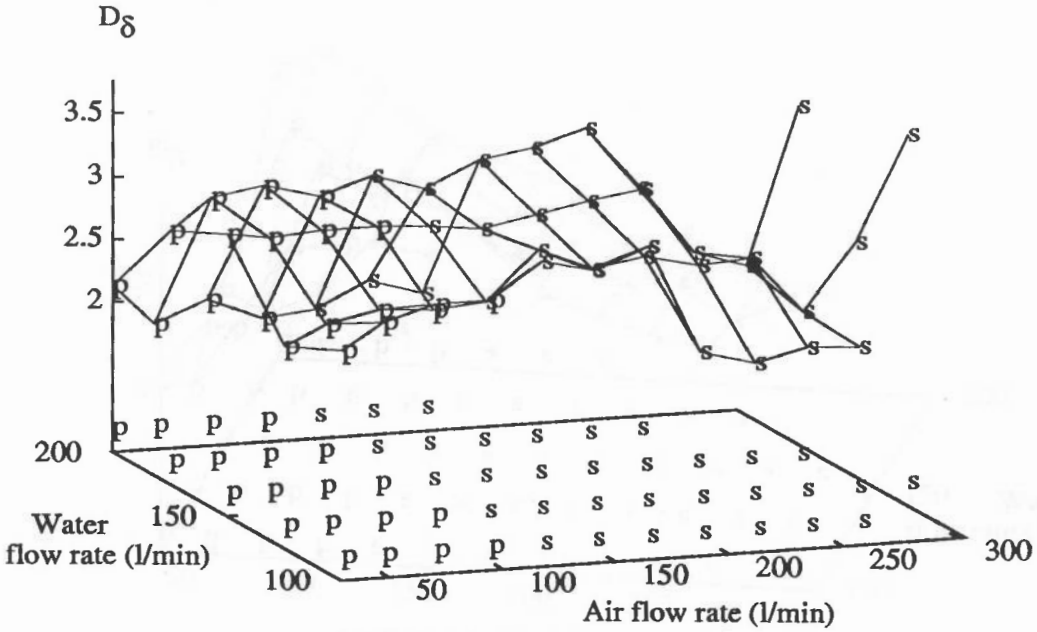

Figure B.17 D_δ : Large range pressure tranducer
(Horizontal 50mm pipe)

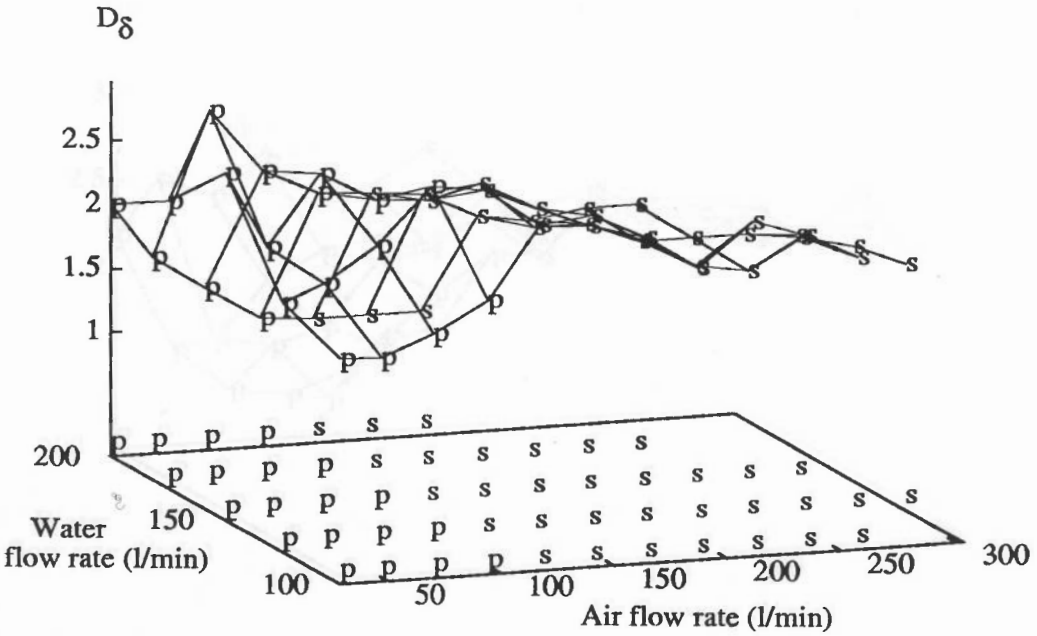

Figure B.18 D_δ : Small range pressure transducer
(Horizontal 50mm pipe)

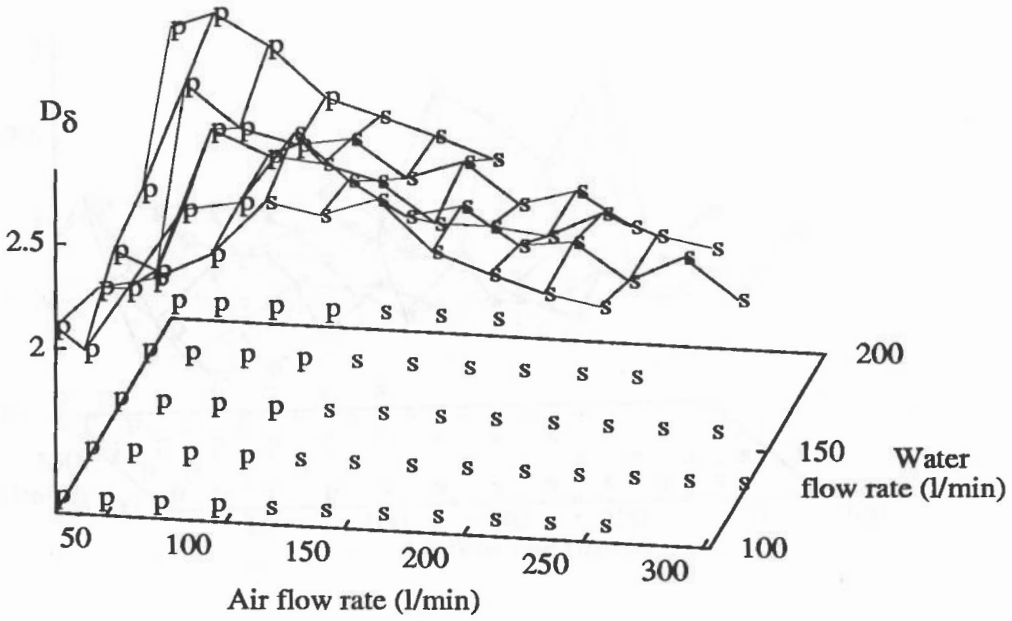

Figure B.19 D_δ: Light tranducer (τ = 0.00125 s)
(Horizontal 50mm pipe)

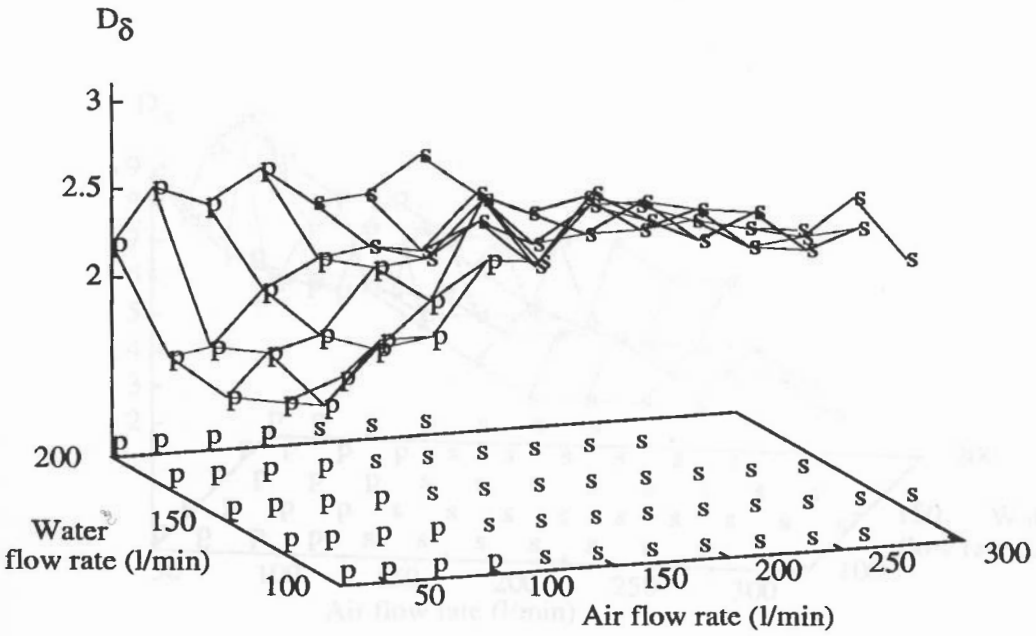

Figure B.20 D_δ: Light tranducer (τ = 0.00375 s)
(Horizontal 50mm pipe)

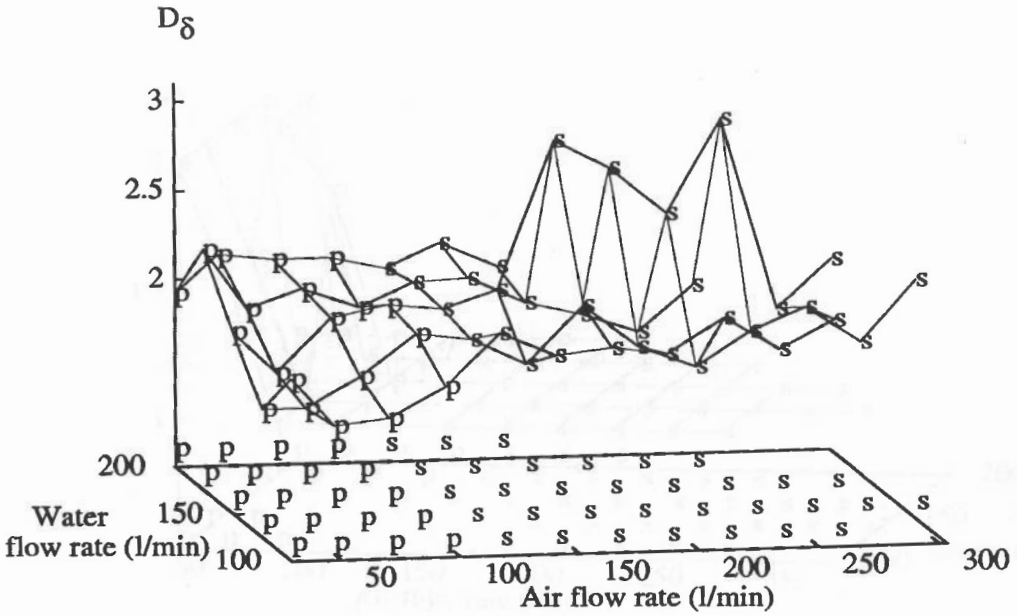

Figure B.21 D_δ : Electrical transducer
(Horizontal 50mm pipe)

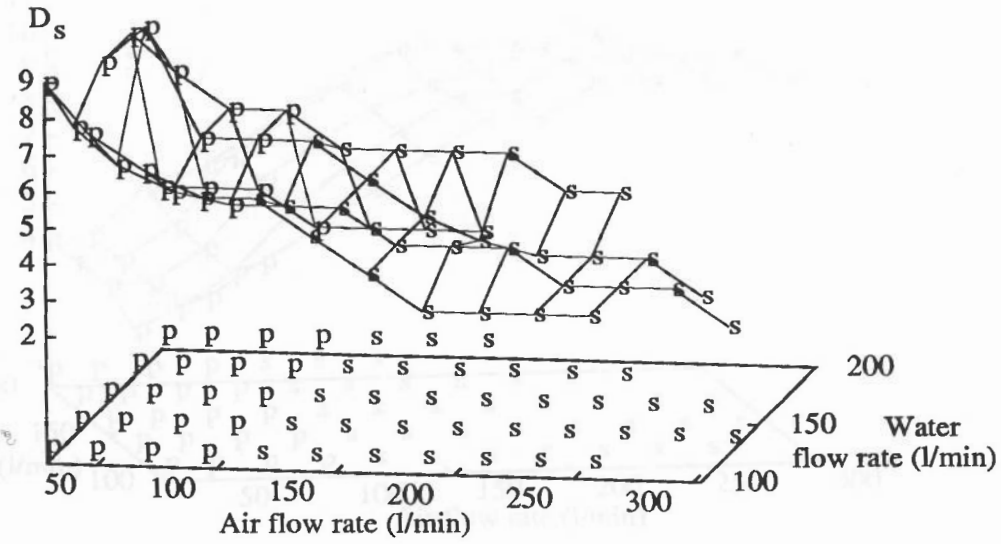

Figure B.22 D_s : Large pressure transducer (τ = 0.00375 s)
(Horizontal 50mm pipe)

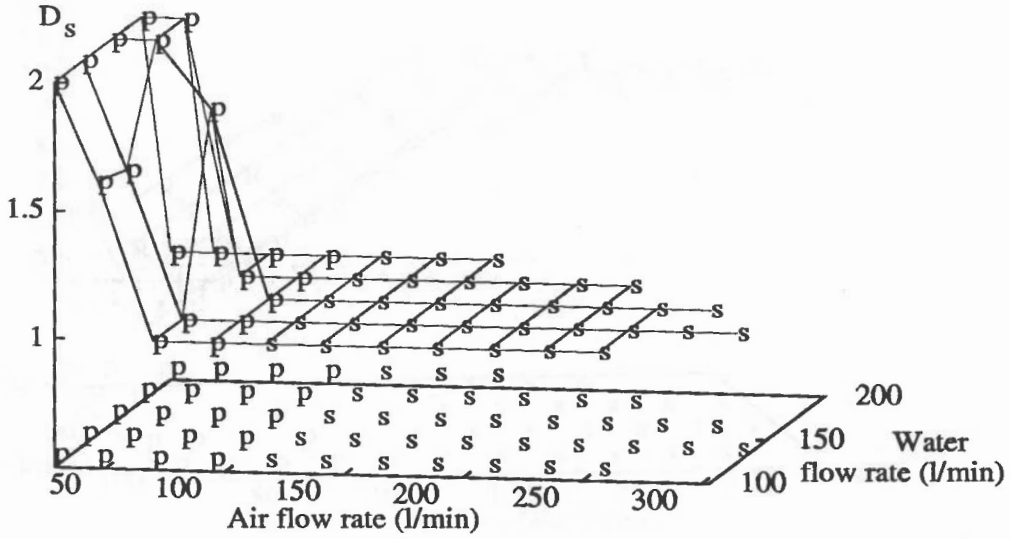

Figure B.23 D_s : Small pressure transducer
(Horizontal 50mm pipe)

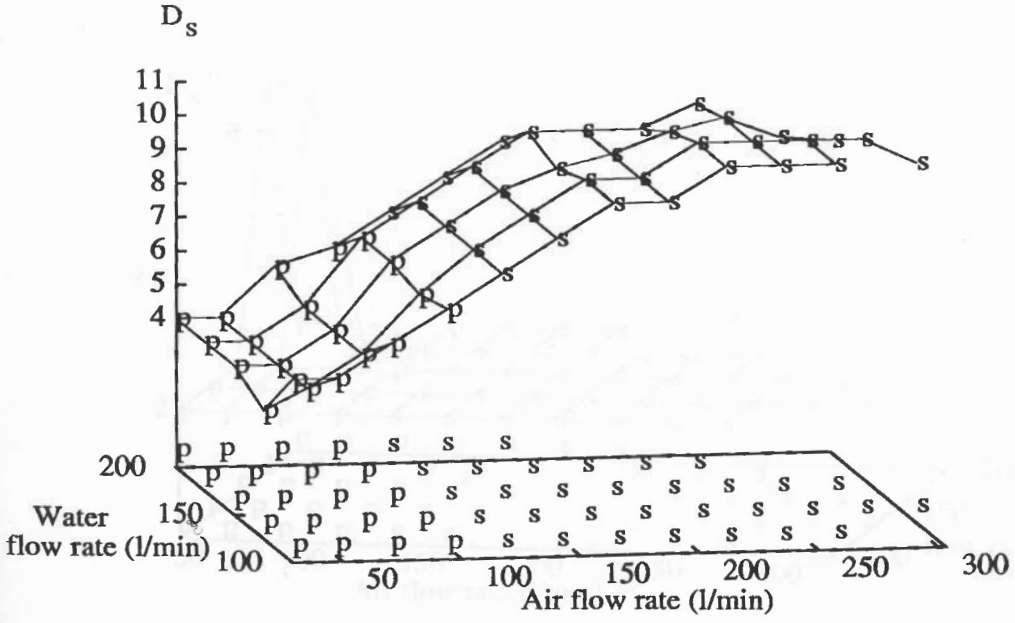

Figure B.24 D_s : Light transducer (τ = 0.00125 s)
(Horizontal 50mm pipe)

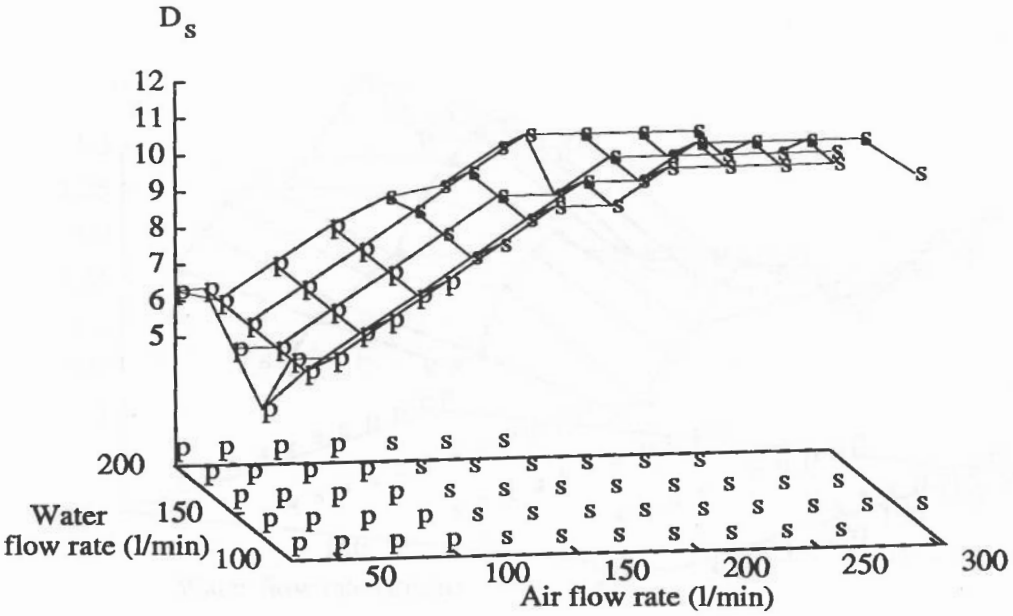

Figure B.25 D_s : Light transducer (τ = 0.00375 s)
(Horizontal 50mm pipe)

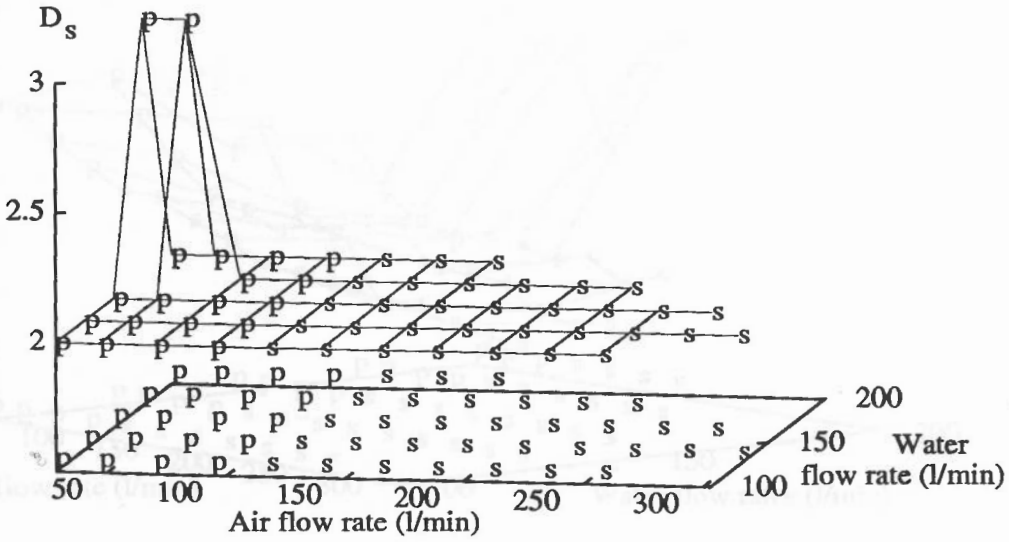

Figure B.26 D_s : Electrical transducer (τ = 0.00375 s)
(Horizontal 50mm pipe)

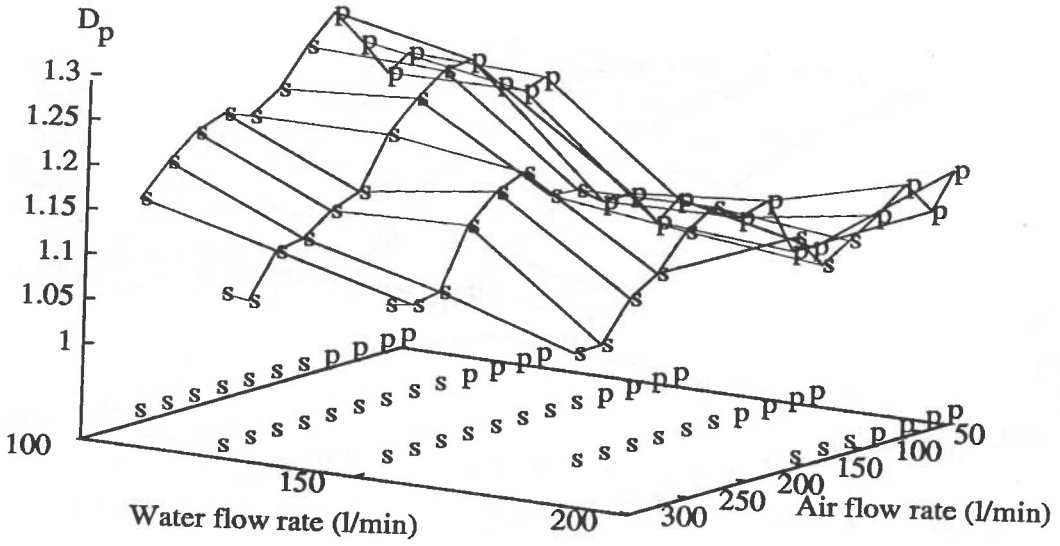

Figure B.27 D_p : Large range pressure tranducer (Horizontal 50mm pipe)

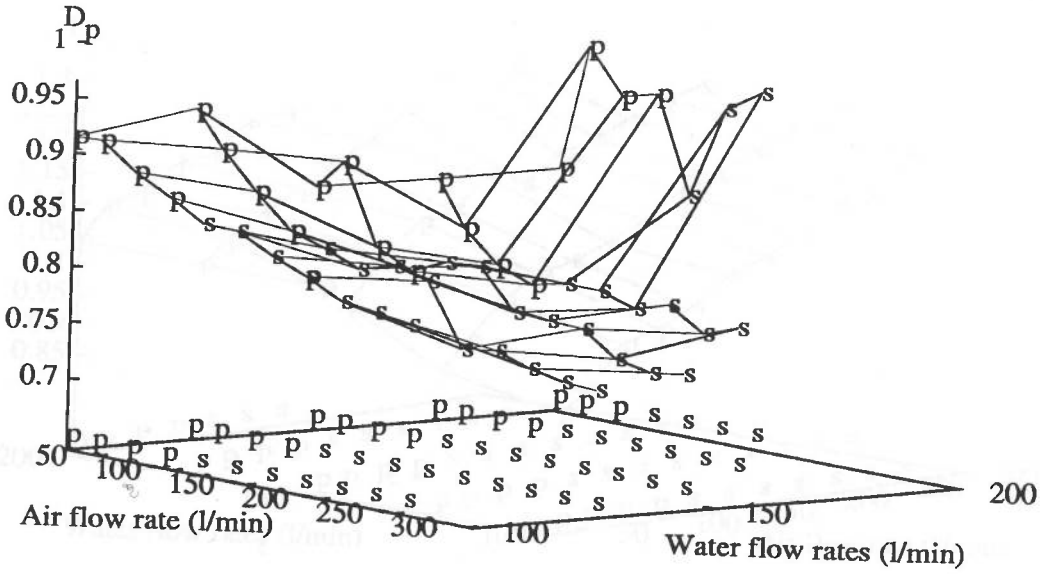

Figure B.28 D_p : Small range pressure transducer (Horizontal 50mm pipe)

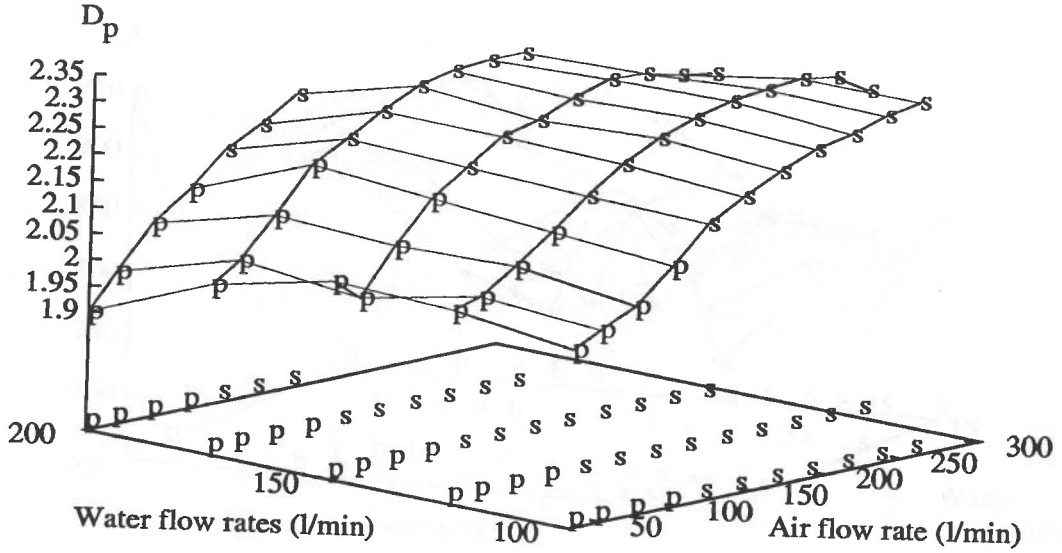

Figure B.29 D_p : Light transducer
(Horizontal 50mm pipe)

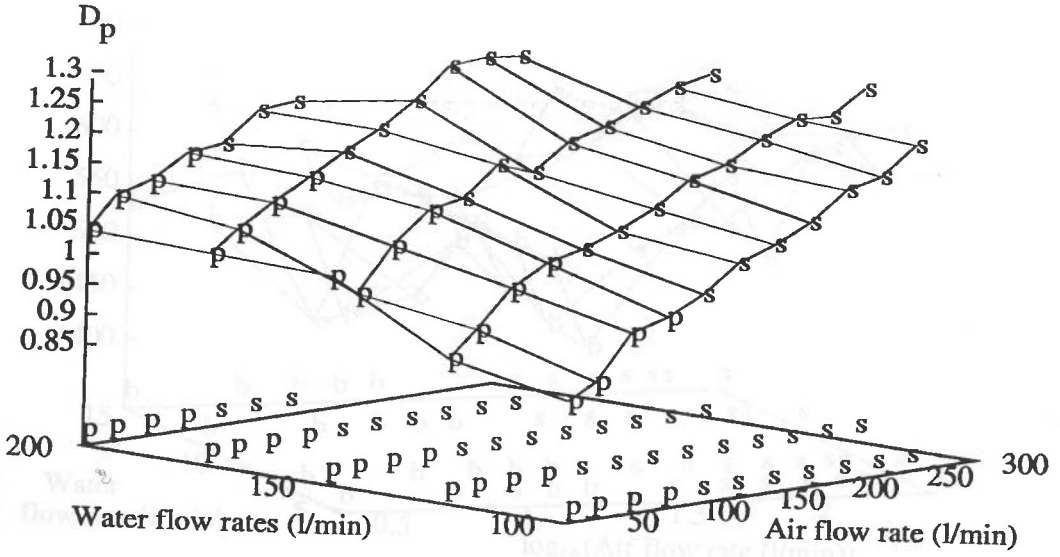

Figure B.30 D_p : Electrical transducer
(Horizontal 50mm pipe)

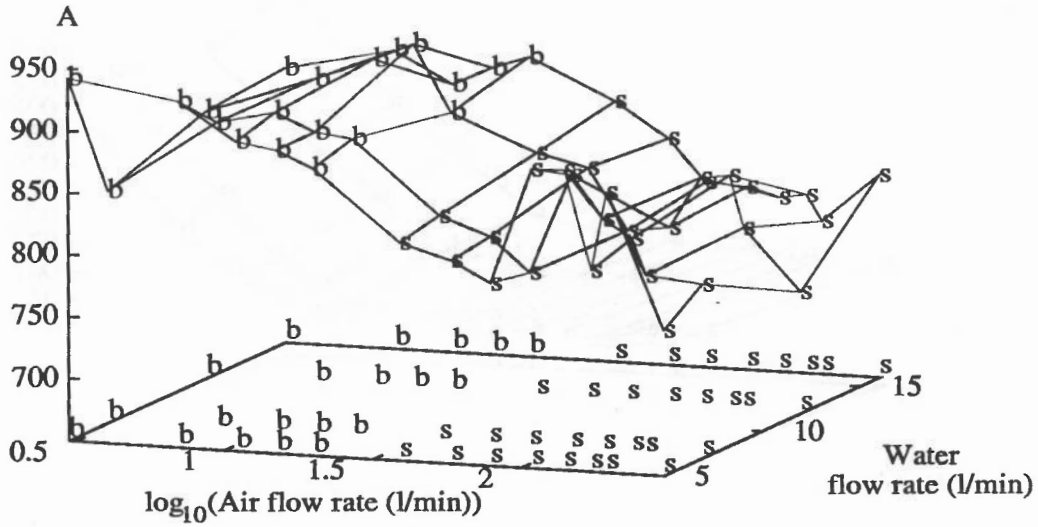

Figure B.31 A : Large range pressure transducer
(Vertical 50mm pipe)

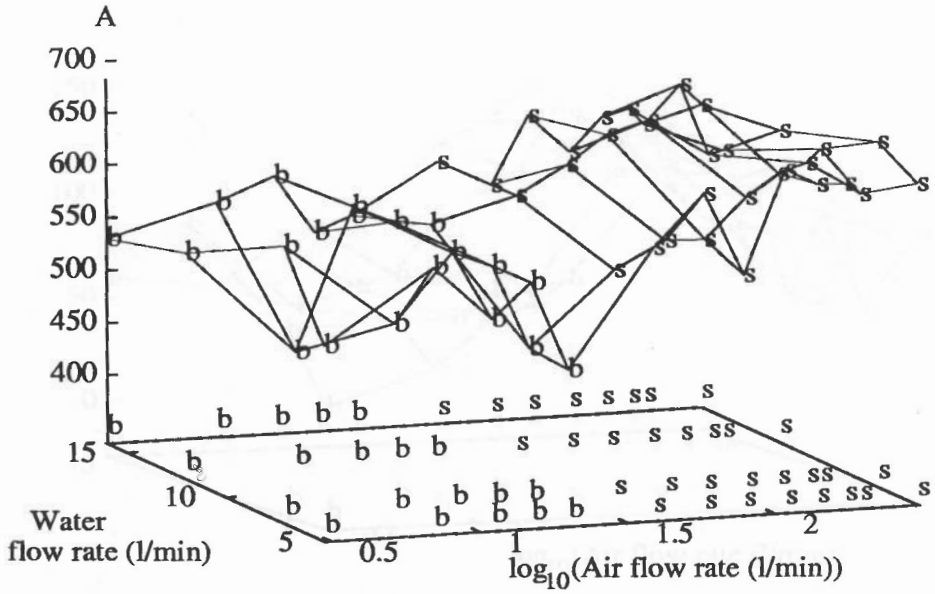

Figure B.32 A : Electrical transducer
(Vertical 50mm pipe)

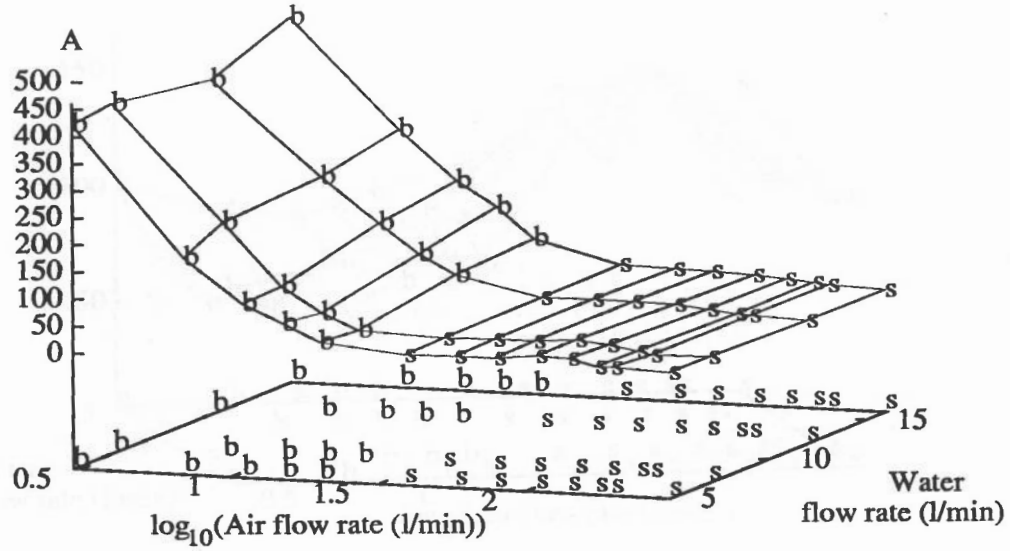

Figure B.33 A : Light transducer
(Vertical 50mm pipe)

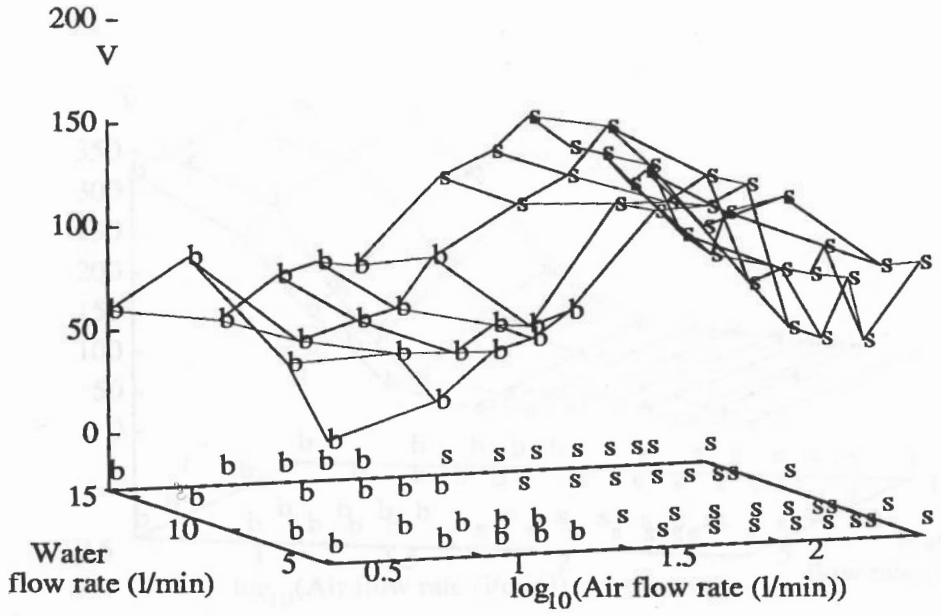

Figure B.34 V : Large range pressure transducer
(Vertical 50mm pipe)

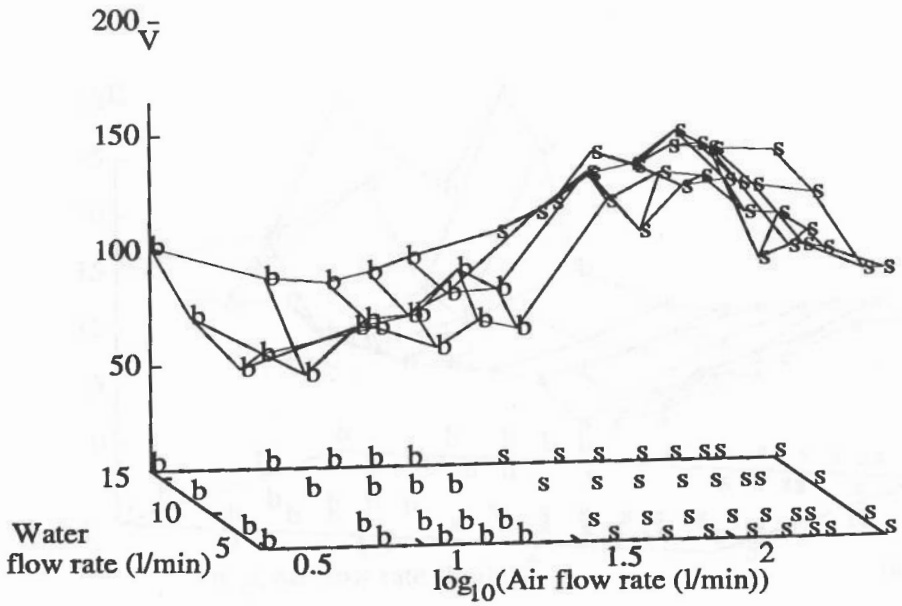

Figure B.35 V : Electrical transducer
(Vertical 50mm pipe)

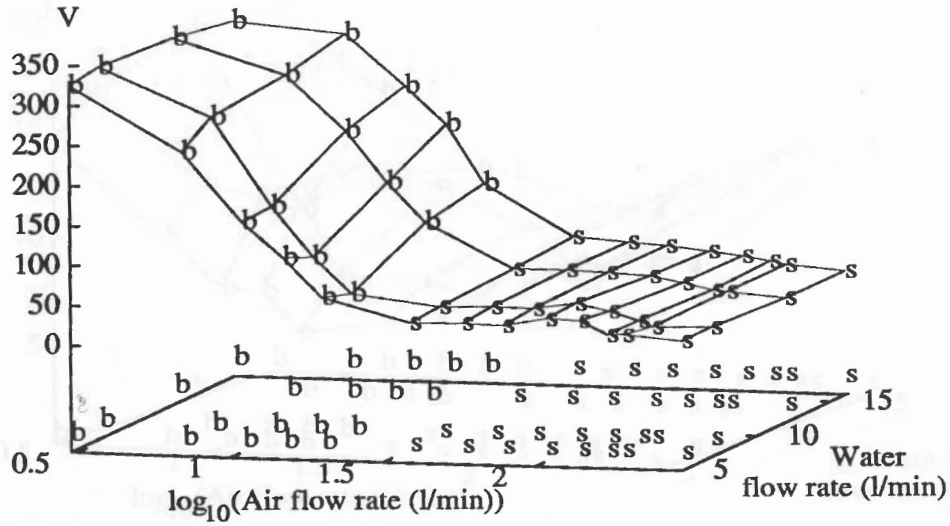

Figure B.36 V : Light transducer
(Vertical 50mm pipe)

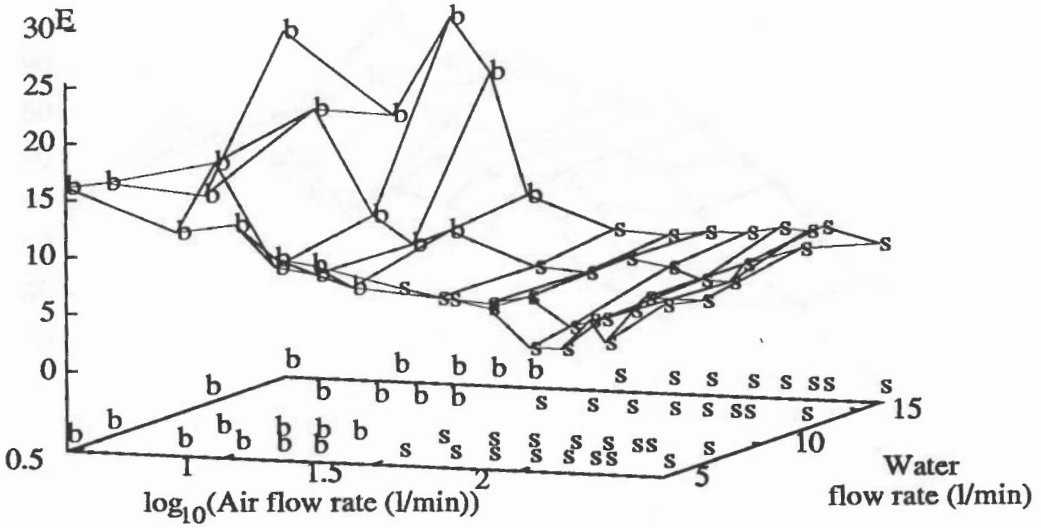

Figure B.37 E : Large range pressure transducer
(Vertical 50mm pipe)

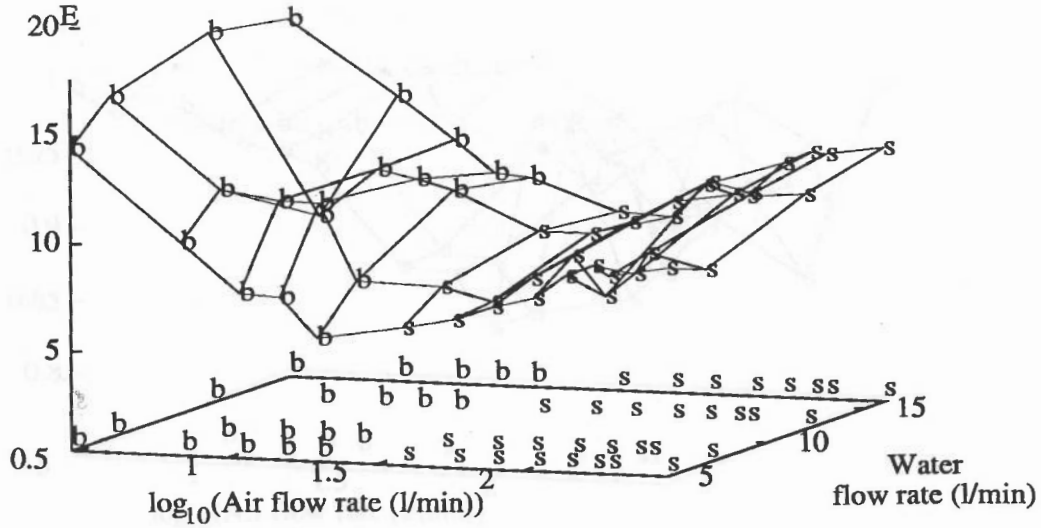

Figure B.38 E : Electrical transducer
(Vertical 50mm pipe)

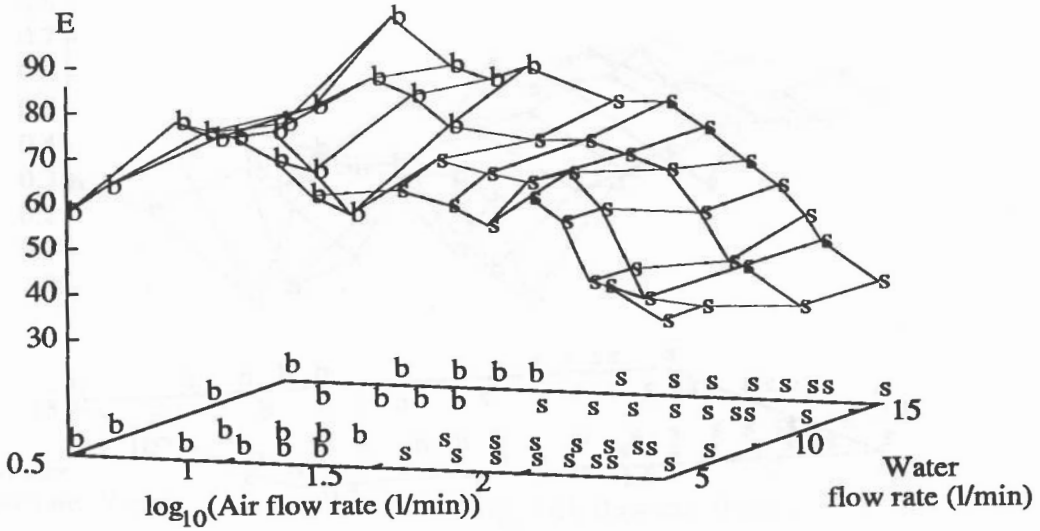

Figure B.39 E : Light transducer
(Vertical 50mm pipe)

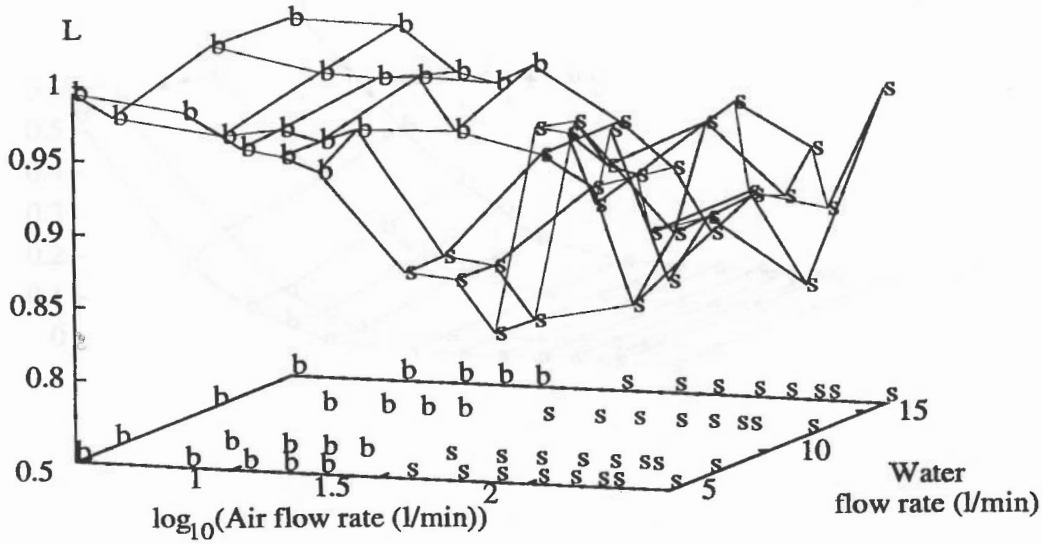

Figure B.40 L : Large range pressure transducer
(Vertical 50mm pipe)

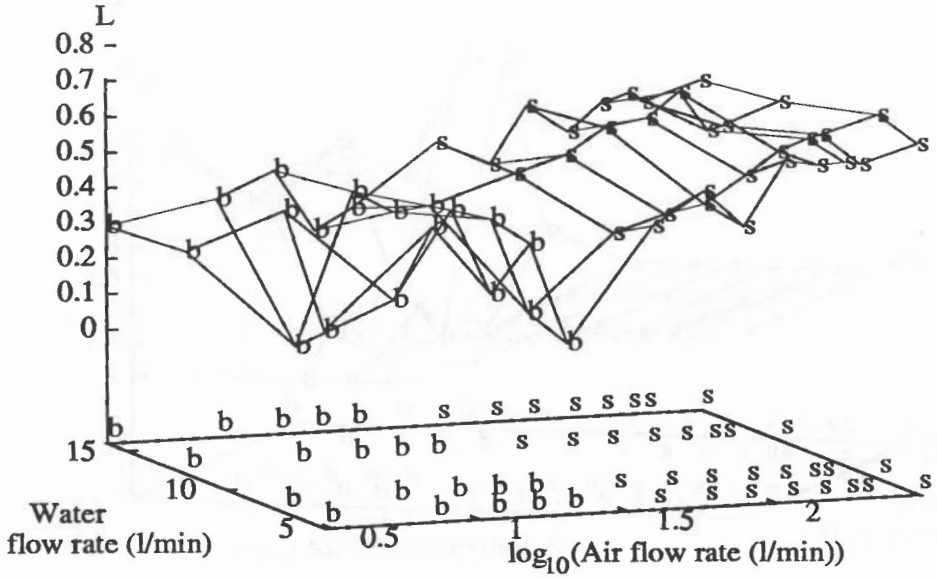

Figure B.41 L : Electrical transducer
(Vertical 50mm pipe)

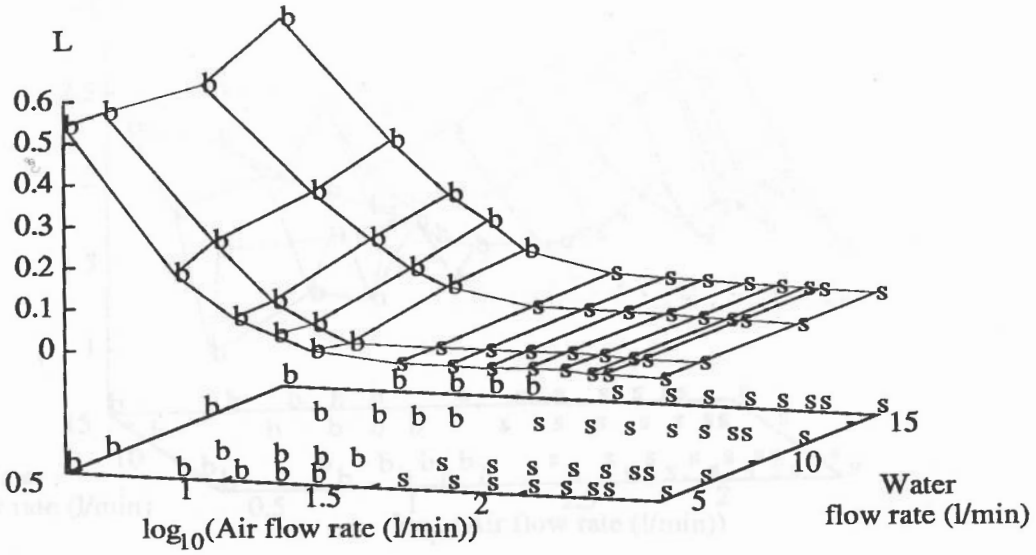

Figure B.42 L : Light transducer
(Vertical 50mm pipe)

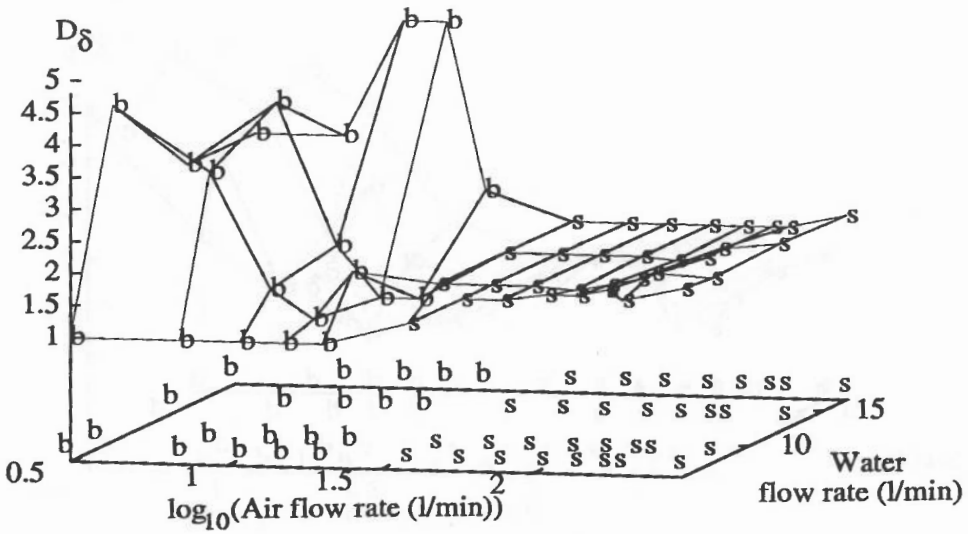

Figure B.43 D_δ : Large range pressure transducer
(Vertical 50mm pipe)

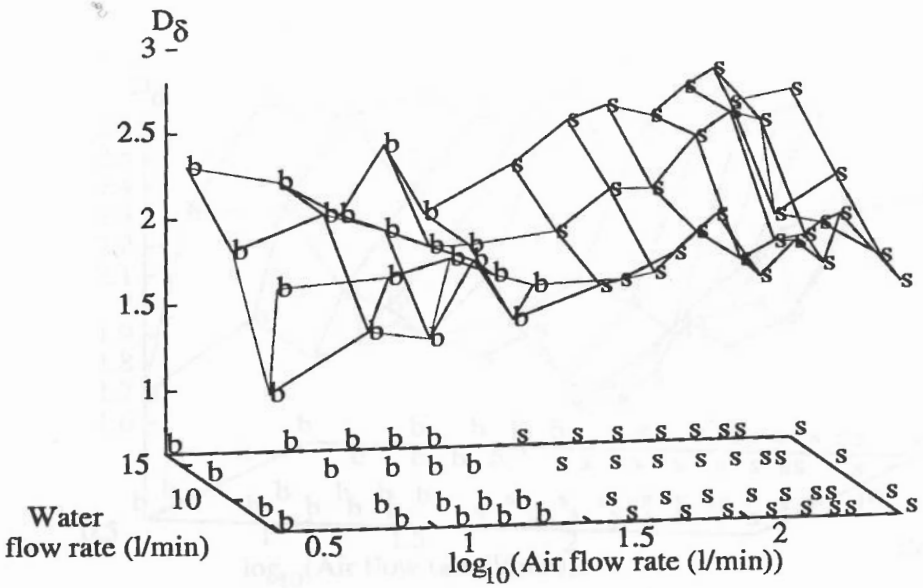

Figure B.44 D_δ : Electrical transducer
(Vertical 50mm pipe)

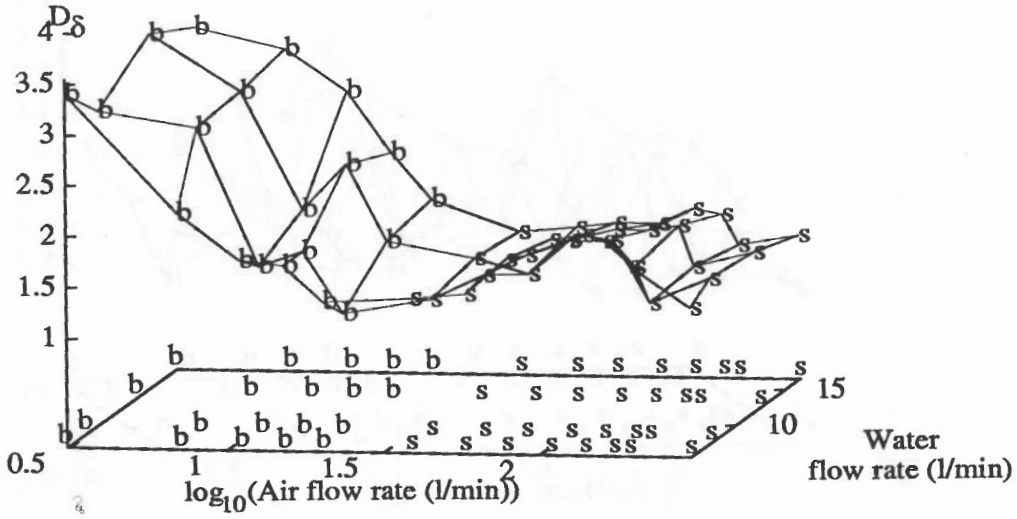

Figure B.45 D_δ : Light transducer
(Vertical 50mm pipe)

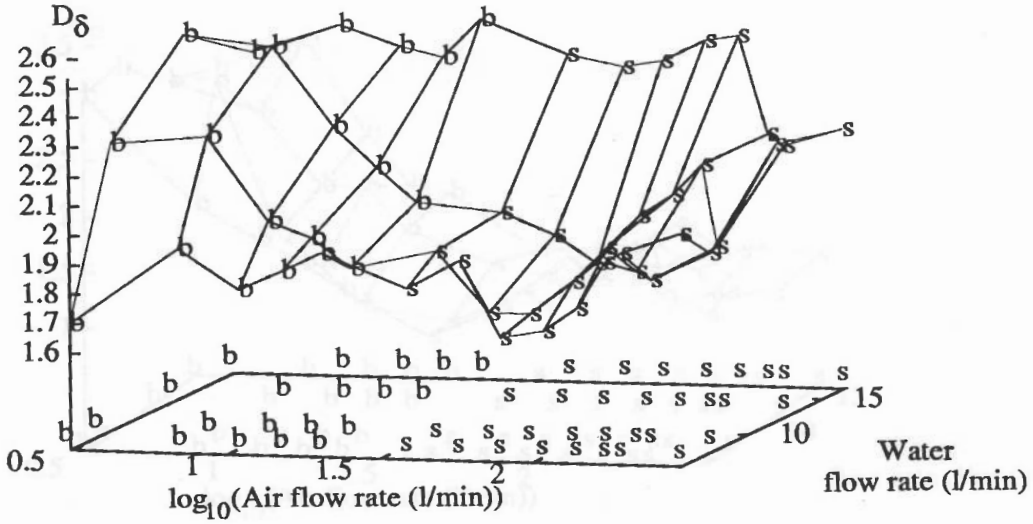

Figure B.46 D_δ : Large range pressure transducer
($\tau = 0.027$s) (Vertical 50mm pipe)

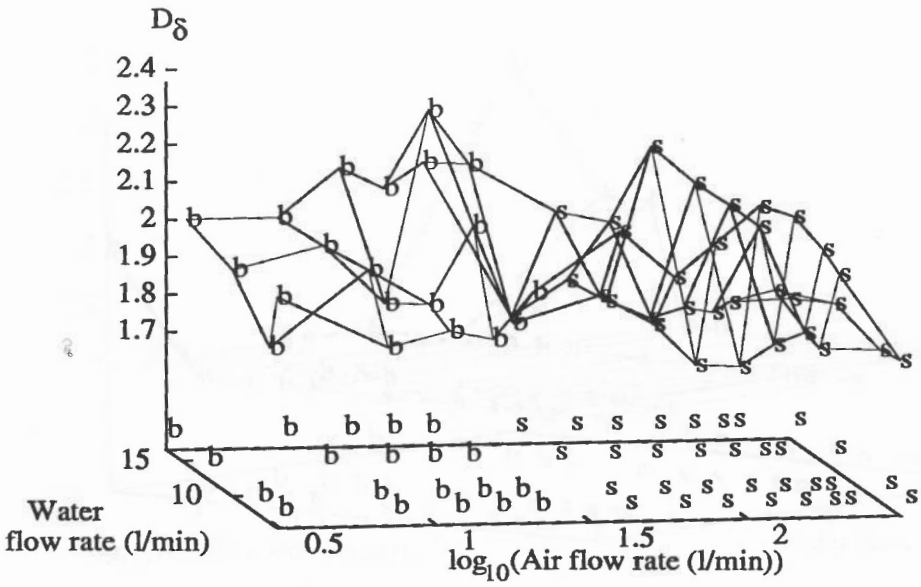

Figure B.47 D_δ : Electrical transducer
(τ = 0.027s) (Vertical 50mm pipe)

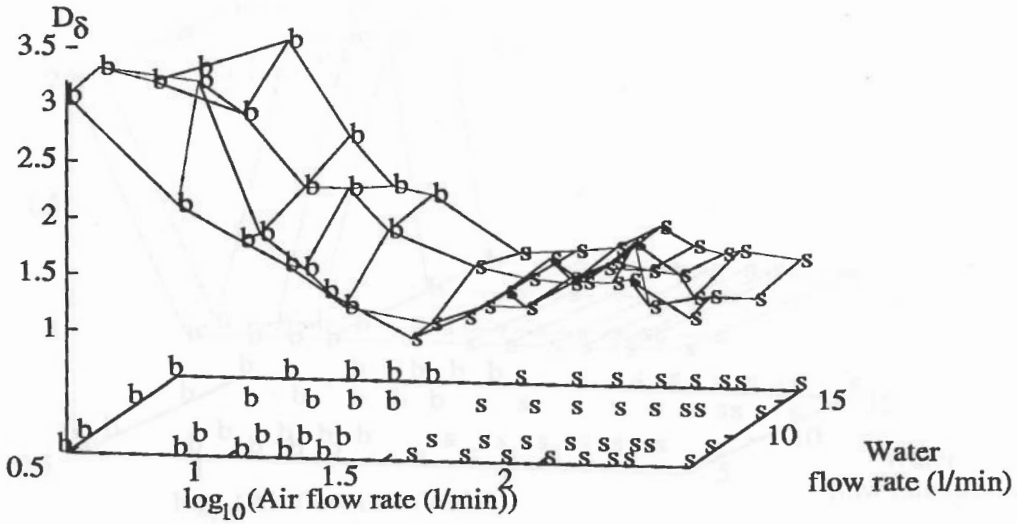

Figure B.48 D_δ : Light transducer
(τ = 0.027s) (Vertical 50mm pipe)

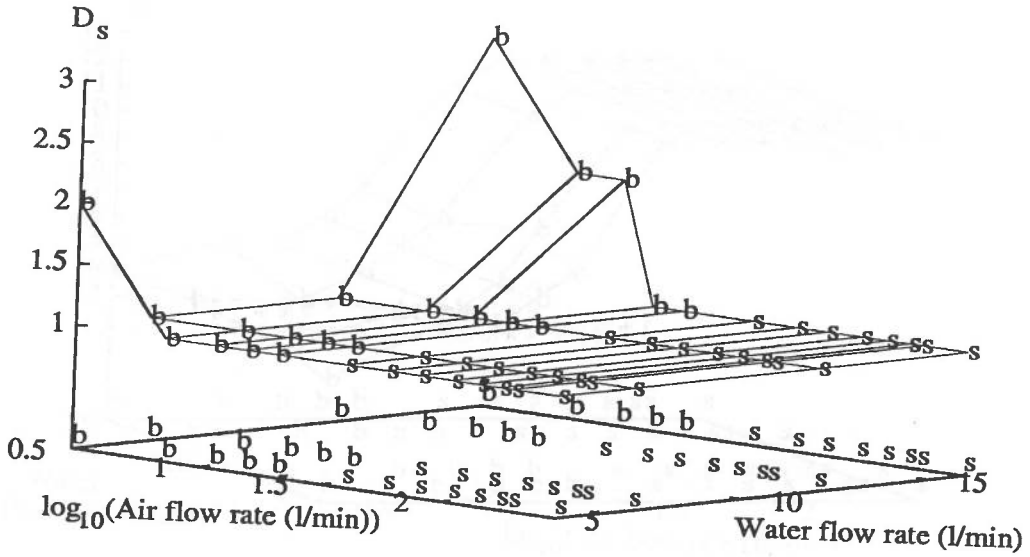

Figure B.49 D_s : Large range pressure transducer
(Vertical 50mm pipe)

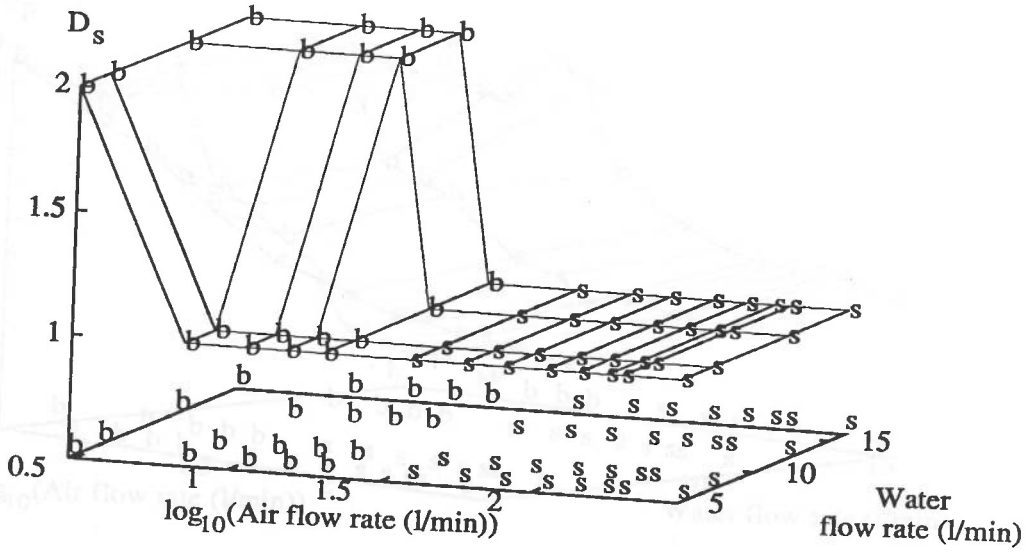

Figure B.50 D_s : Electrical transducer
(Vertical 50mm pipe)

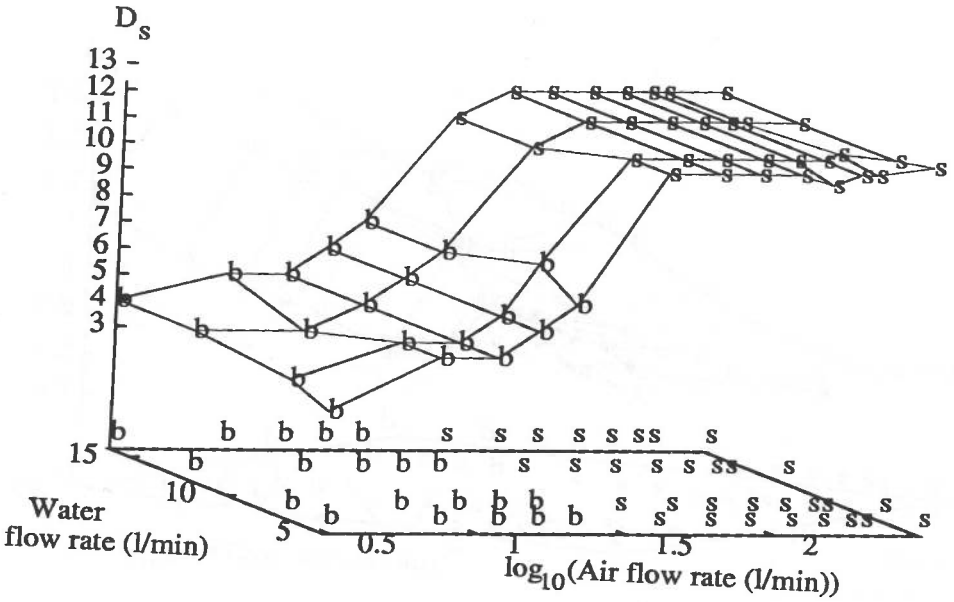

Figure B.51 D_s : Light transducer
(Vertical 50mm pipe)

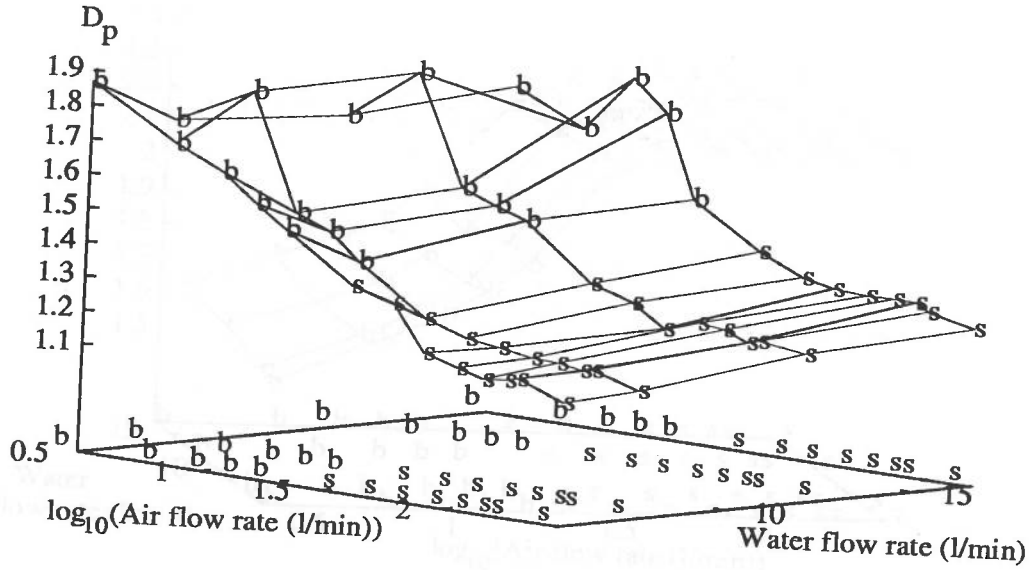

Figure B.52 D_p : Large range pressure transducer
(Vertical 50mm pipe)

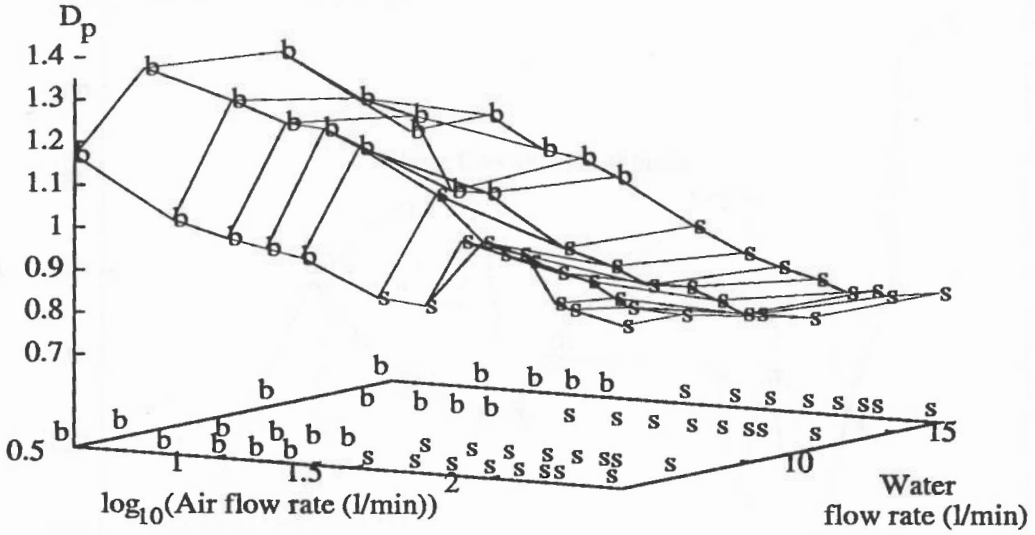

Figure B.53 D_p : Electrical transducer
(Vertical 50mm pipe)

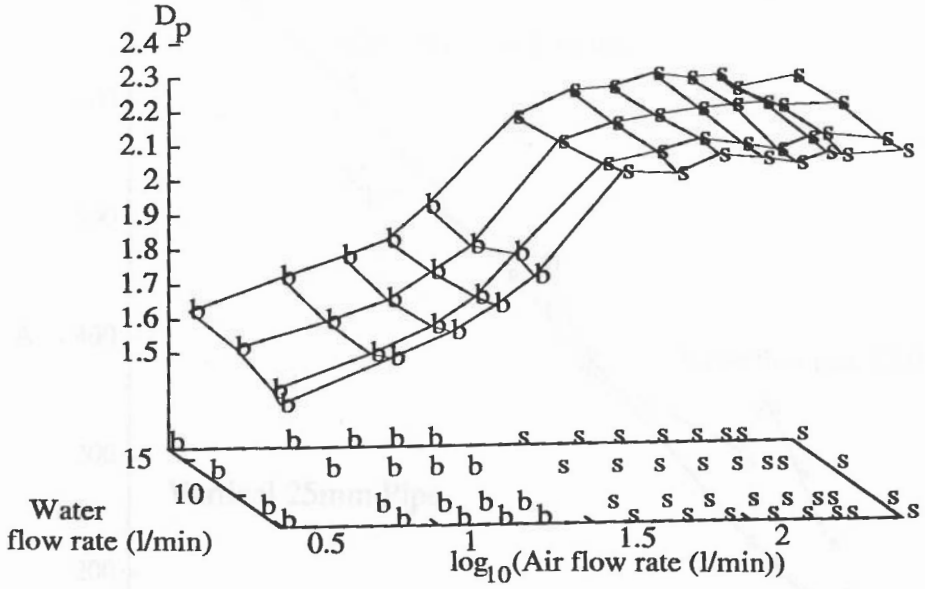

Figure B.54 D_p : Light transducer
(Vertical 50mm pipe)

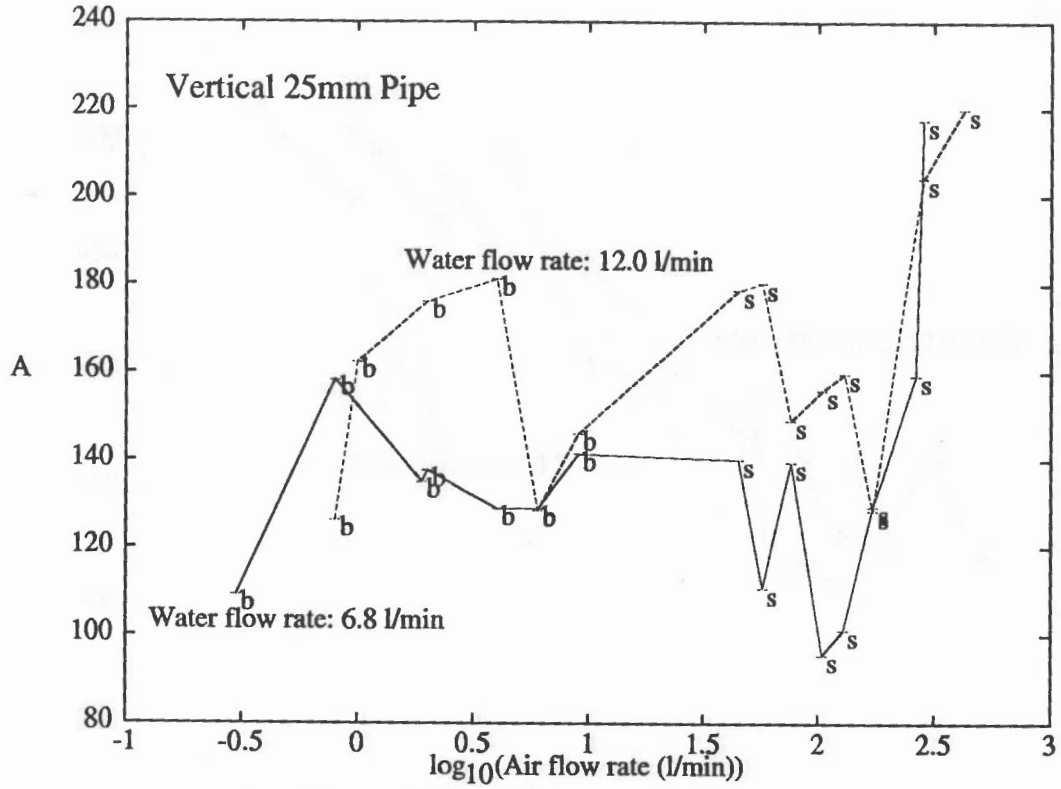

Figure B.55 A : Ultrasonic transducer

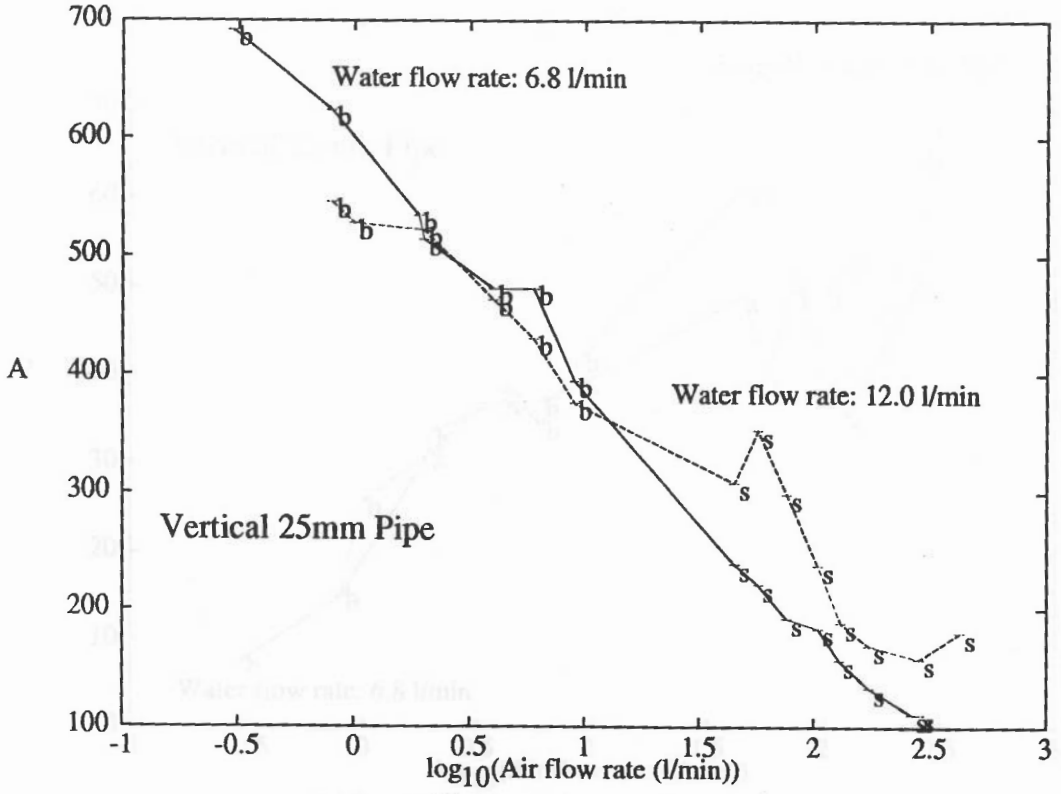

Figure B.56 A : Light transducer

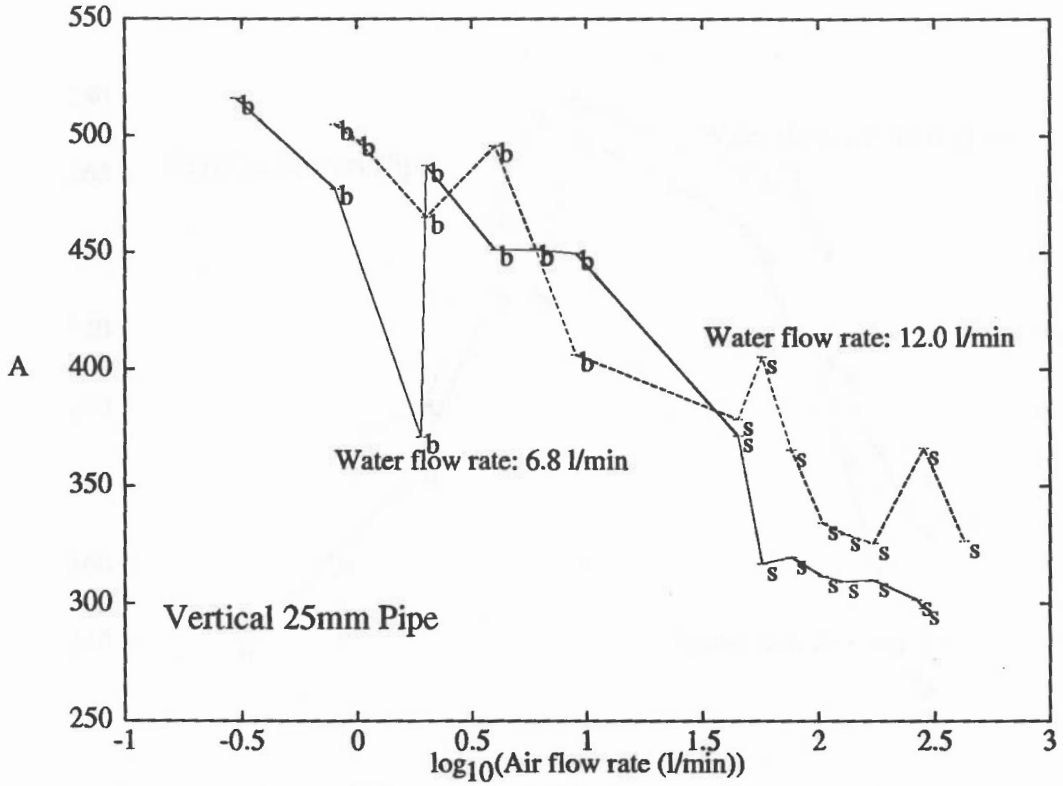

Figure B.57 A : Large range pressure transducer

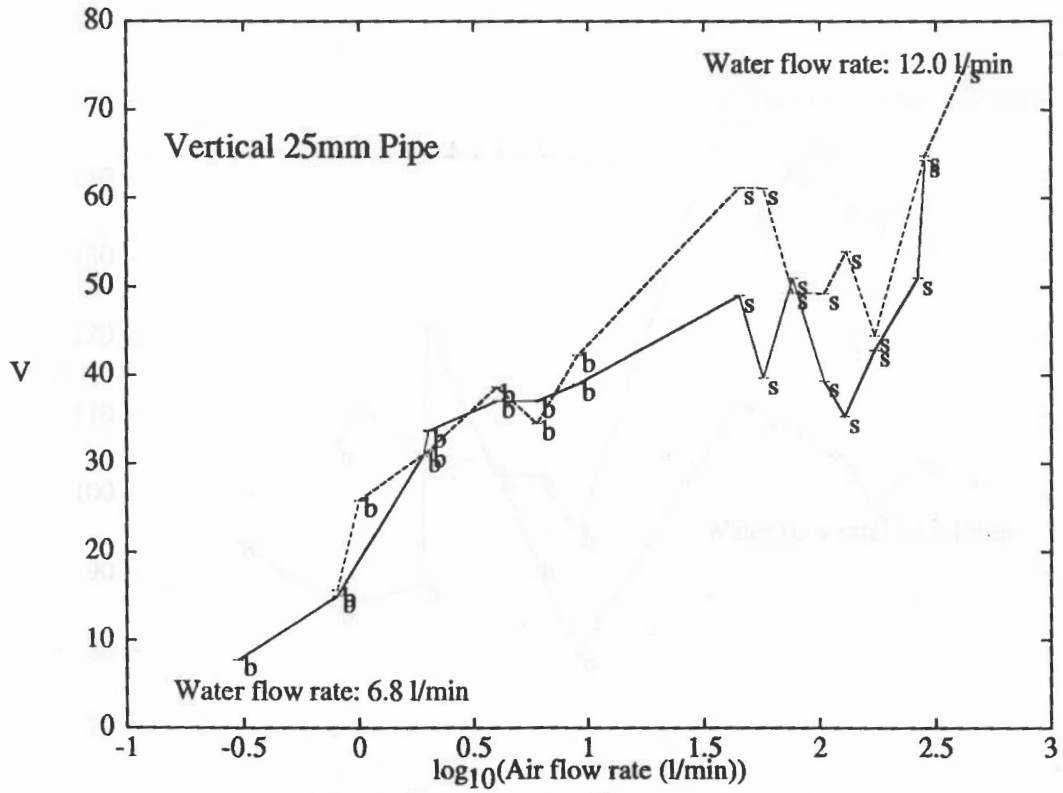

Figure B.58 V : Ultrasonic transducer

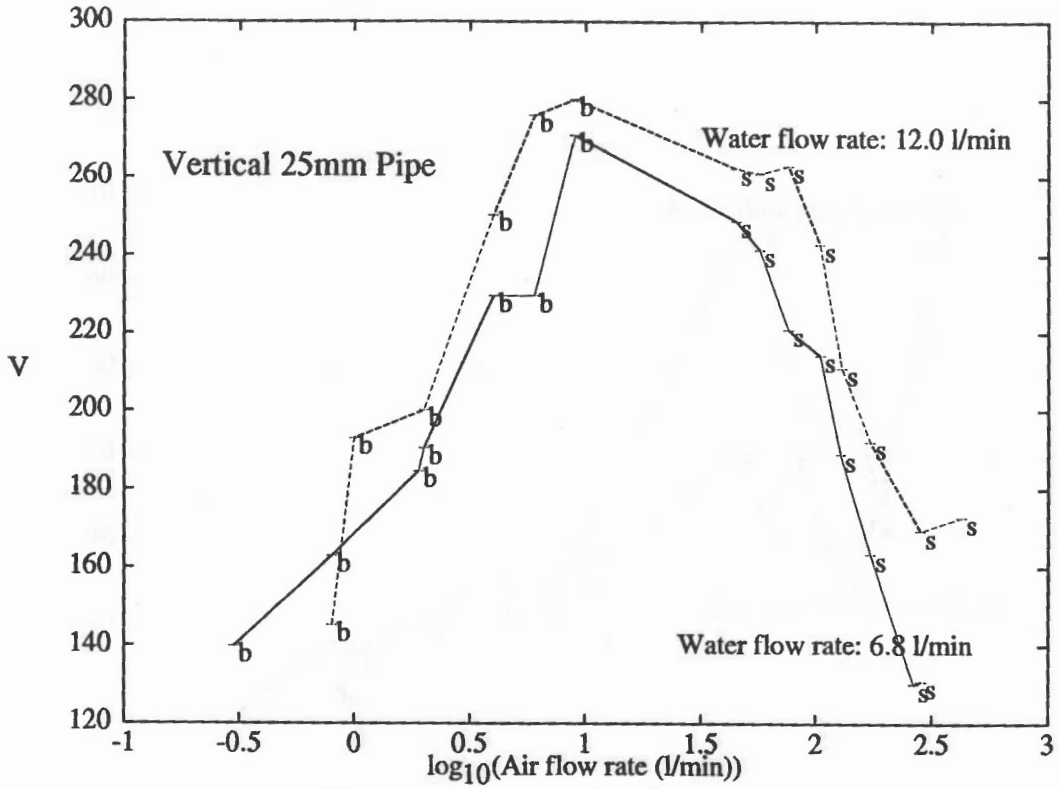

Figure B.59 V : Light transdducer

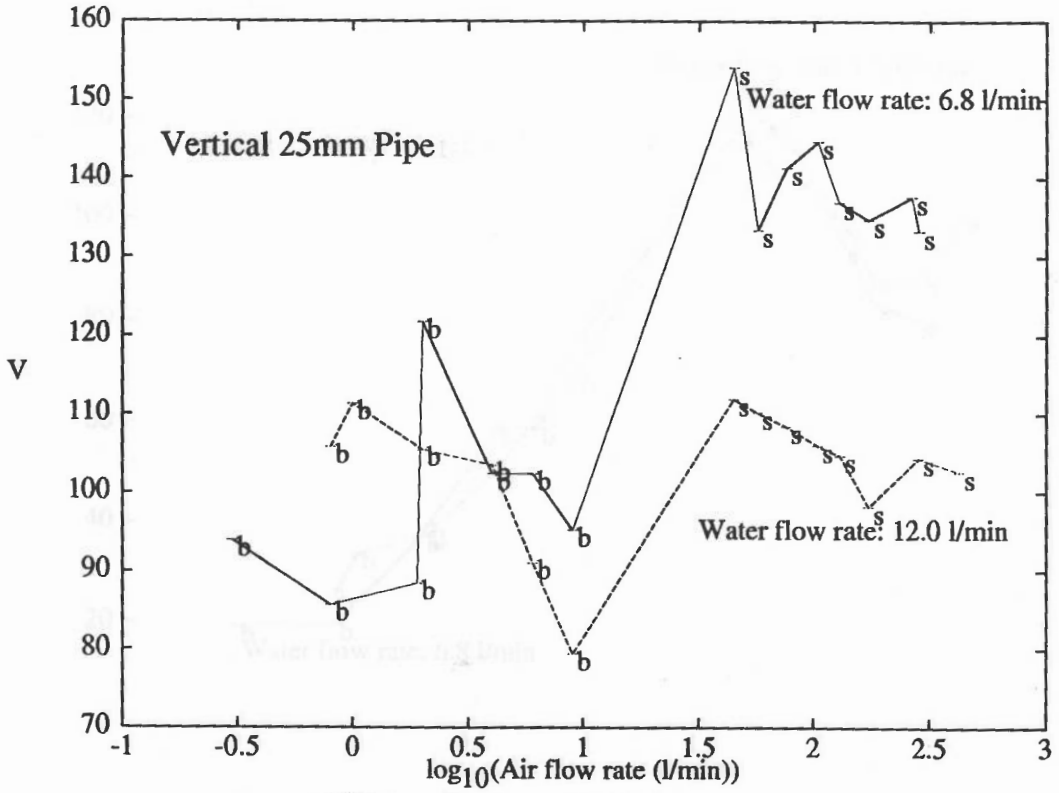

Figure B.60 V : Large range pressure transducer

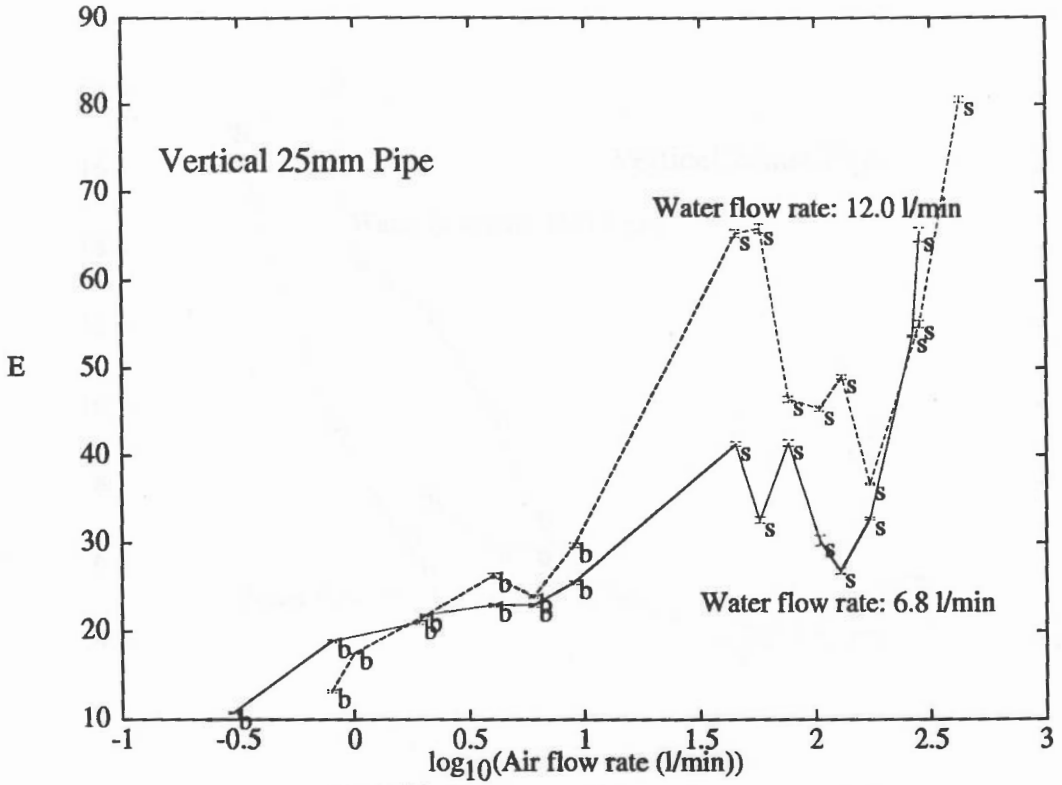

Figure B.61 E : Ultrasonic transducer

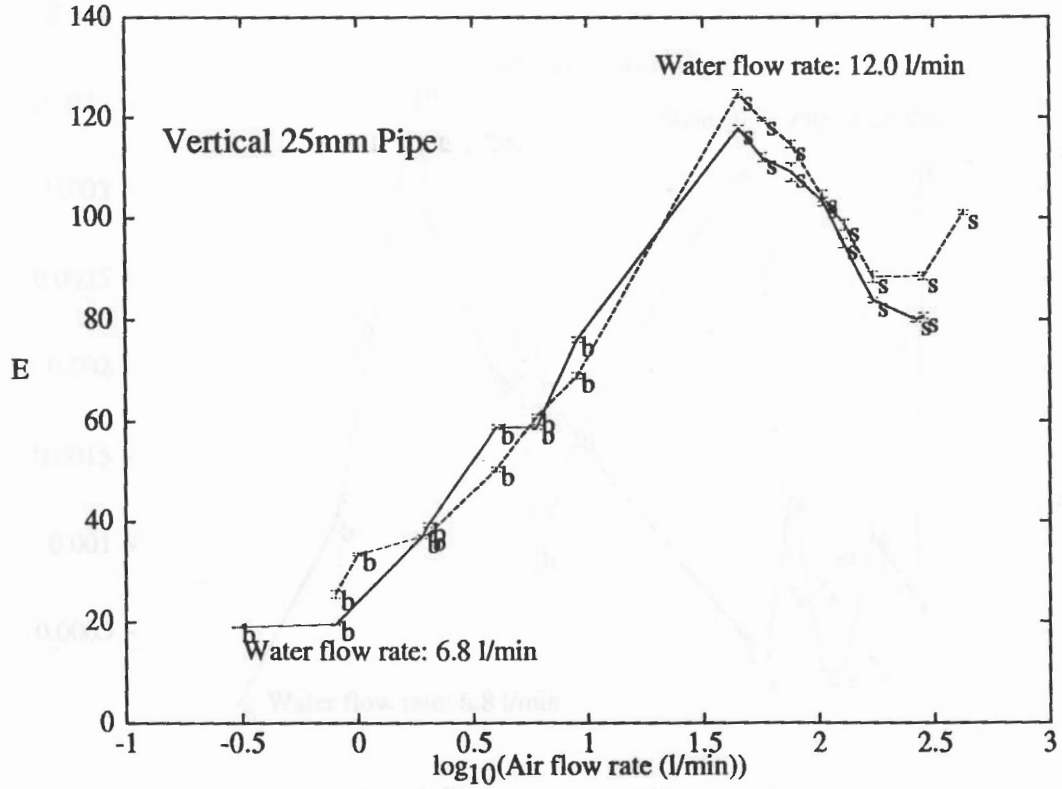

Figure B.62 E : Light transducer

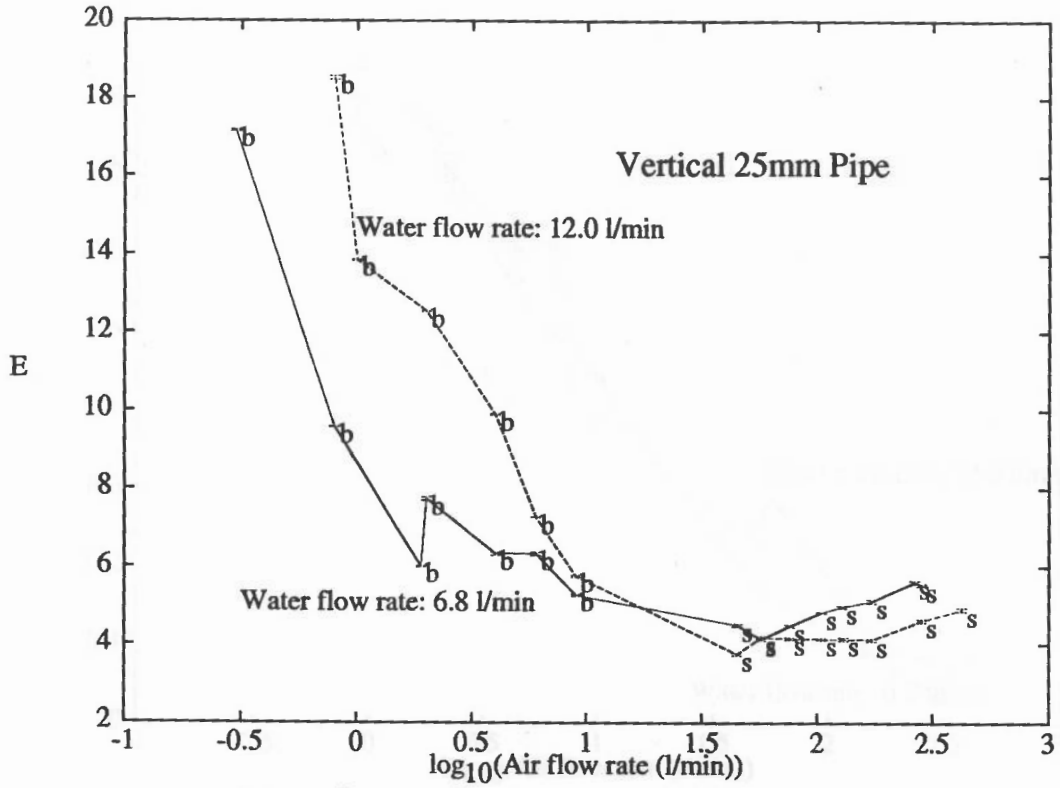

Figure B.63 E : Large range pressure transducer

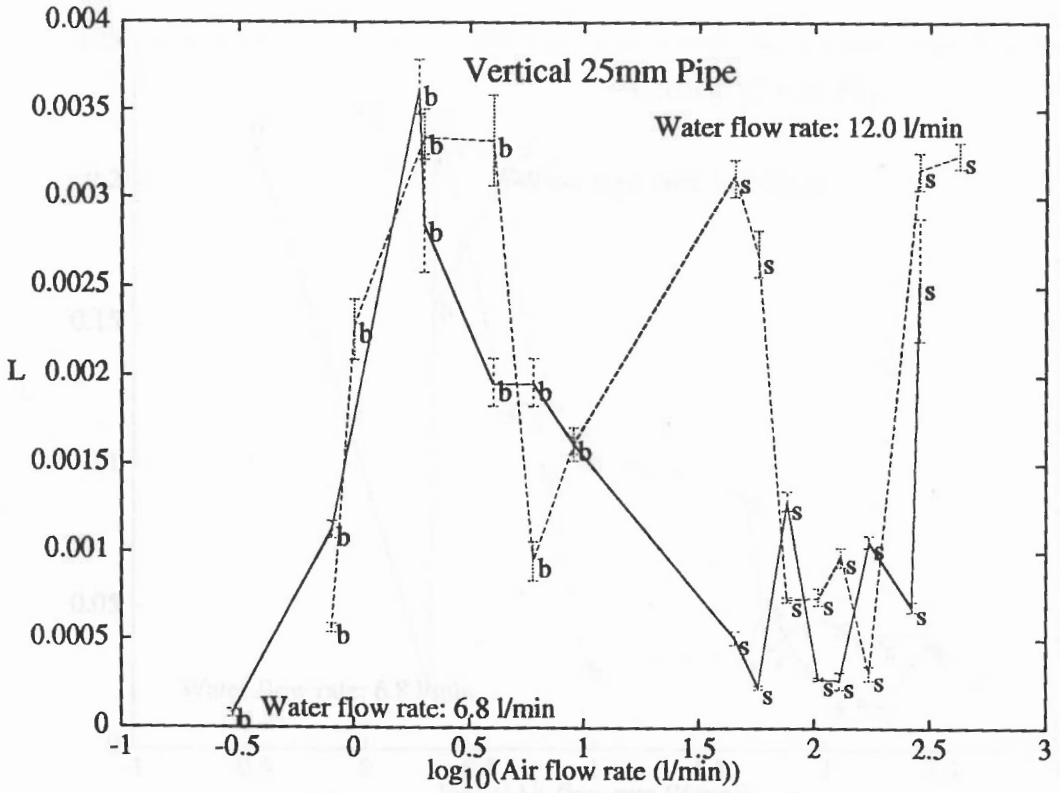

Figure B.64 L : Ultrasonic transducer

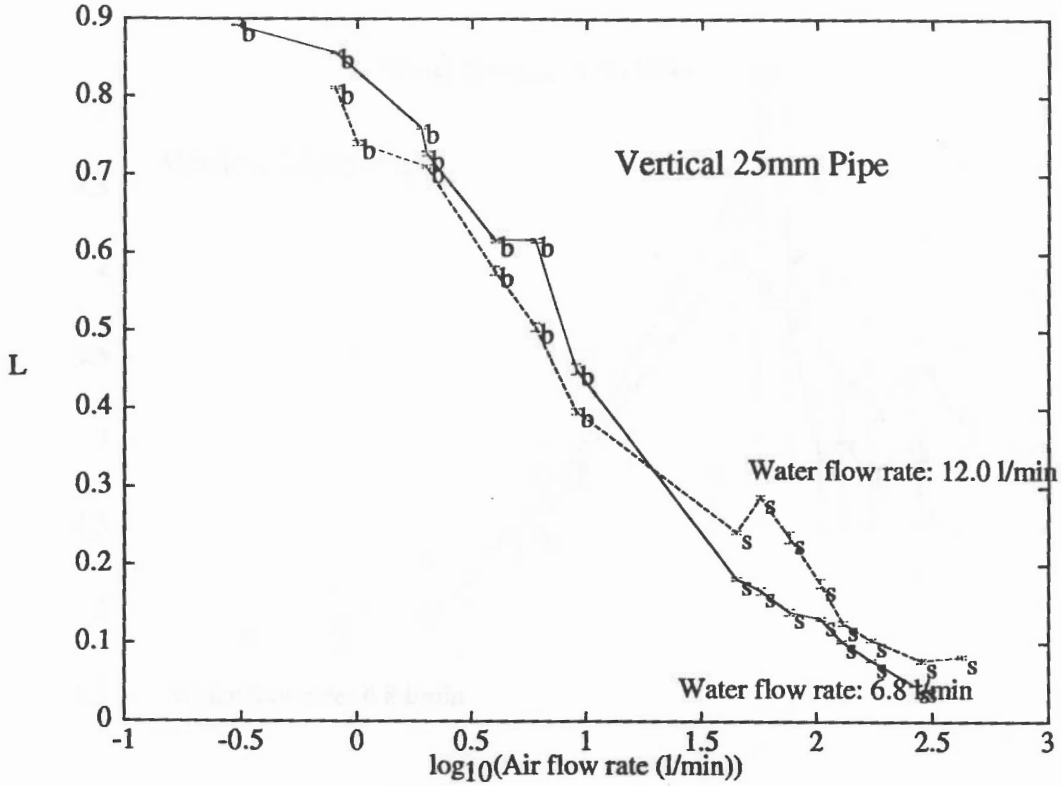

Figure B.65 L : Light transducer

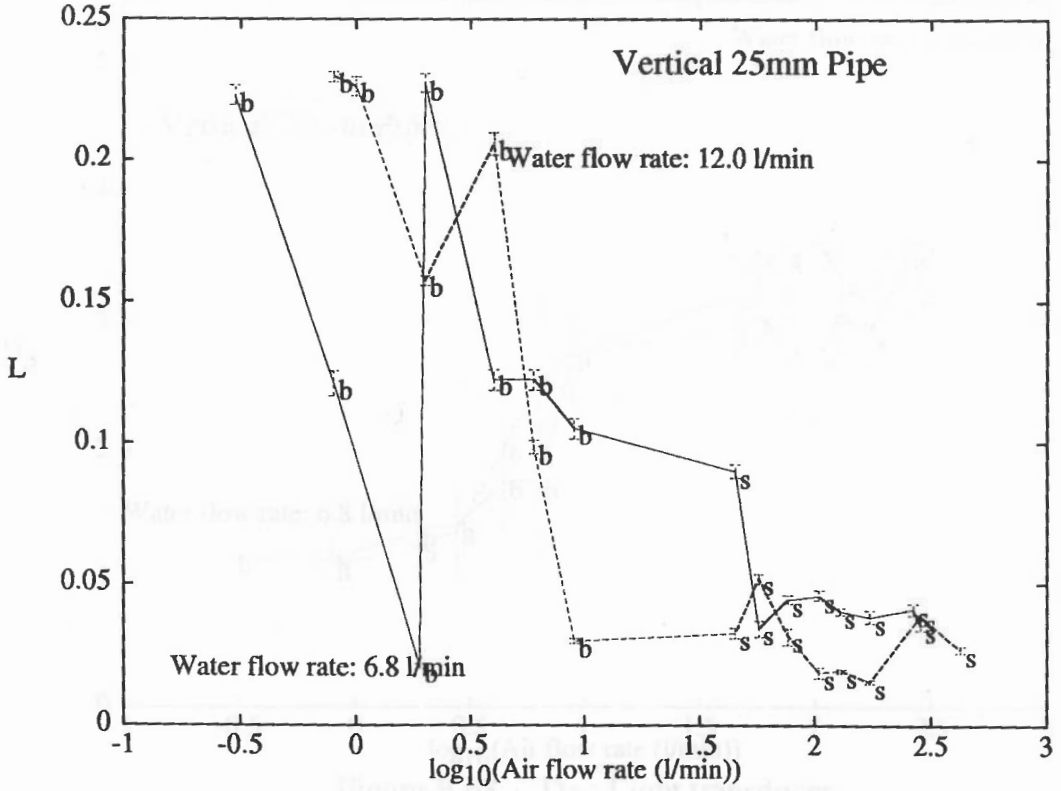

Figure B.66 L : Large range pressure transducer

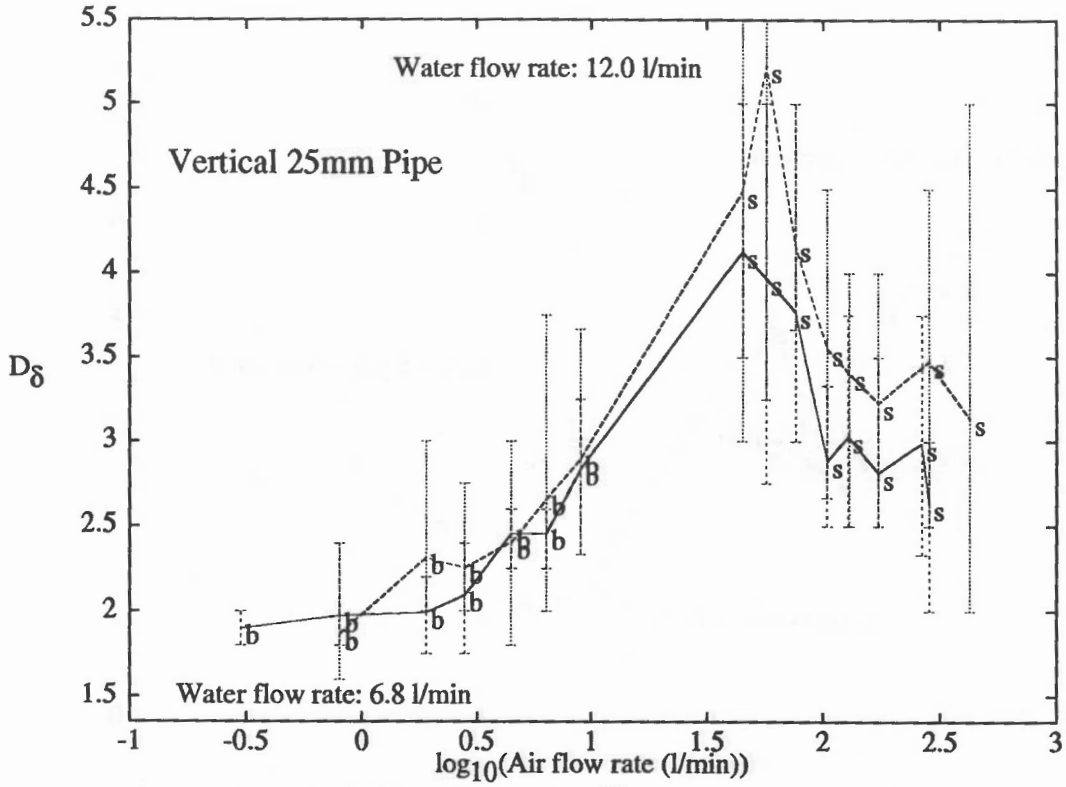

Figure B.67 D_δ : Ultrasonic transducer

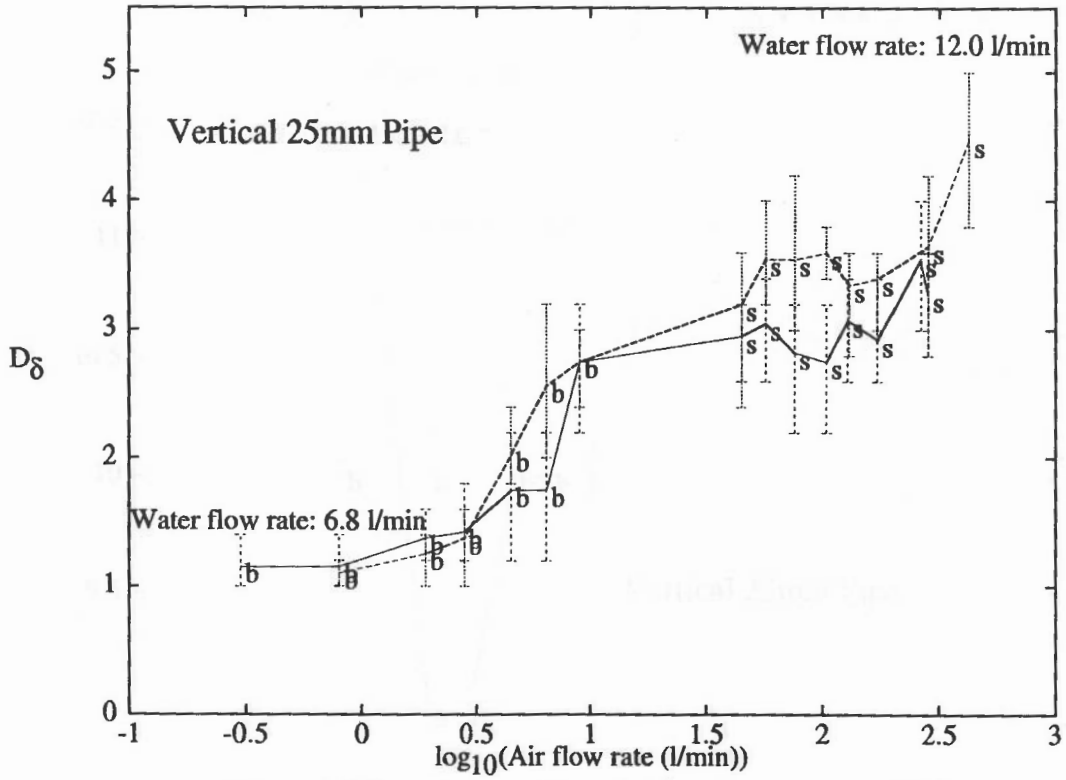

Figure B.68 D_δ : Light transducer

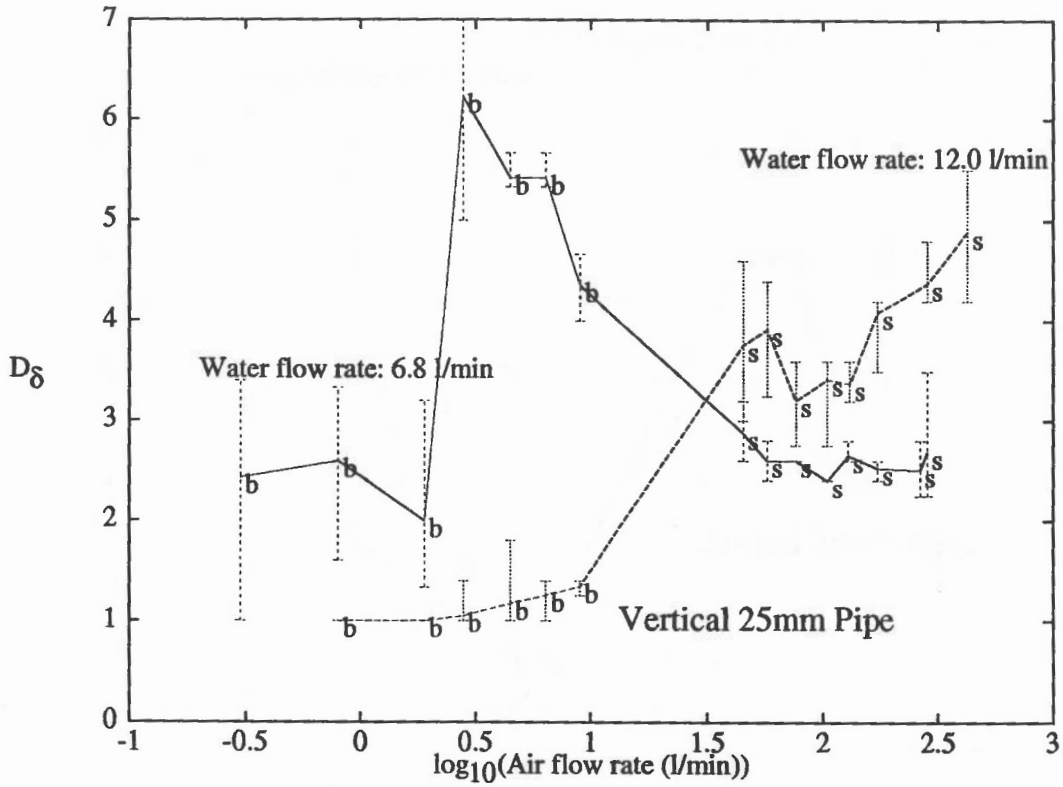

Figure B.69 D_δ : Large range pressure transducer

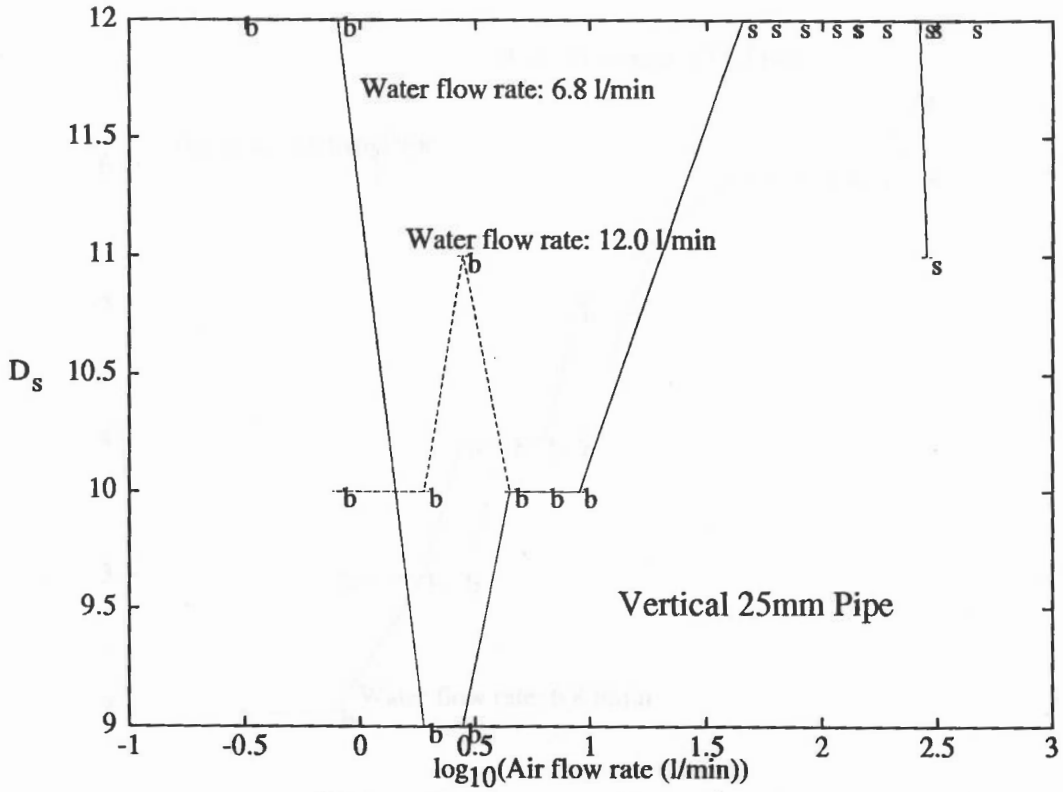

Figure B.70 D_s : Ultrasonic transducer (t =0.0055s)

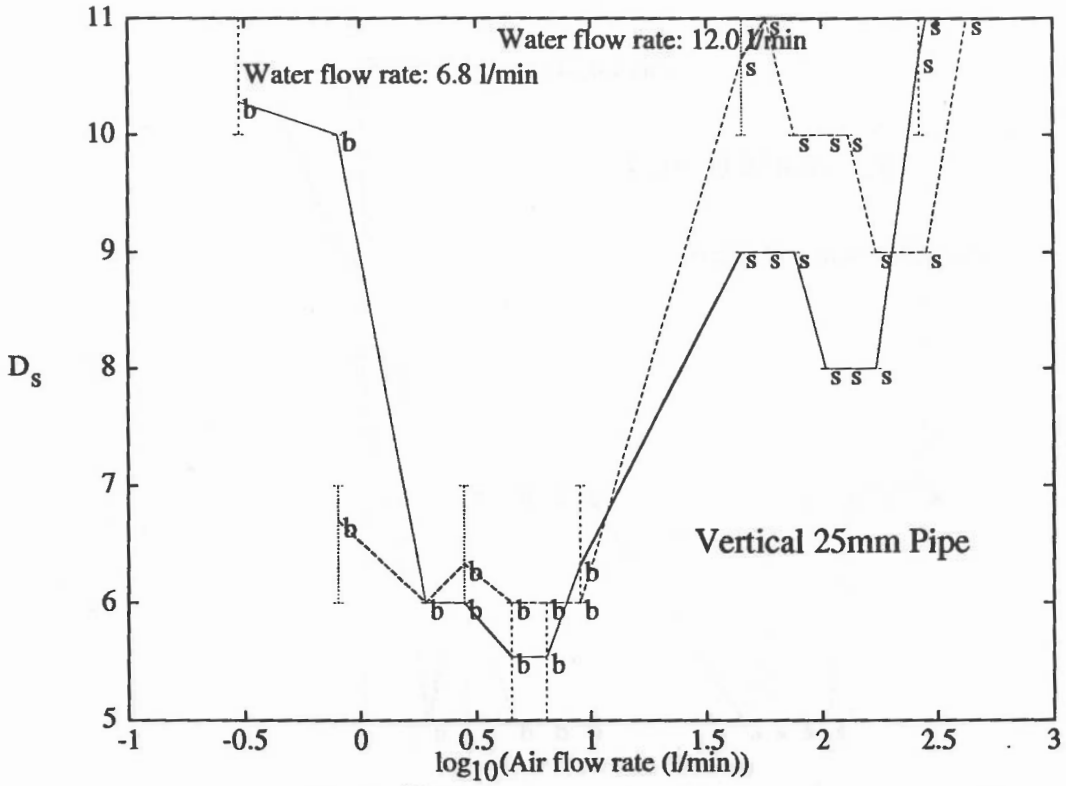

Figure B.71 D_s : Ultrasonic transducer

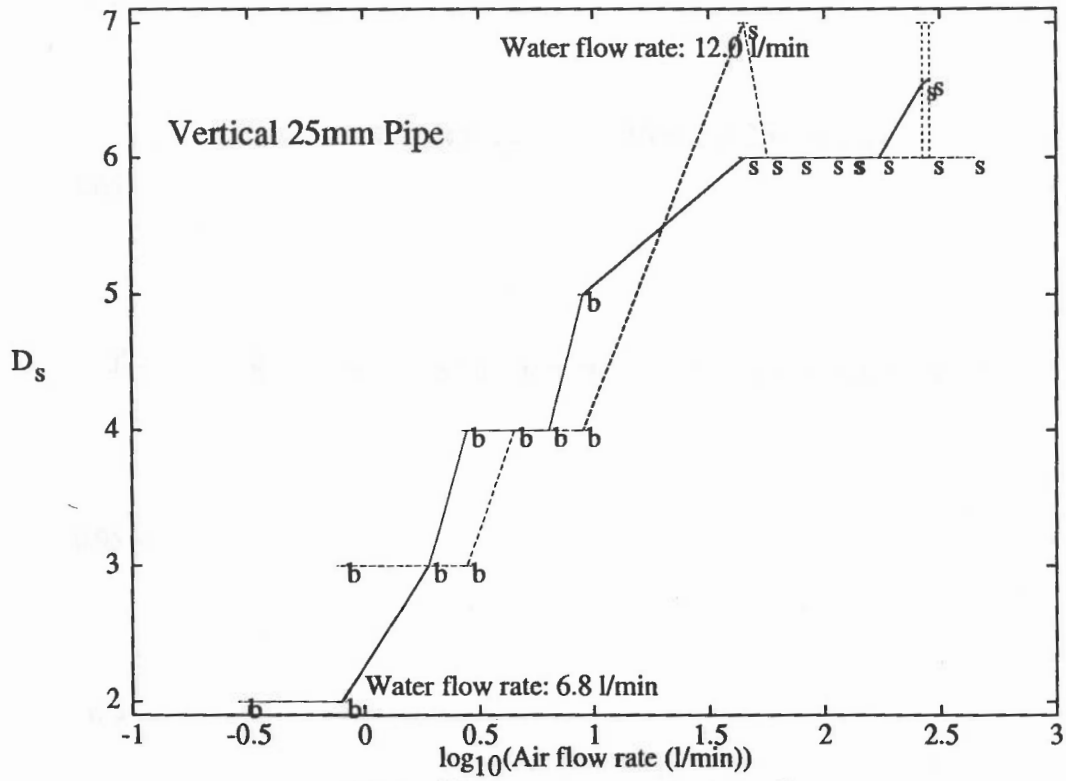

Figure B.72 D_s : Light transducer

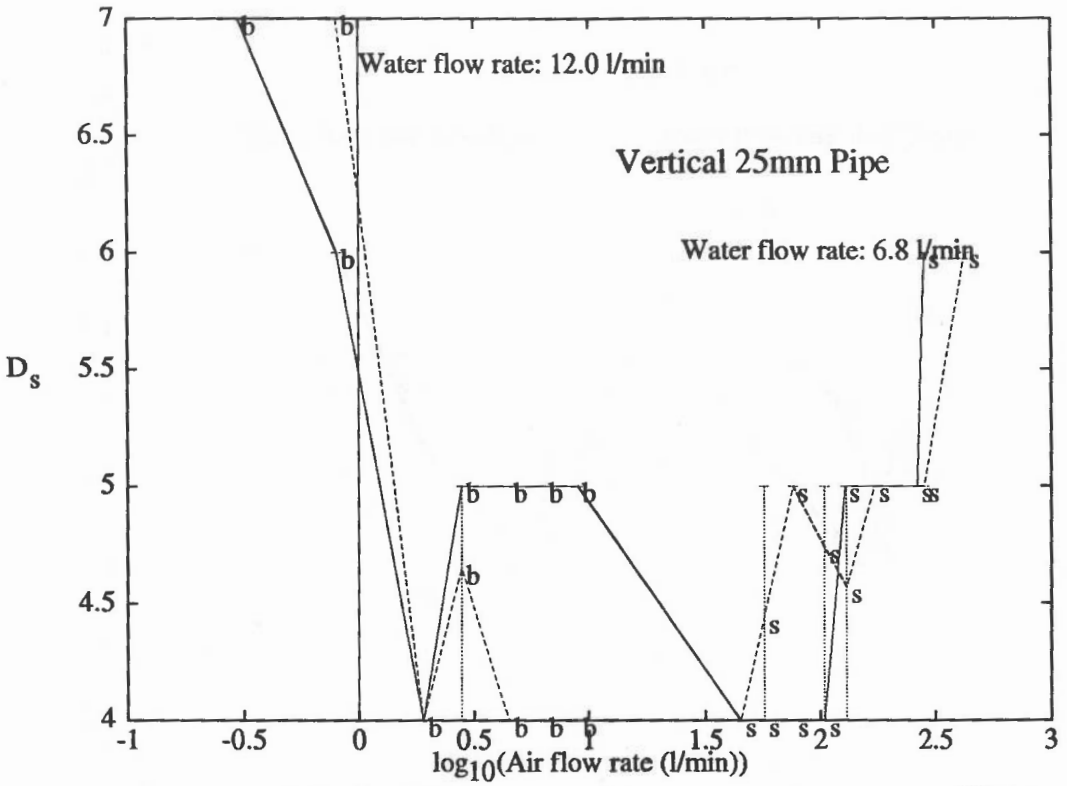

Figure B.73 D_S : Large range pressure transducer (τ=0.0055s)

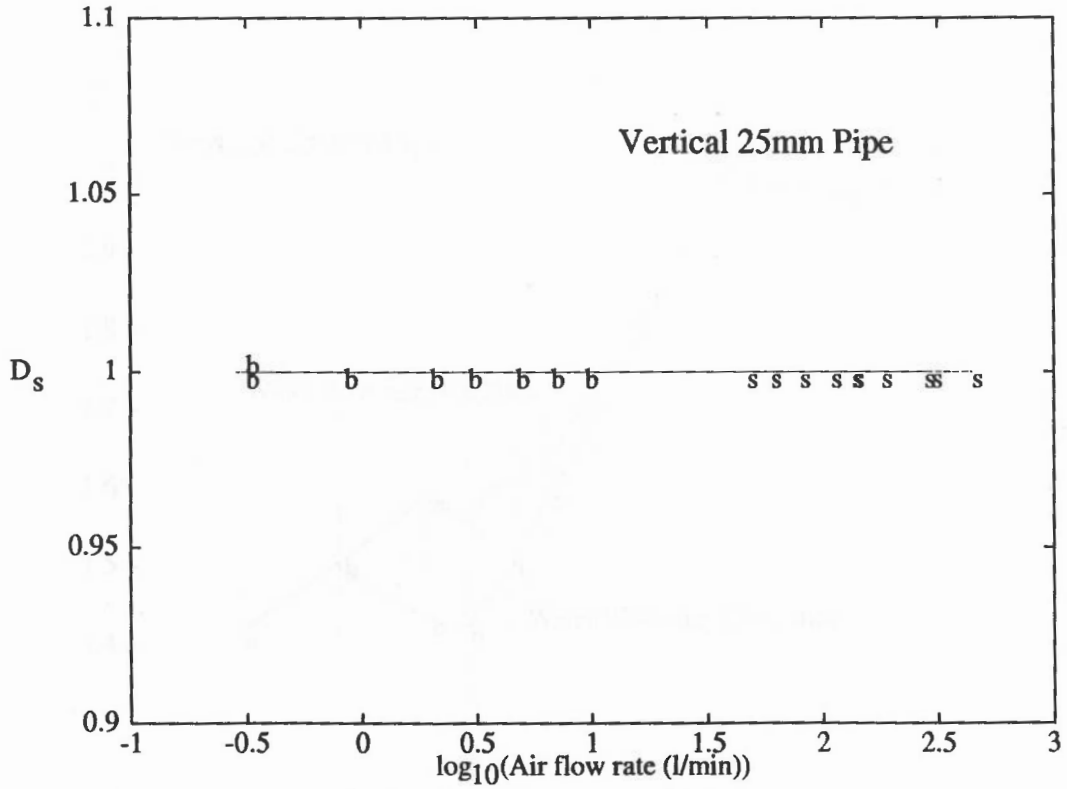

Figure B.74 D_S : Large range pressure transducer

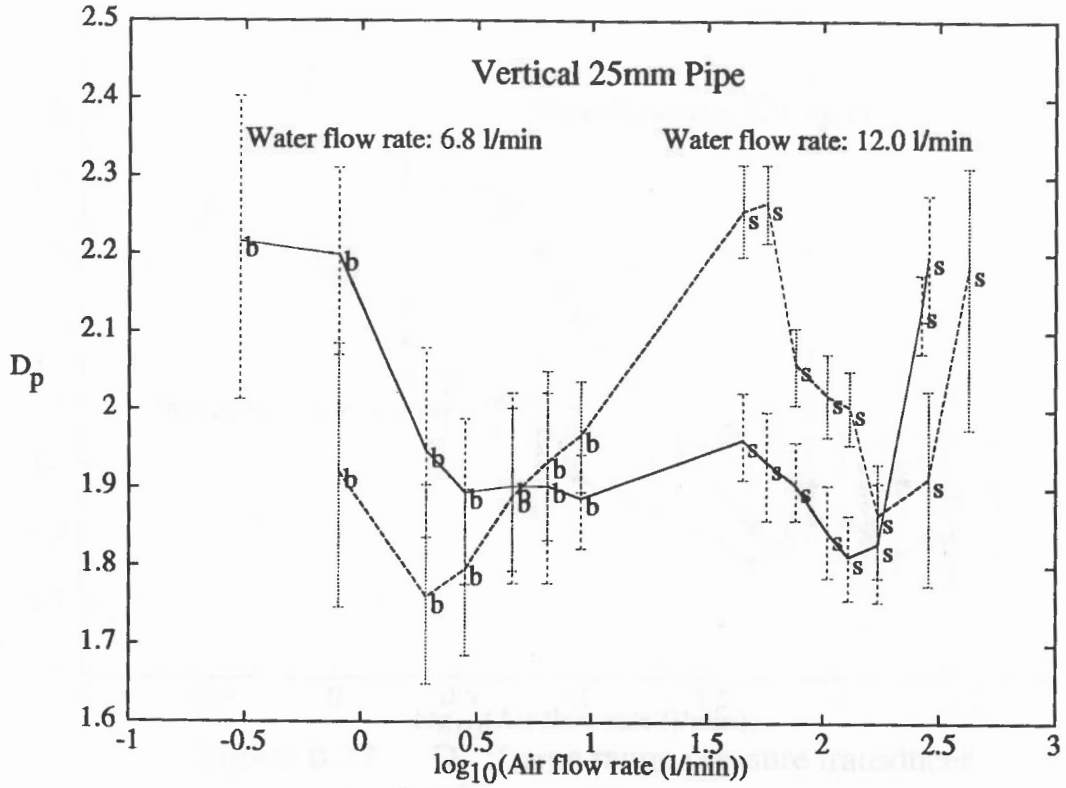

Figure B.75 D_p : Ultrasonic transducer

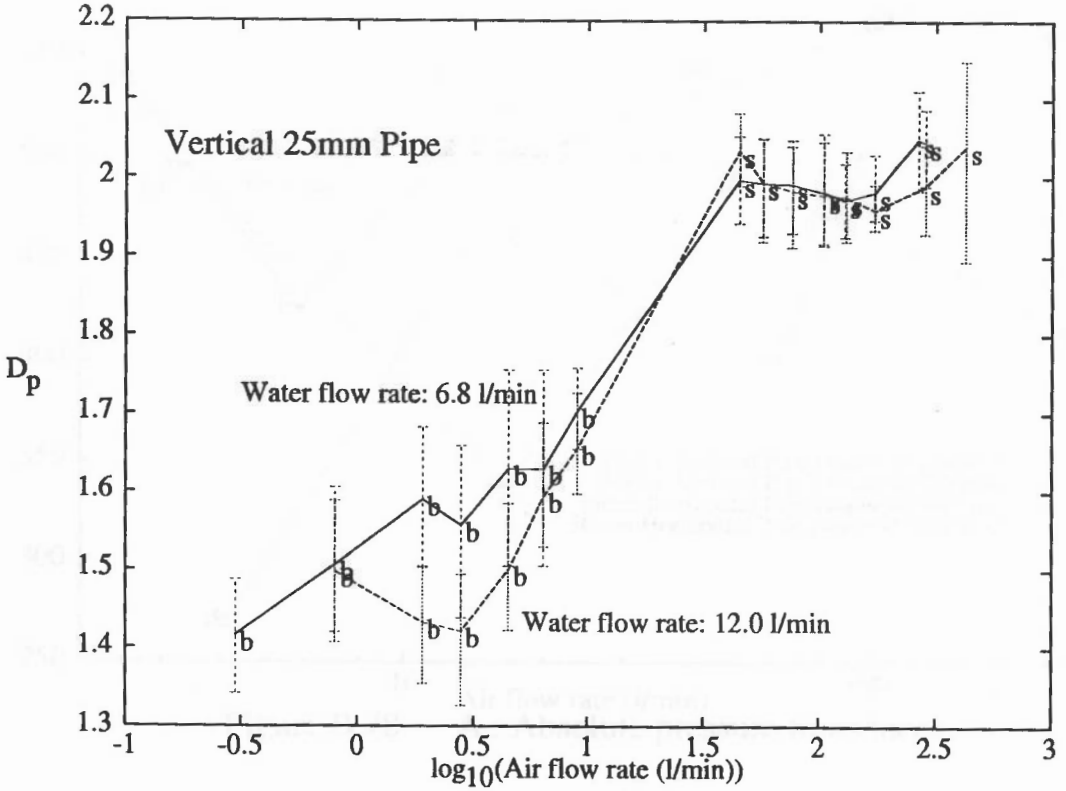

Figure B.76 D_p : Light transducer

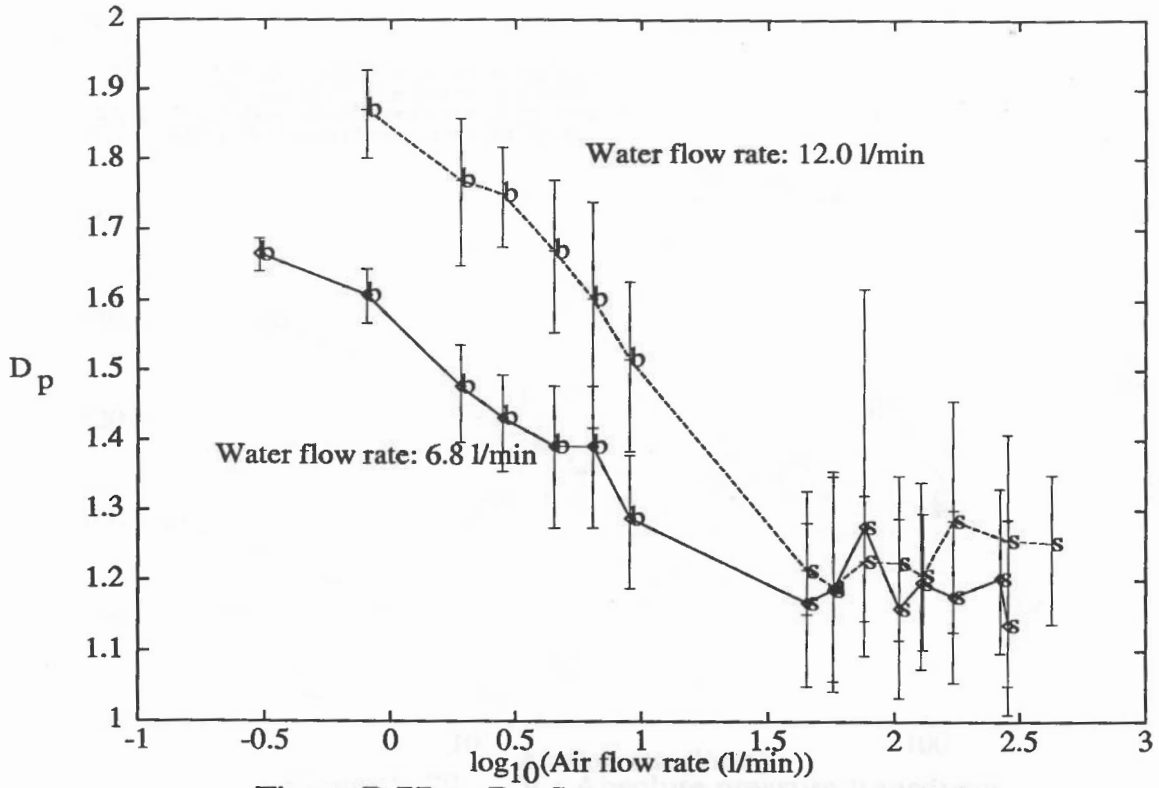

Figure B.77 D_p :Large range pressure transducer

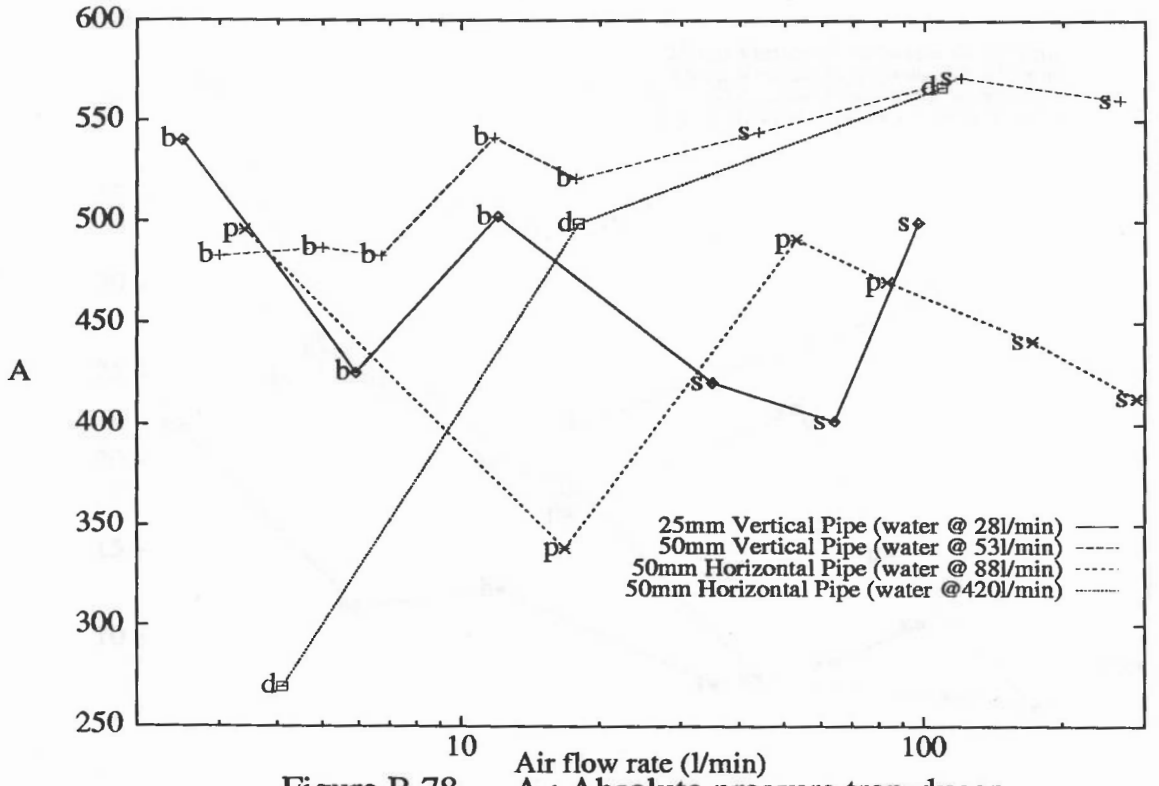

Figure B.78 A : Absolute pressure transducer

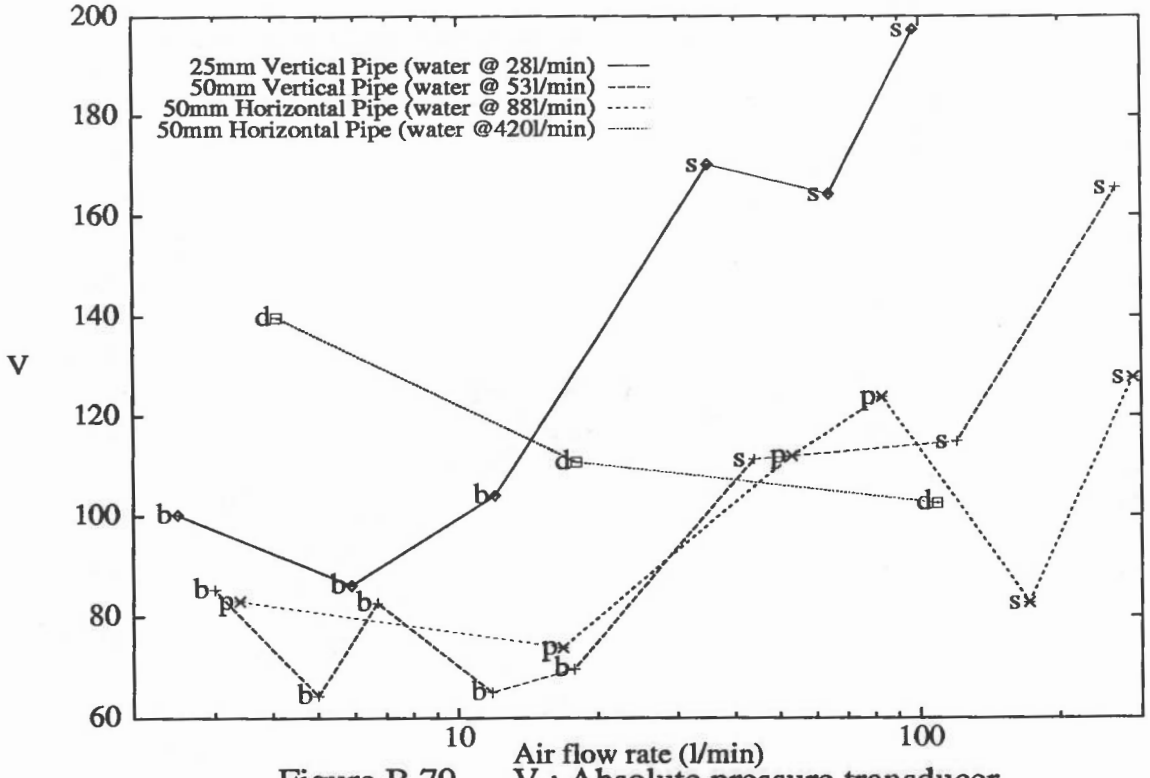

Figure B.79 V : Absolute pressure transducer

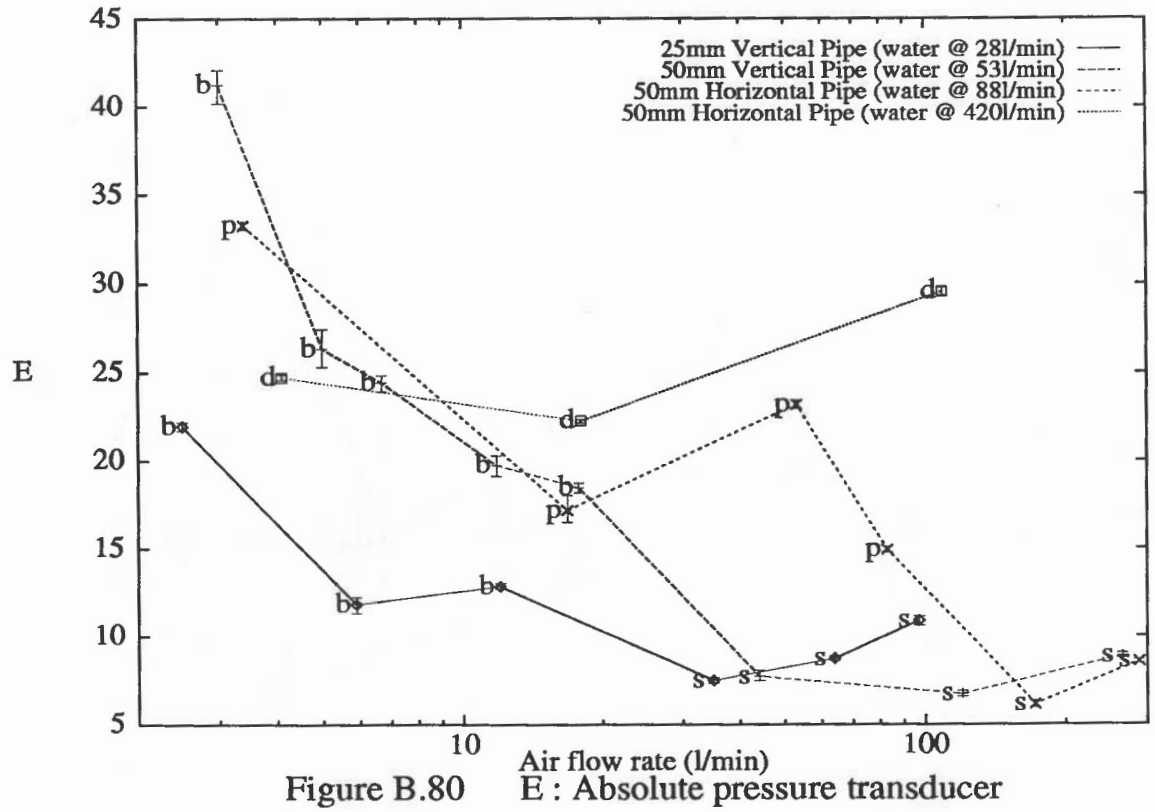

Figure B.80 E : Absolute pressure transducer

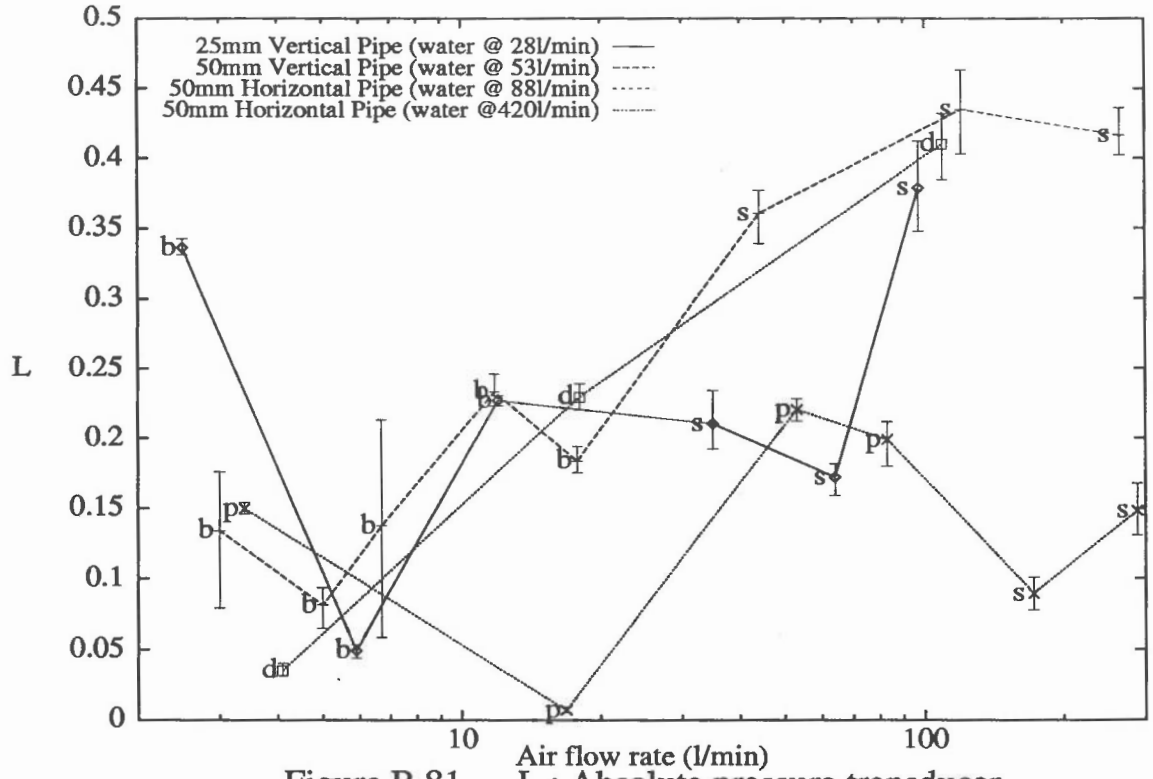

Figure B.81 L : Absolute pressure transducer

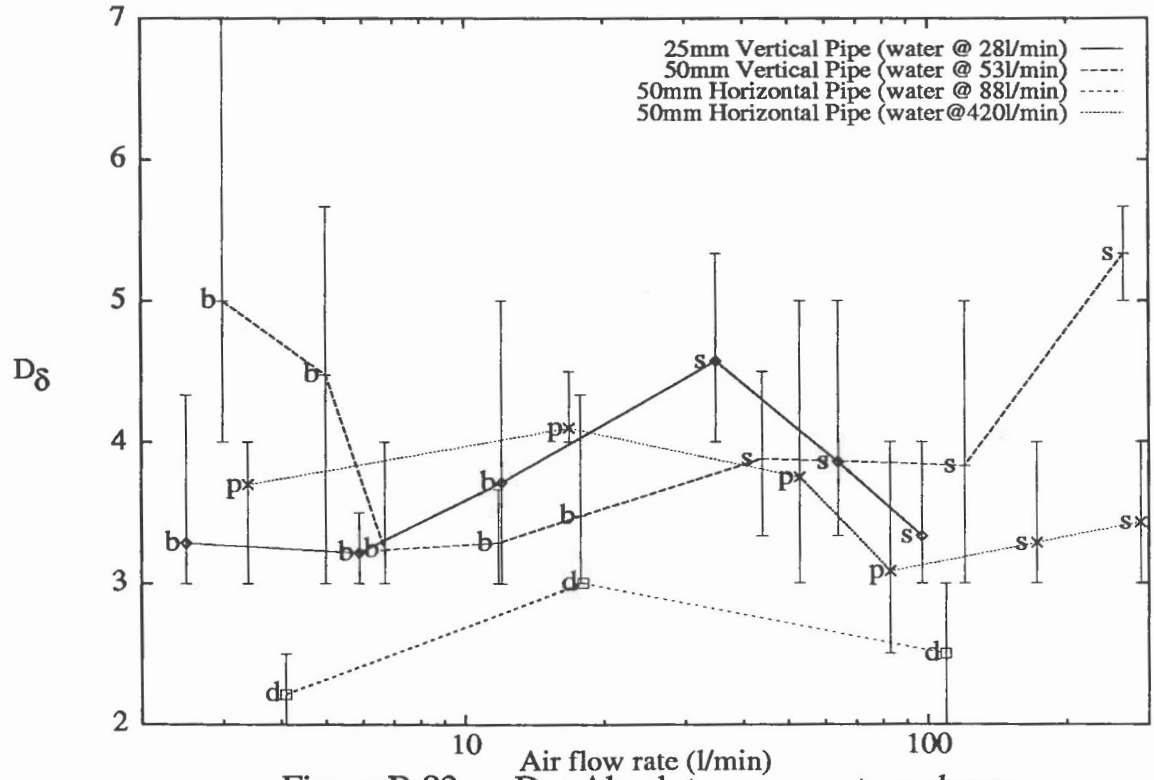

Figure B.82 D_δ: Absolute pressure transducer

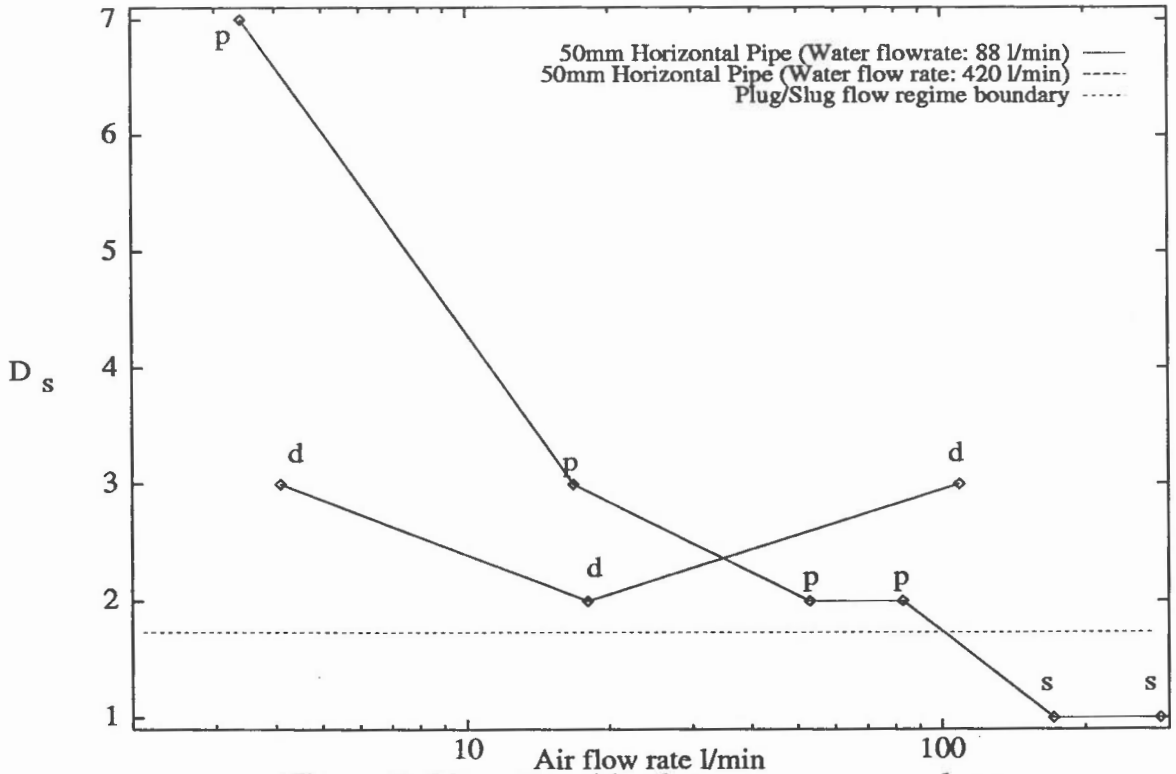

Figure B.83 D_S: Absolute pressure transducer (τ =0.00275s)

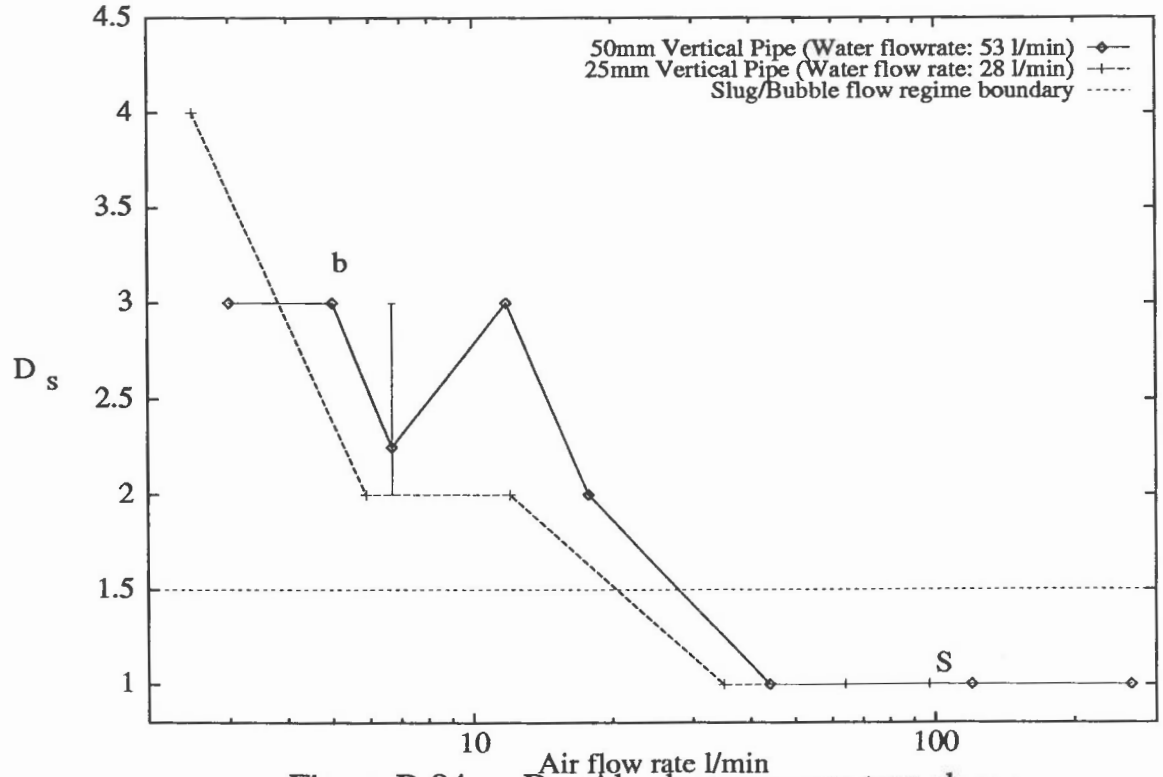

Figure B.84 D_S: Absolute pressure transducer

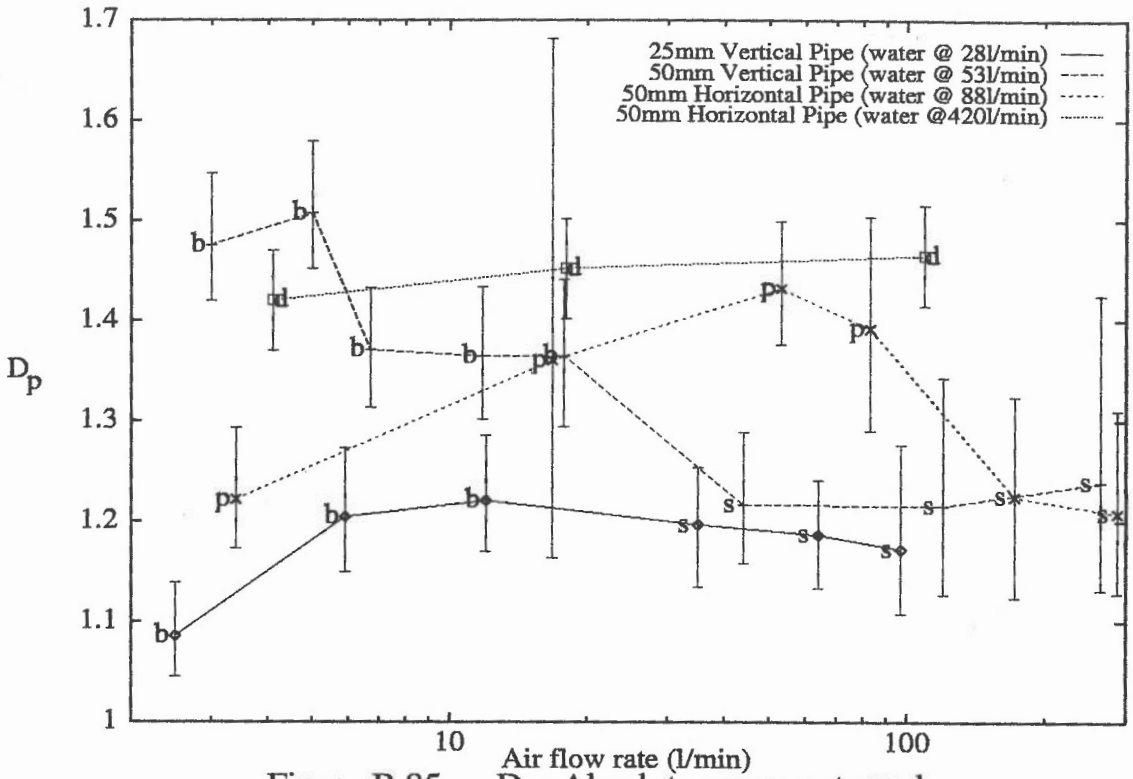

Figure B.85 D_p: Absolute pressure transducer